博 士 論 文

STUDY ON ENERGY SHARING IN PV COMMUNITIES CONSIDERING SOLAR RADIATION PREDICTION

日射量予測を考慮した太陽光発電コミュニティにおけるエネルギーシェアリングに関する研究

2023 年 3 月

李　游

LI YOU

Acknowledgements

Foremost, I would like to express my sincere gratitude to Prof. Hiroatsu FUKUDA and Prof. Weijun GAO for their continuous support of my Ph. D study and research, for their patience, motivation, enthusiasm, and immense knowledge. Their guidance helped me in all the time of research and writing of this thesis.

I could not have imagined having a better advisor and mentor for my Ph. D study.

Besides my advisor, I would like to thank the rest of my thesis committee: Prof. Hidehiro KOYAMADA, Prof. Masayuki SATO, for their encouragement, insightful comments, and questions. And I would like to thank Prof. Wanxiang YAO, for enlightening me the first glance of research field in solar radiation.

I thank my fellow lab mates in Kitakyushu FUKUDA Group, for the stimulating discussions, for the sleepless nights we were working together before deadlines, and for all the fun we have had in the last five years.

Last but not the least, I would like to thank my parents and Yafei WANG, for supporting me throughout my life.

Study on Energy Sharing in PV Communities Considering Solar Radiation Prediction

ABSTRACT

The power sector plays an important role in energy conservation and emission reduction. Renewable energy, especially solar PV, has been growing steadily in recent years. The development of solar energy can not only reduce the use of fossil energy, but also increase the energy self-sufficiency rate. After the implementation of the FiT system in 2011, there has been an explosive growth in the import of solar PV. However, solar power generation exhibits unstable output characteristics as it is affected by weather conditions. Large-scale introduction can affect the stability of the grid (e.g., the severe curtailment of generation or lack of resilience in the face of failures and disturbances). Therefore, this study considers the unstable weather conditions (mainly, solar radiation) and proposes the concept of energy sharing to increase the chances of local energy self-consumption and renewable energy penetration in the future. At the same time, we aim to explore the interactions between smart grids, smart buildings, and distributed energy storage to achieve better energy management practices.

Firstly, because high-resolution data for solar radiation are particularly significant for building thermal simulation and photovoltaic systems. Whereas, applying low-cost data to construct a highly accurate and reliable solar radiation model has been a challenge. In this work, a new weakening solar radiation model is proposed based on a formal analysis of exiting models and as well as on new understandings of the seasonal and stochastic feature of solar radiation. As a result, in first part of main body, surface meteorological parameters (such as relative humidity, weather, cloud cover, etc.) that can be simply obtained are used to construct the model. Over 200,000 sets of data are collected from seven locations in Japan were used for modeling as well as validation. Considering the ease of data acquisition. Furthermore, most hourly solar models are only developed for clear sky conditions. And it is increasingly required that hourly solar radiation models maintain a high level of accuracy and confidence in complex weather conditions. In contrast, the proposed model is established and calibrated from over 20 years of meteorological data and under a variety of weather conditions in Japan. Meanwhile, the weakening effect of solar radiation is taken as the main body of this work. The stochastic feature can be well characterized by turbidity parameters in cloudy and even rainy days. Simultaneously, the proposed model has strong extensibility, and the inclusion of interaction variables (especially sunshine duration and cloud cover) leads to a significant improvement in the interpretability as well as the accuracy of the model.

Secondly, based on the solar radiation prediction in various weather conditions, the solar penetration of the building community can be accurately captured. However, the building community is still faced with the problem of surplus energy consumption resulting from the dynamic mismatch between solar energy and local demand. Thus, in the second part of the main body, energy sharing is proposed, which refers to energy transactions between consumers and

producers or between producers, where surplus electricity from producers can be shared between neighbors. The potential of energy sharing is explored based on historical monitoring data in a Japanese smart community. Then, the size and number of the BESS are determined by developing a genetic algorithm-based constraint model. Then, the participation of the BESS in grid demand response is discussed to bring more economic benefits. And the proposed method of battery sharing is compared to the traditional user-owned BESS to verify its feasibility.

Furthermore, the energy sharing is enabled to optimize the control strategy and allocation method of the distributed battery system that can be exploited to achieve better optimization for load leveling through investigating the interaction between buildings with the distributed battery system and the distribution network. we provide an analysis of battery sharing by establishing a coordinated control model for a distributed battery system. In our case study design, we selected 39 buildings with different capacities of energy storage systems as a battery-sharing community to optimize sharing schedules and the load-leveling performance.

The results indicate that the optimal solution obtained with the energy sharing structure performs possible to import more solar energy and load leveling effectively. Compared with the individual operation, the energy sharing model achieves better load leveling performance of the public grid, while it reduces the battery capacity at aggregation level. Also, the energy sharing is a generic framework for decomposing the optimal BESS allocation problem into individual optimal sizes of BESS within buildings. This approach allows to obtain optimal solutions by reducing unnecessary energy exchange between buildings. The proposed method highlights the possibility of cooperation between consumers. It provides a blueprint for the implementation of a better use of solar energy and regional energy sharing.

李 游 博士論文の構成

Study on Energy Sharing in PV Communities Considering Solar Radiation Prediction

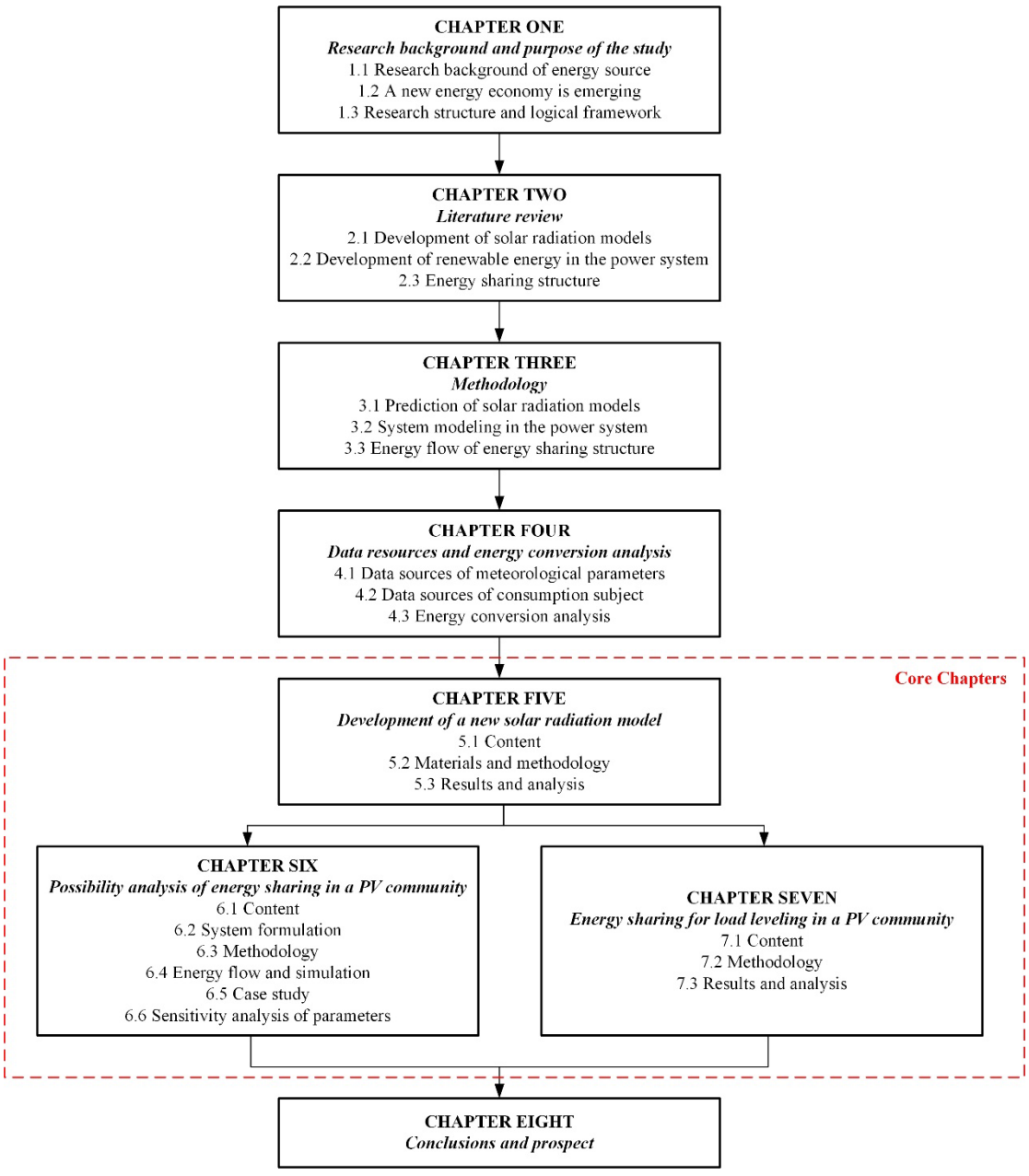

TABLE OF CONTENTS

ABSTRACT I

STRUCTURE OF THIS PAPER IV

CHAPTER 1: RESEARCH BACKGROUND AND PURPOSE OF THE STUDY

1.1 Research background of energy resource 1-1

1.1.1 Current status of energy supply 1-1

1.1.2 Government policy 1-8

1.1.3 Climate change and weather stochastics 1-15

1.2 A new energy economy is emerging 1-19

1.3 Research structure and logical framework 1-22

1.3.1 Research purpose and core content 1-22

1.3.2 Chapter content overview and related instructions 1-24

Reference 1-27

CHAPTER 2: LITERATURE REVIEW

2.1 Development of solar radiation models 2-1

2.1.1 Existing coarse-grained models 2-1

2.1.2 Existing fined-grained models 2-2

2.2 Development of solar PV generation models 2-4

2.3 Application of solar PV generation in urban area 2-5

2.4 Application of PV battery system in urban area 2-6

2.5 Battery sharing in urban area 2-13

Reference 2-23

CHAPTER 3: METHODOLOGY

3.1 Methodology of solar radiation model development 3-1

3.1.1 Analysis of global solar radiation models 3-1

3.1.2 Methods 3-1

3.1.3 Processing flow 3-2

3.1.4 Statistical test methods 3-2

3.2 Methodology of solar PV generation model 3-3

3.2.1 PV cell 3-3

3.3 Methodology of battery bank model 3-4

3.4 Methodology of PV battery system 3-5

3.4.1 System description 3-5

3.4.2 Energy balance 3-6

3.4.3 Aggregated control 3-6

3.4.4 Adaptive power dispatch 3-11

3.5 Methodology of energy sharing 3-15

3.5.1 Internal pricing mechanism 3-15

3.5.2 Aggregator managed demand response 3-15

3.5.3 Energy flow and simulation 3-16

3.5.4 Energy losses 3-20

3.5.5 Intelligent optimization algorithm 3-21

3.5.6 Processes 3-23

3.5.7 Evaluation Indicators 3-25

Reference 3-25

CHAPTER 4: DATA RESOURCES AND ENERGY CONVERSION ANALYSIS

4.1 Weather data sources 4-1

4.2 Energy sources 4-3

4.2.1 Load sources 4-3

4.2.2 Distributed network 4-12

4.2.3 Data Processing 4-14

Reference 4-16

CHAPTER 5: DEVELOPMENT OF A NEW SOLAR RADIATION MODEL

5.1 Contents 5-1

5.2 Materials and Methodology 5-4

5.2.1 Analysis of global solar radiation models 5-4

5.2.2 A new concept from layer-by-layer weakening theory 5-5

5.2.3 Methods 5-6

5.2.4 Solar Geometry 5-7

5.2.5 Data collection 5-9

5.2.6 Processing flow 5-10

5.2.7 Statistical test methods 5-12

5.3 Result and discussion 5-13

5.3.1 Model Establishment....5-13
5.3.2 Overall forecast result....5-18
5.3.3 Available for rainy and cloudy conditions....5-26
5.3.4 Interpretability....5-29
5.3.5 Comparison and Expansion....5-29
5.4 Application....5-33
5.5 Conclusion....5-35
Appendix A....5-36
References....5-39

CHAPTER 6: POSSIBILITY ANALYSIS OF ENERGY SHARING IN A PV COMMUNITY

6.1 Contents....6-1
6.2 System formulation....6-7
6.2.1 Basic idea of energy sharing structure....6-7
6.2.2 Introduction of typical design scenarios of BESS....6-8
6.3 Methodology....6-9
6.3.1 Data sources....6-9
6.3.2 PV and battery modeling....6-10
6.3.3 Internal pricing mechanism....6-11
6.3.4 Aggregator managed demand response....6-12
6.4 Energy flow and simulation....6-13
6.4.1 Energy flow....6-13
6.4.2 Energy losses....6-17
6.4.3 Objective functions....6-18
6.4.4 Optimization....6-18
6.5 Case study....6-21

6.5.1 Situation analysis 6-21
6.5.2 Energy sharing participation willingness evaluation 6-23
6.5.3 The results of optimized BESS configuration 6-26
6.5.4 Losses comparison at community-levels 6-27
6.5.5 Transmission loss optimization during battery sharing process 6-28
6.5.6 Performance comparison of single building 6-29
6.5.7 DR performance evaluation (Scenario SCB&SDB) 6-31
6.5.8 Economic performance comparison 6-33
6.6 Sensitivity analysis of parameters 6-34
6.7 Conclusions 6-36
Reference 6-37

CHAPTER 7: ENERGY SHARING FOR LOAD LEVELING IN A PV COMMUNITIY

7.1 Contents 7-1
7.2 System description 7-4
7.2.1 Basic concept of cloud-based battery sharing framework 7-4
7.3 Methodology 7-5
7.3.1 General process 7-5
7.3.2 Battery energy storage system 7-7
7.3.3 Energy flow 7-7
7.3.4 Energy flow modeling 7-10
7.3.5 Performance metrics 7-11
7.3.6 Optimization 7-12
7.4 Case study 7-15
7.4.1 Situational analysis 7-15
7.4.2 Optimal battery capacity at aggregation level 7-16

7.4.3 Result of BESS in implementing load leveling 7-16
7.4.4 Aggregated battery capacity comparison with individual design 7-19
7.4.5 Optimization at single building level 7-19
7.4.6 Building features and optimal sizing of BESS 7-21
7.4.7 Closing day 7-22
7.5 Future direction of battery sharing 7-24
7.6 Conclusions 7-25
Reference 7-26

CHAPTER 8: CONCLUSIONS AND PROSPECT

8.1 Conclusions 8-1
8.2 Prospect 8-3
8.2.1 Future direction of solar energy 8-3
8.2.2 Future direction of battery sharing 8-3

Chapter 1

RESEARCH BACKGROUND AND PURPOSE OF THE STUDY

RESEARCH BACKGROUND AND PURPOSE OF THE STUDY

1.1 Research background of energy resource 1-1

1.1.1 Current status of energy supply 1-1

1.1.2 Government policy 1-8

1.1.3 Climate change and weather stochastics 1-15

1.2 A new energy economy is emerging 1-19

1.3 Research structure and logical framework 1-22

1.3.1 Research purpose and core content 1-22

1.3.2 Chapter content overview and related instructions 1-24

References 1-27

1.1 Research background of energy resource

1.1.1 Current status of energy supply

The world's proven oil reserves were 1,729.7 billion barrels at the end of 2018, and divided by oil production in 2018, the number of years of producible reserves was 50.0 years. During the oil shocks of the 1970s, there were concerns that oil resources would be depleted, but improved recovery rates and new oil resource discoveries [1]. However, due to improvements in recovery rates and the discovery and confirmation of new oil resources, the recoverable life of oil has been maintained at around 40 years since the 1980s. In recent years, the recoverable life of oil has been increasing with the discovery of shale oil in the United States and reserves of extra-heavy oil in Venezuela and Canada [2].

At the end of 2018, Venezuela had the largest proven reserves in the world, while Saudi Arabia, long the number one, has been number two since 2010. Venezuela's proven reserves of 303.3 billion barrels represent a 17.5% share of the global total. Saudi Arabia has proven reserves of 297.7 billion barrels, a 17.2% share of the global total, followed by Canada (167.8 billion barrels, 9.7% share), Iran (155.6 billion barrels, 9.0% share), Iraq (147.2 billion barrels, 8.5% share), Russia (106.2 billion barrels, 6.1% share), and Kuwait (101.5 billion barrels, 5.9% share), and the United Arab Emirates (97.8 billion barrels, 5.7% share). The Middle Eastern countries alone account for about half of the world's total proven crude oil reserves.

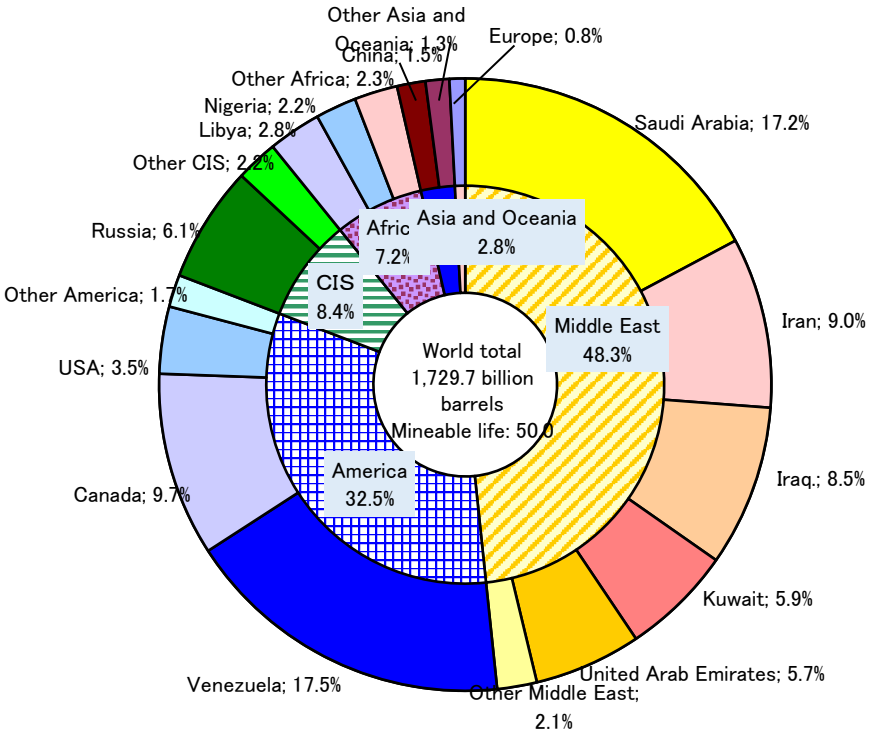

Fig.1-1 World Proved Reserves of Crude Oil (2019)

(Source: based on BP's Statistical Review of World Energy 2019 [2])

In recent years, shale oil (tight oil), which is produced using different production methods than conventional oil, has been attracting attention. The major shale oil producing countries are the United States, Russia, China, Argentina, and Libya. In 2013, the EIA released a shale oil and shale gas resource assessment map.

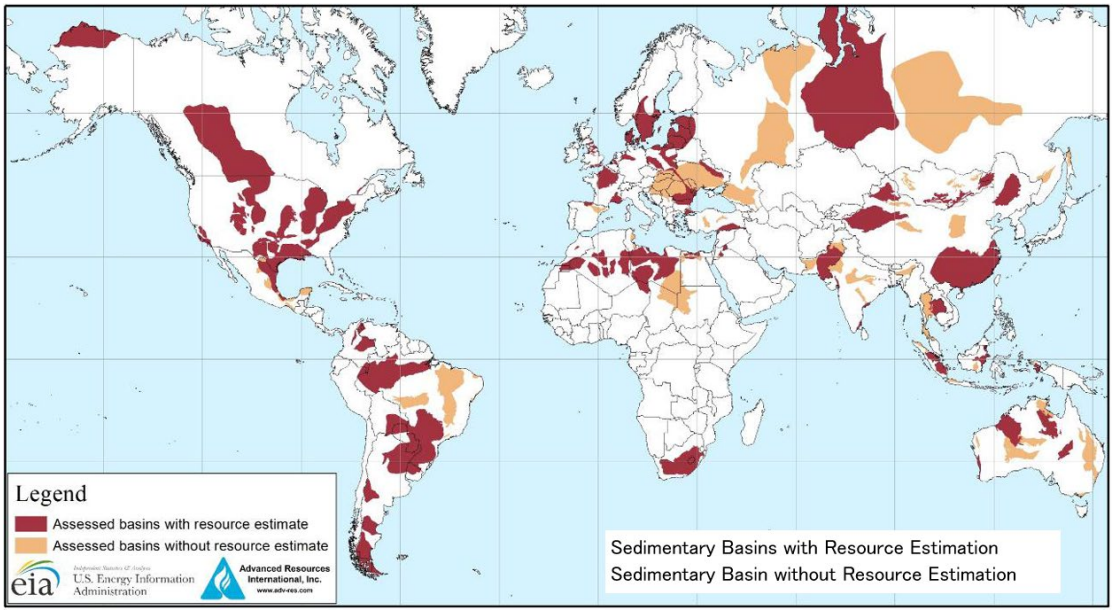

Fig.1-2 Map of basins with assessed shale oil and shale gas formations, as of May 2013

((Note) "Amount of extractable resources" represents the amount of petroleum resources that can be technically produced and represents a wider range of resources than "reserves" in that it does not strictly take into account economic efficiency and certainty of its existence. Source: Based on EIA, "Technically Recoverable Shale Oil and Shale Gas Resources," June 2013. [3])

World oil production has expanded along with the increase in oil consumption, from 58.55 million barrels per day in 1973 to 94.72 million barrels per day in 2018, an increase of about 1.6 times in less than 45 years. By region, production has been declining in Europe since 2000, while production in Asia Pacific and Africa and Latin America has remained mostly flat, and production in Russia, the Middle East, and North America has increased steadily.

After a large increase in production by OPEC oil-producing countries until the 1970s, production by OPEC oil-producing countries declined in the first half of the 1980s due to increased production by non-OPEC oil-producing countries on the back of high oil prices and sluggish world oil consumption but recovered in the second half of the 1980s. As a result, OPEC's share of world oil production declined from around 50% in the early 1970s to below 30% in the mid-1980s but rose again and has remained above 40% since 1993.

Production by non-OPEC oil-producing countries (former Soviet Union countries (CIS), the United States, Mexico, Canada, the United Kingdom, Norway, China, Malaysia, etc.) has generally increased steadily since 1965, reaching 55.38 million barrels per day in 2018, up from 17.85 million barrels per day in 1965. The breakdown of the increase varies by decade, with North America, the CIS, Asia Pacific, and Europe leading the increase in the 1970s and 1980s, Europe and Latin America in the 1990s, and the CIS in the 2000s. In recent years, the U.S.,

which has been rapidly increasing its production volume due to technological innovation in shale oil production (shale revolution), has been attracting particular attention.

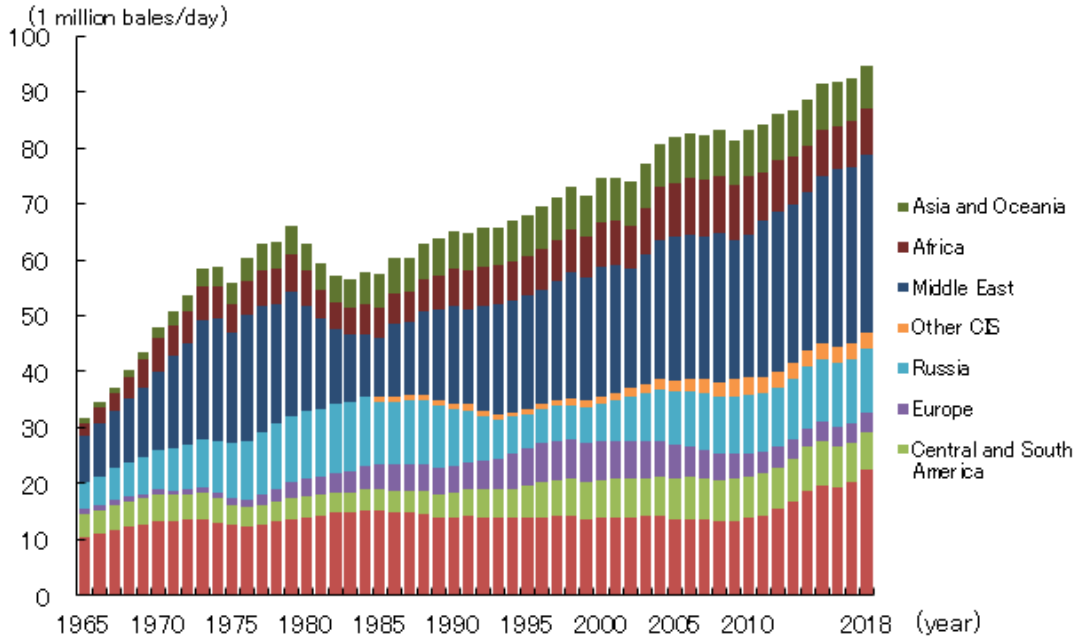

Fig.1-3 World Crude Oil Production Trends by Region

((Note: Russia through 1984 includes other former Soviet Union countries. Source: based on BP's Statistical Review of World Energy 2019 [4])

World oil consumption has followed an increasing trend with economic growth: from 55.66 million barrels per day in 1973, world oil consumption increased to 99.84 million barrels per day in 2018 (average annual growth rate of 1.6%) [2] [4].

Oil consumption in OECD countries declined from 41.28 million barrels per day in 1973 to the early 1980s due to the global economic downturn caused by two oil shocks as well as the shift to alternative energy sources such as nuclear power and natural gas. After 2015, the consumption of oil started to increase again due to the decline in oil prices and continued to increase even in 2018 when oil prices rose to 47.47 million barrels per day [5].

Consumption has increased significantly in non-OECD countries. Oil consumption in these countries increased from 14.38 million barrels per day in 1973 to 52.38 million barrels per day in 2018 (an average annual growth rate of 2.9%) due to robust economic growth. As a result, the share of non-OECD countries in world oil consumption rose from 26% in 1973 to 52% in 2018, while the share of OECD countries fell from 74% to 48% within the same period.

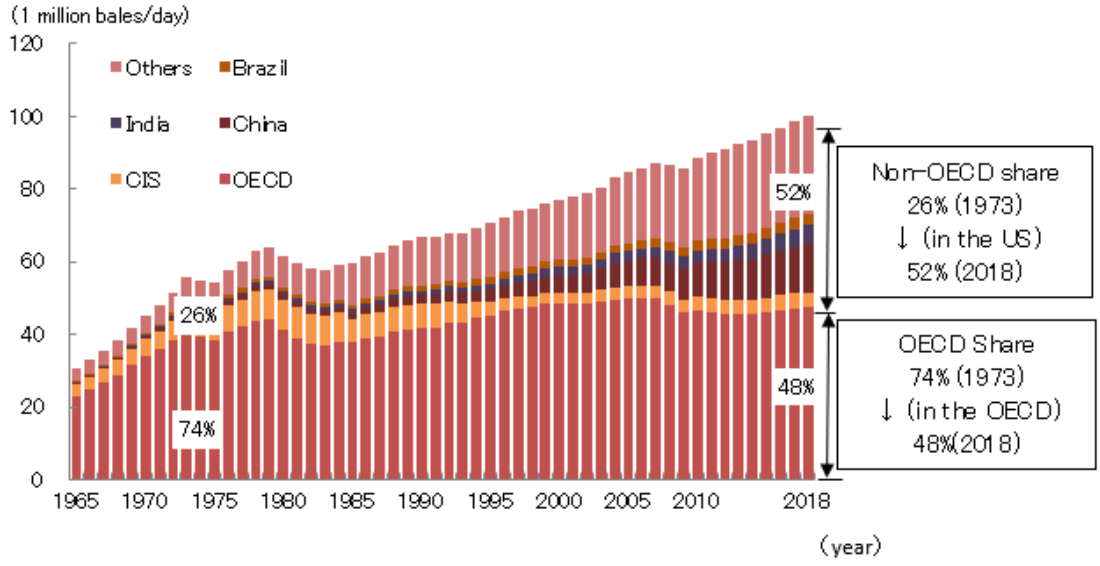

Fig.1-4 World Oil Consumption by Region

(Source: based on BP's Statistical Review of World Energy 2019 [4])

Energy is essential for our daily living and social activities. However, Japan is a country with a low energy self-sufficiency ratio, with a percentage of 12.1% in FY2019, a considerably low level compared with other OECD countries. It was 20.2% in FY2010 before the Great East Japan Earthquake. Thereafter, it decreased substantially due in large part to the shutdowns of nuclear power plants but started to increase gradually in recent years [6].

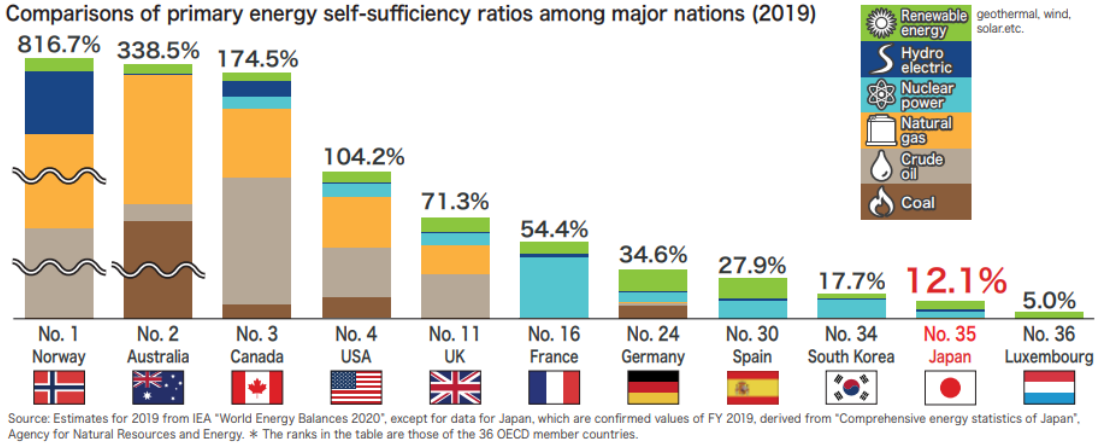

Fig.1-5 Comparisons of primary energy self-sufficiency ratios among major nations (2019) (Source: 2019 estimates from IEA "World Energy Balances 2020"; for Japan only, FY2019 firm data from the Agency for Natural Resources and Energy's Comprehensive Energy Statistics. Rankings in the table are out of 36 OECD countries. [7])

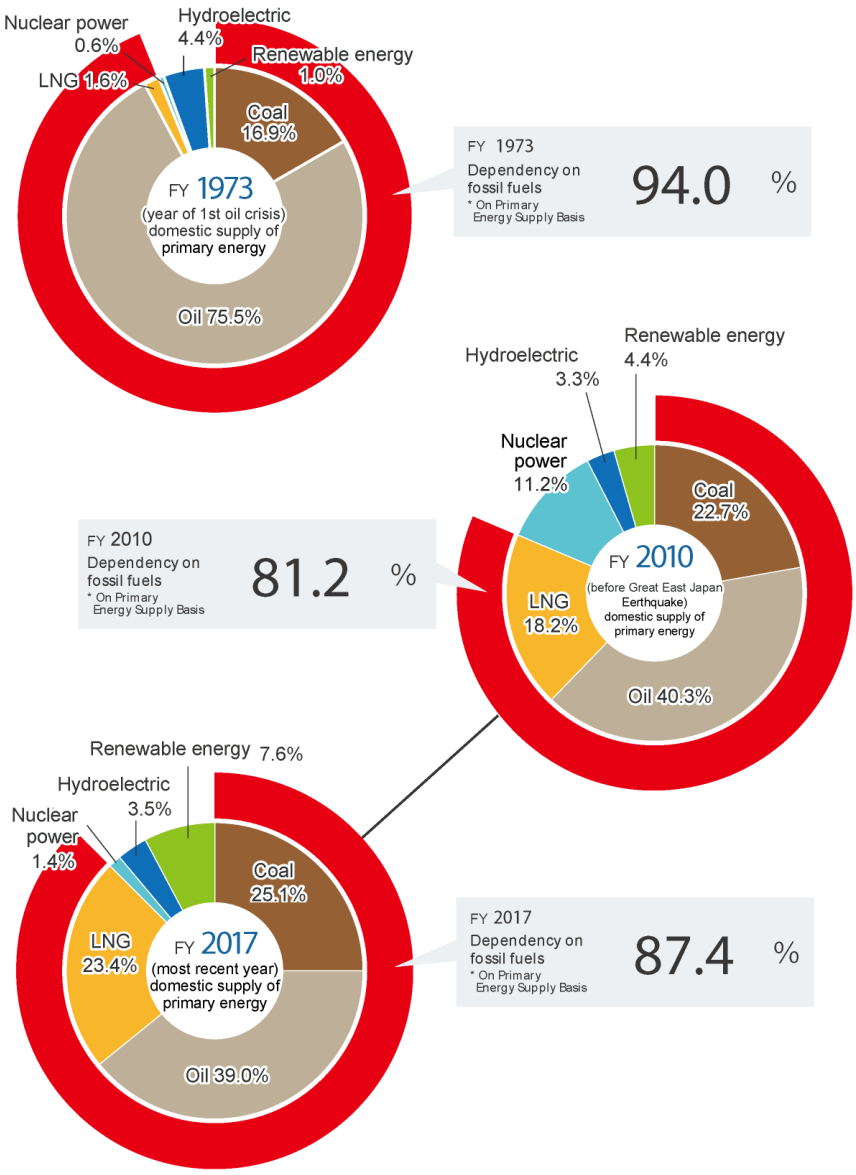

Fig.1-6 Trends in the composition of primary energy supply of Japan [8]

The major reason for this low self-sufficiency ratio is that energy resources are scarce in Japan. Japan depends largely on fossil fuels such as oil, coal and liquefied natural gas (LNG), most of which are imported from overseas. Having experienced oil crises in the 1970s, Japan reduced its dependency on fossil fuels to a certain extent. However, since the Great East Japan Earthquake in 2011, thermal power generation has increased with dependency on fossil fuels in FY2019 being 84.8%.

Many countries and regions have been working to expand the use of renewable energy in recent years. In addition to research and development, demonstration, and subsidies for the introduction of renewable energy, feed-in tariffs (FIT) and renewable energy portfolio standards (RPS), which are also in place in Japan, have been introduced to promote the introduction of renewable energy. RPS (Renewables Portfolio Standards), which are also in place in Japan. As of 2018, FITs have been introduced in 111 countries/regions and RPSs in 33 countries/regions. In recent years, many countries have introduced competitive bidding systems to determine the

purchase price.

These measures have led to a dramatic increase in investment in renewable energy since the mid-2000s, with over US$200 billion invested annually since 2010 (excluding large hydropower); in 2018, this figure was about US$288.9 billion, down about 11.5% from 2017. This is because China, which accounts for the majority of investments, implemented changes to its feed-in tariffs mid-year, resulting in a significant decrease in investment. On the other hand, investment in developed and developing countries increased. Investment in renewable energy is estimated to be about three times the amount invested in coal-fired and gas-fired power generation combined. By energy source, investments are almost consistently concentrated in solar energy and wind power.

① Solar power generation

The introduction of photovoltaic power generation worldwide has accelerated since the late 2000s, reaching a cumulative total of approximately 510 MW in 2018. The expansion of introduction was largely due to the FIT introduced in European countries around 2000, with Germany, Italy, Spain, and other countries showing remarkable growth due to the high purchase price set for solar power generation. The introduction of the FIT in Japan in July 2012 also led to a significant expansion of PV installation, with Japan (56.16 million kW) ranking third in the world in terms of cumulative installation in 2018, behind China (175.4 million kW) and the United States (62.5 million kW). The significant expansion of the photovoltaic power generation market has also led to a decline in the cost of installing power generation equipment, and in recent years, the introduction of this technology has spread to emerging countries as well. In particular, China surpassed Germany in 2015 to become the world's No. 1 country in terms of installed capacity.

The economic ripple effect of the increased introduction of solar power generation is expected to create jobs, etc. On the other hand, however, there are concerns about an increase in the cost burden because the purchase cost of FIT is ultimately passed on to consumers in the form of a levy. For example, in Germany, it has been announced that the FIT levy, which is added to electricity bills, will be 6.756-euro cents16 per kWh in 2020, which means that the monthly burden for a model consumer who uses 260 kWh of electricity per month will be approximately 17.3 euro 17 (approximately 2,100 yen). On the other hand, in Japan, the FIT levy for FY2020 is 2.98 yen/kWh, and the monthly burden for a consumer model with a monthly electricity consumption of 260 kWh is estimated to be 774 yen18.

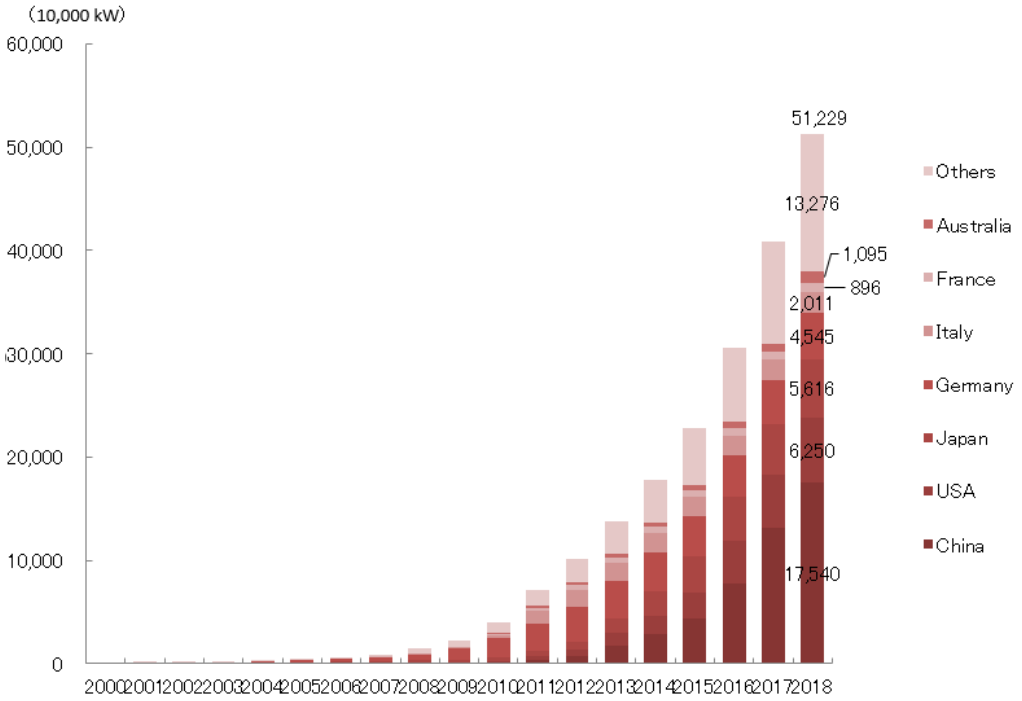

Fig.1-7 Global PV deployment (cumulative total installed base)
(Source: based on IEA "PVPS TRENDS 2019" [9])

② Wind power generation

Global wind power installed capacity has grown rapidly in recent years, reaching approximately 650 MW in 2019. The largest installed capacity is in China (23,640 MW), which accounts for about one-third of the world's total, followed by the United States (10,547 MW) and Germany (6,141 MW). These three countries therefore account for approximately 60% of the world's installed wind power capacity.

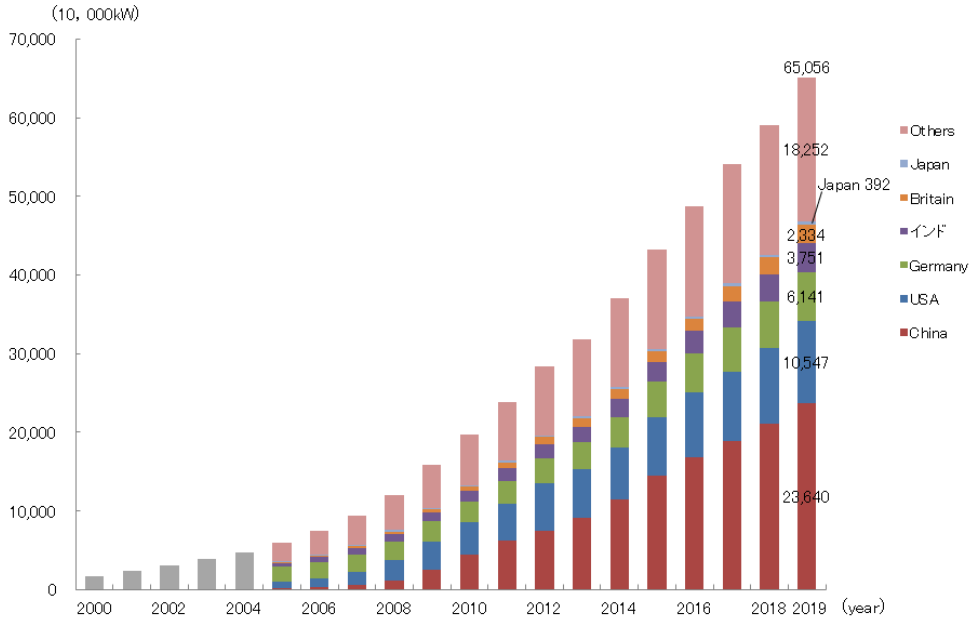

Fig.1-8 Global Wind power deployment (cumulative total installed base) [10]

(Source: Based on Global Wind Energy Council (GWEC) "Global Wind Report (each year) [7])

Globally, the cost of generating renewable energy is declining. Some renewable energy power generation has become cost competitive enough to compete with coal- and gas-fired power generation without subsidies. In Asia, the average cost of renewable energy generation is generally lower than in other regions, driven by China and India, which have favorable climates and cheap labor for solar and wind power. In Japan, however, the cost of generating renewable energy is high compared to thermal and nuclear power generation, and this is one of the challenges for making renewable energy a main source of power.

Such cost reduction has been supported mainly by policies promoting renewable energy and by technological innovation. Daily advances in technology have reduced manufacturing costs and improved maintenance and management efficiency, and economies of scale have been a factor. In addition, the bidding system introduced in many countries, whereby purchase prices are determined, has encouraged competition and led to lower power generation costs.

The average cost of solar PV and onshore wind power has been declining significantly, with the average cost of solar PV that started operation in 2018 being $0.09/kWh, down about 77% from $0.37/kWh in 2010. This is believed to have lowered the cost of electricity generation. Onshore wind has likewise seen a decline in average generation costs as turbine prices have fallen, from $0.08/kWh in 2010 to $0.06/kWh in 2018. Solar thermal has not been technically established and has limited installed capacity, so the cost of generating electricity has remained higher than solar and wind, but with new projects starting in China, Morocco, and South Africa in 2018, the average cost of generating electricity in 2018, compared to 2010, has and decreased by 46%.

1.1.2 Government policy

Indeed, renewable energy will reshape the geopolitical landscape. A country's relative position in the international system is influenced by a range of factors, including its gross domestic product (GDP), population, land area, natural resources, geostrategic location, military resources and "soft power. Having control of and access to important energy resources and markets is an important asset because it protects national interests and leverages foreign economic and political influence. Over the past two centuries, the development of fossil energy has increased global energy use 50-fold, shaping the geopolitical landscape of the modern world. IREAN assesses the influence of selected countries and groups based on the share of national oil, gas and coal imports in total primary energy consumption, and the cumulative number of renewable energy technology patents. The assessment finds that the United States is close to energy self-sufficiency and is well positioned to compete for clean energy; China is leading innovation and deployment of manufacturing and renewable energy technologies. Resources. Harmonizing Ecological Protection and Mineral Resource Development China's Natural Resource Economics 25 would benefit from an energy transition in terms of energy security; the EU and Japan also hold significant positions in renewable energy technologies, with Germany in particular holding nearly 31,000 renewable energy patents, making it a leader in renewable energy deployment; Russia is the world's largest exporter of natural gas and the second largest exporter of oil that may face challenges in adapting to growing renewable energy sources [11]. On this basis, IREAN calculated the share of net fossil energy imports and exports

in GDP for each region and analyzed the impact of the energy transition on the region; calculated the share of fossil energy rents in GDP and analyzed the share of fossil energy exporters. Vulnerability: The analysis of countries' dependence on fossil energy rents and economic resilience argues that renewable energy has become central to the global energy landscape in the context of the energy transition. Renewable energy sources exist in a different form than fossil energy sources that are concentrated in specific geographic locations. Most renewables are energy streams that do not run themselves out and are more difficult to disrupt. Renewable energy can be deployed at almost any scale and is better used in decentralized forms of energy production and consumption, increasing the democratizing effect of renewable energy; the marginal cost of renewable energy is almost zero, as in the case of solar and wind. Doubling production capacity would reduce costs by nearly 20%. Thus, the rapid growth of renewable energy makes it possible for countries that can use new renewable energy technologies to increase their global reach. Among them, countries with high-tech potential for renewable energy generation have abundant mineral resources that could become necessary for renewable energy technologies. All three categories of countries, including those leading technological innovation, have the potential to become new leaders in renewable energy, take the initiative in the energy transition, and reshape the geopolitical landscape of the 21st century.

Therefore, the United States, Germany, Japan and China were selected as the typical countries for renewable energy policy research. On the one hand, these four countries have an important influence on the world economic and technological development due to their economic aggregates ranking among the top in the world. On the other hand, these four countries have led the development of renewable energy in different periods. We analyze the evolution of renewable energy institutional arrangements, clarify the characteristics and background of renewable energy policies, explore the ideological basis and changing trends of renewable energy policy formulation in these countries, and provide references for the rapid development of renewable energy.

① The United State

The promotion of renewable energy is a major policy in the United States. Its overall policy framework is characterized by a combination of bottom-up state policies and top-down federal policies. State policies primarily use market mechanisms to promote renewable energy. In 1983, Iowa pioneered the implementation of a Renewable Portfolio Standard (RPS). As of 2015, 34 states have implemented the RPS. this policy, implemented with market mechanisms, has provided the conditions for the subsequent development of renewable energy in the U.S. It provides a solid foundation for the development of the company. The federal policy system is mainly centered on fiscal policy, which can effectively reduce project costs, promote technological progress and accelerate industrialization. The main policy measures of the federal fiscal policy include the following aspects. First, long-term tax incentives based on the Investment Tax Credit (ITC) and the Production Tax Credit (PTC). Second, the implementation of priority planning and strong financial support to enhance technology development and project promotion. Finally, in 2013, the U.S. proposed a government green procurement system. The share of renewable energy electricity consumption in government agencies' electricity consumption gradually increased from 7% in 2013 to 10% in 2015, and will reach more than 20% in 2020.

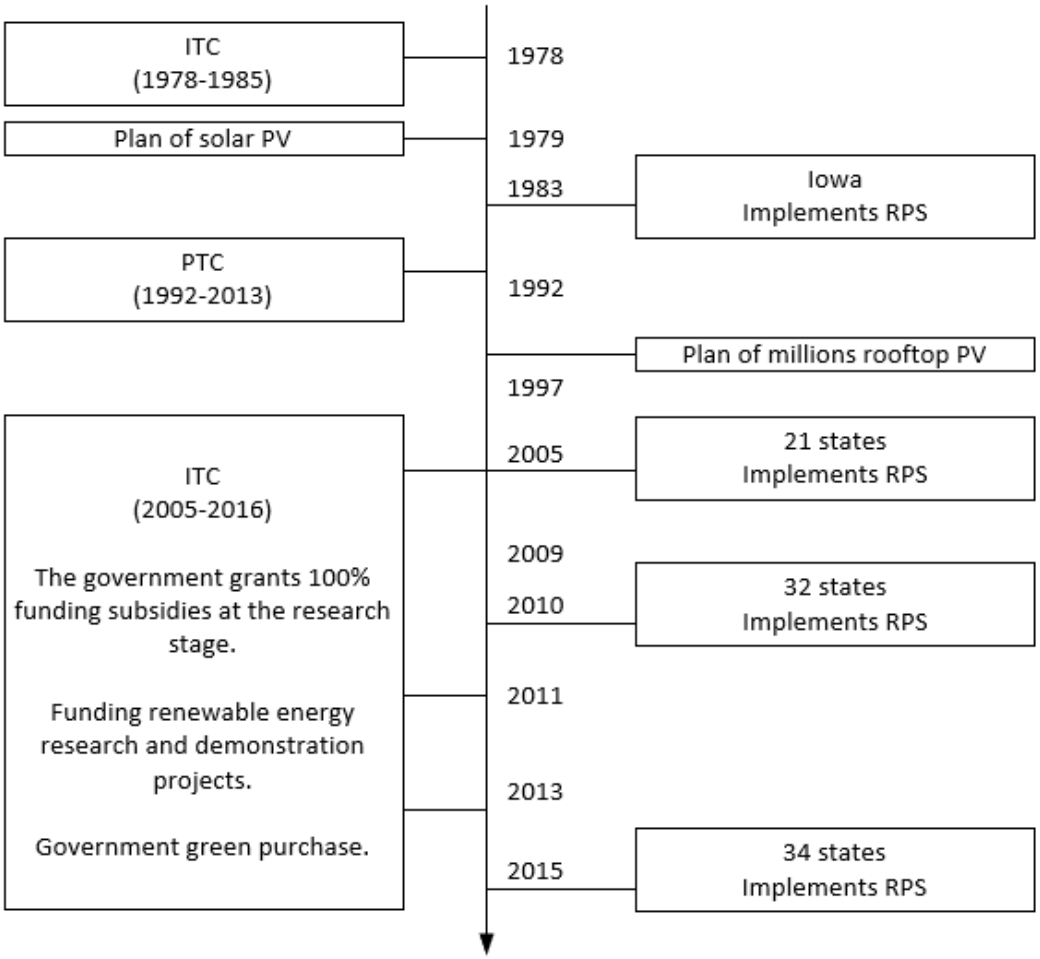

Fig.1-9 The Historical Evolution of U.S. Implementation of Renewable Energy Policy

② China

China's renewable energy policy focuses on planning projects to promote renewable energy start-up first; second, the use of fiscal and tax price policies to ensure the rapid development of renewable energy. Now the policy has begun to shift to a market-based policy system based on quota system. For multi-body, multi-level quota system, quota system is internationally recognized as an effective measure to promote the development of renewable energy. The share of renewable energy growth is allocated from the installed capacity of renewable energy, power generation and regions. And on this basis, combined with the green certificate trading mechanism launched by the Energy Bureau to provide solutions for market based.

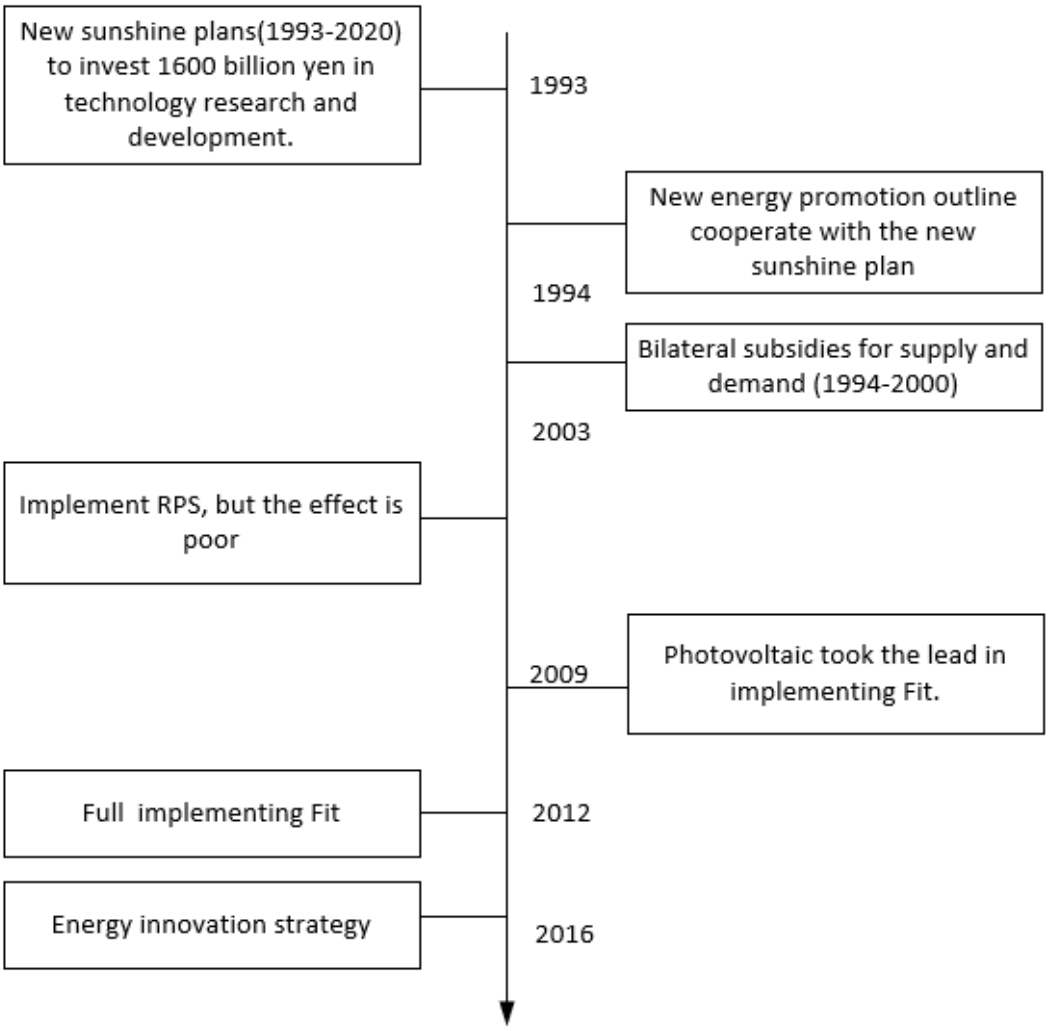

Fig.1-10 The Historical Evolution of Chinese Implementation of Renewable Energy Policy

③ Germany

German renewable energy policy system is divided into four typical parts, gradually from the government-led fiscal support policy to the market-oriented policy system transition is very clear. The first is to enhance the installed renewable energy base capacity with key projects. Install rooftop PV for every household. The second is to carry out ecological tax reform to enhance the competitiveness of renewable energy. This is reflected in tax incentives for wind, solar and geothermal energy generation. Then promote a feed-in tariff subsidy system (FiT) to set solid tariffs in the form of loyalty degrees. However, as the scale of renewables increases and government subsidies increase, the additional cost of renewables in the final tariff increases. To address the distortions in the electricity market and the rapid increase in end-use electricity prices, Germany reformed the Renewable Energy Act in 2014 and introduced a feed-in tariff subsidy policy (FIP). The shift to renewable energy generation was encouraged to participate in the feed-in tariffs in the electricity market. The sales price is determined by the prevailing market supply and demand. The government then provides premium subsidies to power generators based on the average of the stipulated tariff levels for various renewable energy sources and the monthly market price to promote the promotion of renewable energy. Energy

generation market competitiveness. New renewable energy generation must enter the electricity market like conventional power sources and assume the obligation of power system balancing.

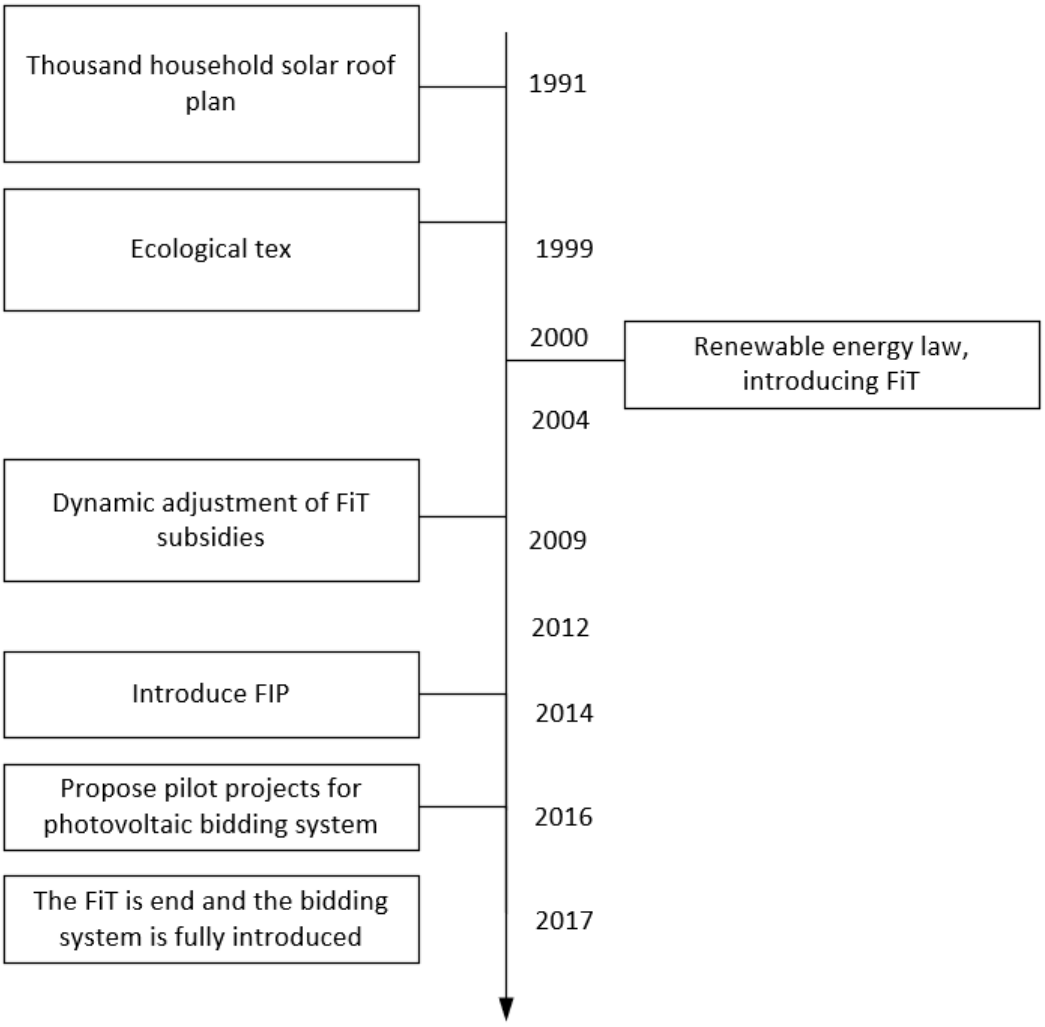

Fig.1-11 The Historical Evolution of German Implementation of Renewable Energy Policy

④ Japan

One of Japan's most effective practices for distributing renewable energy has been the Feed-In Tariff (FIT) scheme introduced in July 2012 by the Ministry of Economy, Trade, and Industry (METI) under the Act on Special Measures Concerning the Procurement of Renewable Energy by Operators of Electric Utilities. The new FIT scheme made it mandatory for power companies to buy electricity generated by certified power generating renewable sources, including solar, wind, hydro, geothermal, and biomass at fixed prices set by the government for a given period, so that the prospect of stable revenue would facilitate investment in renewable power generation.

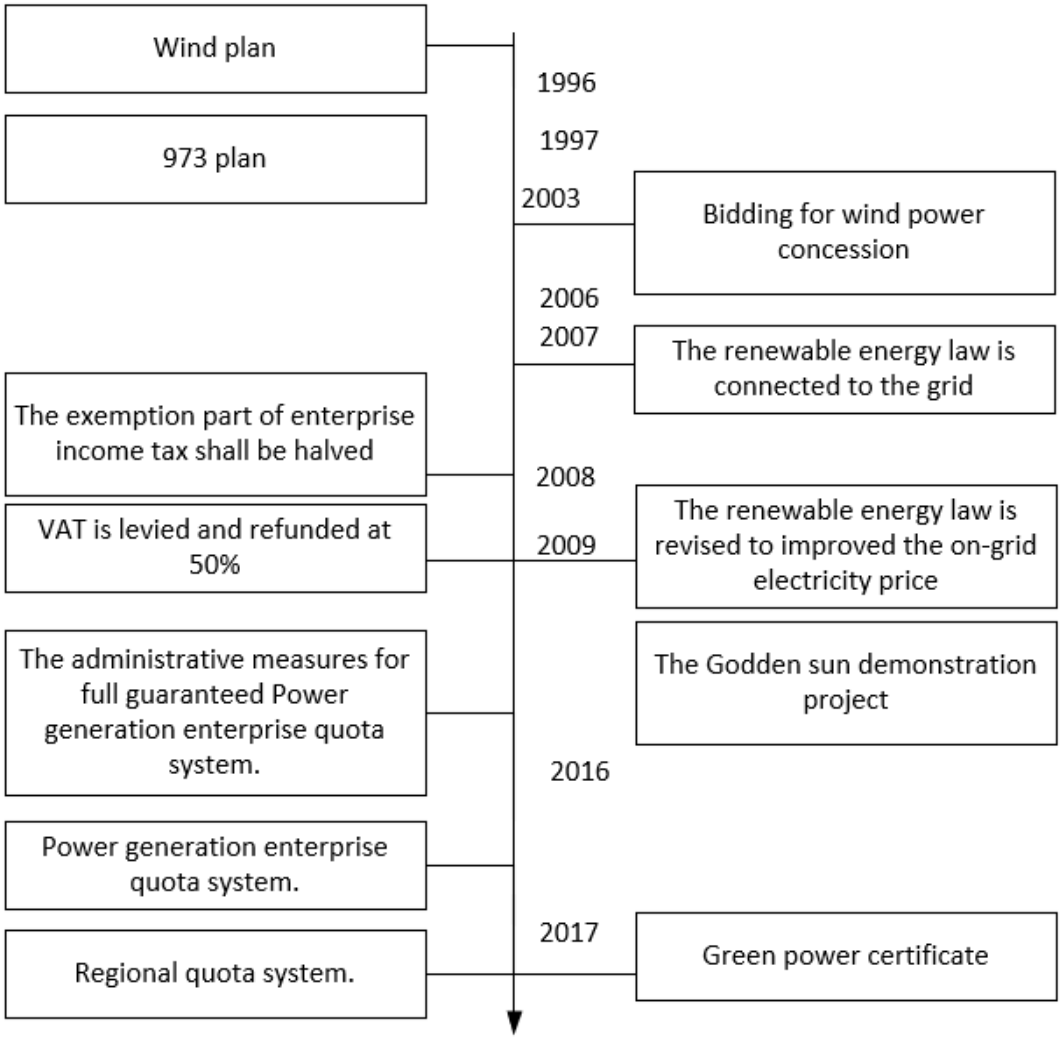

Fig.1-12 The Historical Evolution of Japanese Implementation of Renewable Energy Policy

The system has indeed sharply boosted the introduction of solar power, whose facilities can be built relatively easily and quickly. Prior to 2012, the accumulated Japanese solar PV capacity had amounted to just 5.6 GW, of which 84% was for residential purposes[12]. Solar power output during the peak-demand period in summer 2014 reached 6.33 million kilowatts—the equivalent of six nuclear reactors. By the end of April 2014, 9.77 gigawatts of renewable energy capacity had been installed and started operation, a much faster pace than in the previous ten years. The new FIT scheme further altered the dynamic of residential vs nonresidential use. For example, by the end of 2017, nonresidential use accounted for about 75% of the total shipments PV modules until the end of the FY 2017, and about 79% of the total capacity installed in 2017.

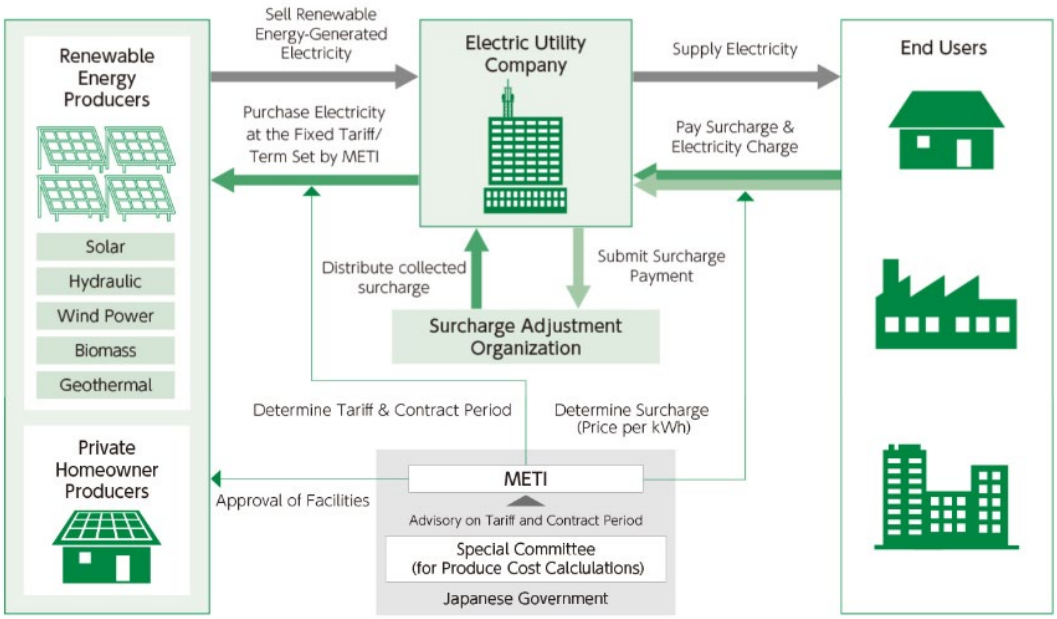

Fig.1-13 Basic mechanism of the Feed-In Tariff system [13]

By that time, the newly installed generation capacity from renewables certified by the FIT scheme had exceeded 72 million kilowatts, but approximately 96% of that capacity was from solar power. To further scale-up the proliferation of renewable energy under the FIT scheme, the government can seek to harness the potential of other kinds of renewable energy. Today, this FIT scheme has enabled Japan to be on track of reaching its target of renewable power capacity accounting for 22% to 24% of the total power mix installed by 2030 as long as half the already-approved projects under the FIT scheme will be built [12].

The new FIT scheme was intended as a temporary system to encourage the transition to renewable energy, and a revision is expected to be introduced by March 31st, 2021. It must target the limits identified above. A FIT system is highly recommended for use in other countries as it holds great potential for diversifying the participation of different sectors into renewable energy, including local governments, businesses, and citizens [13].

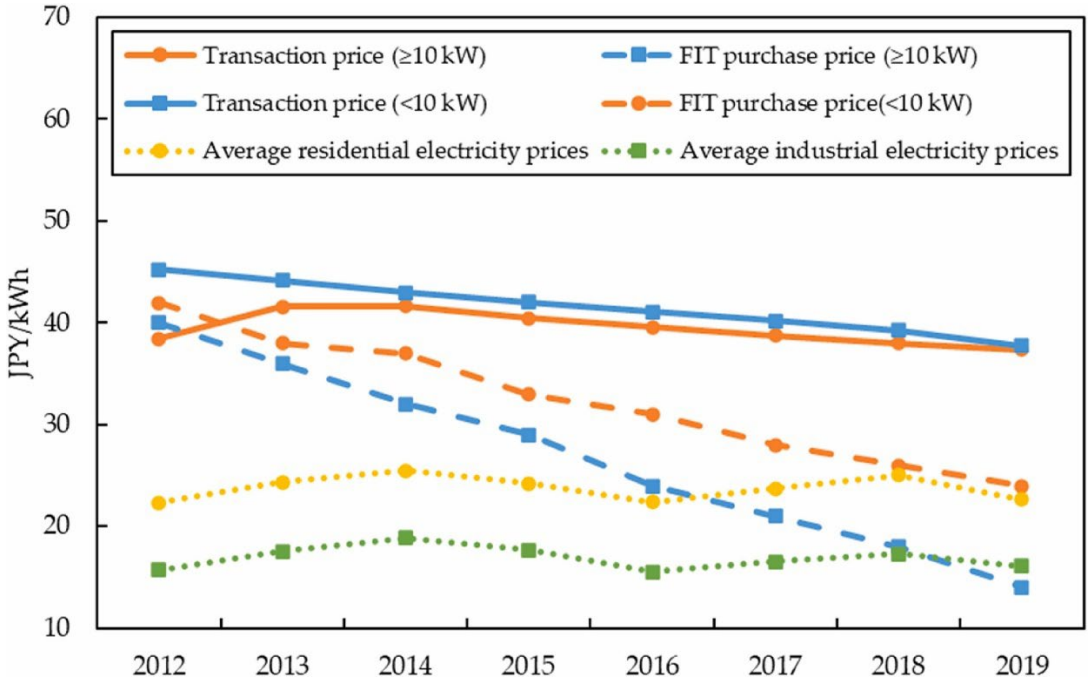

Fig.1-14 Trends in average electricity prices, the PV transaction price, and the FIT fixed purchase price in the residential and non-residential sectors from 2012 to 2019. (Data source: METI Statistics).

1.1.3 Climate change and weather stochastics

① Greenhouse gas emissions

About half of the carbon dioxide (CO2) emitted by human activity today remains in the atmosphere. The rest is absorbed by the oceans and terrestrial ecosystems. The fraction of emissions remaining in the atmosphere, called the airborne fraction (AF), is an important indicator of the balance between sources and sinks. The AF varies considerably from year to year, with relatively uncertain annual averages varying between 0.2 (20%) and 0.8 (80%) over the last 60 years. However, statistical analysis shows that over the long term (~60 years), the average AF is 0.42, with no clear trend (see Figure 1). This means that only 42% of human CO2 emissions remain in the atmosphere. CO2 sinks on land and in the oceans continue to increase proportionally with increasing emissions. Because the absorption process is sensitive to climate and land use changes, it is uncertain how AF will change in the future [14].

Changes in AF will have strong implications for achieving the Paris Agreement goal of limiting global warming to well below 2°C and will require adjustments in the timing and/or scale of emission reduction commitments [15]. Ongoing climate change and related feedbacks, such as more frequent droughts and associated increases in the incidence and intensity of wildfires, may reduce the uptake of CO2 by terrestrial ecosystems. Oceanic uptake may also be reduced due to increased sea surface temperatures, decreased pH due to CO2 uptake, and slower meridional overturning circulation due to increased sea ice melting. Timely and accurate information on adaptive changes is essential to detect changes in the unsourced/sink balance.

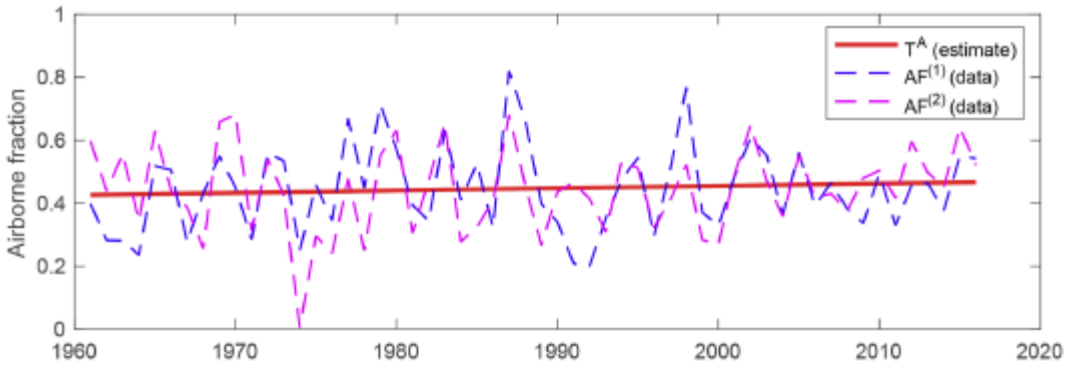

Fig.1-15 Fitted estimate of the linear trend in AF (TA) over the period 1960–2016 (Data source: METI Statistics).

Carbon dioxide is the most important anthropogenic greenhouse gas in the atmosphere, accounting for about 66% of the radiative forcing of inland greenhouse gases. It represents about 82% of the increase in radiative forcing over the last decade and about 82% of the increase over the last five years. The pre-industrial level of 278 ppm represents the flux balance between the atmosphere, oceans, and terrestrial biosphere. the global average molar fraction of CO2 in 2020 is 413.2 ± 0.2 ppm. the increase in the annual average from 2019 to 2020 (2.5 ppm) is slightly lower than the increase from 2018 to 2019, but slightly higher than the average growth rate over the past decade (2.40 ppm yr^{-1}), despite a decrease in fossil fuel CO2 emissions of about 5.6% in 2020 due to constraints associated with the COVID-19 pandemic [16]. Note that the 2019 global surface CO2 average reported in the 16th GHG Bulletin is adjusted from 410.5 ppm to 410.7 ppm due to the upgrade of all reported values to the new CO2 X2019 calibration scale.

In 2020, atmospheric CO2 reaches 149% of pre-industrial levels, mainly due to emissions from fossil fuel combustion and cement production. According to the International Energy Agency, CO2 emissions from fossil fuels reach 31.5 GtCO2 in 2020 (5), down from 33.4 GtCO2 in 2019 [14]. According to the Global Carbon Project 2020 analysis, deforestation and other land use changes contribute 5.7 GtCO2 yr-1 (average of 2010-2019). Of the total anthropogenic emissions for the period 2010-2019, about 46% accumulate in the atmosphere, 23% in the ocean, and 31% on land, with an unattributed budget imbalance of 0.4% [15]. The fraction of CO2 emitted from fossil fuel combustion that remains in the atmosphere (the fraction in the air) varies from year to year, due to the large natural variability of CO2 sinks and the absence of a confirmed global trend [17].

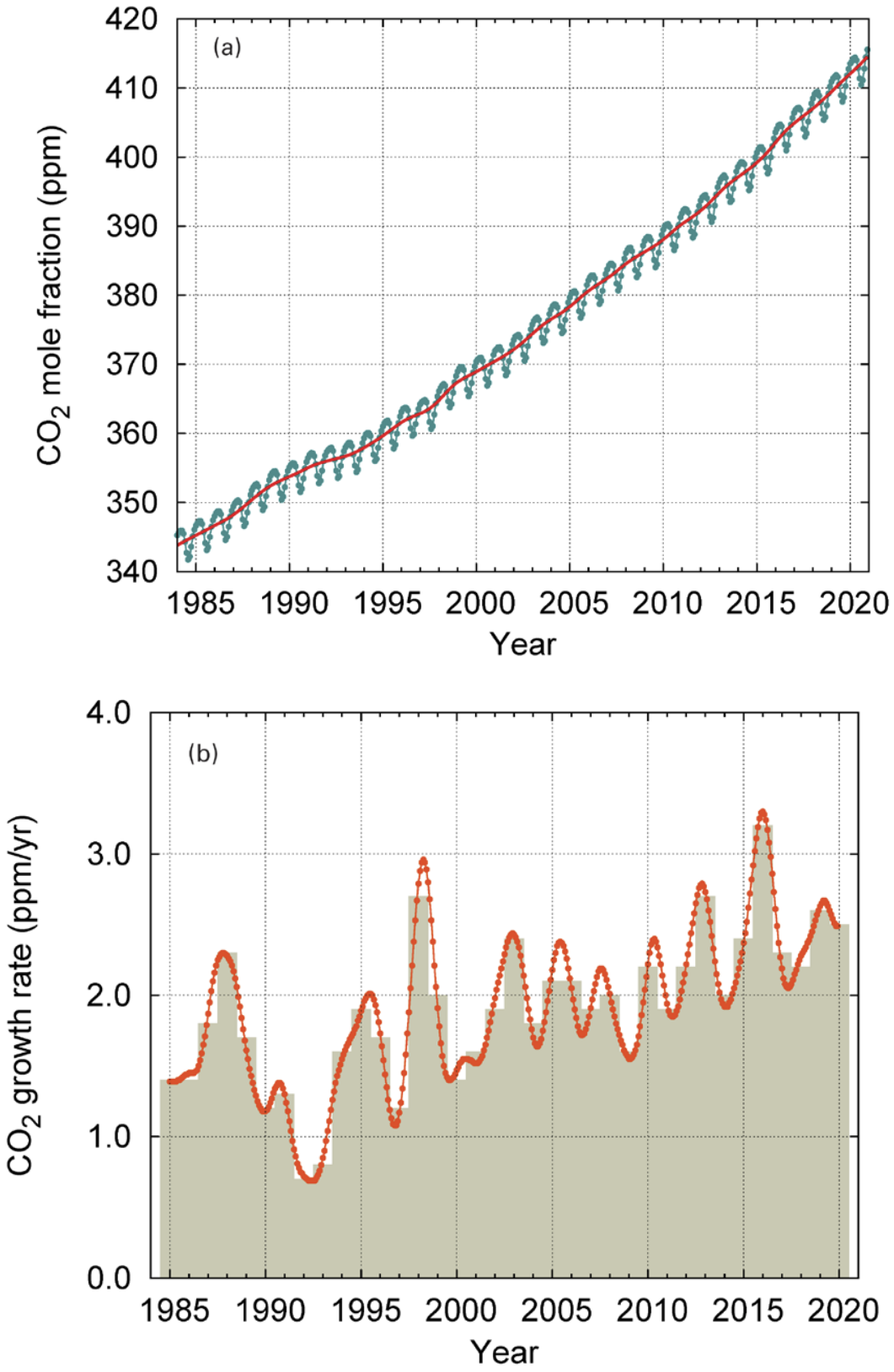

Fig.1-16 Globally averaged CO2 mole fraction (a) and its growth rate (b) from 1984 to 2020. Increases in successive annual means are shown as shaded columns in (b). The red line in (a) is the monthly mean with the seasonal variation removed; the blue dots and blue line in (a) depict the monthly averages. Observations from 139 stations were used for this analysis.

② Climate change

Figure 2.1-1 shows the distribution of the difference in mean temperature between present climate 1 and future climate 2 by year and season according to the regional climate model.

The figure shows the regional mean temperature values (Table 1.3-1) by semi-season for one year for the present and future climates based on the regional climate model.

The figure shows the semi-annual values of regional mean temperatures for the present and future climate by region (Table 1.3-1) for one year according to the regional climate model. Annual mean temperatures increase significantly across the country, with a 4.5°C increase in the national average. By region, the temperature increases by 4.5°C on the

4.8°C on the Sea of Japan side of northern Japan, 4.9°C on the Pacific side of northern Japan, 4.5°C on the Sea of Japan side of eastern Japan, 4.3°C on the Pacific side of eastern Japan, and 4.5°C on the Pacific side of western Japan. The increase is larger at higher latitudes, such as 4.1°C on the Sea of Japan side of western Japan, 4.1°C on the Pacific side of western Japan, and 3.3°C in Okinawa/Amami. The increase is larger in higher latitudes (Figs. 2.1-1 and 2.1-2). This is the case, for example, for Tokyo, which belongs to the Pacific side of eastern Japan. The current (1981-2010 average) annual mean temperature is 15.4°C, which means that the temperature will increase by 4.3°C by the end of the 21st century, which is the same as the present annual mean temperature in Yakushima. This corresponds to an increase of 4.3°C by the end of the 21st century, which is close to the current value of 19.4°C on Yakushima Island (the average of 1981 - 2010 observations)3 .

This trend is common among all members and is the same as the results of the analysis in Murata et al. (2015). Although the average annual mean temperature rises by 4.9°C on the Pacific side of northern Japan, where the increase in annual mean temperature is the largest, it varies from year to year, with years in the range of 4.2 to 5.6°C more likely to appear higher than the present4 (hereafter denoted as 4.9 ± 0.7°C). Similarly, the RCPs for the Sea of Japan in northern Japan, the Sea of Japan in eastern Japan, the Pacific Ocean in eastern Japan, and Okinawa/Amami in western Japan increase by 4.8±0.7°C, 4.5±0.6°C, 4.3±0.6°C, 4.1±0.5°C, and 3.3±0.4°C, respectively. According to the projection results under the RCP8.5 scenario in AR5 (i.e., the change in the 2081 - 2100 average with respect to the 1986 - 2005 average), the global average is estimated to increase by 3.3 ± 0.4°C over the period from 2081 to 2100.

The annual average temperature increase for the world as a whole is about 3.7°C, and the temperature increase near Japan is larger than the global average, according to the results of the projection under the RCP8.5 scenario in AR5 (change in the average of 2081-2100 relative to the average of 1986-2005). This is because the temperature increase tends to be larger at higher latitudes due to the melting of sea ice and snow cover as temperatures rise, which makes it easier to absorb solar radiation, and this tendency is manifested in the Japanese archipelago, which is located at a relatively high latitude.

The seasonal mean temperatures also show the same trend as the annual mean temperatures, but the increase is larger at higher latitudes in each season, and the increase is larger in winter than in summer, when the melting of sea ice and snow cover has a greater impact. In particular, large increases are seen in winter and spring in some parts of Hokkaido, reflecting the decrease

in sea ice in the Sea of Okhotsk.

In annual and seasonal mean temperatures, the average increase is larger than the range of inter-annual variability in the present climate, meaning that in the future, temperatures will be averaged in such a way that they rarely appear as that season in the present climate.

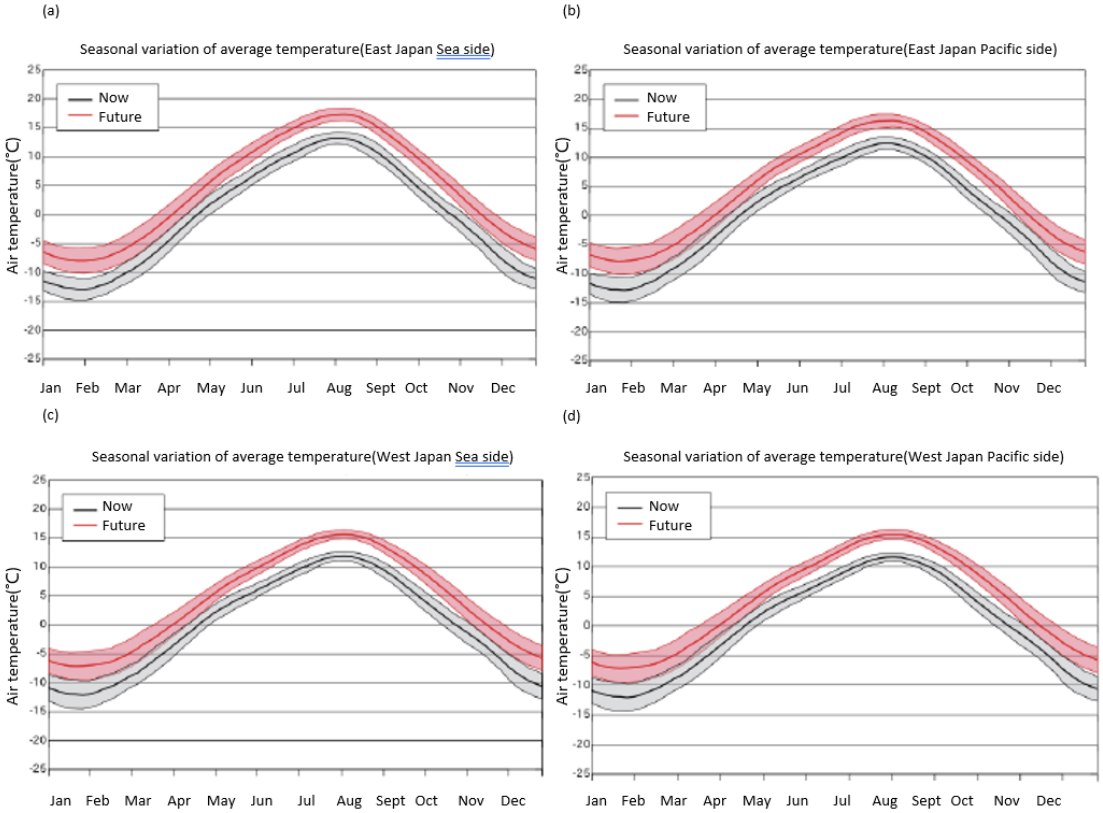

Fig.1-17 Seasonal progression of average temperature by region (unit: °C)

1.2 A new energy economy is emerging

In October 2020, the new Prime Minister of Japan declared that by 2050 Japan will aim to reduce greenhouse gas emissions to net-zero and to realize a carbon-neutral, decarbonized society. This declaration is a defining moment for Japan's future energy and climate policies, and the government is developing additional policies and measures to achieve this target. In November 2020, a bipartisan group of lawmakers declared a climate emergency in a symbolic vote to support the earlier announcement by the Prime Minster. This IEA in-depth review comes timely, as it makes numerous recommendations that can be helpful in developing policies and measures to support achieving the new goal [18] [19].

Over the last decade, Japan made substantial progress in implementing its vision of an efficient, resilient and sustainable energy system. The gradual restart of nuclear power generation, expansion of renewable energy and energy efficiency gains have reduced the need for imported fossil fuels and contributed to a continuous decline in greenhouse gas (GHG) emissions. These reached an historic peak in 2013, as fossil fuels filled the gap caused by the temporary shutdown of all nuclear power plants after the Fukushima accident. In 2018, GHG emissions had decreased by 12% compared to 2013, back to same level they had in 2009 [19].

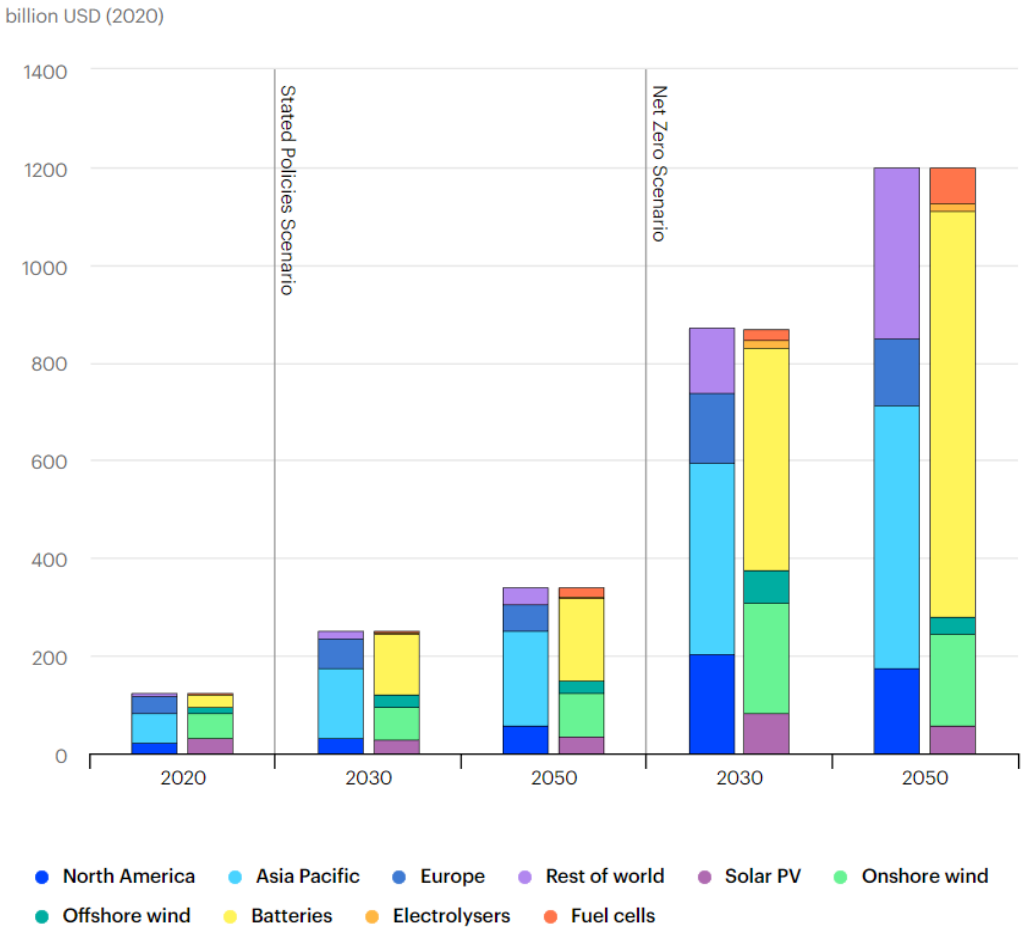

Fig.1-18 Estimated market sizes for selected clean energy technologies by technology and region, 2020-2050

Grid-scale storage plays an important role in the Net Zero Emissions by 2050 Scenario, providing important system services that range from short-term balancing and operating reserves, ancillary services for grid stability and deferment of investment in new transmission and distribution lines, to long-term energy storage and restoring grid operations following a blackout [20].

The rapid scaling up of energy storage systems are critical to address the hour-to-hour variability of wind and solar PV electricity generation on the grid, especially as their share of generation increases rapidly in the Net Zero Scenario [21]. Meeting rising flexibility needs while decarbonizing electricity generation is a central challenge for the power sector, so all sources of flexibility need to be tapped, including grid reinforcements, demand-side response, grid-scale batteries and pumped-storage hydropower.

Grid-scale battery storage grows significantly. In the Net Zero Scenario, installed grid-scale battery storage capacity expands 44-fold between 2021 and 2030 to 680 GW. Nearly 140 GW of capacity is added in 2030 alone, up from 6 GW in 2021. To get on track with the Net Zero Scenario, annual additions must pick up significantly, to an average of over 80 GW per year over the 2022-2030 period.

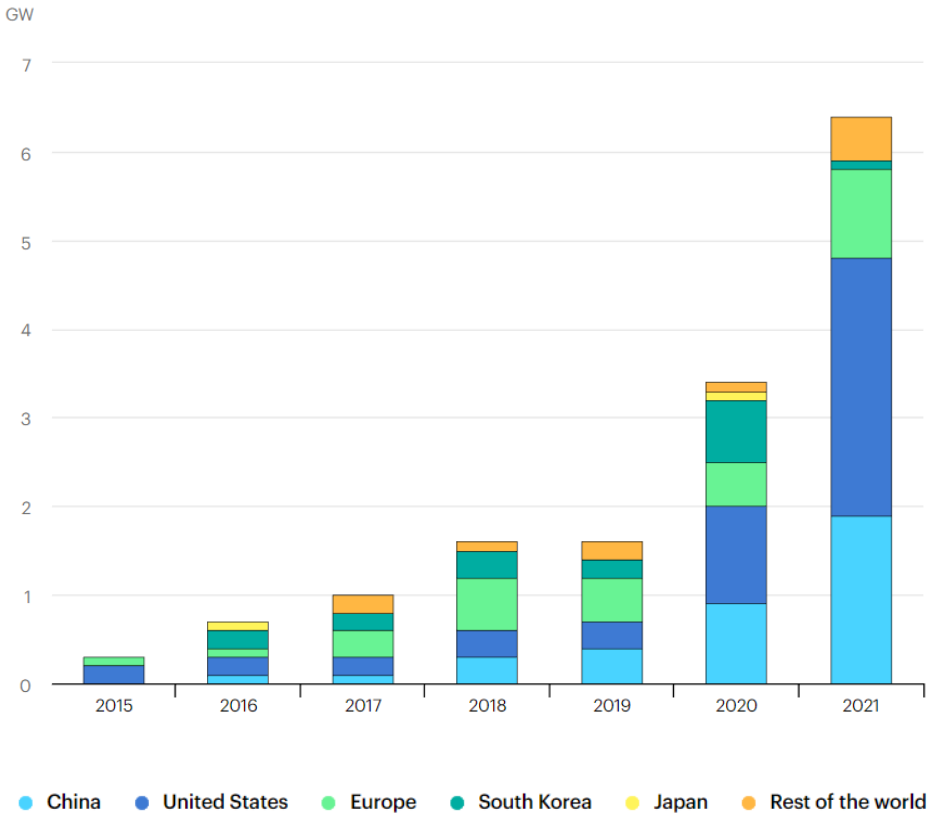

Fig.1-19 Annual grid-scale battery storage additions, 2016-2021

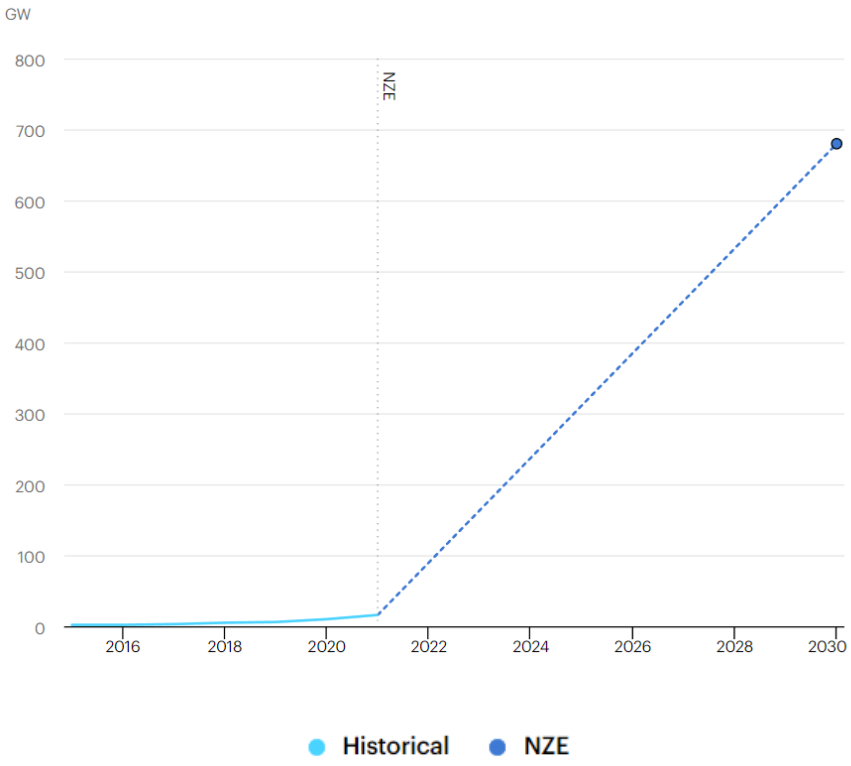

Fig.1-20 Installed grid-scale battery storage capacity in the Net Zero Scenario, 2015-2030

1.3 Research structure and logical framework

1.3.1 Research purpose and core content

In the background of safe energy use and the reduced of energy self-sufficiency, the development of renewable energy is imperative. At present, the proportion of the world's dependence on fossil energy still exceeds 50% of the total energy consumption, and it is also a general trend to strengthen the conversion of the power sector. Therefore, the power sector is responsible for energy conservation, emission reduction and energy supply.

At the same time, there is a growing demand for high-precision solar power forecasts to maintain a high degree of accuracy and credibility under complex weather conditions, especially with the frequent occurrence of extreme weather today. At the same time, the energy system is able to maintain stable operation.

Therefore, the main contributions of this work are as follows:

① Low-cost meteorological parameters (relative humidity, precipitation, weather, etc.) are used to construct a highly accurate hourly solar radiation model. Based on the classical layer-by-layer weakening solar radiation theory, a new weakening solar radiation model is proposed. The proposed model is established and calibrated under a variety of weather conditions to maintain more strong adaptability to cloudy and rainy days.

② Energy sharing and battery sharing are enabled to increase the self-consumption of renewable energy in the community, thereby eliminating the requirement for large-sized BESS and power feedback to the grid. The optimal number and position in the private battery sharing community are optimized by a constrained multivariate genetic algorithm. The BESS’s effect on system benefits through an aggregator is discussed, which can be the different application of demand response (DR).

③ we develop an energy sharing framework between the distribution network and the individual batteries for allocation of distributed ESS for community load leveling application. Representative load profiles (RLP) for non-residential buildings were extracted by clustering and feature analysis methods, and the optimal deployment of BESS in the RLP with sharing framework was discussed, and these results provide promising insights into battery sharing.

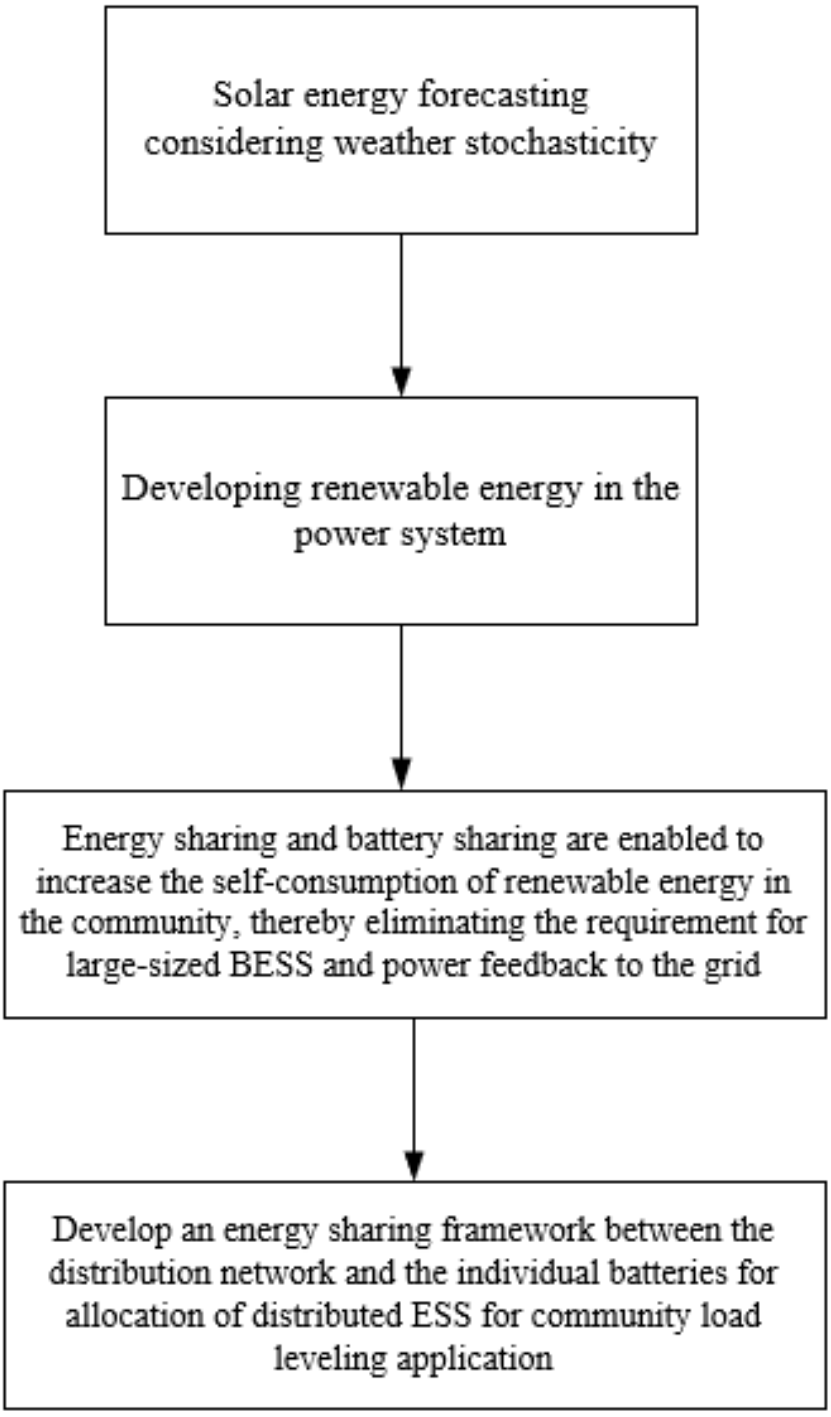

Fig.1-21 Research logic of this work

1.3.2 Chapter content overview and related instructions

The chapter names and basic structure of this paper are shown in Fig 1-26. Besides, the brief introduction of chapters schematic is shown in Fig 1-22.

In Chapter 1, Research Background and Purpose of the Study:

Given the shortage of energy and the need for secure supply, the development of renewable energy is imperative. This chapter analyzes the international energy situation, the bottlenecks and the historical evolution. In this way, the necessity of developing renewable energy can be derived. Secondly, it summarizes the international and Japanese regional renewable energy trends. The international level combines the evolution of the energy mix and renewable energy promotion strategies of typical countries such as the United States, Germany, Japan and China. The Japanese region details how renewable energy sources are penetrating into the grid. This demonstrates the importance of the power system in terms of stable energy supply and reduction of greenhouse gas emissions Finally, the background and chapter structure of the paper are presented for the reader's reference.

In Chapter 2, Literature Review of Renewable Energy System:

This chapter provides a detailed review of existing solar radiation models and the application of solar PV in the power grid. Section 2.1 reviews the commonly used solar radiation models and the calculation methods, and then summarizes the characteristics of the existing models and the application scenarios. Section 2.2 begins with a review of the performance of power generation systems combining renewable energy sources with energy storage devices and their applications in urban grids. Section 2.3 provides a detailed description and summary of the emerging types of sharing economies, reviewing the economic performance of energy sharing as well as the technical means. Overall, the review in this section focuses on the development of solar radiation models, the application of renewable energy in the grid, the metrics for assessing the impact of renewable energy on the grid, and the methodology.

In Chapter 3, Methodology:

This chapter describes the research methodology used in this paper. It includes methods for predicting global solar radiation based on general meteorological parameters, as well as the calculation methods and use of solar photovoltaic power. Section 3.1 shows the technical aspects of the grid impact of renewable energy penetration and the energy flow of the proposed energy sharing framework. the modeling of batteries and the optimization methods are documented in detail in section 3.2. Section 3.3 shows the economics metrics, where the dynamic payback period of PV is used. Compared to the static payback period, the dynamic payback period adds a time cost.

In Chapter 4, Data Resource and Energy Conversion Analysis:

The data resources and energy conversion analysis in this paper are presented in Chapter 4. The parameters of weather are obtained from historical data observed by the Japan Meteorological Agency. In this paper, the regional power grid of the Higashida Smart Community in Kyushu is selected to describe the generation composition and load profile.

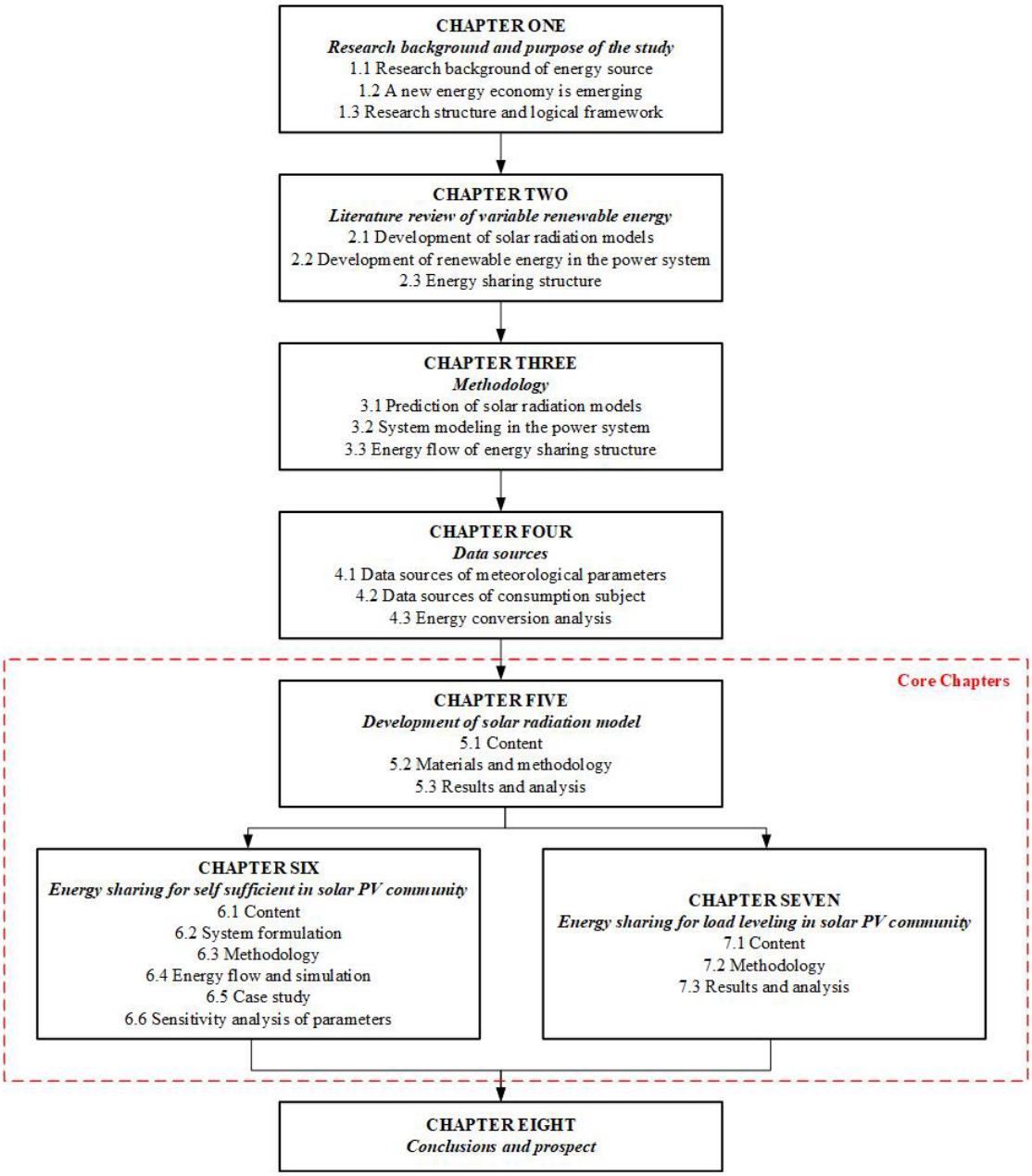

Fig.1-22 Brief chapter introduction

In Chapter 5, Development of a new solar radiation model:

As the population grows and urbanization accelerates, the energy crisis and environmental issues are becoming increasingly prominent. Solar energy is one of the most attractive renewable sources of electricity and heat, as it has the advantages of no pollution, wide distribution, and abundant reserves. For economic reasons, there are far fewer weather stations that observe hourly solar radiation than those that observe general meteorological parameters (e.g., temperature, relative humidity, wind speed, and sunshine duration). Accordingly, in an effort to overcome these difficulties, it is necessary to develop models for estimating solar radiation based on general meteorological parameters. In this chapter, a new hourly weakening solar radiation model was developed based on the layer-by-layer weakening theory. Over 200,000 sets of data collected from seven locations in Japan were used for

modeling as well as validation. Considering the ease of data acquisition, we selected only six meteorological parameters that are easily available at weather stations as input variables. In addition, the accuracy of the model is tested in this paper under different weather conditions.

In Chapter 6, Energy sharing for self-sufficient in solar PV community:

With the rapid decline in the price of photovoltaic (PV), the growth in installation of solar PV systems has increased significantly, and the trend is likely to continue. The lower prices have attracted many commercial buildings to become producers who generate electricity from local renewable energy resources (RES) and consume it locally or sell it to the grid. However, as PV penetration increases, and its intermittent output puts management pressure on the public grid. Therefore, energy sharing has increased opportunities to improve the local energy self-consumption rate and the spread-ability of RES in the future. With direct energy sharing, communities still face the issue of not being able to consume all the surplus energy. in this chapter, two different BESS sharing structures, namely shared design for centralized BESS and the shared design for distributed BESS have been compared with the traditional user owned BESS (Individual design for distributed BESS). First, we optimize the BESS size under different battery sharing structures and then discuss the BESS installation position and quantity by a multi-objective genetic algorithm. In terms of economics, aggregation control of shared BESS and participation in grid demand response are used to improve the economic performance, and their effectiveness is verified by whole-life cost analysis. The performance of surplus sharing and storage sharing within the energy sharing community was investigated in the context of the Kyushu region of Japan.

In Chapter 7, Energy sharing for load leveling in solar PV community:

The irregularity of buildings in consumption leads to inefficiencies in energy supply as well as uncertainty (because conventional electricity suppliers were designed and built with average electricity demand rather than maximum demand). To worsen the situation, energy consumption in the building sector continues to grow due to population growth and increasing per capita income. Integrating energy storage systems (ESS) into the power system is one of the solutions being proposed to improve the grid's reliability and performance. In this chapter, we enabled the energy sharing framework to optimize the control strategy and allocation method of the distributed battery system that can be exploited to achieve better optimization for load leveling through investigating the interaction between buildings with the distributed battery system and the distribution network. Firstly, we proposed the advantages of energy sharing to analyze the differences and of centralized and distributed energy storage in dealing with load-leveling problems. And we establish a strategy to move the peak-to-valley difference for the battery management system. Then we combine the advantages of centralized energy storage and propose a size allocation method in distributed energy storage to optimize load leveling performance and reduce the battery capacity at the aggregation level. The proposed distributed battery system, which is applied in typical community with 39 buildings in Japan, is simulated to analyze the load leveling performance.

In Chapter 8, Conclusion and Prospect:

The conclusion of each Chapter is concluded.

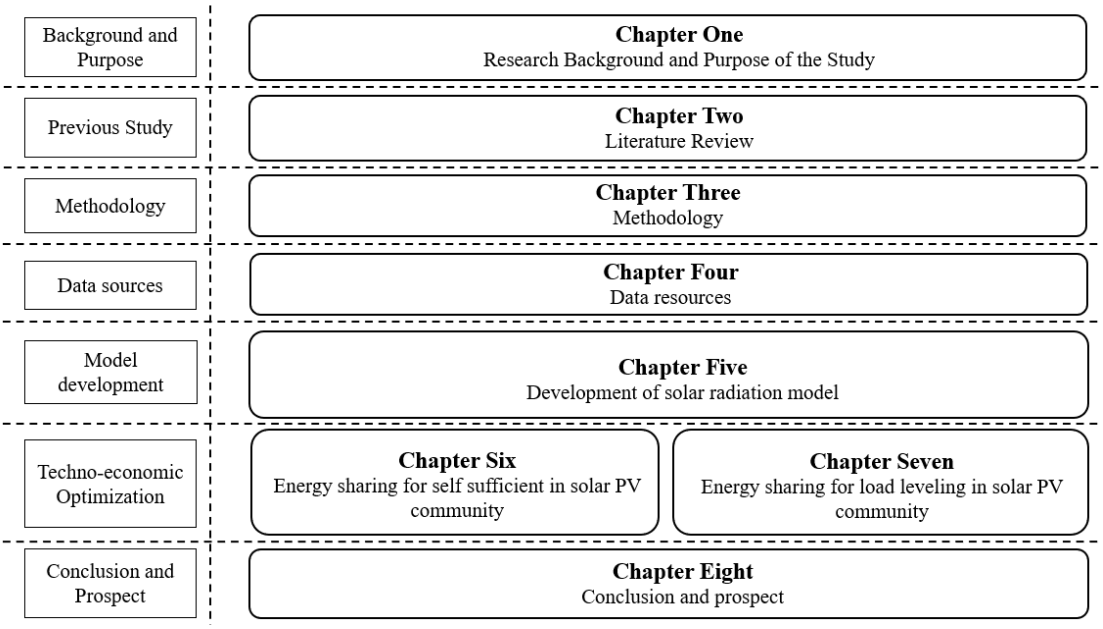

Fig.1-23 Research overview of this work

References

[1] Masters CD, Root DH, Attanasi ED, Tedeschi M, Singh S, du Plessis M, et al. World resources of crude oil and natural gas. Energy Exploration & Exploitation. 1991:354-74.

[2] Nashawi IS, Malallah A, Al-Bisharah M. Forecasting world crude oil production using multicyclic Hubbert model. Energy & Fuels. 2010;24:1788-800.

[3] Jiang S, Zhang J, Jiang Z, Xu Z, Cai D, Chen L, et al. Geology, resource potentials, and properties of emerging and potential China shale gas and shale oil plays. Interpretation. 2015;3:SJ1-SJ13.

[4] Zhang Z, He M, Zhang Y, Wang Y. Geopolitical risk trends and crude oil price predictability. Energy. 2022;258:124824.

[5] Gumus M, Kiran MS. Crude oil price forecasting using XGBoost. 2017 International conference on computer science and engineering (UBMK): IEEE; 2017. p. 1100-3.

[6] Brown SP. New estimates of the security costs of US oil consumption. Energy policy. 2018;113:171-92.

[7] Vitunskienė V, Aleksandravičienė A, Ramanauskė N. Spatio-temporal assessment of biomass self-sufficiency in the European Union. Sustainability. 2022;14:1897.

[8] Sharvini SR, Noor ZZ, Chong CS, Stringer LC, Yusuf RO. Energy consumption trends and their linkages with renewable energy policies in East and Southeast Asian countries: Challenges and opportunities. Sustainable Environment Research. 2018;28:257-66.

[9] Almarshoud A, Adam E. Towards VLS-PV deployment in Saudi Arabia: Challenges, opportunities and recommendations. Energy policy. 2018;114:422-30.

[10] Adams AS, Keith DW. Are global wind power resource estimates overstated?

Environmental Research Letters. 2013;8:015021.

[11] Del Río P, Gual MA. An integrated assessment of the feed-in tariff system in Spain. Energy policy. 2007;35:994-1012.

[12] Tomar V, Tiwari G. Techno-economic evaluation of grid connected PV system for households with feed in tariff and time of day tariff regulation in New Delhi–A sustainable approach. Renewable and Sustainable Energy Reviews. 2017;70:822-35.

[13] Ye L-C, Rodrigues JF, Lin HX. Analysis of feed-in tariff policies for solar photovoltaic in China 2011–2016. Applied energy. 2017;203:496-505.

[14] Gillingham K, Stock JH. The cost of reducing greenhouse gas emissions. Journal of Economic Perspectives. 2018;32:53-72.

[15] O'Connor RE, Bord RJ, Yarnal B, Wiefek N. Who wants to reduce greenhouse gas emissions? Social Science Quarterly. 2002;83:1-17.

[16] Ritchie H, Roser M, Rosado P. CO_2 and greenhouse gas emissions. Our world in data. 2020.

[17] Herzog T. World greenhouse gas emissions in 2005. World Resources Institute. 2009;7:2009.

[18] Chen T, Jin Y, Lv H, Yang A, Liu M, Chen B, et al. Applications of lithium-ion batteries in grid-scale energy storage systems. Transactions of Tianjin University. 2020;26:208-17.

[19] Bowen T, Chernyakhovskiy I, Denholm PL. Grid-scale battery storage: frequently asked questions. National Renewable Energy Lab.(NREL), Golden, CO (United States); 2019.

[20] Castillo A, Gayme DF. Grid-scale energy storage applications in renewable energy integration: A survey. Energy Conversion and Management. 2014;87:885-94.

[21] Cho KT, Albertus P, Battaglia V, Kojic A, Srinivasan V, Weber AZ. Optimization and analysis of high-power hydrogen/bromine-flow batteries for grid-scale energy storage. Energy Technology. 2013;1:596-608.

Chapter 2

LITERATURE REVIEW

LITERATURE REVIEW

2.1 Development of solar radiation models 2-1

2.1.1 Existing coarse-grained models 2-1

2.1.2 Existing fined-grained models 2-2

2.2 Development of solar PV generation models 2-4

2.3 Application of solar PV generation in urban area 2-5

2.4 Application of PV battery system in urban area 2-6

2.5 Battery sharing in urban area 2-13

References 2-23

2.1 Development of solar radiation models

In recent years, scholars and researchers have conducted a lot of research around solar radiation forecasting and have achieved satisfactory results. Depending on the difference in input parameters, it can be roughly divided into two categories, models based on general meteorological data (which includes empirical formulations and machine learning models) and models based on satellite data.

2.1.1 Existing coarse-grained models

Firstly, general meteorological parameters can be analyzed by regression with solar radiation to establish empirical models. Due to the simplicity of the expression form, it is widely used in its long development. The parameters commonly used in this empirical solar model are sunshine duration, temperature, or a mixture of other meteorological parameters. The initial sunshine duration model was first proposed by Angstrom in 1924 [1]. It is based on the analysis of the ratio of measured daily solar radiation to theoretical clear-sky solar radiation and the ratio of measured daily sunshine duration to the theoretical maximum possible sunshine duration. Then Prescott (1940) modify this model by replacing the clear-sky solar radiation with theoretical extraterrestrial solar radiation, which is more readily available; this modified form is called the Angstrom-Prescott model [2]. Since then, based on the Angstrom-Prescott model, different scholars have refined and improved the model [3] [4] [5] [6] [7]. Similarly, some scholars have developed linear, polynomial, exponential, and power functions between the clear sky index and the maximum, minimum, and average temperatures, and temperature differences [8] [9] [10] [11]. One of the classic models is the power function model proposed by Hargreaves using daily temperature differences and extraterrestrial solar radiation [8]. The models mentioned above are convenient for calculating daily solar radiation. Daily solar radiation is valuable for some specific applications, such as assessing the maximum output potential of solar generation. Nevertheless, for other scientific engineering applications, such as thermal utilization and heat gain in buildings, hourly solar radiation are increasingly required.

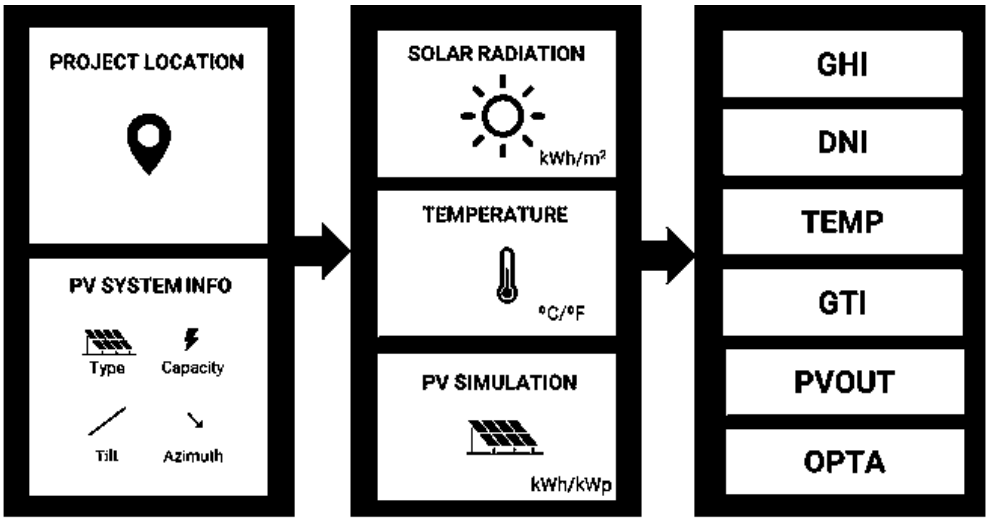

Fig.2-1 The input and output items of Solar radiation model

2.1.2 Existing fined-grained models

An hourly solar model is initially developed by Zhang and Huang for Beijing and Guangzhou, China [12]. Zhang and Huang use common meteorological parameters such as temperature, humidity and cloud cover to establish a polynomial relationship with hourly solar radiation [13]. It uses observed cloud cover data to reflect the effect of clouds on solar radiation under all-day conditions. The accuracy of the Zhang model has been verified in many previous studies [14] [15] [16]. Despite the fact that the many advantages of the Zhang and Huang model the cloud data used are not recorded numerically but as described: clear, scattered, broken, overcast, obscured and partially obscured [12]. Hence, the Zhang and Huang model needs to be deeply studied. In addition, although the authors claim that the proposed model can be adapted to all-sky conditions, there are still many technical difficulties in the study of clouds, and more evidence is needed to show that cloud cover is correlated with all-sky conditions.

In recent years, there has been an increasing interest in machine learning models, such as different artificial neural networks and support vector machine (SVM) models to estimate solar radiation. AI-Alawi and AI-Hinai [17] use a multi-layer feed-forward network and back-propagation training algorithm for analyzing the relationship between global radiation and climate variables. The results show that using location, month, average pressure, average temperature, average vapor pressure, average relative humidity, average wind speed and average sunshine hours as inputs, an accuracy of approximately 93% and an average absolute percentage error of 7.30 are achieved. Lazzús, J.A.et al. [18] have developed an artificial neural network using data measured from weather stations to estimate the hourly global solar radiation in La Serena (Chile). Then, an R-square value of 0.94 is found, indicating a strong correlation between hourly global solar radiation and meteorological data. Kaba, K. et al. [19] train the model using the Self-Regulating Particle Swarm Optimization algorithm. The parameters sunshine hours, cloud cover, maximum temperature, and minimum temperature are selected as inputs and 16 different input combinations were constructed. The results show that the deep learning model produces very accurate and comparable results in estimating the daily global solar radiation. Hassan, M.A. et al. have compared gradient boosting decision tree, random forest, multilayer perception, decision tree and SVM and concluded that SVM produced the highest accuracy but is 39 times more computationally expensive than the other models. As a result, many improved SVM models have been proposed [20]. In addition, researchers are keen to integrate multiple deep learning techniques, called Ensemble-based machine-learning models. Basaran, K., A. et al. [21] develop Ensemble-based machine-learning models based on SVM, multilayer perception, and decision tree, then give us a reference conclusion as compared to the single models, Ensemble-based machine-learning models improved the RMSE significantly. Gao, Y. et al. [22] develop a deep Long short-term memory-based generative model for multi-step solar irradiation prediction for at least 24 hours in the future. Peng, T. et al. [23] propose a hybrid model by combining the Bi-directional long short-term memory model sine cosine algorithm and complete ensemble empirical mode decomposition with adaptive noise for solar radiation prediction. The effectiveness of the Bi-directional long short-term memory network in processing solar radiation time series data and improving the prediction accuracy is demonstrated. Zhou Y. et al. [24] provide a comprehensive and systematic review

of all important aspects of machine learning models, including input parameters, feature selection, and model development and presents a guide for machine learning models in solar radiation prediction. This is despite the fact that many studies have shown that the prediction accuracy of machine learning is generally higher than that of general empirical models, as a branch of data science, machine learning models have difficulty in giving proper interpretation among the input parameters. Some researchers are trying to construct appropriate models to improve the interpretability as well as the credibility of the results. Gao, Y. et al. [25] investigate the interpretability of the temporal and spatial dependence of the prediction process through attentional mechanisms and graph neural networks. The results show that solar radiation is directly related to month, time, temperature, infiltration rainfall, water vapor pressure and radiation time. However, current findings are far from satisfactory.

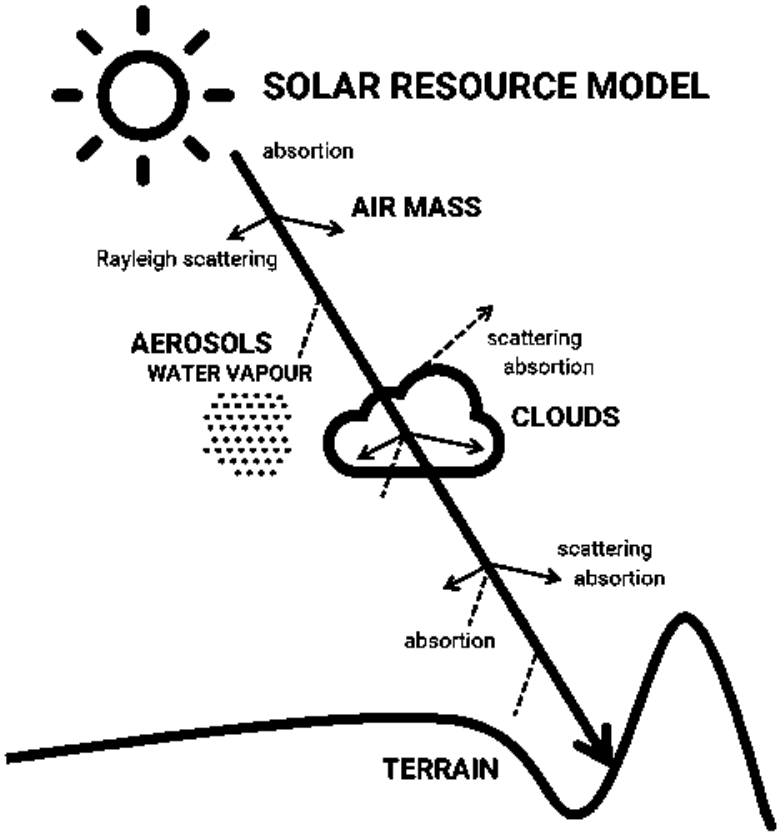

Fig.2-2 Reduction of Solar radiation

The solar radiation estimation models mentioned above have high accuracy and wide applicability, they are mostly statistical or data-driven models. But it is difficult to guarantee that the forecasts will remain convincing when conditions change (e.g., geographic climate and weather conditions). Consequently, a proper theoretical basis is necessary for high-precision solar radiation prediction. In 1981, Richard E. Bird and Roland L. Hulstrom [26] first proposed a layer-by-layer weakening solar radiation model which divided the weakening layers into six layers: mixed gas layer, ozone layer, Rayleigh layer, water vapor layer, aerosol layer and cloud layer. The model is theoretically clear and consistent with the laws of nature. However, in the calculation of Bird model, the weakening effect is reflected by the transmittance, and it is

necessary to consider the transmittance of each layer, which is complicated to use in practice. Chen et al. [27] refer to some data from NCEP/NCAR and some information about the terrain to improve the Bird model as input items. The results show that the accuracy of the model is improved by 7.58%, but it is greatly reduced in cloudy conditions. The accuracy of the model is limited by the resolution of the data. Su, G. et al. [28] modify the weakening solar radiation model by using relative humidity and air quality index. The result show that the R value of the layer-by-layer weakening model is increased by 5.74% and 41.27% compared with the existing beam solar radiation model and diffuse solar radiation model. Unfortunately, typical weakening models use data from satellite observations and invert them with specialized software. The collection and processing of satellite data is a huge challenge for the general weather station. The low resolution of satellite data also makes it difficult to meet the spatial and temporal adaptability requirements in practical applications.

2.2 Development of solar PV generation models

Among the latest challenges of our time, the need to reduce energy dependence on fossil fuels and to limit air pollution and CO2 concentration certainly occupies an important place on the world stage. On the other hand, population growth and improved living conditions lead to a growing energy demand, which needs to be met in accordance with sustainable development. The Earth's surface receives about 120,000 TW of solar radiation [29], which is a thousand times greater than the energy needs of the entire planet. Therefore, solar energy seems to be an attractive solution for the conversion of electrical energy through more complex solar systems or in a simpler way PV modules are seen as an important means to achieve environmental sustainability.

There are two main parameters that affect the performance of photovoltaic devices: incident solar radiation and operating cell temperature. In fact, only a small fraction of the incident solar radiation is converted into electrical energy, the rest is converted into heat, which raises the cell operating temperature. As a result, the module efficiency decays almost linearly with increasing temperature (from 0.40% to 0.65% per degree increase in temperature relative to the PV technology under consideration) [30]. The cell temperature is the result of a combination of external air temperature, incident solar radiation, wind speed and wind direction. Different methods have been proposed for estimating cell temperatures, ranging from simple empirical correlations to more structured thermal and electrical models.

The empirical correlation uses environmental variables and numerical parameters determined with reference to specific configurations (geometry, material and environmental context) [31]. The most common implicit relationship provides the cell temperature starting from the NOCT (Nominal Operating Cell Temperature) value, incident solar radiation, and outdoor air temperature. Further correlations based on NOCT have been developed, suggesting the use of a factor instead of incident solar radiation, taking into account the different possible configurations of PV module installations and considering other parameters such as peak factors, global annual average heat exchange coefficients, weather indicators, reference cell efficiencies and annual average cell temperatures. Comprehensively, correlations including wind speed, which plays a key role in convective heat exchange between the module and the

external environment, have been proposed [32] [33] [34].

The advantage of developing a thermal model is to avoid the estimation of parameters (I-V characteristics of PV modules) required for different electrical models, which are usually not provided by the manufacturer and are difficult to obtain. The thermal approach can be implemented in either a steady-state or transient model, whether the variables considered are assumed to be constant with time or time-dependent, including the panel thermal mass. The energy balance of the PV module in the transient state was developed to simulate the thermal energy exchange with the external environment, assuming uniform module temperature across the layer. The fitted coefficients for forced convection were found to lead to more accurate predictions. In a similar way, a model considering the heat exchange between the module and the environment was developed and solved numerically by fine-tuning several parameters to improve the model accuracy [35].

These studies suggest that in the case of PV systems, it seems more appropriate to use a more simplified 1D model that provides sufficient accuracy to predict energy production.

2.3 Application of solar PV generation in urban area

With the rapid decline in PV system prices in recent years, there has been a significant increase in interest in using grid-connected PV and/or battery systems. Traditionally, PV systems have been used in two configurations, grid-tied without batteries and off-grid (stand-alone) with batteries. The main challenge for PV technology is the infinite size of the system and its inability to meet the full electricity demand of a typical household customer. PV systems cannot meet electricity demand beyond daytime hours. Therefore, in off-grid applications, power storage becomes an integral part of PV generation (ignoring cost issues) to ensure higher power reliability [36].

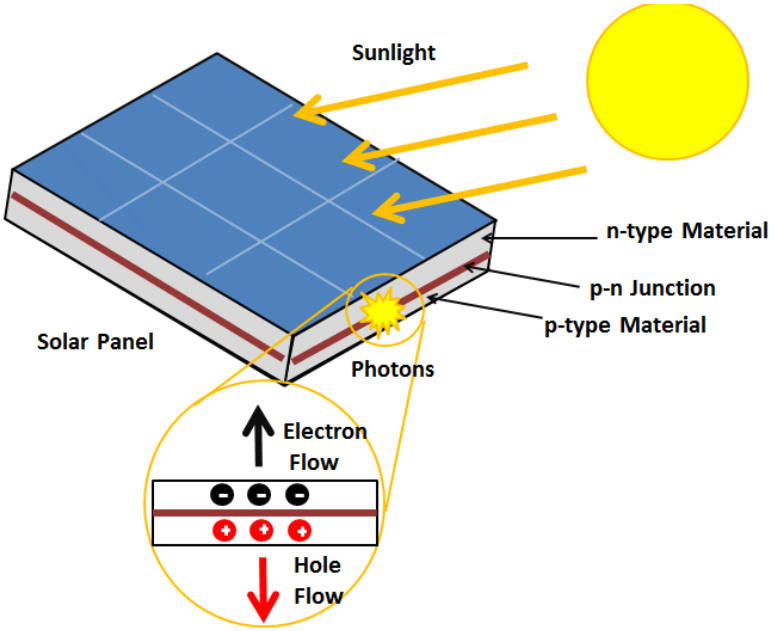

Fig.2-3 A diagram showing the photovoltaic effect

Some researchers have focused on the efficient operation of photovoltaic cell systems. According to Halliday et al. [37], although PV systems account for a large portion of the initial investment in PV cell systems, their share of the life-cycle capital cost of the system (over 20 years) is about one-third. In contrast, cells account for half of the total capital cost due to lower expected cell life due to inefficient cell operation (high temperature, low SOC, etc.). Therefore, optimal control of battery charge/discharge (SOC) is a key component of improving overall system economics. one of the first studies of efficient battery operation was by Appelbaum et al. [38].

Photovoltaic (PV) systems are widely used as an important alternative energy source for residential applications. However, due to the intermittent nature of solar energy, which is related to climatic conditions, PV systems should be integrated with other power sources to ensure a stable power supply [39] [40]. Hybrid energy systems consisting of photovoltaic modules, fuel cells, batteries, and residential energy loads can be proposed [41].

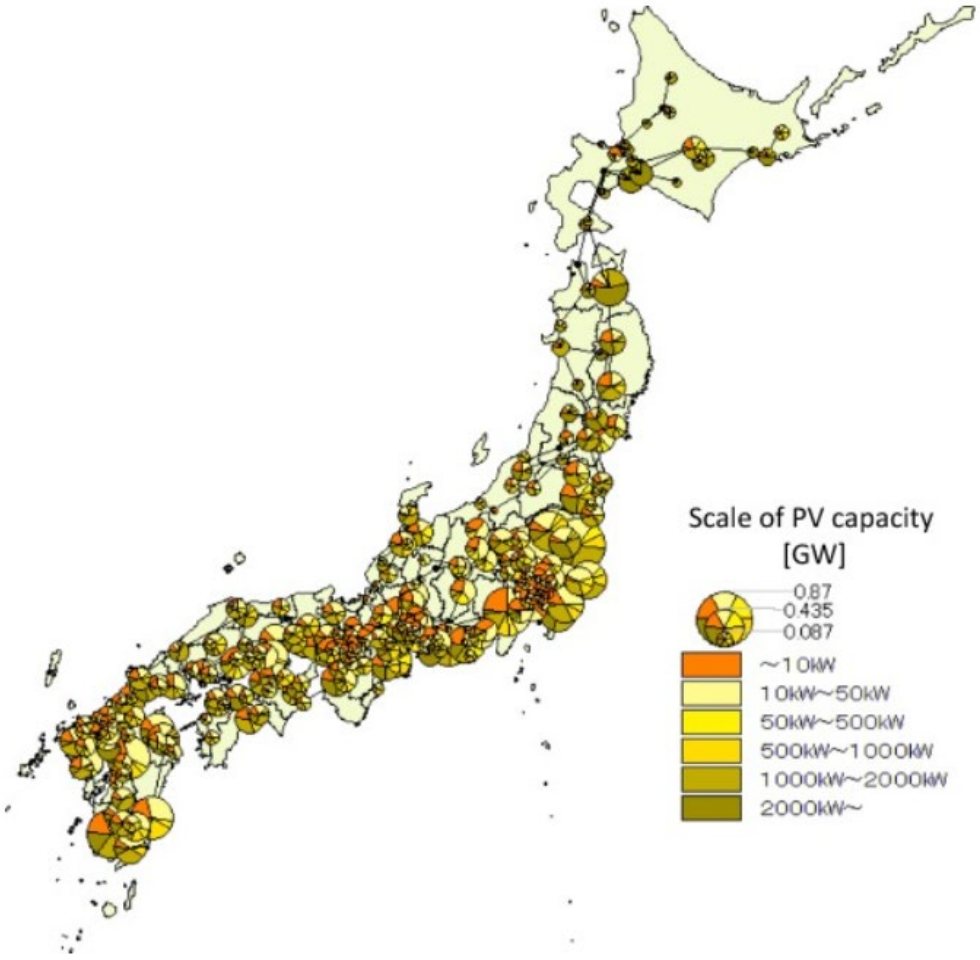

Fig.2-4 Installed PV capacity in Japan in 2017 [42]

2.4 Application of PV battery system in urban area

This irregularity in consumption leads to inefficiencies in energy supply as well as uncertainty (because conventional electricity suppliers were designed and built with average

electricity demand rather than maximum demand) [43] [44] [45] [46]. To worsen the situation, energy consumption in the building sector continues to grow due to population growth and increasing per capita income [47] [48]. In Japan, after the Great East Japan Earthquake in 2011 [49] [50], the safety of nuclear energy has been seriously questioned, thus, it remains heavily dependent on imported fossil fuels which provides 88% of the Japan's total primary energy supply (TPES) in 2019 [51, 52]. Large-scale power outages and year-round electricity bill hikes are also plaguing Japan due to insufficient conventional power generation capacity and changes in the international situation. As a result, Japan is urgently upgrading its energy system. Integrating energy storage systems(ESS) into the power system is one of the solutions being proposed to improve the grid's reliability and performance [53, 54]. Distribution networks can utilize ESS for a number of grid applications including mitigating the renewable resources uncertainties [55], micro-grid applications [56] risk mitigation in electricity market [57].The other significant benefit at distribution side is that ESS can contribute in time shifting of energy output[58], for example excess generated energy is stored energy at off peak or low price periods and then stored energy is dispatched during the high demand, high price or low generation periods. It also achieve the performance on smoothing the load pattern be decreasing the on-peak and increasing the off-peak loads in one day, knowns as load leveling [59]. In addition, the planners would need to build only sufficient generating capacity to meet average rather than peak electrical demand by installing large-scale electricity storage facilities. [60]. Consequently, ESS can be a critical element in helping to regulate the city's peak demand by implementing load leveling. Among the various available ESS technology types, Battery Energy Storage System (BESS) has attracted considerable attention with clear advantages like a fast response, controllability, and geographical independence [61-64].

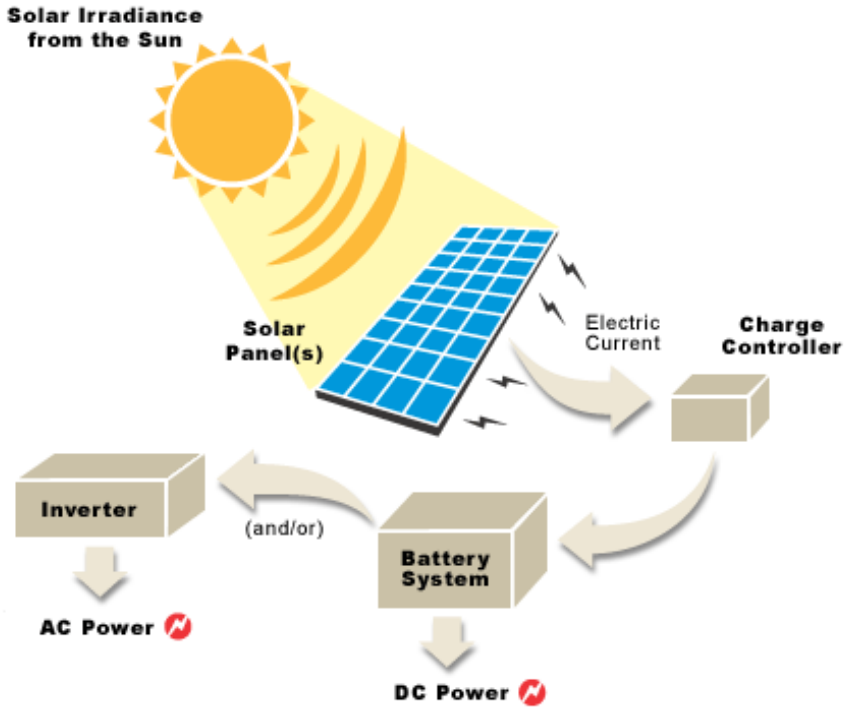

Fig.2-5 A diagram showing of PV battery system

In order to reduce the difference between peak and valley, three countermeasures: peak cut, peak shift, valley up are proposed. Currently, users are required to use low-power equipment to reduce the peak power consumption is a common measure of power generation companies. Meanwhile, distributed photovoltaic production can directly reduce the burden on the grid by reducing the peak demand of users. But, it is well-known that renewable energy production strongly depends on local weather and climate conditions. The consequent intermittent and stochastic characteristics of non-dispatchable renewable energy can bring about instability into power systems [65]. These stability issues, due to the fluctuating features of the resources, can be exacerbated when a high penetration of RE is present. For example, in recent studies [66] [67], the overgeneration of PV led to a very low net demand during midday in California, but the net demand in the morning and evening, when PV cannot deliver power, was still high. This net demand profile, when further PV is included, would see the net demand trough in the middle portion of the day deepen, leading to the so called “duck” curve. As a consequence, with a limited capability to accommodate this huge ramp, solar energy needs to be curtailed, thereby reducing the economic and environmental benefits of renewable energy integration. Currently, there are some studies on hybrid PV and BESS to reduce peaks. Yan L. et.al [49] investigate the technical and economical performances of residential PV system with nominal capacity of 5.0 kWp with and without battery system over months in Kyushu, Japan. It is found that optimal control on dispatch of battery flows can release the peak pressure against needed grid flexibility, aggregated residential PV battery system (assume 2% of total grid load) can participate in shaving 1.1% of net peak load. Luthander R et. al [68] focused on enhancing self-consumption and peak shaving of residential photovoltaics using shared storage and curtailment, results indicated that profit for the PV-battery system can increase by changing from individual to shared storage, the maximum power from community to the grid can be halved, which can effectively relieve the pressure on the public grid. Ref. [69] proposed the dynamic programming for residential PV-battery system to maximize the residential economic profits in Norway, the application of battery storage can help to curtail the power fed into the grid and maintain voltage profile during peak generator hours.

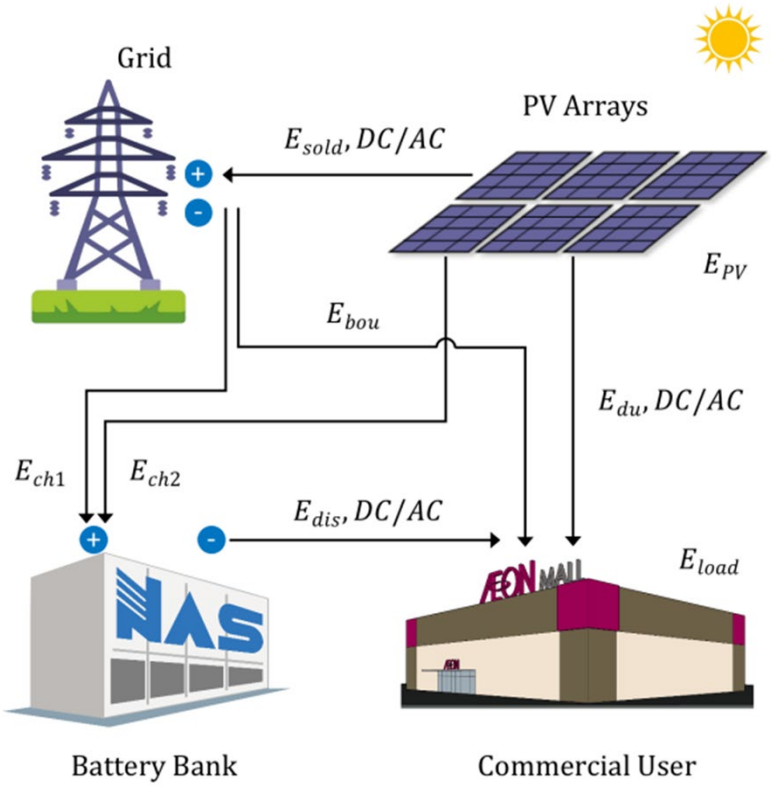

Fig.2-6 PV battery system

In addition, change the business day and business hours of the factory in a planned manner, and use heat accumulators to store the air-conditioning heat used at night and during the day, or the power company adopts effective incentives and inducing measures to work with users to improve terminal power efficiency and change the way of electricity consumption (demand-side management) to achieve peak shift. However, the widespread deployment of demand response programs in the building sector still faces significant challenges. Smart technology deployment, the lack of common standardized assessment procedures and metrics, the absence of established regulatory frameworks are among the main obstacles limiting the development of portfolios of competitive flexibility assets [70].

Our knowledge is limited in the power shifting technical demand response potential covering all sectors and the achievable demand response potential of all sectors.

Pang Y. et al [71] assessed electricity load shifting technical demand response potential and achievable demand response potential in western Inner Mongolia, the results show that, in secondary sectors, over half of the enterprises' power load shifting technical demand response potential is less than 10%.

Moreover, the use of Energy Storage Systems (ESS) to facilitate the increasing penetration of renewable energy by absorbing and releasing power in different time horizons and lead to

greater load balance has been extensively studied [72] [73] [74] [75]. Of the various types of ESS technology available, Battery Energy Storage Systems (BESS) have attracted considerable attention with clear advantages like fast response, controllability, and geographical independence [76]. Meanwhile, one example for a grid connected battery is through energy arbitrage — the principle of buying energy when it is cheaper and selling it when it is more expensive in order to make a profit [77].

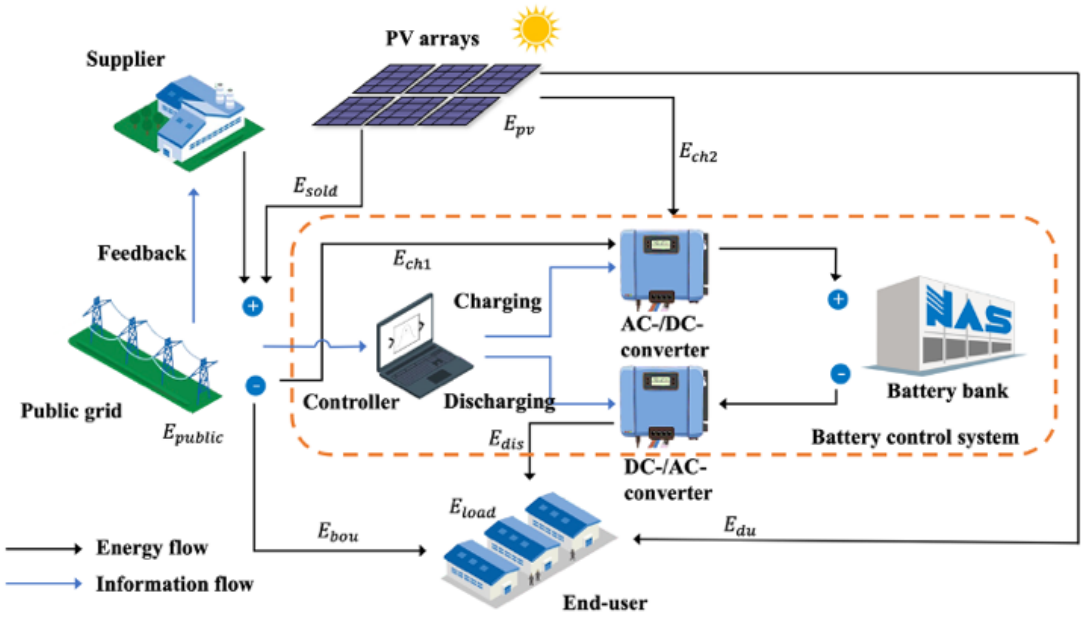

Fig.2-7 Layout of the grid-connected PV-battery system

Table 2-1. Optimization technologies for application strategy

Optimization technologies	Performance metric	Decision variables	Application strategy	Target
Rule-based algorithm	Peak shaving Economic dispatching	Power flow	Control	Grid-connected microgrid of a sport center facility
	Self-consumption	Power flow Capacity	Control/Sizing	
	Price arbitrage			
Deterministic Optimization	NPV Self-consumption	Power flow	Control	Building with PV system
	Cost in the time	Capacity	Control	
	Total cost of grid electricity	Power flow P2P trading	Control	
	5-year NPV value	Power flow		
	Total greenhouse gas emissions		Control	
	Self-sufficiency rate	Power flow	Control	
Stochastic optimization	Self-consumption ratio	Capacity	Control/Energy sizing	High-rise building with renewable energy systems
	Cycling aging	Charging/Discharging rates	Control	
	Load cover ratio	Capacity	Control	Building with PV system, battery, EV
	LCOE	Power flow	Control	

Daily electricity cost Annual economic benefit Daily operational cost		Buildings with hybrid energy system

In spite of the fact that the use of BESS for load leveling can bring significant economic advantages, the high overall investment of BESS remains an issue [78]. It is therefore crucial that the BESS is optimally sized. Those on the application of BESS to cope with load leveling problem can be broadly categorized as two categories, centralized battery storage and distributed battery storage. The majority of the existing studies in the literature propose optimal manipulation and sizing for BESS. Some researchers also examine the optimal policy for charging and discharging power based on two different optimization objectives [79]. The first is to minimize the difference between the peak and valley demand, the second is to minimize the daily variance in load. The storage devices have been used to reduce the peak of the load profile and therefore, lessen the planning and operational costs. Allocation of the ESS is incorporated into the network planning problem [80]. A mixed integer nonlinear programming (MINLP) model was proposed to solve it utilizing a particle swarm optimization algorithm (PSO) [81]. As a result of the simulation, both the cost and technical performance of the network is improved. To improve the reliability level of the distribution network, Saboori H et.al have been proposed as an investment plan of ESSs. With the energy not supplied (ENS) index, the level of system reliability is elevated, and system failures are minimized through optimal ESS planning. In order to perform load leveling and improve voltage curve in the networks, a bi-objective optimization model was proposed [59]. For economic assessment, a stochastic cost–benefit analysis framework for allocating centralized energy storage systems (ESS) in the networks is proposed to achieve load balancing [82]. An algorithm was presented to solve the issue of load leveling and losses minimization in the networks impacted by temporary service restoration activities but they have not considered optimal allocation [83]. [84] introduced a metric of five indexes to evaluate the technical performances of load peak shaving for a test house in Northern Ireland but have not considered optimal operation. In addition, the mobile BESS technology can provide services and economic benefits by connecting to the grid (such as vehicle-to-grid system). However, some researchers pointed out that the increased integration of electric vehicles is expected to have a negative impact on power quality, and investment costs of the microgrid. Hence, a decentralized energy management system, based on multi-agent systems, was developed for the efficient charging of electric vehicles [85], to achieve approximately 17% peak load reduction and 29% load variances reduction.

The various papers mentioned above discuss strategies for the placement of BESS to improve the load leveling performance of the building sector and propose solutions in terms of optimal location and size. Most importantly, it demonstrates the feasibility of BESS participation in grid management in terms of economics. As the price of battery systems decreases, battery systems, whether centralized or distributed (It will be explained in detail in section 3.3), are expected to become an attractive application for the building sector. Centralized energy storage not only requires operational and size optimization considerations but also requires additional consideration of battery siting and distribution system upgrades due to large transient branch circuit current changes over long distances. The conventional design methods of distributed system are based on single building energy allocation for sizing the distributed batteries, so, they neglect the interaction that we call it 'energy sharing' in this paper, between the smart grid, smart buildings and distributed energy storage to achieve better energy management practices.

2.5 Battery sharing in urban area

① Battery type

The basic operating logic of the BESS used for electrochemical storage technologies is that it converts chemical energy stored in electrodes into electrical power using electric potential difference [86]. There are various types of BESS using electrochemical storage technologies in the energy storage market, and they can be classified according to the operation principles and electrolyte types [87]. Table 1 shows a summary of characteristics and usage (i.e., applications suitable to apply in the grid system) according to the electrolyte type and oxidation-reduction reaction at the electrode [88] [76].

1). Lithium-ion Battery (Li-ion): A rechargeable lithium-ion battery consists of a positive electrode, a negative electrode, an electrolyte and a diaphragm. During charging, lithium ions move from the positive to the negative electrode and vice versa during discharge. It offers high energy density, relatively long service life and higher storage efficiency than batteries of the same size and weight for stationary applications.

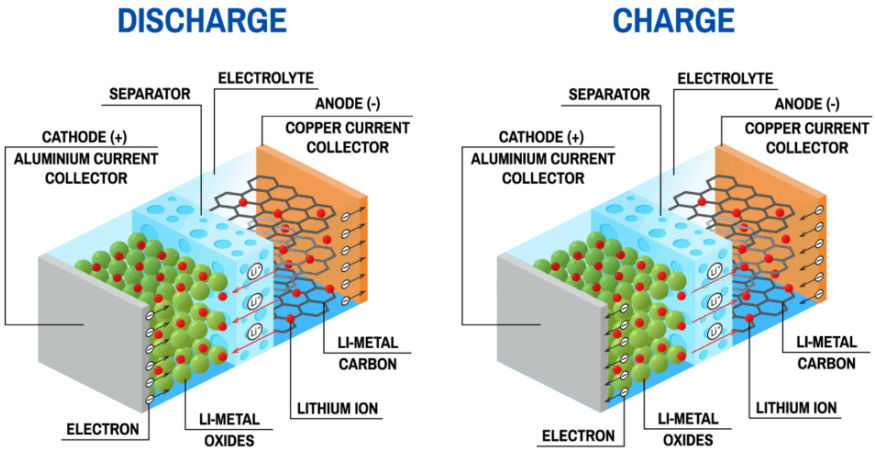

Fig.2-8 Lithium-ion batteries

2). Lead-Acid Battery (Pb-acid): It is one of the most developed and durable battery technologies. In this type of battery, electrons move from an electrode with a greater ionization to opposite electrodes in a circuit consisting of two electrodes with different ionization. In addition, these heavyweight lead-acid batteries have been used in vehicles where weight is not an issue, such as forklifts and golf carts, while lead toxicity remains a safety concern.

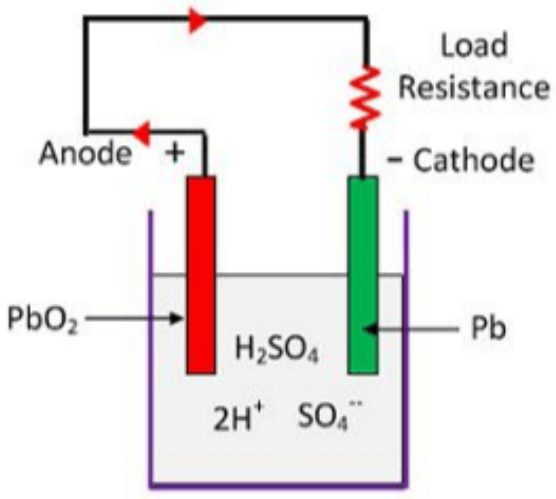

Fig.2-9 Lead-Acid batteries

3). Sodium–Sulfur battery (NaS): When the sodium ion is charged and discharged, it uses the electron flow generated when the sodium ion is separated and combined with sulfur to generate electricity. Unlike other batteries that use a liquid electrolyte, it uses a solid electrolyte in a different way. This makes it difficult to be used universally because it can only be operated at high temperatures to ensure the molten state of sodium, so it is mainly used to connect large power facilities and renewable energy systems.

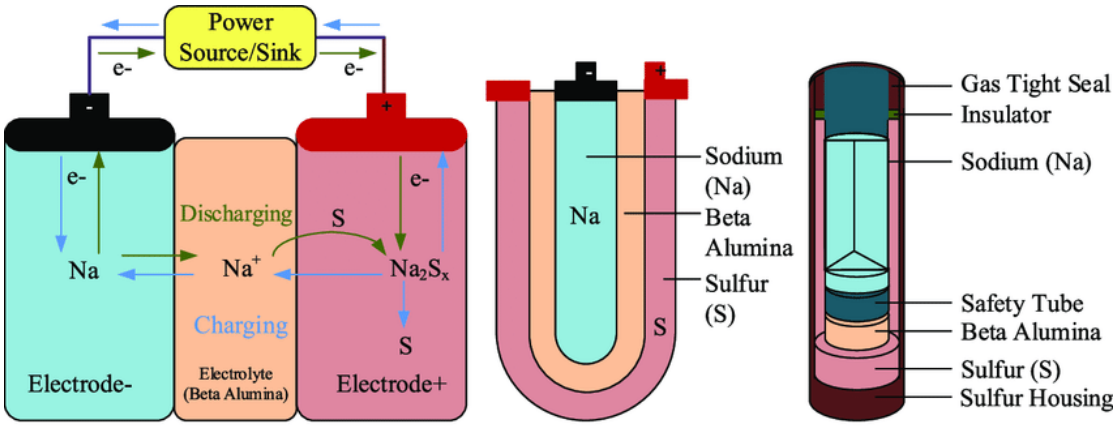

Fig.2-10 Sodium-sulfur batteries

4). Sodium–Nickel Chloride battery (Na–NiCl2): It operates at temperatures similar to sodium-sulfur batteries. A solid sodium cell with a robust steel shell around each cell provides high conductivity potential and storage efficiency. It has long life, deep cycling and fast response and is suitable for mass storage in large power plants as a typical stationary application for peaking and load shifting.

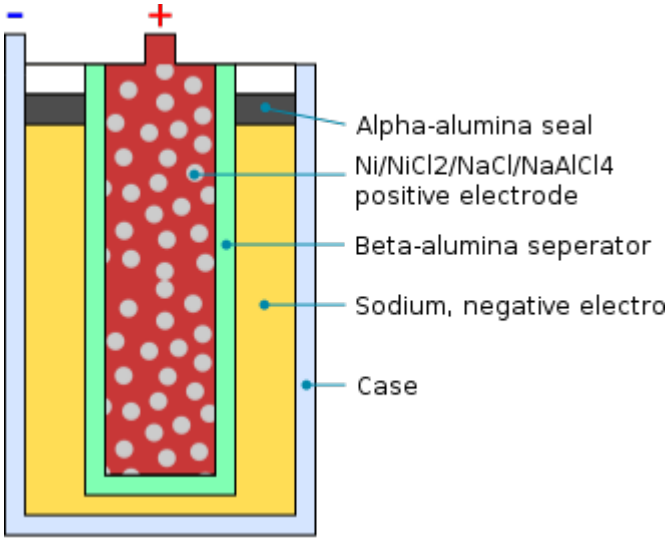

Fig.2-11 Sodium–Nickel Chloride batteries

5). Vanadium Redox Flow Battery (VRFB): The anode electrolyte is produced by dissolving the electrolyte-based active material in the cathode electrolyte, storing it in a tank, and then using a pump to supply the electrode surface of the electrolyte. It can be charged and discharged using the electrode potential difference of several redox pairs within the cell Since the electrolyte is stored in liquid form in an external tank rather than in the cell, it has a complex structure that includes a pump, sensors, controls, and a tank.

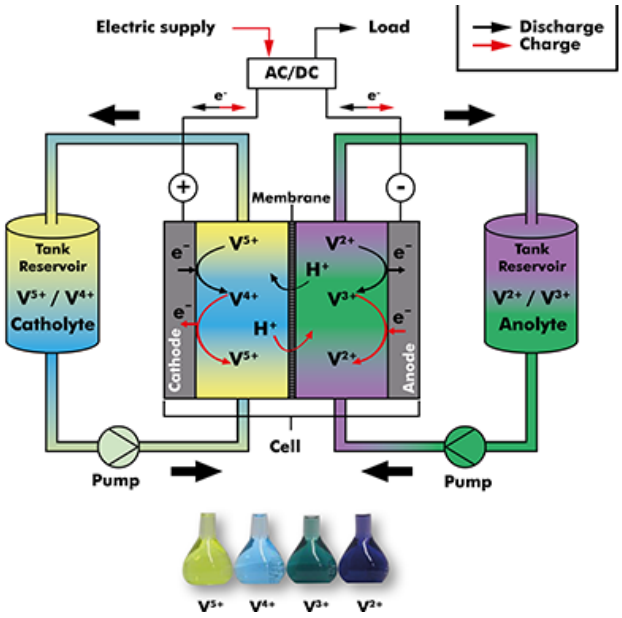

Fig.2-12 Vanadium Redox Flow batteries

Table 2-2. BESS types according to the operation principles and electrolyte types

Types	Lithium-ion Battery (Li-ion)	Lead-acid Battery (Pb-acid)	Sodium-Sulfur Battery (NaS)	Sodium-Nickel Chloride Battery (Na-$NiCl_2$)	Vanadium Redox Flow Battery (VRFB)
Operation Principles	Potential difference caused by the ion movement between the negative and positive electrodes				Redox reaction of ions at the electrode
Electrolyte types	Liquid	Liquid	Solid	Solid	Liquid
Operation degree (C)	5 to 45	-35 to 45	300 to 350	270 to 350	-5 to 50
Self-discharging rate(%/day)	0.1 to 0.3	0.1 to 0.3	0.05 to 20	15	0.2
Round-trip efficiency (%)	90 to 97	70 to 90	78 to 90	85 to 90	75 to 85
Discharge duration (hour)	Minutes to 4	Seconds to 10	Seconds to 8	Seconds to 5	Seconds to 12
Cycle (cycles)	1,000 to 10,000	400 to 1,500	2,500 to 10,000	At least 4,500	12,000 to 18,000
Lifetime (year)	5 to 15	5 to 15	10 to 15	10 to 15	10 to 20

Usage in the grid system	Frequency regulation Load shifting Power quality	Frequency regulation Load adjustment	Load shifting Standby power	Load shifting Spinning reserve Frequency regulation	Load leveling Emergency standby

② Battery sharing

With the rapid decline in the price of photovoltaic (PV), the growth in installation of PV systems has increased significantly, and the trend is likely to continue according to International Energy Agency Photovoltaic Power Systems Programme (IEA PVPS, 2020) [89]. The lower prices have attracted many commercial buildings to become producers who generate electricity from local renewable energy resources (RES) and consume it locally or sell it to the grid. The surplus energy generated by the dynamic mismatch between solar power and local demand can be sold to the grid through a feed-in tariff (FIT). However, as PV penetration increases and its intermittent output puts management pressure on the public grid, governments have had to promote local consumption of distributed energy resources (DERs) by reducing the FIT to reduce the impact on public grid stability [49]. Meanwhile, under the impact of the pandemic, the governments have understandably redistributed public funding to combat the Covid-19 in a way that leaves less available for renewable energy incentives and tax credits [90]. Japan has fully opened its retail electricity market since April 2016 [91]. The resulting positive impact is that the liberalization of the energy market has increased public support for RES [92]. Therefore, energy sharing [93], [94] have increased opportunities to improve the local energy self-consumption rate and the spread-ability of RES in the future. With direct energy sharing, communities still face the issue of not being able to consume all the surplus energy. Battery sharing [95], [96] is considered to be an effective solution to the above issue.

With the rapid growth of the sharing economy around the world, a new proprietary idea of community centric sharing has recently emerged into the energy market [97]. Unlike traditional individually owned BESSs and large utility-level BESSs, customers in a community can provide optimal energy management services through energy sharing (for example, using remaining power to match the power needs in the same community) and storage sharing (for example, using the battery to take remaining power to or out of the building community) [98, 99]. A peer-to-peer (P2P) energy sharing paradigm involving hybrid solar-wind renewable energy systems, battery storage, and grid-connected commercial prosumers (a high-rise office and hotel) was proposed[100]. And they found that the proposed P2P sharing operation with storage sharing can promote the self-consumption from 0.591 to 0.795 and reduce the net cost.

[101] established a shared economy model that enables residential communities to share solar power generation and storage capacity is investigated. The result is that it saves an average of €615 per year compared to operating alone. Peer-to-peer (P2P) energy trading framework was proposed [102], enabling distributed photovoltaic (PV) consumers and prosumers to participate in a community sharing market created by a stakeholder. [103] proposed a bi-objective mixed-integer linear programming approach for managing clusters of buildings equipped with shared electrical energy storage. Therefore, the uneconomic use case for batteries may become profitable when individual EES assets are aggregated into a large portfolio to provide grid-scale ancillary services [104].

At this stage, large-scaled battery is mainly utilized for load levelling in electricity plants by supplying power. The power generated by the electricity suppliers due to low needs (for example at dawn or on the off-peak hours [105]) and charged to the battery during periods of overgeneration and discharged to the buildings during the electricity shortage periods because of high needs (for example on the peak hours). Economic viability is the major critical element in large battery implementations because of the high initial costs. However, the utilization rate of large BESS for load levelling can be low due to fluctuating demand. In addition, large BESS also have high transmission loss due to size and distance limitations. On the other side, the ability to perform energy arbitrage is the biggest motivation for individual users to install BESS. Therefore, through energy sharing, private BESSs can perform in load levelling to reduce the peaking stress of the power supply, saving expenses for peaking power generators. Electricity suppliers are also willing to cooperate with individuals to share information and optimize energy use by paying a fee. As a result, stakeholder-based information exchange is essential to enable energy sharing between buildings where load balancing is performed and electricity suppliers. Hence, wide area monitoring system (WAMS) based on real-time measurement and monitoring is becoming a key solution in the key areas of online stability, situational awareness, grid planning. The possibility of monitoring and controlling the operation of the whole power system for achieve real-time, dynamic control of the power has been proved [106]. [107] studied the performance of communication in dense networks with wireless energy harvesting (WEH)-enabled sensor nodes. [108] proposed an information sharing strategy based on linked data for improved management of Net-zero communities. This strategy systematically integrates stakeholders' engagement by using energy performance indicators as information carriers and linked data as engagement channels.

Energy sharing refers to energy transactions between consumers and producers or between producers, where surplus electricity from producers can be shared between neighbors. Energy sharing allows producers to sell energy to their neighbors for more profit, as well as makes the DERs to be better utilized [94]. Energy sharing networks can be broadly split into two categories, autonomous energy sharing and supervised sharing. In autonomous energy sharing mode, it allows users with full control over their DERs, without requiring a central control system. Most of the existing literature on energy sharing has focused on different mechanisms based on this community framework. A small-scale local market needs to be formed within the community. This market is mainly based on a decentralized model through auction model [96], [109], blockchain [110], [111] and bilateral contracts [112]. Game theory provides a good

theoretical framework for this structure. Cintuglu et al.[113] presented a real-time implementation of multiagent-based game theory reverse auction for microgrid market operations featuring conventional and DERs. Cui et al.[114] used the Stackelberg approach realized a distributed game-based pricing market for solar PV prosumers within a microgrid to undertake energy sharing. In this mode, the advantages are, selling energy locally can be more profitable than selling to the grid, so incentives to engage producers in energy sharing are usually not needed in this model. The disadvantage is, in order to prevent long waits in the transaction process, communication systems with a lot of computational power are usually needed to perform the bidding of energy prices [115]. In addition, everyone in the community will participate individually without any cooperation. However, several studies have pointed out the Nash equilibrium of a non-cooperative game may not be the best solution [94], [116].

Under the supervised energy sharing mode, energy sharing within the community is managed by a third-party entity. Simpler communication systems and less data processing are required within the community because no bids need to be executed. Olivella-Rosell et al. [117] proposed a new aggregator type called Smart Energy Service Provider to schedule flexible energy resources. Ottesen et al. [118] considered the capability of an aggregator providing flexibility services to the broader grid. Motalleb et al. [119] constructed a theoretical model of the competition between demand response aggregators for selling energy previously stored in an aggregation of storage devices.

Due to the limitations of load characteristics, direct energy sharing is not sufficient for communities to achieve high penetration of energy self-consumption. Existing studies have shown that energy sharing networks with battery energy storage systems (BESS) can save significant amounts of money for producers in a community while increasing energy self-consumption within the community [120]. Nguyen et al. [121] proposed an optimization model to maximize the economic benefits for rooftop PV-battery distributed generation in an energy trading environment. The goal of the proposed model is to investigate the feasibility of such renewable source participated energy trading by examining the economic benefits. Dong et al.[122] proposed an agent-based model to investigate and analyze community energy storage based on a range of criteria. Parra et al.[123] optimized the performance including equivalent full cycles and round trip efficiency of lead-acid and lithium-ion batteries performing demand load shifting are quantified as a function of the size of the community. BESSs with different sharing structures (distributed and centralized, respectively) of the kind found in sharing communities have also been shown to have different techno-economic properties. Rodrigues et al. [124] considered the optimal BESS sizing and operation in an energy sharing network under different BESS ownership structures. Huang and Sun et al.[125] proposed a hierarchical design method of distributed batteries in solar power shared building communities, with the purpose of reducing the battery capacity and minimizing the energy loss in the sharing process. The above study demonstrates that both different BESS structure designs (distributed and centralized) are economically feasible in energy sharing communities. But the interaction between energy sharing and BESS size and the optimal location of BESS units is ignored.

In modern power system, all system operators have a fundamental need to be responsive to the appropriate level to which they will function to achieve maximum reliability of overall

power system [126, 127]. The overview of recent advances and future key benefits of demand-side management states that distributed generation should be integrated with demand response (DR) mechanisms which is an emerging strategy to deal with peak demand, energy management, reliability and economy of contemporary distribution system [128]. The combination of smart grid and energy storages and resultant policy recommendations have been discussed by Amoretti et al.[129] and Zame et al.[130]. Contreras-Ocanaet al. [131]showed that aggregators and storage units are likely to cooperate in the long-term using Nash bargaining theory. F. Mohamad et al. [132] proposed a method that optimally deployed BESSs and determined their capacity in a two-part framework to minimize solar energy curtailment, by considering network topology and power flow constraints to maximize their cooperation among BESSs by pooling all their capacities to store surplus solar power. Chen et al.[133] studied the coordination of groups of residential consumers for demand response. In addition, many scholars have pointed out that at this stage in Japan, the economic performance of BESS is heavily dependent on government subsidies, and we must seek new ways to improve the economic performance of BESS [134], [135]. Excitingly, through aggregation, BESS can participate in DR to relieve the pressure on the grid for peaking, saving the supply side expenditure on peaking plants. Therefore power companies are also willing to work with aggregators by paying a fee when there are enough regulable users to participate in DR. Astriani Y et al [136] indicated that the power companies needs to allocate around 40% of its DR profit so that the commercial customer's DR deployment costs are paid back within its lifetime. Thus, there is a great prospect for providing services through aggregating BESSs.

③ Energy aggregators

The overview of recent advances and future key benefits of demand-side management states that distributed generation should be integrated with demand response (DR) mechanisms[137] [138]. The combination of smart grid and energy storages and resultant policy recommendations have been discussed by Amoretti et al. and Zame et al. [139]. Contreras-Ocanaet al. showed that aggregators and storage units are likely to cooperate in the long-term using Nash bargaining theory. F. Mohamad et al. proposed a method that optimally deployed BESSs and determined their capacity in a two-part framework to minimize solar energy curtailment, by considering network topology and power flow constraints to maximize their cooperation among BESSs by pooling all their capacities to store surplus solar power. Chen et al. [140] studied the coordination of groups of residential consumers for demand response. In addition, many scholars have pointed out that at this stage in Japan, the economic performance of BESS is heavily dependent on government subsidies, and we must seek new ways to improve the economic performance of BESS. Excitingly, through aggregation, BESS can participate in DR to relieve the pressure on the grid for peaking, saving the supply side expenditure on peaking plants. Therefore, power companies are also willing to work with aggregators by paying a fee when there are enough regulable users to participate in DR. Astriani Y et al [141] indicated that the power companies needs to allocate around 40% of its DR profit so that the commercial customer's DR deployment costs are paid back within its lifetime. Thus, there is a great prospect for providing services through aggregating BESSs [142].

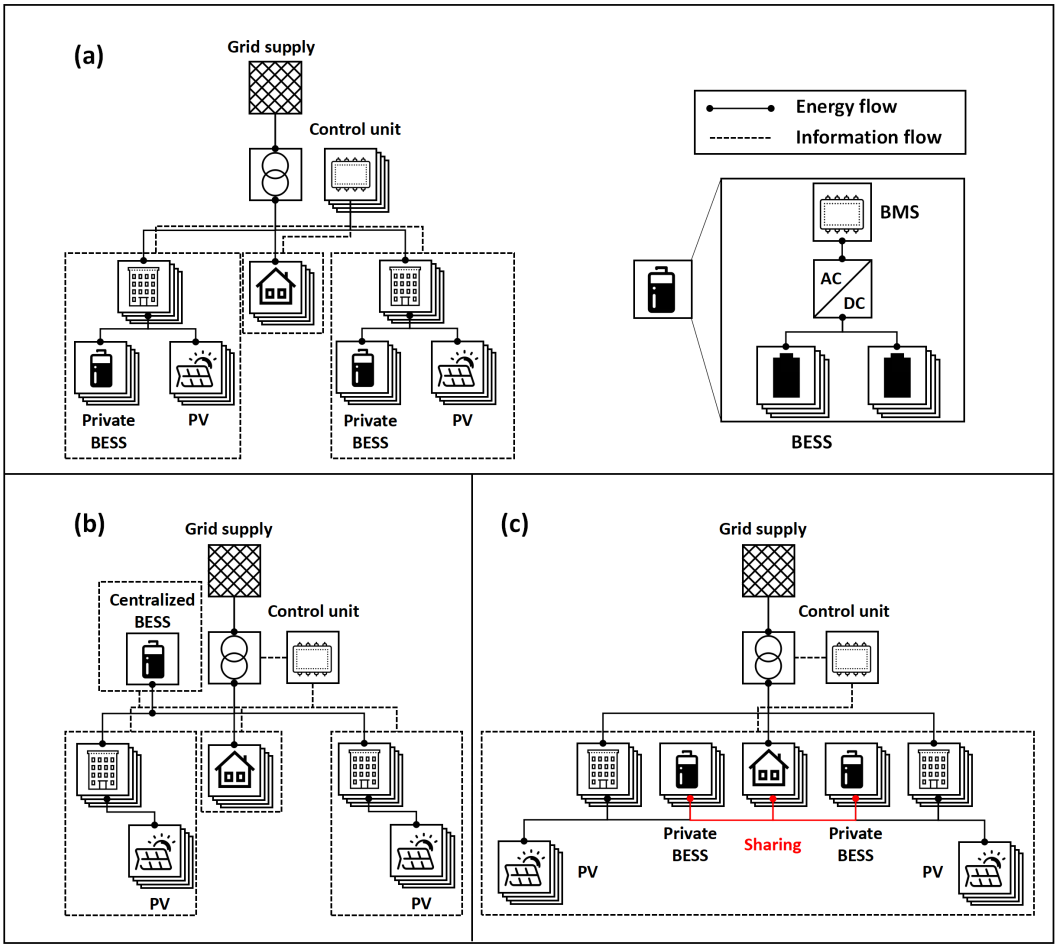

Fig.2-13 The operation strategies of three BESS sharing structure design approaches. (a), Individual design for distributed BESS; (b), Shared design for centralized BESS; (c), Shared design for distributed BESS

④ BESS ownership

To overcome the risk of accidents, high prices, and other barriers to BESS adoption, the type of ownership of BESS is gradually shifting from full ownership to shared ownership, resulting in a variety of business models [143] [144]. BESS-based energy sharing within the solar PV building community can refer to either energy sharing or storage sharing. Full ownership may pose a risk to the system owner due to high investment costs and risk liability, so shared ownership is often preferred by adopters in the early stages of BESS diffusion. Therefore, the type of ownership of BESS is an important factor to consider when planning for urban energy sharing. The ownership of BESS can be classified into the following three types: (i) individually owned BESS; (ii) community-owned BESS; and (iii) utility-owned BESS.

(i) Individually owned BESS: This is the most traditional type of ownership for owning and using BESS. In this type of ownership, an individual can own a BESS by purchasing it (i.e., assuming the full initial investment cost of the BESS) or by leasing it from a third party (i.e., paying for the use of the BESS.) An individually owned BESS is designed to maximize the

owner's profits through three business models: (i) net metering (i.e., billing the consumer for the net amount of electricity used); (ii) power purchase agreements (PPAs) (i.e., consumers can sell surplus electricity back to the grid); and (iii) peer-to-peer (P2P) energy trading (i.e., consumers can sell surplus electricity directly to their neighbors). Although this is the simplest type of having BESS, the utilization of BESS can be very low due to demand fluctuations. In addition, while BESS can potentially provide economic and environmental benefits, the upfront costs can be financially burdensome to consumers [145].

(ii) Community-owned BESS: With the rapid growth of the sharing economy worldwide, a new ownership concept of community-centric sharing has recently been introduced in the energy market. As part of this trend, community owned BESSs have emerged, where a group of consumers located in a community with defined boundaries own the BESS and share the electricity stored in it. The advantage of this ownership is that electricity is shared between groups within the energy sharing boundary without the high installation costs of BESS and renewable energy facilities. While the business model for BESS owned through the community depends on the installation environment of the BESS, customers within the community can essentially purchase or lease a portion of the energy facility or share the stored electricity.

(iii) Utility-owned BESS: Utility-owned BESS is a form of BESS ownership by the utility, primarily for the provision of industrial or grid-connected services. It is designed to maximize the social welfare of electricity consumers in the grid system. It allows electricity generated from renewable energy systems to be stored in the BESS and supplied to electricity consumers. In particular, large utility power plants can reduce peak demand and provide ancillary power services (i.e., frequency regulation, voltage control and load control).

⑤ The limitation of BESS sharing

Despite the academic and industrial results achieved with the development of BESS technologies, operations and management approaches, the applied technologies are still not sufficient to achieve carbon neutral cities. The following challenges need to be further addressed through the literature review.

First, since the application of BESS cannot be separated from the analysis, utilization and interaction of data, the current data collection and utilization technology of BESS application needs to be improved. Second, the current technology for BESS applications is segmented, allowing solutions and strategies for only one component of the microgrid. Second, the current technology of the BESS application is segmented, allowing solutions and strategies for only one component of the microgrid. Despite the evolving technologies in the field of energy and batteries, the lack of connectivity between individual technologies makes it difficult to fully integrate the various factors that affect energy generation and consumption. In addition, current technologies mainly analyze the initial investment costs of BESS in the planning phase. In the operational phase, truly integrated data-based solutions should be developed to effectively manage the energy performance of shared communities, including buildings with BESS, PV and EV. Third, BESS-related energy management systems have difficulty monitoring operational data. Therefore, inter operation ability must be ensured through technology integration to support a variety of smart devices and applications.

References

[1] Angstrom A. Solar and terrestrial radiation. Report to the international commission for solar research on actinometric investigations of solar and atmospheric radiation. Quarterly Journal of the Royal Meteorological Society. 1924;50:121-6.

[2] Prescott J. Evaporation from a water surface in relation to solar radiation. Trans Roy Soc S Aust. 1940;46:114-8.

[3] Asilevi PJ, Quansah E, Amekudzi LK, Annor T, Klutse NAB. Modeling the spatial distribution of Global Solar Radiation (GSR) over Ghana using the Ångström-Prescott sunshine duration model. Scientific African. 2019;4:e00094.

[4] Liu X, Mei X, Li Y, Porter JR, Wang Q, Zhang Y. Choice of the Ångström–Prescott coefficients: Are time-dependent ones better than fixed ones in modeling global solar irradiance? Energy Conversion and Management. 2010;51:2565-74.

[5] Liu X, Xu Y, Zhong X, Zhang W, Porter JR, Liu W. Assessing models for parameters of the Ångström–Prescott formula in China. Applied energy. 2012;96:327-38.

[6] Morf H. A stochastic solar irradiance model adjusted on the Ångström–Prescott regression. Solar Energy. 2013;87:1-21.

[7] Paulescu M, Stefu N, Calinoiu D, Paulescu E, Pop N, Boata R, et al. Ångström–Prescott equation: Physical basis, empirical models and sensitivity analysis. Renewable and Sustainable Energy Reviews. 2016;62:495-506.

[8] Hargreaves GH, Samani ZA. Estimating potential evapotranspiration. Journal of the irrigation and Drainage Division. 1982;108:225-30.

[9] Hargreaves GH, Samani ZA. Reference crop evapotranspiration from temperature. Applied engineering in agriculture. 1985;1:96-9.

[10] Almorox J, Bocco M, Willington E. Estimation of daily global solar radiation from measured temperatures at Cañada de Luque, Córdoba, Argentina. Renewable Energy. 2013;60:382-7.

[11] Li M-F, Tang X-P, Wu W, Liu H-B. General models for estimating daily global solar radiation for different solar radiation zones in mainland China. Energy conversion and management. 2013;70:139-48.

[12] Chang K, Zhang Q. Development of a solar radiation model considering the hourly sunshine duration for all-sky conditions – A case study for Beijing, China. Atmospheric Environment. 2020;234.

[13] Zhang Q, Huang J, Lang S. SYMPOSIUM PAPERS-HI-02-16 Recent Developments in Availability of International Weather Data-Development of Typical Year Weather Data for Chinese Locations. ASHRAE Transactions-American Society of Heating Refrigerating

Airconditioning Engin. 2002;108:1063-78.

[14] Chang K, Zhang Q. Improvement of the hourly global solar model and solar radiation for air-conditioning design in China. Renewable Energy. 2019;138:1232-8.

[15] Kim KH, Oh JK-W, Jeong W. Study on solar radiation models in South Korea for improving office building energy performance analysis. Sustainability. 2016;8:589.

[16] Kim KH, Baltazar J-C, Haberl JS. Evaluation of meteorological base models for estimating hourly global solar radiation in Texas. Energy Procedia. 2014;57:1189-98.

[17] S.M.Al-Alawi, H.A.Al-Hinai. An ANN-based approach for predicting global radiation in locations with no direct measurement instrumentation. Renewable Energy. 1998;14:199-204.

[18] Lazzús JA, Pérez Ponce AA, Marín J. Estimation of global solar radiation over the city of La Serena (Chile) using a neural network. Applied Solar Energy. 2011;47:66-73.

[19] Kaba K, Sarıgül M, Avcı M, Kandırmaz HM. Estimation of daily global solar radiation using deep learning model. Energy. 2018;162:126-35.

[20] Hassan MA, Khalil A, Kaseb S, Kassem MA. Exploring the potential of tree-based ensemble methods in solar radiation modeling. Applied Energy. 2017;203:897-916.

[21] Basaran K, Özçift A, Kılınç D. A new approach for prediction of solar radiation with using ensemble learning algorithm. Arabian Journal for Science and Engineering. 2019;44:7159-71.

[22] Gao Y, Miyata S, Akashi Y. Multi-step solar irradiation prediction based on weather forecast and generative deep learning model. Renewable Energy. 2022;188:637-50.

[23] Peng T, Zhang C, Zhou J, Nazir MS. An integrated framework of Bi-directional long-short term memory (BiLSTM) based on sine cosine algorithm for hourly solar radiation forecasting. Energy. 2021;221.

[24] Zhou Y, Liu Y, Wang D, Liu X, Wang Y. A review on global solar radiation prediction with machine learning models in a comprehensive perspective. Energy Conversion and Management. 2021;235.

[25] Gao Y, Miyata S, Akashi Y. Interpretable deep learning models for hourly solar radiation prediction based on graph neural network and attention. Applied Energy. 2022;321.

[26] Bird RE, Hulstrom RL. Simplified clear sky model for direct and diffuse insolation on horizontal surfaces. Solar Energy Research Inst., Golden, CO (USA); 1981.

[27] Chen R, Kang E, Ji X, Yang J, Wang J. An hourly solar radiation model under actual weather and terrain conditions: A case study in Heihe river basin. Energy. 2007;32:1148-57.

[28] Su G, Zhang S, Hu M, Yao W, Li Z, Xi Y. The modified layer-by-layer weakening solar radiation models based on relative humidity and air quality index. Energy. 2022;239.

[29] Chaisson EJ. Long-term global heating from energy usage. Eos, Transactions American

Geophysical Union. 2008;89:253-4.

[30] Stritih U. Increasing the efficiency of PV panel with the use of PCM. Renewable Energy. 2016;97:671-9.

[31] Skoplaki E, Palyvos JA. Operating temperature of photovoltaic modules: A survey of pertinent correlations. Renewable energy. 2009;34:23-9.

[32] Faiman D. Assessing the outdoor operating temperature of photovoltaic modules. Progress in Photovoltaics: Research and Applications. 2008;16:307-15.

[33] Koehl M, Heck M, Wiesmeier S, Wirth J. Modeling of the nominal operating cell temperature based on outdoor weathering. Solar Energy Materials and Solar Cells. 2011;95:1638-46.

[34] Skoplaki E, Boudouvis A, Palyvos J. A simple correlation for the operating temperature of photovoltaic modules of arbitrary mounting. Solar energy materials and solar cells. 2008;92:1393-402.

[35] Lobera DT, Valkealahti S. Dynamic thermal model of solar PV systems under varying climatic conditions. Solar energy. 2013;93:183-94.

[36] Khalilpour KR, Vassallo A. Technoeconomic parametric analysis of PV-battery systems. Renewable Energy. 2016;97:757-68.

[37] Halliday J, Markvart T, Ross J. Battery management for PV systems. Power Engineer. 2003;17:46-.

[38] Appelbaum J, Braunstein A, Bani J. Performance analysis of a solar-electrical system with a load and storage batteries. Energy Conversion. 1977;16:105-10.

[39] Mokhtari G, Nourbakhsh G, Zare F, Ghosh A. Improving the penetration level of PVs using DC link for residential buildings. Energy and Buildings. 2014;72:80-6.

[40] Akinyele D, Rayudu R, Nair N. Development of photovoltaic power plant for remote residential applications: The socio-technical and economic perspectives. Applied Energy. 2015;155:131-49.

[41] Karakoulidis K, Mavridis K, Bandekas D, Adoniadis P, Potolias C, Vordos N. Techno-economic analysis of a stand-alone hybrid photovoltaic-diesel–battery-fuel cell power system. Renewable Energy. 2011;36:2238-44.

[42] Komiyama R, Fujii Y. Optimal integration assessment of solar PV in Japan's electric power grid. Renewable Energy. 2019;139:1012-28.

[43] Guichi A, Talha A, Berkouk EM, Mekhilef S. Energy management and performance evaluation of grid connected PV-battery hybrid system with inherent control scheme. Sustainable cities and society. 2018;41:490-504.

[44] Wu Z, Tazvinga H, Xia X. Demand side management of photovoltaic-battery hybrid system. Applied Energy. 2015;148:294-304.

[45] Nandi SK, Ghosh HR. A wind–PV-battery hybrid power system at Sitakunda in Bangladesh. Energy Policy. 2009;37:3659-64.

[46] Rai N, Rai B. Control of fuzzy logic based PV-battery hybrid system for stand-alone DC applications. Journal of Electrical Systems and Information Technology. 2018;5:135-43.

[47] Al Shawa B. The ability of Building Stock Energy Models (BSEMs) to facilitate the sector's climate change target in the face of socioeconomic uncertainties: A review. Energy and Buildings. 2022;254:111634.

[48] Tofighi A, Kalantar M. Power management of PV/battery hybrid power source via passivity-based control. Renewable Energy. 2011;36:2440-50.

[49] Li Y, Gao W, Ruan Y. Performance investigation of grid-connected residential PV-battery system focusing on enhancing self-consumption and peak shaving in Kyushu, Japan. Renewable energy. 2018;127:514-23.

[50] Shaqour A, Farzaneh H, Yoshida Y, Hinokuma T. Power control and simulation of a building integrated stand-alone hybrid PV-wind-battery system in Kasuga City, Japan. Energy Reports. 2020;6:1528-44.

[51] Global A. Global status report for buildings and construction. Global Alliance for Buildings and Construction. 2020.

[52] Cozzi L, Gould T, Bouckart S, Crow D, Kim T, Mcglade C, et al. World Energy Outlook 2020. vol. 2020;2050:1-461.

[53] Child M, Bogdanov D, Breyer C. The role of storage technologies for the transition to a 100% renewable energy system in Europe. Energy Procedia. 2018;155:44-60.

[54] Zhang C, Wei Y-L, Cao P-F, Lin M-C. Energy storage system: Current studies on batteries and power condition system. Renewable and Sustainable Energy Reviews. 2018;82:3091-106.

[55] Zhao H, Wu Q, Hu S, Xu H, Rasmussen CN. Review of energy storage system for wind power integration support. Applied energy. 2015;137:545-53.

[56] Comodi G, Giantomassi A, Severini M, Squartini S, Ferracuti F, Fonti A, et al. Multi-apartment residential microgrid with electrical and thermal storage devices: Experimental analysis and simulation of energy management strategies. Applied Energy. 2015;137:854-66.

[57] Zheng Y, Dong ZY, Luo FJ, Meng K, Qiu J, Wong KP. Optimal allocation of energy storage system for risk mitigation of DISCOs with high renewable penetrations. IEEE Transactions on Power Systems. 2013;29:212-20.

[58] Wong LA, Ramachandaramurthy VK, Taylor P, Ekanayake J, Walker SL, Padmanaban S. Review on the optimal placement, sizing and control of an energy storage system in the distribution network. Journal of Energy Storage. 2019;21:489-504.

[59] Mehrjerdi H. Simultaneous load leveling and voltage profile improvement in

distribution networks by optimal battery storage planning. Energy. 2019;181:916-26.

[60] Van der Linden S. Bulk energy storage potential in the USA, current developments and future prospects. Energy. 2006;31:3446-57.

[61] Energy stroage study-Funding and knowledge sharing priorities. 2015.

[62] Divya KC, Østergaard J. Battery energy storage technology for power systems—An overview. Electric Power Systems Research. 2009;79:511-20.

[63] Dunn BK, Haresh; Tarascon, Jean-Marie. Electrical Energy Storage for the Grid: A Battery of Choices. Materials for grid energy. 2011.

[64] Mahlia TMI, Saktisahdan TJ, Jannifar A, Hasan MH, Matseelar HSC. A review of available methods and development on energy storage; technology update. Renewable and Sustainable Energy Reviews. 2014;33:532-45.

[65] Mahmud N, Zahedi A. Review of control strategies for voltage regulation of the smart distribution network with high penetration of renewable distributed generation. Renewable and Sustainable Energy Reviews. 2016;64:582-95.

[66] Denholm P, O'Connell M, Brinkman G, Jorgenson J. Overgeneration from solar energy in california. a field guide to the duck chart. National Renewable Energy Lab.(NREL), Golden, CO (United States); 2015.

[67] Doroshenko M, Keshav S, Rosenberg C. Flattening the duck curve using grid-friendly solar panel orientation. Proceedings of the Ninth International Conference on Future Energy Systems2018. p. 375-7.

[68] Luthander R, Widén J, Munkhammar J, Lingfors D. Self-consumption enhancement and peak shaving of residential photovoltaics using storage and curtailment. Energy. 2016;112:221-31.

[69] Ranaweera I, Midtgård O-M. Optimization of operational cost for a grid-supporting PV system with battery storage. Renewable Energy. 2016;88:262-72.

[70] Pallonetto F, De Rosa M, D'Ettorre F, Finn DP. On the assessment and control optimisation of demand response programs in residential buildings. Renewable and Sustainable Energy Reviews. 2020;127:109861.

[71] Pang Y, He Y, Jiao J, Cai H. Power load demand response potential of secondary sectors in China: The case of western Inner Mongolia. Energy. 2020;192:116669.

[72] Whittingham MS. History, evolution, and future status of energy storage. Proceedings of the IEEE. 2012;100:1518-34.

[73] Mahlia T, Saktisahdan T, Jannifar A, Hasan M, Matseelar H. A review of available methods and development on energy storage; technology update. Renewable and sustainable energy reviews. 2014;33:532-45.

[74] Ibrahim H, Ilinca A, Perron J. Energy storage systems—Characteristics and comparisons.

Renewable and sustainable energy reviews. 2008;12:1221-50.

[75] Lund PD, Lindgren J, Mikkola J, Salpakari J. Review of energy system flexibility measures to enable high levels of variable renewable electricity. Renewable and sustainable energy reviews. 2015;45:785-807.

[76] Australia A. Energy Storage Study: Funding and Knowledge Sharing Priorities. Sydney, Australia: AECOM Australia; 2015.

[77] Walawalkar R, Apt J, Mancini R. Economics of electric energy storage for energy arbitrage and regulation in New York. Energy Policy. 2007;35:2558-68.

[78] Sparacino RJKGFRAR. Economic analysis of grid level energy storage for the application of load leveling. 2012 IEEE Power and Energy Society General Meeting. 2012.

[79] Lu C, Xu H, Pan X, Song J. Optimal Sizing and Control of Battery Energy Storage System for Peak Load Shaving. Energies. 2014;7:8396-410.

[80] Saboori H, Hemmati R, Abbasi V. Multistage distribution network expansion planning considering the emerging energy storage systems. Energy Conversion and Management. 2015;105:938-45.

[81] Saboori H, Hemmati R, Jirdehi MA. Reliability improvement in radial electrical distribution network by optimal planning of energy storage systems. Energy. 2015;93:2299-312.

[82] Trivedi A, Chong Aih H, Srinivasan D. A stochastic cost–benefit analysis framework for allocating energy storage system in distribution network for load leveling. Applied Energy. 2020;280.

[83] Duerr S, Ababei C, Ionel DM. A Case for Using Distributed Energy Storage for Load Balancing and Power Loss Minimization in Distribution Networks. Electric Power Components and Systems. 2020;48:1063-76.

[84] Jankowiak C, Zacharopoulos A, Brandoni C, Keatley P, MacArtain P, Hewitt N. Assessing the benefits of decentralised residential batteries for load peak shaving. Journal of Energy Storage. 2020;32:101779.

[85] Boglou V, Karavas CS, Karlis A, Arvanitis K. An intelligent decentralized energy management strategy for the optimal electric vehicles' charging in low - voltage islanded microgrids. International Journal of Energy Research. 2022;46:2988-3016.

[86] Mengelkamp E, Gärttner J, Rock K, Kessler S, Orsini L, Weinhardt C. Designing microgrid energy markets: A case study: The Brooklyn Microgrid. Applied Energy. 2018;210:870-80.

[87] Morstyn T, Teytelboym A, McCulloch MD. Bilateral contract networks for peer-to-peer energy trading. IEEE Transactions on Smart Grid. 2018;10:2026-35.

[88] An J, Yan D, Guo S, Gao Y, Peng J, Hong T. An improved method for direct incident solar radiation calculation from hourly solar insolation data in building energy simulation.

Energy and Buildings. 2020;227.

[89] Gandhi O, Kumar DS, Rodríguez-Gallegos CD, Srinivasan D. Review of power system impacts at high PV penetration Part I: Factors limiting PV penetration. Solar Energy. 2020;210:181-201.

[90] Sovacool BK, Furszyfer Del Rio D, Griffiths S. Contextualizing the Covid-19 pandemic for a carbon-constrained world: Insights for sustainability transitions, energy justice, and research methodology. Energy Research & Social Science. 2020;68.

[91] Shin KJ, Managi S. Liberalization of a retail electricity market: Consumer satisfaction and household switching behavior in Japan. Energy Policy. 2017;110:675-85.

[92] Nicolli F, Vona F. Energy market liberalization and renewable energy policies in OECD countries. Energy Policy. 2019;128:853-67.

[93] Vand B, Ruusu R, Hasan A, Manrique Delgado B. Optimal management of energy sharing in a community of buildings using a model predictive control. Energy Conversion and Management. 2021;239.

[94] Jiang A, Yuan H, Li D. A two-stage optimization approach on the decisions for prosumers and consumers within a community in the Peer-to-peer energy sharing trading. International Journal of Electrical Power & Energy Systems. 2021;125.

[95] Taşcıkaraoğlu A. Economic and operational benefits of energy storage sharing for a neighborhood of prosumers in a dynamic pricing environment. Sustainable Cities and Society. 2018;38:219-29.

[96] Tushar W, Chai B, Yuen C, Huang S, Smith DB, Poor HV, et al. Energy Storage Sharing in Smart Grid: A Modified Auction-Based Approach. IEEE Transactions on Smart Grid. 2016;7:1462-75.

[97] Kang H, Jung S, Lee M, Hong T. How to better share energy towards a carbon-neutral city? A review on application strategies of battery energy storage system in city. Renewable and Sustainable Energy Reviews. 2022;157:112113.

[98] Huang P, Lovati M, Zhang X, Bales C. A coordinated control to improve performance for a building cluster with energy storage, electric vehicles, and energy sharing considered. Applied Energy. 2020;268:114983.

[99] Roberts M. Impact of shared battery energy storage systems on photovoltaic self-consumption and electricity bills in apart.

[100] Zheng S, Huang G, Lai AC. Techno-economic performance analysis of synergistic energy sharing strategies for grid-connected prosumers with distributed battery storages. Renewable Energy. 2021;178:1261-78.

[101] Henni S, Staudt P, Weinhardt C. A sharing economy for residential communities with PV-coupled battery storage: Benefits, pricing and participant matching. Applied Energy. 2021;301:117351.

[102] He L, Liu Y, Zhang J. Peer-to-peer energy sharing with battery storage: Energy pawn in the smart grid. Applied Energy. 2021;297:117129.

[103] Dai R, Charkhgard H. Bi-objective mixed integer linear programming for managing building clusters with a shared electrical energy storage. Computers & Operations Research. 2018;96:173-87.

[104] Rappaport RD, Miles J. Cloud energy storage for grid scale applications in the UK. Energy Policy. 2017;109:609-22.

[105] Datta M, Senjyu T, Yona A, Funabashi T, Kim C-H. A coordinated control method for leveling PV output power fluctuations of PV–diesel hybrid systems connected to isolated power utility. IEEE Transactions on Energy Conversion. 2009;24:153-62.

[106] Karavas C-SG, Plakas KA, Krommydas KF, Kurashvili AS, Dikaiakos CN, Papaioannou GP. A review of wide-area monitoring and damping control systems in Europe. 2021 IEEE Madrid PowerTech. 2021:1-6.

[107] Mekikis P-V, Antonopoulos A, Kartsakli E, Lalos AS, Alonso L, Verikoukis C. Information exchange in randomly deployed dense WSNs with wireless energy harvesting capabilities. IEEE Transactions on Wireless Communications. 2016;15:3008-18.

[108] Li Y, Hu S, Hoare C, O'Donnell J, García-Castro R, Vega-Sánchez S, et al. An information sharing strategy based on linked data for net zero energy buildings and clusters. Automation in Construction. 2021;124:103592.

[109] Bandara KY, Thakur S, Breslin J. Flocking-based decentralised double auction for P2P energy trading within neighbourhoods. International Journal of Electrical Power & Energy Systems. 2021;129.

[110] Mengelkamp E, Gärttner J, Rock K, Kessler S, Orsini L, Weinhardt C. Designing microgrid energy markets. Applied Energy. 2018;210:870-80.

[111] Khalid R, Javaid N, Almogren A, Javed MU, Javaid S, Zuair M. A Blockchain-Based Load Balancing in Decentralized Hybrid P2P Energy Trading Market in Smart Grid. IEEE Access. 2020;8:47047-62.

[112] Morstyn T, Teytelboym A, McCulloch MD. Bilateral Contract Networks for Peer-to-Peer Energy Trading. IEEE Transactions on Smart Grid. 2019;10:2026-35.

[113] Cintuglu MH, Martin H, Mohammed OA. Real-Time Implementation of Multiagent-Based Game Theory Reverse Auction Model for Microgrid Market Operation. IEEE Transactions on Smart Grid. 2015;6:1064-72.

[114] Cui S, Wang YW, Liu N. Distributed game‐based pricing strategy for energy sharing in microgrid with PV prosumers. IET Renewable Power Generation. 2017;12:380-8.

[115] Long C, Wu J, Zhou Y, Jenkins N. Peer-to-peer energy sharing through a two-stage aggregated battery control in a community Microgrid. Applied Energy. 2018;226:261-76.

[116] Jia L, Tong L. Dynamic Pricing and Distributed Energy Management for Demand Response. IEEE Transactions on Smart Grid. 2016;7:1128-36.

[117] Olivella-Rosell P, Bullich-Massagué E, Aragüés-Peñalba M, Sumper A, Ottesen SØ, Vidal-Clos J-A, et al. Optimization problem for meeting distribution system operator requests in local flexibility markets with distributed energy resources. Applied Energy. 2018;210:881-95.

[118] Ottesen SØ, Tomasgard A, Fleten S-E. Prosumer bidding and scheduling in electricity markets. Energy. 2016;94:828-43.

[119] Motalleb M, Ghorbani R. Non-cooperative game-theoretic model of demand response aggregator competition for selling stored energy in storage devices. Applied Energy. 2017;202:581-96.

[120] Lüth A, Zepter JM, Crespo del Granado P, Egging R. Local electricity market designs for peer-to-peer trading: The role of battery flexibility. Applied Energy. 2018;229:1233-43.

[121] Nguyen S, Peng W, Sokolowski P, Alahakoon D, Yu X. Optimizing rooftop photovoltaic distributed generation with battery storage for peer-to-peer energy trading. Applied Energy. 2018;228:2567-80.

[122] Dong S, Kremers E, Brucoli M, Rothman R, Brown S. Techno-enviro-economic assessment of household and community energy T storage in the UK. Energy Conversion and Management. 2020.

[123] Parra D, Norman SA, Walker GS, Gillott M. Optimum community energy storage system for demand load shifting. Applied Energy. 2016;174:130-43.

[124] Rodrigues DL, Ye X, Xia X, Zhu B. Battery energy storage sizing optimisation for different ownership structures in a peer-to-peer energy sharing community. Applied Energy. 2020;262.

[125] Huang P, Sun Y, Lovati M, Zhang X. Solar-photovoltaic-power-sharing-based design optimization of distributed energy storage systems for performance improvements. Energy. 2021;222.

[126] Jimada-Ojuolape B, Teh J. Impact of the Integration of Information and Communication Technology on Power System Reliability: A Review. IEEE Access. 2020;8:24600-15.

[127] Jimada-Ojuolape B, Teh J. Surveys on the reliability impacts of power system cyber–physical layers. Sustainable Cities and Society. 2020;62.

[128] Kakran S, Chanana S. Smart operations of smart grids integrated with distributed generation: A review. Renewable and Sustainable Energy Reviews. 2018;81:524-35.

[129] Amoretti M. Towards a peer-to-peer hydrogen economy framework. International Journal of Hydrogen Energy. 2011;36:6376-86.

[130] Zame KK, Brehm CA, Nitica AT, Richard CL, Schweitzer Iii GD. Smart grid and energy storage: Policy recommendations. Renewable and Sustainable Energy Reviews. 2018;82:1646-54.

[131] Contreras-Ocana JE, Ortega-Vazquez MA, Zhang B. Participation of an Energy Storage Aggregator in Electricity Markets. IEEE Transactions on Smart Grid. 2019;10:1171-83.

[132] Mohamad F, Teh J, Lai C-M. Optimum allocation of battery energy storage systems for power grid enhanced with solar energy. Energy. 2021;223.

[133] Chen C, Wang J, Kishore S. A Distributed Direct Load Control Approach for Large-Scale Residential Demand Response. IEEE Transactions on Power Systems. 2014;29:2219-28.

[134] Wang Y, Gao W, Qian F, Li Y. Evaluation of economic benefits of virtual power plant between demand and plant sides based on cooperative game theory. Energy Conversion and Management. 2021;238.

[135] Qian F, Gao W, Yang Y, Yu D. Economic optimization and potential analysis of fuel cell vehicle-to-grid (FCV2G) system with large-scale buildings. Energy Conversion and Management. 2020;205.

[136] Astriani Y, Shafiullah GM, Shahnia F. Incentive determination of a demand response program for microgrids. Applied Energy. 2021;292.

[137] Hocaoglu FO, Serttas F. A novel hybrid (Mycielski-Markov) model for hourly solar radiation forecasting. Renewable Energy. 2017;108:635-43.

[138] Sun L, Qiu J, Han X, Yin X, Dong ZY. Capacity and energy sharing platform with hybrid energy storage system: An example of hospitality industry. Applied Energy. 2020;280:115897.

[139] Prina MG, Manzolini G, Moser D, Nastasi B, Sparber W. Classification and challenges of bottom-up energy system models-A review. Renewable and Sustainable Energy Reviews. 2020;129:109917.

[140] Das CK, Bass O, Kothapalli G, Mahmoud TS, Habibi D. Overview of energy storage systems in distribution networks: Placement, sizing, operation, and power quality. Renewable and Sustainable Energy Reviews. 2018;91:1205-30.

[141] Hwangbo S-W, Kim B-J, Kim J-H. Application of economic operation strategy on battery energy storage system at Jeju. 2013 IEEE PES Conference on Innovative Smart Grid Technologies (ISGT Latin America): IEEE; 2013. p. 1-8.

[142] Wang Y, Gao W, Qian F, Li Y. Evaluation of economic benefits of virtual power plant between demand and plant sides based on cooperative game theory. Energy Conversion and Management. 2021;238:114180.

[143] Sharda S, Singh M, Sharma K. Demand side management through load shifting in IoT based HEMS: Overview, challenges and opportunities. Sustainable Cities and Society.

2021;65:102517.

[144] Kim S, Kwon M, Choi S. Operation and control strategy of a new hybrid ESS-UPS system. IEEE Transactions on Power Electronics. 2017;33:4746-55.

[145] Berrada A, Loudiyi K, Zorkani I. Valuation of energy storage in energy and regulation markets. Energy. 2016;115:1109-18.

Chapter 3

METHODOLOGY

METHODOLOGY

3.1 Methodology of solar radiation model development 3-1

3.1.1 Analysis of global solar radiation models 3-1

3.1.2 Methods 3-1

3.1.3 Processing flow 3-2

3.1.4 Statistical test methods 3-2

3.2 Methodology of solar PV generation model 3-3

3.2.1 PV cell 3-3

3.3 Methodology of battery bank model 3-4

3.4 Methodology of PV battery system 3-5

3.4.1 System description 3-5

3.4.2 Energy balance 3-6

3.4.3 Aggregated control 3-6

3.4.4 Adaptive power dispatch 3-11

3.5 Methodology of energy sharing 3-15

3.5.1 Internal pricing mechanism 3-15

3.5.2 Aggregator managed demand response 3-15

3.5.3 Energy flow and simulation 3-16

3.5.4 Energy losses 3-20

3.5.5 Intelligent optimization algorithm 3-21

3.5.6 Processes 3-23

3.5.7 Evaluation Indicators 3-25

References 3-25

3.1 Methodology of solar radiation model development

3.1.1 Analysis of global solar radiation models

Many global solar radiation models attempt to estimate the ratio between the radiation incident on the surface water plane and a radiation threshold (usually extraterrestrial radiation). Firstly, it is dimensionless and has a clear physical meaning, it can be expressed as the transmittance of solar radiation in the atmosphere on a clear or cloudy day. Therefore, the ratio can be referred to as the clearness index. As described in Section 1.2, a large number of studies [1] [2]have tried to establish a functional relationship between the clearness index and general meteorological parameters (e.g. sunshine duration, temperature, humidity, and their combinations), and this class of models can be described by the following equation:

$$I/I_0 = f(\sigma) \tag{3-1}$$

where I is the global solar radiation. I_0 is the extraterrestrial solar radiation. $f(\sigma)$ is a function expression containing meteorological parameters. They are mostly accurate when dealing with monthly values or daily resolution forecasts. This is because the meteorological parameters used provide feedback on the seasonal variation of solar radiation (accumulated values over time). But most of these models are not applicable when the resolution becomes hourly or instantaneous values. The reason is that a denominator close to zero due to the formal characteristics of the fraction can lead to a large amount of computational error in the prediction results. Normally, the daily accumulated value of extraterrestrial solar radiation in Japan is about 10~40 MJ/m2, while at sunrise and sunset, the extraterrestrial solar radiation is close to zero and this cannot be ignored. Also, the distribution of solar radiation is not continuous and does not satisfy L'Hospital's rule. Therefore, the limit value of the ratio of two infinitesimals cannot be found by deriving the derivative. In addition, since the negative quadrature of X is a growth function, errors in the observation and recording process can also cause unacceptable errors.

In addition, in fine-grained solar radiation forecasting efforts, transient changes in the state of the sky can lead to a substantial increase in the randomness of the solar radiation distribution. Individual seasonal meteorological parameters such as temperature do not correlate well with instantaneous solar radiation. Therefore, a combination of multiple meteorological parameters especially physical quantities describing the state of the sky is a better choice.

3.1.2 Methods

The typical solar radiation weakening model for global solar radiation can be obtained using Eq.(A1) to Eq.(A7) in A.2. It is easy to understand that the typical weakening model functions the layer-by-layer weakening process of solar radiation as the transmittance of each layer to the radiation as shown in the Eq.(A2). Although the physical meaning of the expression is well defined, the complexity of the equation is significant. In addition, cloud cover is neglected in the typical weakening model because it is difficult to obtain by satellite retrieval, which is regarded as an influential factor in solar radiation estimation.

In an attempt to reduce the computational complexity while maintaining the physical meaning of the model. We propose the conceptual weakening model as follows:

$$I = I_0 - \Delta I \tag{3-2}$$

$$\Delta I = c_4 \cdot (c_1 \cdot L_a + c_2 \cdot L_w + c_3 \cdot L_c + c_0) \tag{3-3}$$

3.1.3 Processing flow

In this paper, based on the layer-by-layer weakening solar radiation, easily obtainable surface meteorological parameters are utilized to establish the weakened layer as a function of solar radiation in the following process:

① Data filtering. The raw data is first screened for missing values and outliers. Due to limitations in observation technology, weather stations will only provide weather type, cloud cover, and visibility at 3-hour resolution until 2019. Therefore, in order to maintain data consistency, data sets containing all of the above parameters are selected as data sources for the following analysis. After screening, the constructed dataset contains 205,722 sets of measurement data, of which 184,382 sets of data are used to build the model and 21,340 sets of data are used to verify the accuracy of the model. The data availability for each observation point is shown in.

② Modeling of solar radiation. The weakening value of solar radiation in the atmosphere is used as a medium to establish the functional relationship between meteorological parameters and the actual solar radiation received on the horizontal surface. Using the solar radiation data set from 1st January 2000 to 31st December 2018, the conventional functional forms such as exponential function, linear function, quadratic polynomial, and cubic polynomial are compared and analyzed. The best functional equation is determined.

③ Model Validation. Finally, the proposed model is validated by the solar radiation measured in seven locations in Japan from 1st January 2019 to 31st December 2021 under 15 different weather conditions (which is summarized into three sky states), and the performance of the proposed model is evaluated.

3.1.4 Statistical test methods

In the existing literature, there are several statistical test methods used to evaluate the performance of the hourly solar radiation methods. The relative standard error (RSE), the root mean square error (RMSE), the relative root mean square error (rRMSE), Correlation coefficient (R), and Nash-Sutcliffe Equation (NSE) and are adopted in this study.

① Relative standard deviation (RSE)

The relative standard error can be calculated as follow:

$$RSE = \sqrt{\frac{1}{n}\sum_{i=1}^{n}\left(\frac{e_i - m_i}{m_i}\right)^2} \tag{3-4}$$

where e_i is the estimated value and m_i is the measured value.

② Root mean square error [3] (RMSE)

The root mean square error can be calculated as follow:

$$RMSE = \sqrt{\frac{1}{n}\sum_{i=1}^{n}(e_i - m_i)^2} \tag{3-5}$$

where e_i is the estimated value and m_i is the measured value.

③ Relative root mean square error (rRMSE)

The relative root mean square error can be calculated as follow:

$$rRMSE = \frac{\sqrt{\frac{1}{n}\sum_{i=1}^{n}(e_i - m_i)^2}}{m_a} \times 100\% \tag{3-6}$$

where e_i is the estimated value and m_i is the measured value. where is the average value of the measured value.

④ Correlation coefficient (R)

The correlation coefficient can be calculated as follow:

$$R = \frac{\sum\left((m_i - m_a)(e_i - e_a)\right)}{\sqrt{\sum(m_i - m_a)^2 \sum(e_i - e_a)^2}} \tag{3-7}$$

where e_i is the estimated value and m_i is the measured value. where is the average value of the measured value.

⑤ Nash-Sutcliffe equation [4] (NSE)

The Nash-Sutcliffe equation can be calculated as follow:

$$NSE = 1 - \frac{\sum(m_i - e_i)^2}{\sum(m_i - m_a)^2} \tag{3-8}$$

3.2 Methodology of solar PV generation model

3.2.1 PV cell

In order to accurately design the considered hybrid system, it is crucial to have the hourly solar radiation. The weather data in Fukuoka is provided by Japan Meteorological Agency. This paper adopt the Panasonic module HIT N245 as the objection of PV module. The basic information is shown in Table 2. The generated power of the PV module, by considering the received solar irradiance, can be determined by using Eq. (9) [5] [6]:

$$p_{pv}(t) = P_{R,pv} \times (\frac{R}{R_{ref}}) \times [1 + NT \times (T_c - T_{ref})] \tag{3-9}$$

where $p_{pv}(t)$, $P_{R,PV}$, and R refer to the produced power by a PV module at time (t), the rated power of the utilized panel, and solar radiation, respectively. R_{ref} and T_{ref} denote the reference solar radiation (1000 W/m^2) and reference temperature (conventionally considered equal to 25℃), respectively. The panel temperature coefficient is shown by N_T and equals to

$-3.7 \times 10^{-3}(1/℃)$ for mono and polycrystalline silicon cells [7]. The temperature of the cell can be determined by employing Eq. (10) as:

$$T_c = T_{air} + [(\frac{NOCT - 20}{800}) \times R] \tag{3-10}$$

where T_{air}, R and T_c are the ambient temperature (℃), solar radiation and the normal operating cell temperature (℃), respectively. $NOCT$ is a specification of the cell and is declared by the cell producer. By considering the number of panels as N_{pv}, the total generated power is determined by employing Eq. (11) as:

$$C_{pv} = N_{pv} \times p_{pv}(t) \tag{3-11}$$

Table 3-1 The parameters of PV array

Parameters of PV	Values
Max power (Wp)	245
Voc (V)	53.0
Isc (A)	5.86
Temperature (NOCT)	44
Lifetime (year)	30
Price (yen/kW)	250000

3.3 Methodology of battery bank model

In recent years, battery energy storage technology has developed greatly [8]. Among the many battery technologies that meet the requirements of large-scale energy storage, the overall characteristics of NAS batteries are most suitable for large-scale energy storage system applications, based on a combination of factors such as energy efficiency, installation cost, rated power discharge capacity and the size of the installation site [9, 10]. We chose NAS batteries as the power storage technology. NAS batteries have high capacity with no significant self-discharge and are very safe because they do not use toxic metals [10]. In addition, it has a high charge/discharge tolerance with an expected lifetime of 15 years. A crucial feature of BESS [11]is the time coupling characteristic related to state of charge (SOC). During the charging and discharging process, the SOC (%) dynamics are defined by (12) and (13), respectively as:

$$SOC(t+1) = SOC(t) + \frac{\eta_{cha} \cdot \sum pw^j(t) \cdot \Delta T}{Cap^j} \tag{3-12}$$

$$SOC(t+1) = SOC(t) - \frac{\sum pw^j(t) \cdot \Delta T}{\eta_{dis} \cdot Cap^j} \tag{3-13}$$

where $SOC(t)$, s, yr denotes the state of charge of ESS at time period t in the year yr, η_{cha} , $\eta_{dis}$and Cap^j denote the charging and discharging efficiency and energy capacity of building j, respectively, of BESS. The BESS operation optimization is subject to the following constraints.

① SOC limit constraint

$$SOC_{\min} \le SOC(t) \le SOC_{\max} \tag{3-14}$$

where SOC_{min} and SOC_{max} are the lower and upper limits of SOC.

② ESS operation power limit constraint

$$-pwc \le pw \le pwc \tag{3-15}$$

where pwc denotes the rated power capacity of BESS. In our paper, in order to investigate the long-term economic potential of batteries with different sharing structures, we adopted a mature and commercially available NAS battery system for its field-proven 4,500 full cycle discharges and stabilized capability of charging and discharging. The rated power capacity of BESS is 16% of its capacity [10].

Table 3-2 The parameters of battery bank

Parameters of battery	Values
Type	NAS
Working temperature (℃)	300
Max duration (h)	6
Cycle number	4500
Lifetime (year)	15
Price (yen/kWh)	25000

3.4 Methodology of PV battery system

3.4.1 System description

In this study, the grid-connected photovoltaic battery (PVB) system contains photovoltaic (PV) modules, battery bank, converter, controller, the load, the public grid, and the power supplier illustrated in Fig.2. The control system is a critical component of accepting hourly peak shaving instructions and executing on the demand side. The main principle of peak shaving and energy flow is plotted in Fig. 6. The energy flow based on the hourly distribution of influential factors is obtained. The procedure involves the calculation of the energy production by each source, which makes the modeling of components necessary. The details of the modeling and dispatch strategy are represented in this section.

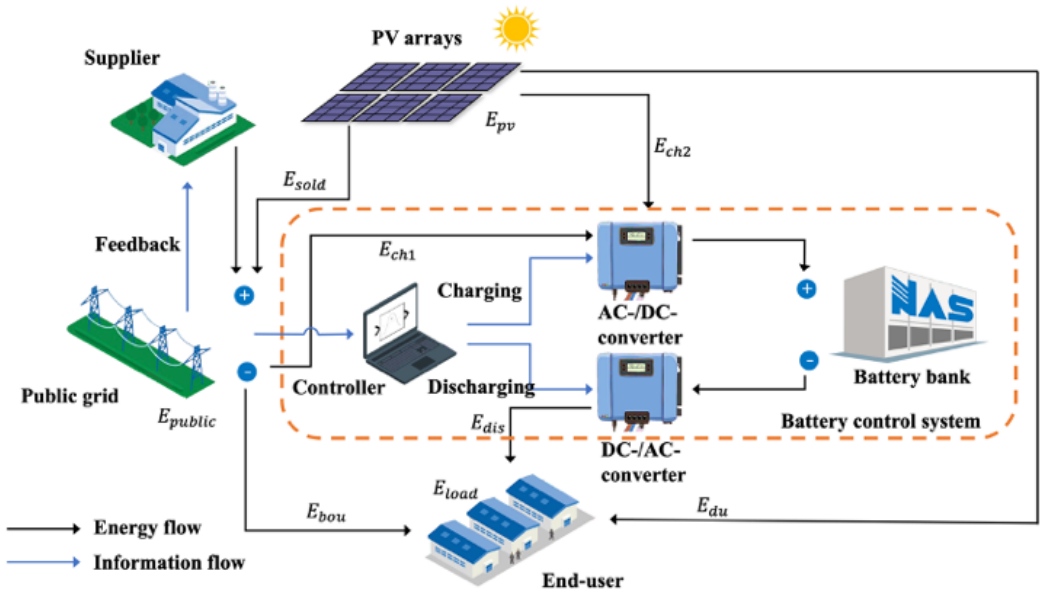

Fig. 3-1 Layout of the grid-connected PV-battery system

3.4.2 Energy balance

Energy balance is the core part of any renewable energy-based system. As expressed in Eq. (1~3), the fist equation is determined as electricity balance of PV system, including PV generation production E_{pv} (kWh), PV direct-used production E_{du} (kWh), electricity sold back to the grid E_{sold} (kWh), battery charge from the PV production E_{ch1} (kWh), energy loss in different electricity conversion steps E_{loss1} (kWh). The second equation is determined as electricity balance of battery system, including battery charge from the grid E_{ch1} (kWh), battery charge from the PV production E_{ch2} (kWh), energy loss in different electricity conversion steps E_{loss2} (kWh). The third equation is determined as electricity balance of Grid-Connected system, including grid injection E_{bou} (kWh), PV direct-used production E_{du} (kWh), battery discharge E_{dis} (kWh) and load demand E_{load} (kWh).

$$E_{pv} = E_{du} + E_{sold} + E_{ch2} + E_{loss1} \tag{3-16}$$

$$E_{ch1} + E_{ch2} = E_{dis} + E_{loss2} \tag{3-17}$$

$$E_{load} = E_{du} + E_{bou} + E_{dis} \tag{3-18}$$

In this study, the time step of the simulation is one hour due to the time step of the available weather and load data and the relatively long simulation period.

The time step of the simulations could be modified according to the various application and different requirements by the decision makers.

3.4.3 Aggregated control

The aggregated control algorithm implements a flexible and easily applicable approach that results in smoother public load. It accomplishes this task by adjusting the available load of the participating users.

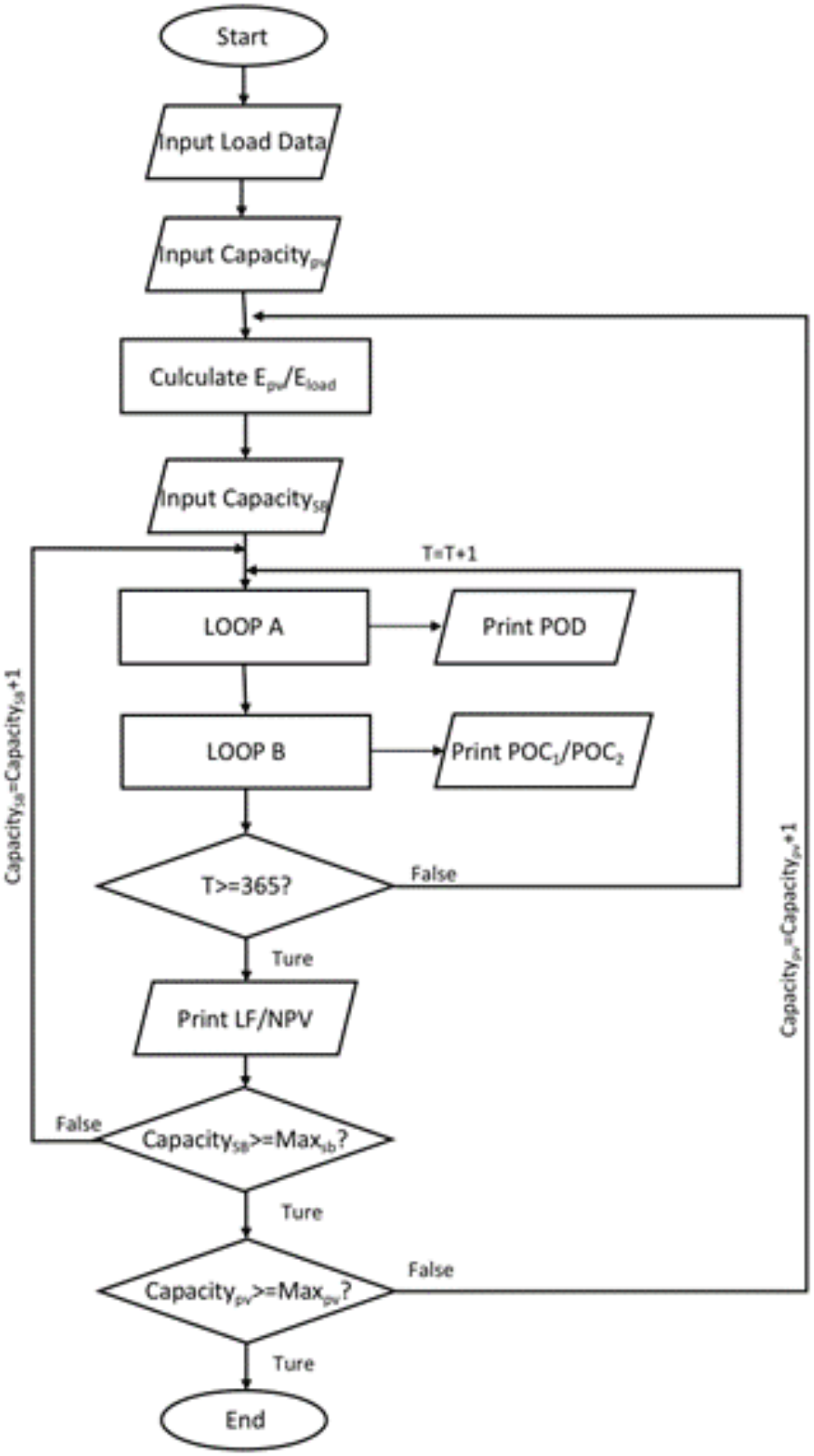

Fig. 3-2 Operating strategy for calculation

The algorithm will automatically identify the peak-valley difference of the public load during the calculation period in the case of no battery installation. Subsequently, the algorithm iteratively runs in steps of 1kWh and ends with the length of the effective capacity of the battery. In each iteration, the actuator of the algorithm determines the optimal flow direction and final position of the 1kWh of the user. Due to the limitation of the battery's power rating and the available load of the user, the protector of the algorithm continuously calculates the shape of these curves, ensuring that the battery's power rating will not be exceeded at all times and overcharging.

Initially, the three basic 24-value vectors representing the calculating day's E_{load}, $E_{kyushu}$and E_{pv} are inserted into the algorithm. Additional inputs of the algorithm are the available capacity and power rating of the battery. The main body of the algorithm is formed by two independent subroutines whose task is calculate the shape of the corresponding level curves, namely charge level and discharge level. Afterwards, those load data at off-peak and on-peak time after PV shaving are insert into two subroutines. The working mechanism of the subroutines are to dynamically capture the highest value or the lowest value of the public load under adjustable load of the user and perform charge and discharge to the user.

Table 3-3 Pseudocode loop A

LOOP A

For i=1:Effective C_{sb}

%The iteration is the size of the effective battery capacity

Max position=find($Kyuload_{peak}$ ==max(max($Kyuload_{peak}$)));

%Find the maximum load value in the charging interval

Max position'=Max position(1);

%If there are more than two maximum values, the first moment is selected by default

$Load_{peak}$(Max position')=$Load_{peak}$(Max position')-1;

%Discharge in steps of 1kWh

dis=$Load_{peak}$-$Loado_{peak}$;

%Calculate the charging status at each time in the iteration

$Kyuload_{peak}$=$Kyuloado_{peak}$-$Loado_{peak}$*k+$Load_{peak}$*k;

%update the reference

for n=1:length($Load_{peak}$)

if dis(n)==fix(Xsb1/6)

$Kyuload_{peak}$(n)=-10000;

end

End

%Protection to prevent charging at this moment when the battery reaches its maximum power

for n_2=1:length($Load_{peak}$)

if $Load_{peak}$(n_2)<=0

$Kyuload_{peak}$(n)=-10000;

end

end

%Protection to prevent charging at each moment when the load is fully satisfied by the

BESS

if sum($Kyuload_{peak}$)=-140000

Final Effective C_{sb}=i;

break

end

%Protection to prevent charging at this moment when the load at the peak moment is fully satisfied by the BESS

Table 3-4 Pseudocode loop B

LOOP B

For i=1:Final Effective C_{sb}

%The iteration is the size of the effective battery capacity

Minposition=find($Kyuload_{valley}$==min(min($Kyuload_{valley}$)));

%Find the minimum load value in the charging interval

Min position'=Min position(1);

%If there are more than two minimum values, the first moment is selected by default

$Load_{valley}$(Min position')=$Load_{valley}$(Min position')+1;

%Charge in steps of 1kWh

cha=$Load_{valley}$-$Loado_{valley}$;

%Calculate the charging status at each time in the iteration

$Kyuload_{valley}$=$Kyuloado_{valley}$-$Loado_{valley}$*k+$Load_{valley}$*k;

%update the reference

for n=1:length($Load_{valley}$)

if dis(n)==fix(Xsb1/6)

$Kyuload_{valley}$(n)=100000000;

end

%Protection to prevent discharging at this moment when the battery reaches its maximum power

end

for n_2=1:length($Load_{valley}$)

if $Load_{valley}$(n_2)<=0

$Kyuload_{valley}$(n_2)=100000000;

end

end

%Protection to prevent discharging at this moment when the PV power generation is completely stored in the BESS

Based on the adaptive power dispatch algorithm, the yearly simulation and throughout the lifetime of different system combinations of PV and battery are conducted to examine the influence of technical and economic indicators on system sizing. Fig.6 displays the performance matrixes of indicators, peak demand with the variance of PV and battery capacities.

Fig.3 represents the technical performance of the system, which decreases rapidly with the increase of battery capacity but is rarely influenced by PV size. Meanwhile, it easily achieves minimum value (14147 MW), which shows the system can participate in max1073 MW peak reduction of the public grid. In the other hand, another important technical indicator (load factor) of equipment utilization, which has the inverse trend with peak demand. It firstly climbs up with the increase of battery capacity then stabilizes at a specific value (0.7~0.71). Combining the analysis of two indicators of peak demand and load factor, it indicates load factor decreases with the increase of PV capacity when peak demand achieves the minimum value (14147 MW), which means the power supply of the public grid is lower due to the participation of larger PV capacity even if in case of the same peak load of the public grid.

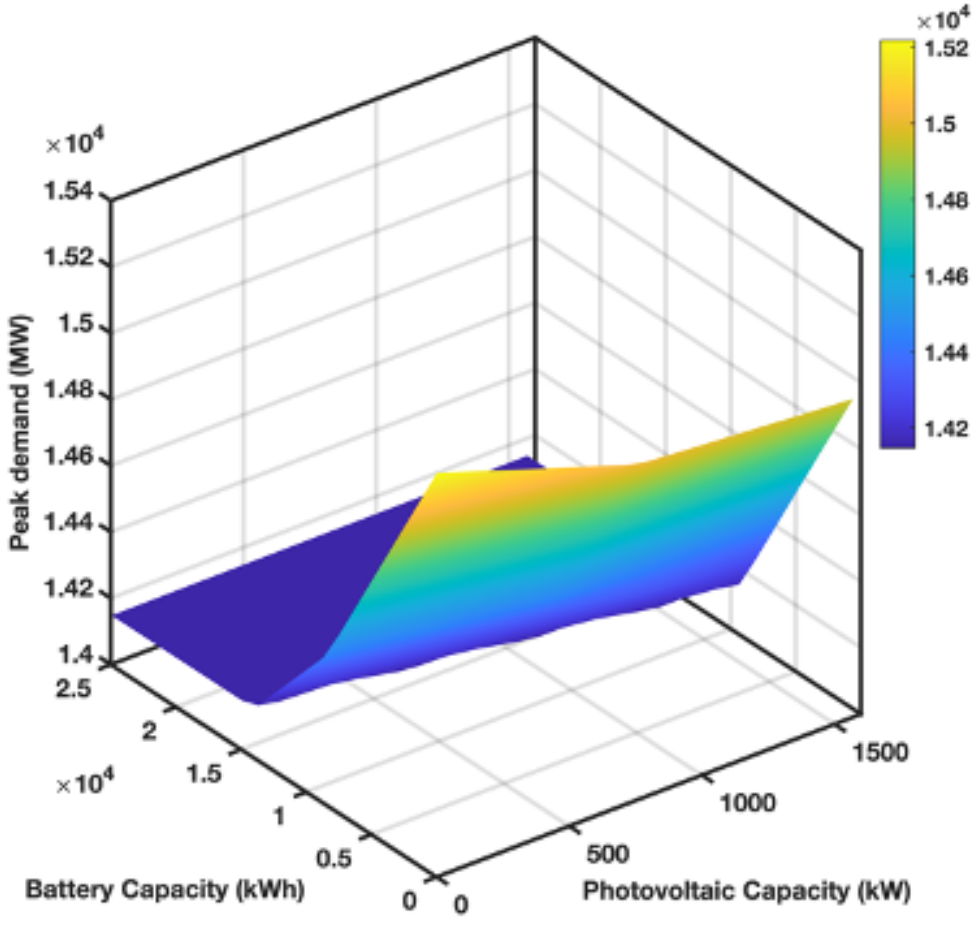

Fig. 3-3 Peak demand performance

The optimal system configurations of the SB-to-PV ratio are discussed, based on the economic evaluation of the supply and full-sized PV capacity ranging from 0 to 1580kW. From Fig. 4, it is clearly shown that a suitable PV size (0~910kW) will alleviate the fluctuation of the public grid. Still, massive PV penetration (910~1580kW) will decrease the Economic benefit of the supply side without battery participation. The increase of the SB-to-PV ratio will help the PV penetrate into the distributed system while reducing the impact of the public grid. It

indicates when the SB-to-PV ratio is higher than 85%, the full-sized PV capacity contributes to the public grid.

3.4.4 Adaptive power dispatch

BESS can adjust many kinds of load curves to realize energy arbitrage. The user may only pay attention to the economic benefits brought by BESS and ignore the load characteristics after BESS adjustment. However, the change of load characteristics is very important for power suppliers. Adjusting the load characteristics of users adaptively to the characteristics of the public grid can maximize the user's contribution to the power supplier while generating revenue, to achieve a win-win situation. Therefore, we developed a piece of code to simulate the charging and discharging process and recorded the charging and discharging amount at each moment under each system size to evaluate the technical and economic performance of the system.

The code is mainly divided into three parts. The first part is the execution of charge and discharge. The second part is the record of electricity flow. The third part is the protection of overcharge and over-discharge. In the first part, the actuator will automatically charge at the lowest power point and discharge at the highest power point based on the judgment. In the second part, the recorder will record the energy flow at each moment during each iteration. The third part is to prevent BESS from over-charging and over-discharging. According to the BESS system performance and user load characteristics, the protector has three trigger mechanisms. First, because the maximum power of the NAS battery is one-sixth of the battery's nominal capacity. When the power flow reaches 1/6 of the nominal capacity of the battery at a certain moment, the protector will trigger the protection mechanism. Second, to achieve the maximum self-consumption of photovoltaic power generation, BESS prioritizes the storage of the electricity discarded by PV. When the PV power generation is completely stored in the BESS, the protector will trigger the protection mechanism. Third, we must ensure that in a BESS cycle, the stored electricity is completely consumed during the peak period to achieve maximum economic benefits. Therefore, when the load at the peak moment is fully satisfied by the BESS, the protector will also be triggered.

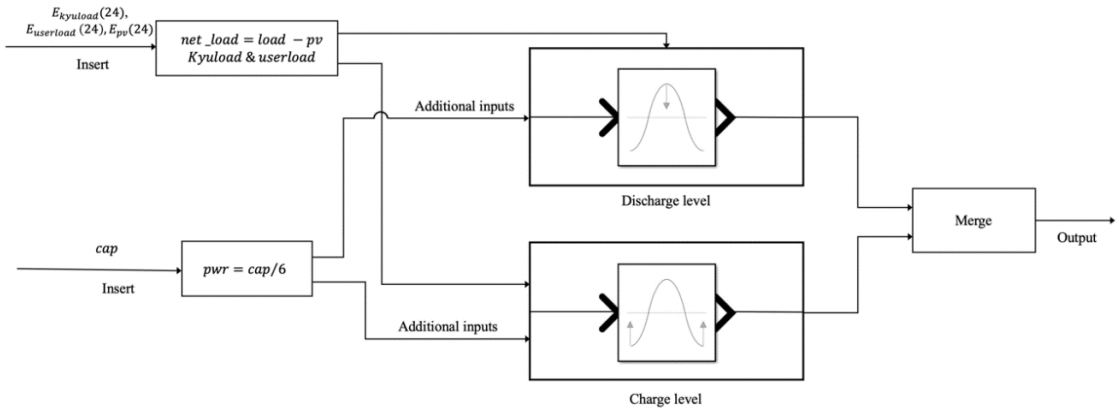

Fig. 3-4 Adaptive power dispatch algorithm flow chart

In the energy allocation scheme optimized for user load, for individual users, within a certain range, due to the uncertainty and instability of photovoltaic power generation, the load factor

(LF) value decreases with the increase of PV sizing, and in the SB sizing in the range of (0~2000kWh), installing a PV system will increase the instability of the user's net load.

The impact of the change of SB size on user load can be divided into three stages. First, as the size of SB increases, the user LF value rises rapidly (0~5000/6500kWh), and after reaching the peak, it rapidly decreases and is lower than the original value of 0.626., And finally stabilized at a relatively low level (0.4~0.45).

For the public grid, due to the same reason, within acertain range (0~17500kWh), the LF value of the public grid decreases with the increase of PV sizing. In this range, the installation of the PV system will increase the instability of net load of the public grid. However, when the SB size is greater than 17500kWh, as the PV size increases, the LF value increases

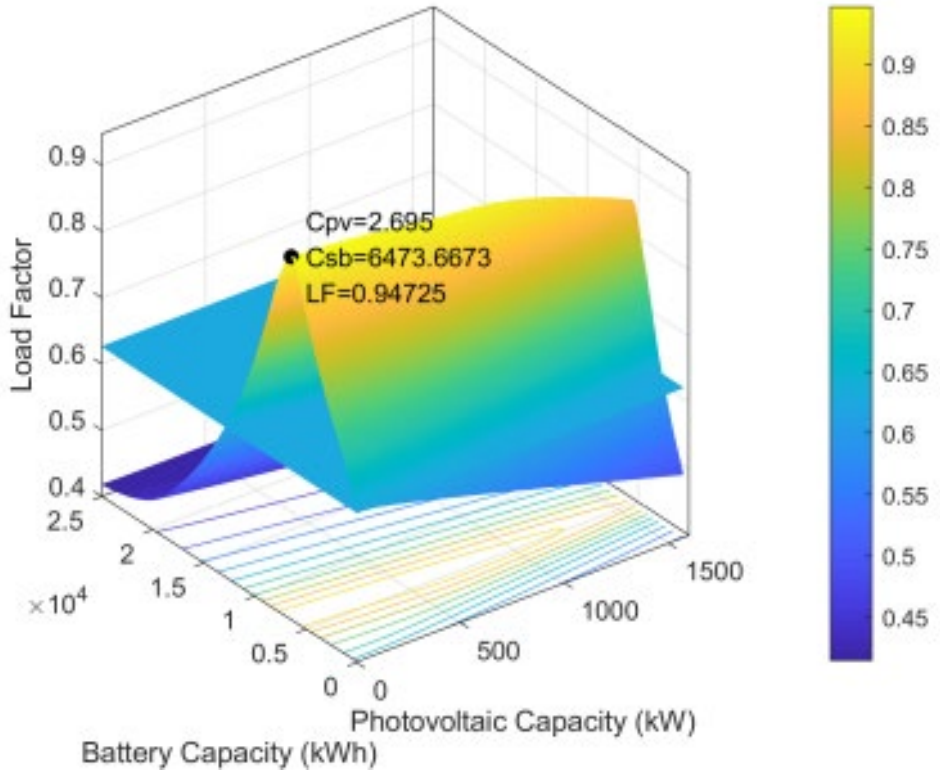

Fig. 3-5 Optimization of public load factor in demand side

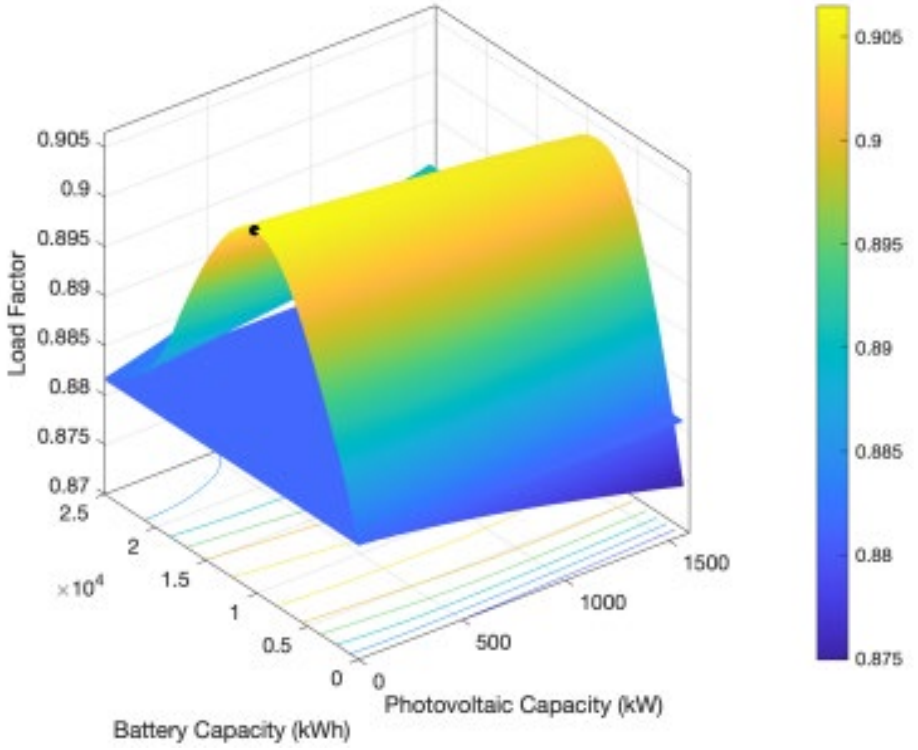

Fig. 3-6 Optimization of user's load factor in supplier side

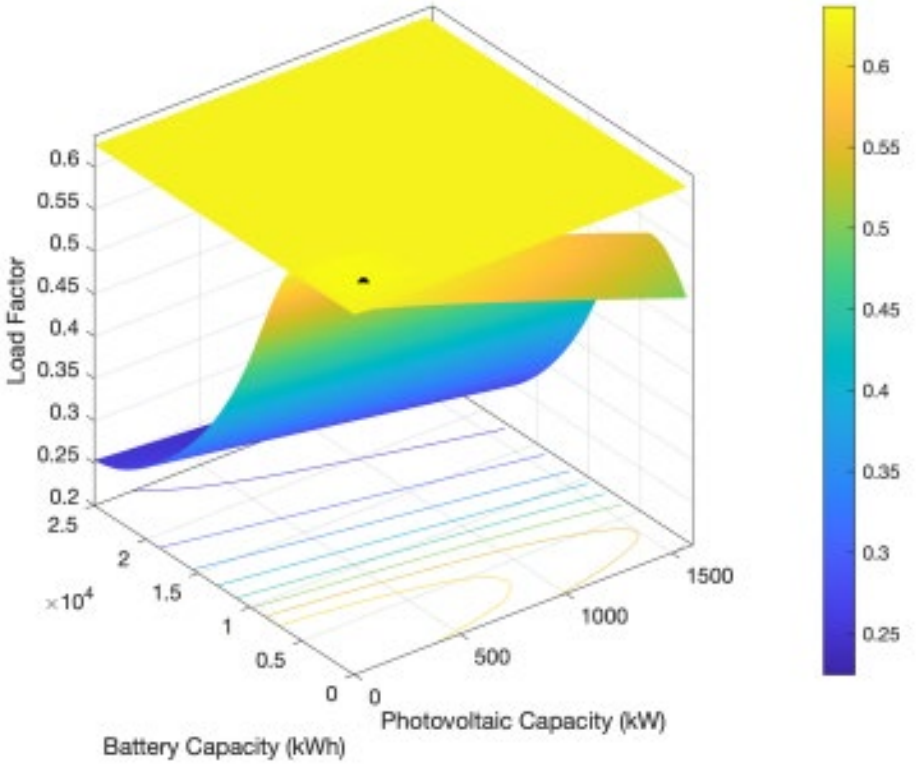

Fig. 3-7 Optimization of user's load factor in demand side

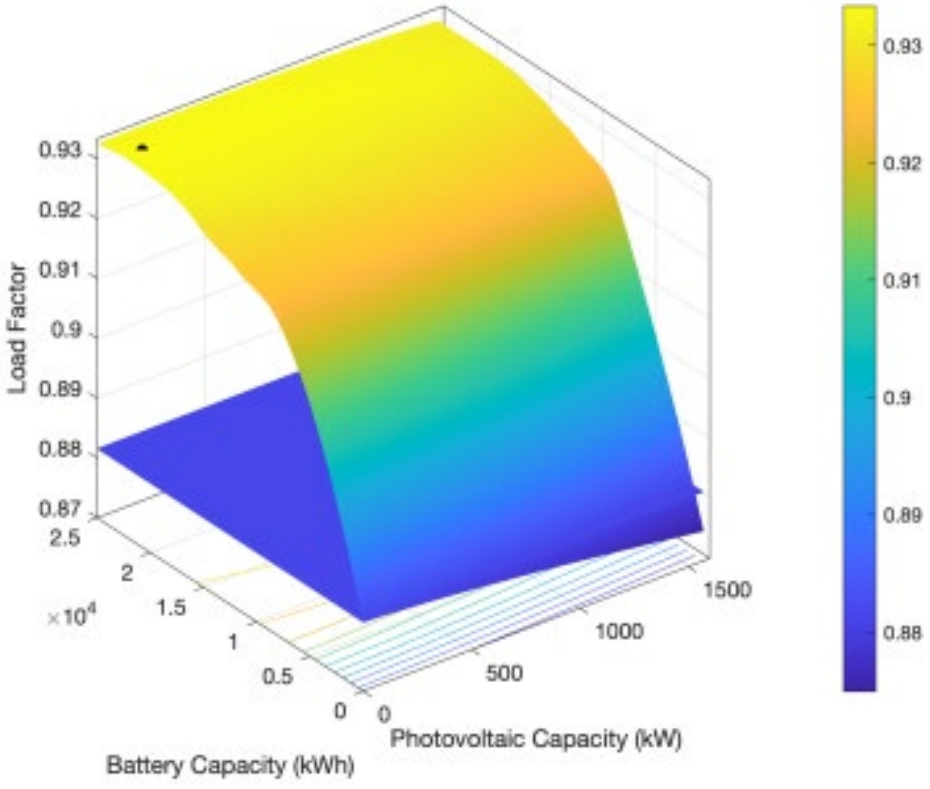

Fig. 3-8 Optimization of public load factor in supplier side

3.5 Methodology of energy sharing

3.5.1 Internal pricing mechanism

In this study, we adopt the SDR internal pricing mechanism with a compensation factor [12]. Because it provides an internal transaction price based on the energy demand conditions within the community during a specified period to ensure a more equitable distribution of benefits in energy trading [13] [14] [15, 16]. The total selling power is from the PV generation and the total buying power is the building's demand. Thus, the SDR at a community at time t is defined as:

$$SDR(t) = \frac{E_{pv}^{tot}(t)}{E_{load}^{tot}(t)} \tag{3-19}$$

where $E_{pv}^{tot}(t)$ is the total supply power (kWh) and $E_{load}^{tot}(t)$ is the total demand power at time t. Buying and selling prices fluctuate at different times of the day and the price set is determined by:

$$Pr_{sell} = [Pr_{sell}(1), Pr_{sell}(2), \cdots Pr_{sell}(T)] \tag{3-20}$$

$$Pr_{buy} = [Pr_{buy}(1), Pr_{buy}(2), \cdots Pr_{buy}(T)] \tag{3-21}$$

where Pr_{sell} is the selling price at time t, Pr_{buy} is the buying price at time t. And T is a time series for a day with a time-step of ΔT, and it is represented as $T = \{1, 2, \ldots, 24\}$. The internal trading prices depends on the buildings demand and solar PV generation at a particular period. Therefore, the selling and buying prices are defined as a function of the SDR. They are determined by:

$$Pr_{sell}(t) = f(SDR(t)) = \begin{cases} \dfrac{\left(\lambda_{sell}(t) + \beta(t)\right) \cdot \lambda_{buy}(t)}{(\lambda_{buy}(t) - \lambda_{sell}(t) - \beta(t)) \cdot SDR(t) + \lambda_{sell}(t) + \beta(t)}, 0 \le SDR(T) \le 1 \\ \lambda_{sell}(t) + \beta(t) / SDR(t), SDR(t) > 1 \end{cases} \tag{3-22}$$

$$Pr_{buy}(t) = f(SDR(t)) = \begin{cases} Pr_{sell}(t) \cdot SDR(t) + \lambda_{buy}(t) \cdot (1 - SDR(t)), 0 \le SDR(T) \le 1 \\ \lambda_{sell}(t) + \beta(t), SDR(t) > 1 \end{cases} \tag{3-23}$$

where $\lambda_{sell}(t)$ is the grid feed-in tariff energy price, (Notice: we adopt $\lambda_{sell} = 0$ in this case). $\lambda_{buy}(t)$ is the grid TOU supply energy price and $\beta(t)$ is the compensating factor restricted by:

$$0 \le \beta(t) \le \lambda_{buy}(t) - \lambda_{sell}(t) \tag{3-24}$$

3.5.2 Aggregator managed demand response

Energy sharing does not mean that the building directly controls its DERs; the building can use a third-party entity, such as an aggregator, to manage its resources [17] [18]. The aggregator has the ability to centrally manage individual decentralized resources. A building participates

in a demand response program by an aggregator, referred to as 'negative trading'. This is an incentive-based demand response program where buildings can save electricity bills during peak hours based on a contract with the aggregator. The aggregator plays the role of a manager that controls the transaction by bundling many buildings and the demand for electricity on a per-building basis.

By shaving or shifting demand at the request of the aggregator, in addition to the reduced electricity bill, the building will receive the following incentives:

KW incentive (fixed per period): Since an event may be activated for any period of time specified in the contract, the building needs to have an appropriate system in place to respond upon activation. Therefore, the incentive will be paid based on the controllable capacity (kW), regardless of whether it is actually activated or not. The incentive is given to the consumer on an annual (kW-year) or monthly (kW-month) basis.

KWh incentive (performance based): Based on the actual performance of the DR events, such as the total kWh reduction during each DR event. The premise of the device is that: (1).The sustainable time for demand reduction is set in the range of 2 to 6 hours. (2).The number of hours required for response is set in the range of 10 to 100 hours as the number of hours of annual demand [19].

Load can be classified as shiftable load, controllable load, and shave-able load [20]. In order to reduce the impact of operations within commercial buildings, we only considered the response effect of shiftable load and the BESSs with shared ability are considered as tools to perform load shifting [21]. (Note: Since aggregators do not have centralized control over individual design-based batteries, individual design for distributed BESS approach do not have the basis to participate in demand response.) The demand response incentives for buildings can be described as:

$$pro_{DR} = \sum (pro_{DR}^{fixed} + pro_{DR}^{perf}) \tag{3-25}$$

where Pro_{DR}^{fixed} is fixed incentive of each consumer, and Pro_{DR}^{perf} is the performance-based incentive of each consumer.

$$pro_{DR}^{fixed} = cap^{j} \times pr_{cont} \tag{3-26}$$

$$pro_{DR}^{perf} = \sum_{d}^{D} \sum_{t}^{T} (RW_{act} \times RD_{act}(t,d)) \tag{3-27}$$

where$cap^{j}$is the capacity of the BESS, $Pr_{cont}$is fixed incentive price. RW_{act} is activation reward (Yen/kWh), and $RD_{act}(t,d)$ is the kWh reduction during DR event at time t.

3.5.3 Energy flow and simulation

For each building in the community a power balance between PV generation, the grid, and the building power demand is to be achieved. This is given by the following equation：

$$E_{net}^{j}(t) = E_{load}^{j}(t) - E_{pv}^{j}(t) \tag{3-28}$$

where $E_{net}^{j}(t)$ is the building j's net power and $\mathrm{E}_{\mathrm{load}}^{\mathrm{j}}(t)$, $\mathrm{E}_{\mathrm{pv}}^{\mathrm{j}}(t)$ are the power demand and PV generation power at time t.

$$E_{net}^{tot}(t) = \sum E_{net}^{j}(t) \tag{3-29}$$

where$E_{net}^{tot}(t)$ is total net power in the building community. According to the total net demand situation of whole community, the PV surplus sharing power of each building $\mathrm{E_{sur}(t)}$ can be described as follow:

$$E_{sur}(t) = \begin{bmatrix} 0 & E_{sur}^{2,1}(t) & \cdots & E_{sur}^{j,1}(t) \\ E_{sur}^{1,2}(t) & 0 & \cdots & E_{sur}^{j,2}(t) \\ \vdots & \vdots & \ddots & \vdots \\ E_{sur}^{1,j}(t) & E_{sur}^{2,j}(t) & \cdots & 0 \end{bmatrix} \tag{3-30}$$

where $E_{sur}(t)$ is a diagonalized vector, whose elements $E_{sur}^{i,j}(t)$ represent the PV surplus sharing from building i to building j at time t. To reduce communication costs, the PV surplus sharing between buildings is uniformly deployed by the aggregator based on demand/surplus. And the elements $E_{sur}^{i,j}(t)$ are limited by equation (20). The relationship with $E_{sur}(t)$ and $E_{net}^{tot}(t)$ is given by equation (21).

$$E_{sur}^{i,j}(t) \geq 0, \forall (E_{net}^{i}(t) \leq 0, E_{net}^{j}(t) \geq 0) \tag{3-31}$$

$$\sum E_{sur}(t) = E_{net}^{tot}(t) \tag{3-32}$$

Hourly energy mismatch of each building after PV surplus sharing can be described as follow:

$$E_{net}^{j'}(t) = E_{net}^{j}(t) - \sum E_{sur}^{i,j}(t) + \eta_{trans} \times \sum E_{sur}^{i,j}(t) \tag{3-33}$$

where $E_{net}^{j\prime}(t)$ is the building j 's net power after surplus sharing. η_{trans} is the transmission efficiency for energy sharing between buildings.

Depending on the BESS sharing structure, the operation of the BESS and energy flow are discussed by category.

(a) IDB:

In scenario IDB, the net load balance is given by equation (23). Each BESS manger its own energy mismatch, so the charge and discharge power can be defined as diagonal matrices, which are determined by equation (24) and equation (25).

$$\left|E_{net}^{j'}(t)\right| = \begin{cases} \dfrac{E_{cha}^{j}(t)}{\eta_{cha}}, if\,(E_{net}^{j'}(t) < 0) \\ 0, if\,(E_{net}^{j'}(t) = 0) \\ E_{dis}^{j}(t) \times \eta_{dis} + E_{grid}^{j}(t), if\,(E_{net}^{j'}(t) > 0) \end{cases} \tag{3-34}$$

$$E_{cha}(t) = \begin{bmatrix} E_{cha}^{1,1}(t) & 0 & \cdots & 0 \\ 0 & E_{cha}^{2,2}(t) & \cdots & 0 \\ \vdots & \vdots & \ddots & \vdots \\ 0 & 0 & \cdots & E_{cha}^{j,j}(t) \end{bmatrix} \tag{3-35}$$

$$E_{dis}(t)=\begin{bmatrix} E_{dis}^{1,1}(t) & 0 & \cdots & 0 \\ 0 & E_{dis}^{2,2}(t) & \cdots & 0 \\ \vdots & \vdots & \ddots & \vdots \\ 0 & 0 & \cdots & E_{dis}^{j,j}(t) \end{bmatrix} \tag{3-36}$$

where η_{cha} and η_{dis} are the chare/discharge efficiency of the BESS. $E_{cha}^{j,j}(t)$ and $E_{dis}^{j,j}(t)$ are the charge and discharge power from building j to building j at time t. The calculation of the charging/discharging states in scenario IDB are described as follows.

Charging state: When the building has surplus PV power generation, (i.e., $E_{net}^{j,\prime}(t)<0$), the private battery is in a charging state. The battery charging rates $E_{cha}^{j,j}(t)$ (kW) should be limited by both the remaining storage capacity of the battery and the battery charging power.

$$E_{cha}^{j,j}(t)=\begin{cases} \left|E_{net}^{j'}(t)\right|\times\eta_{cha}, if\left(\left|E_{net}^{j'}(t)\right|\le pw^{j}\right) \\ pw^{j}, f\left(\left|E_{net}^{j'}(t)\right|> pw^{j}\right) \end{cases} \tag{3-37}$$

Discharging state: When the building has insufficient PV power generation, (i.e., $E_{net}^{j,\prime}(t)>0$), the private battery is in a discharging state. The battery discharging rates $E_{dis}^{j,j}(t)$ (kW) should be limited by both the remaining storage capacity of the battery and the battery discharging power.

$$E_{dis}^{j,j}(t)=\begin{cases} \dfrac{\left|E_{net}^{j'}(t)\right|}{\eta_{dis}}, if\left(\left|E_{net}^{j'}(t)\right|\le pw^{j}\right) \\ pw^{j}, f\left(\left|E_{net}^{j'}(t)\right|> pw^{j}\right) \end{cases} \tag{3-38}$$

(b) SCB:

In scenario SCB, the net load balance is given by equation (28). The centralized BESS manger all energy mismatch, so the charge and discharge power can be defined as vectors, which are determined by equation (29) and equation (30). The calculation of the charging/discharging states in scenario SCB are described as equation (31) and equation (32).

$$\left|\sum E_{net}^{j'}(t)\right|=\begin{cases} \dfrac{E_{cha}(t)}{\eta_{cha}}, if\left(\sum E_{net}^{j'}(t)<0\right) \\ 0, if\left(\sum E_{net}^{j'}(t)=0\right) \\ E_{dis}(t)\times\eta_{dis}+\sum E_{grid}^{j}(t), if\left(\sum E_{net}^{j'}(t)<0\right) \end{cases} \tag{3-39}$$

$$E_{cha}(t)=\begin{bmatrix} E_{cha}^{1,1}(t) & E_{cha}^{2,2}(t) & \cdots & E_{cha}^{j,j}(t) \end{bmatrix} \tag{3-40}$$

$$E_{dis}(t)=\begin{bmatrix} E_{dis}^{1,1}(t) & E_{dis}^{2,2}(t) & \cdots & E_{dis}^{j,j}(t) \end{bmatrix} \tag{3-41}$$

Charging state: When the community has surplus PV power generation, (i.e., $\sum E_{net}^{j,\prime}(t) < 0$), the centralized battery is in a charging state. The battery charging rates $E_{cha}(t)$ (kW) should be limited by both the remaining storage capacity of the battery and the battery charging power.

$$E_{cha}(t)=\begin{cases} \left|E_{net}^{j'}(t)\right|\times\eta_{cha}, if\left(\left|E_{net}^{j'}(t)\right|\le pw^{j}\right) \\ pw^{j}, f\left(\left|E_{net}^{j'}(t)\right|> pw^{j}\right) \end{cases} \tag{3-42}$$

Discharging state: When the community has insufficient PV power generation, (i.e., $\sum E_{net}^{j,\prime}(t) > 0$), the centralized battery is in a discharging state. The battery discharging rates $E_{dis}(t)$ (kW) should be limited by both the remaining storage capacity of the battery and the battery discharging power.

$$E_{dis}(t)=\begin{cases} \dfrac{\left|E_{net}^{j'}(t)\right|}{\eta_{dis}}, if\left(\left|E_{net}^{j'}(t)\right|\le pw^{j}\right) \\ pw^{j}, f\left(\left|E_{net}^{j'}(t)\right|> pw^{j}\right) \end{cases} \tag{3-43}$$

(c) SDB:

In scenario SDB, the net load balance is given by equation (33). The shared private BESS not only manage its own energy mismatch, but also responses to the other building's requirement if there are remaining capacity. So, the charge and discharge power can be defined as matrices, which are determined by equation (34) and equation (35). The calculation of the charging/discharging states in scenario SDB is described as equation (36) and equation (37).

$$\left|\sum E_{net}^{j'}(t)\right|=\begin{cases} \dfrac{\sum E_{cha}^{j}(t)}{\eta_{cha}}, if\left(\sum E_{net}^{j'}(t)<0\right) \\ 0, if\left(\sum E_{net}^{j'}(t)=0\right) \\ \sum E_{dis}^{j}(t)\times\eta_{dis}+\sum E_{grid}^{j}(t), if\left(\sum E_{net}^{j'}(t)>0\right) \end{cases} \tag{3-44}$$

$$E_{cha}(t)=\begin{bmatrix} E_{cha}^{1,1}(t) & E_{cha}^{2,1}(t) & \cdots & E_{cha}^{j,1}(t) \\ E_{cha}^{1,2}(t) & E_{cha}^{2,2}(t) & \cdots & E_{cha}^{j,2}(t) \\ \vdots & \vdots & \ddots & \vdots \\ E_{cha}^{1,j}(t) & E_{cha}^{2,j}(t) & \cdots & E_{cha}^{j,j}(t) \end{bmatrix} \tag{3-45}$$

$$E_{dis}(t)=\begin{bmatrix} E_{dis}^{1,1}(t) & E_{dis}^{2,1}(t) & \cdots & E_{dis}^{j,1}(t) \\ E_{dis}^{1,2}(t) & E_{dis}^{2,2}(t) & \cdots & E_{dis}^{j,2}(t) \\ \vdots & \vdots & \ddots & \vdots \\ E_{dis}^{1,j}(t) & E_{dis}^{2,j}(t) & \cdots & E_{dis}^{j,j}(t) \end{bmatrix} \tag{3-46}$$

Charging state: When the own building has surplus PV power generation, (i.e., $E_{net}^{j,\prime}(t) < 0$), the private battery is in a charging state. And if the other buildings have surplus PV power generation while the battery has remaining capacity, (i.e.,$E_{net}^{j-1,\prime}(t) < 0 \cdots \vee E_{net}^{1,\prime}(t) < 0$), the private battery can also be in a charging state. The battery charging rates $E_{cha}^{j}(t)$ (kW) should be limited by both the remaining storage capacity of the battery and the battery charging power.

$$E_{cha}^{j}(t) = \sum E_{cha}^{j,j}(t) = \begin{cases} pw^{j}, if\left(\left|E_{net}^{j'}(t)\right| > pw^{j}\right) \\ \left|E_{net}^{j'}(t)\right| \times \eta_{cha} + \left|E_{net}^{j-1'}(t)\right| \times \eta_{cha} \times \eta_{trans}, if\left(\left|E_{net}^{j'}(t)\right| \le pw^{j} \le \left|E_{net}^{j'}(t) + E_{net}^{j-1'}(t)\right|\right) \\ \left|E_{net}^{j'}(t)\right| \times \eta_{cha} + \left|E_{net}^{j'}(t) + E_{net}^{j-1'}(t)\right| \times \eta_{cha} \times \eta_{trans}, if\left(\left|E_{net}^{j-1'}(t)\right| \le pw^{j}\right) \end{cases} \tag{3-47}$$

Discharging state: When the own building has insufficient PV power generation, (i.e., $E_{net}^{j,\prime}(t) > 0$), the private battery is in a discharging state. And if the other buildings have insufficient PV power generation while the battery has remaining capacity, (i.e.,$E_{net}^{j-1,\prime}(t) > 0 \cdots \vee E_{net}^{1,\prime}(t) > 0$), the private battery can also be in a discharging state. The battery discharging rates $E_{dis}^{j}(t)$ (kW) should be limited by both the remaining storage capacity of the battery and the battery discharging power.

$$E_{dis}(t) = \sum E_{dis}^{j,j}(t) = \begin{cases} pw^{j}, if\left(\left|E_{net}^{j'}(t)\right| > pw^{j}\right) \\ \left|E_{net}^{j'}(t)\right| / \eta_{dis} + \left|E_{net}^{j-1'}(t)\right| / \eta_{dis} \times \eta_{trans}, if\left(\left|E_{net}^{j'}(t)\right| \le pw^{j} \le \left|E_{net}^{j'}(t) + E_{net}^{j-1'}(t)\right|\right) \\ \left|E_{net}^{j'}(t)\right| / \eta_{dis} + \left|E_{net}^{j'}(t) + E_{net}^{j-1'}(t)\right| / \eta_{dis} \times \eta_{trans}, if\left(\left|E_{net}^{j-1'}(t)\right| \le pw^{j}\right) \end{cases} \tag{3-48}$$

3.5.4 Energy losses

Due to the differences in distance from the BESS to the building in the three scenarios, the extensive energy loss during energy sharing process is bound to have an impact on the performance evaluation. Also, in the scenario SDB, different number and location of cells can produce differentiated results for the optimal operation of the BESS. Therefore, it is essential to discuss the energy losses. The total energy loss occurs during battery charging and discharging process, PV surplus sharing, and battery sharing process, which can be described as:

$$Loss_{tot} = Loss_{cha/dis} + Loss_{sur} + Loss_{pvs} + Loss_{bats} \tag{3-49}$$

where $Loss_{cha/dis}$ is the energy loss in the battery charging and discharging process, $Loss_{sur}$ is the energy loss in the surplus sharing process, $Loss_{pvs}$ is the energy loss in the surplus PV storage sharing process .and $Loss_{bats}$ is the energy loss in the remaining battery sharing process. The transmission losses (including remaining battery energy sharing and surplus PV storage sharing) of battery sharing within the community (within 1km) in this paper was assumed 8% and for the distributed surplus PV storage (inside) we assumed 0% because all energy exchange processes are occurred inside one building.

$$Loss_{cha/dis} = \sum E_{dis}(t) \times (\frac{1-\eta_{cha}}{\eta_{cha}}) \times (\frac{1-\eta_{dis}}{\eta_{dis}}) \tag{3-50}$$

$$Loss_{sur} = \sum E_{sur}(t) \times \eta_{trans} \tag{3-51}$$

$$Loss_{pvs} = \begin{cases} 0, if\,(IDB) \\ \sum E_{cha}(t) \times \eta_{trans}, i(SCB) \\ \sum (E_{cha}^{j}(t) - E_{cha}^{j,j}(t)) \times \eta_{trans}, i(SDB) \end{cases} \tag{3-52}$$

$$Loss_{bats} = \begin{cases} 0, if\,(IDB) \\ \sum E_{dis}(t) \times \eta_{trans}, i(SCB) \\ \sum (E_{dis}^{j}(t) - E_{dis}^{j,j}(t)) \times \eta_{trans}, i(SDB) \end{cases} \tag{3-53}$$

3.5.5 Intelligent optimization algorithm

Genetic algorithm (GA) originated from computer simulation studies on biological systems and is a stochastic global search optimization method, which simulates the replication, crossover and mutation phenomena occurring in natural selection and heredity, starting from any initial population, through random selection, crossover and mutation operations to produce a group of individuals more suitable for the environment, so that the population evolves to an increasingly better region in the search space, so that from one generation to the next, it continues to reproduce and evolve, and finally converges to a group of individuals most suitable for the environment, thus finding a quality solution to the problem [22] [23] [24].

Basic Genetic Algorithm (also called Standard Genetic Algorithm or Simple Genetic Algorithm, SGA for short) is a population-based operation, which takes all individuals in a population as the object and uses only basic genetic operators: selection operator, crossover operator and variation operator. It not only provides a basic framework for various genetic algorithms, but also has some application value. Selection, crossover and mutation are the three main operators of genetic algorithms, which constitute genetic operations and give genetic algorithms features that other methods do not have.

It is expressed as follows.

$$SGA = (C, E, P_0, M, \phi, \Gamma, \varphi, T) \tag{3-54}$$

where C denotes the coding scheme of an individual

E denotes the individual fitness evaluation function

P_0 denotes the initial population.

M denotes the population size.

ϕ denotes the selection operator.

Γ denotes the crossover operator.

φ denotes the variation operator.

T denotes the genetic algorithm termination condition.

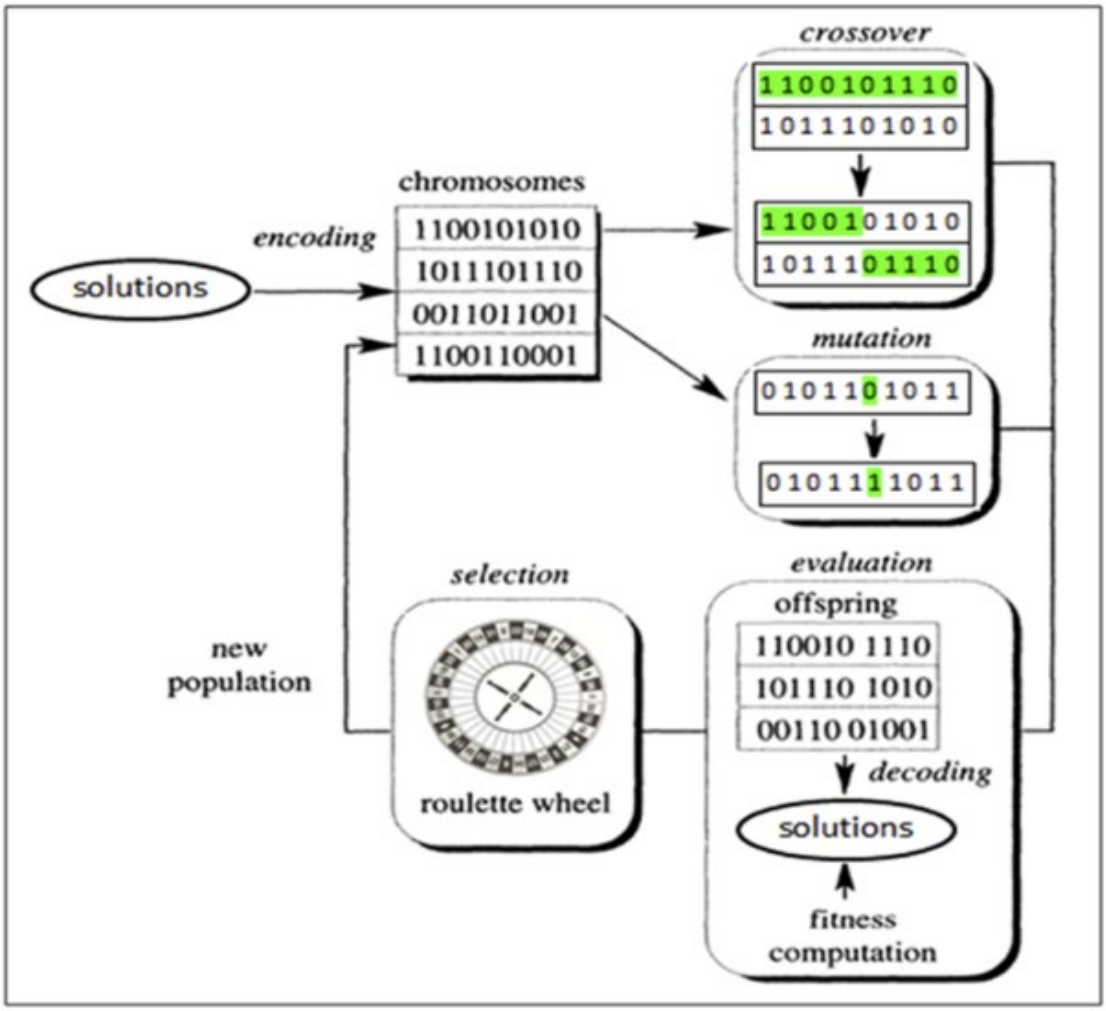

Fig. 3-9 Traditional structure of genetic algorithms

The basic operation procedure of the genetic algorithm is as follows.

(1) Initialization: set the evolutionary algebra counter t=0, set the maximum evolutionary algebra T, and randomly generate M individuals as the initial population P(0).

(2) Individual evaluation: calculate the fitness of each individual in the population P(t).

(3) Selection operation: the selection operator is applied to the population. The purpose of selection is to inherit the optimized individuals directly to the next generation or to generate

new individuals by pairwise crossover and then to the next generation. The selection operation is based on the assessment of the fitness of individuals in the population.

(4) Crossover operation: the crossover operator is applied to the population. The central role in genetic algorithms is played by the crossover operator.

(5) Variation operation: the variation operator is applied to the population. This means that the value of a gene on some locus of a string of individuals in the population is changed. The population P(t) is selected, crossover, and variation operators to obtain the next generation population P(t+1).

(6) Termination condition judgment: if t=T, then the individual with the maximum fitness obtained in the evolutionary process is output as the optimal solution and the calculation is terminated.

Genetic operations include the following three basic genetic operators: selection; crossover; mutation.

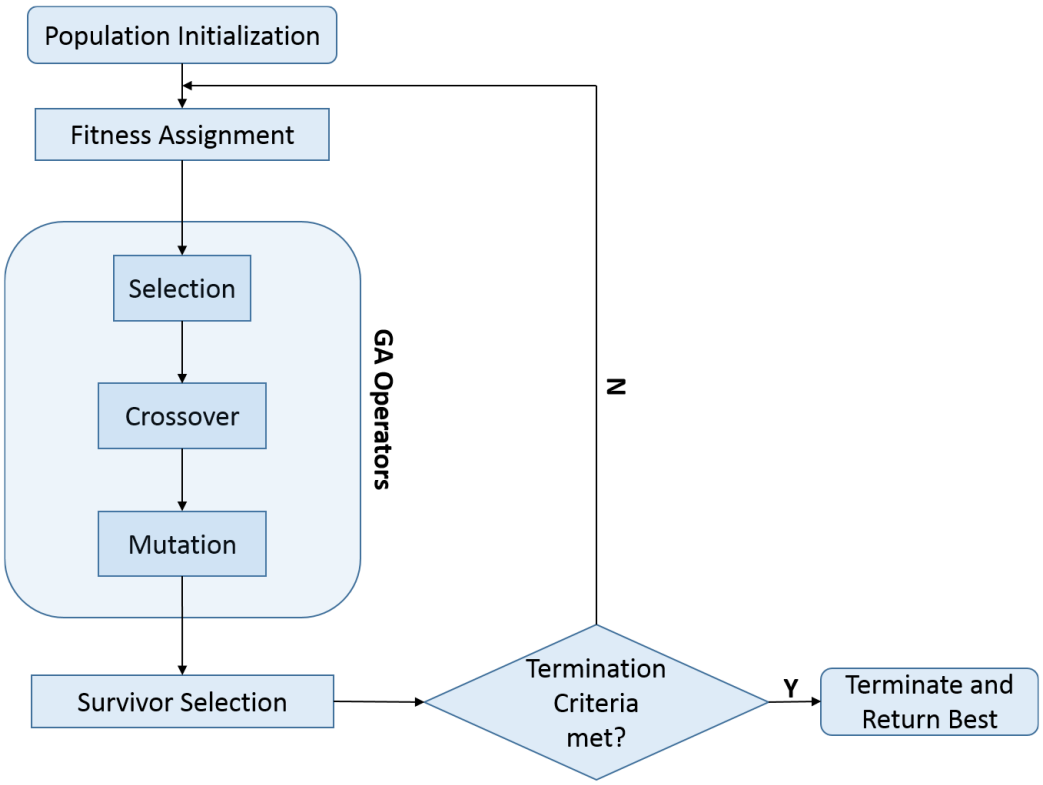

Fig. 3-10 Flow chart of genetic algorithms

3.5.6 Processes

The output of this step is considered to be the minimum capacity required to achieve the required energy performance (load leveling) for the entire community. In step 3, nonlinear programming (NLP) is used to optimize the capacity of the distributed batteries installed in each building) to minimize storage sharing (i.e., power exchange with other batteries) and thus reduce the associated energy losses. A step-by-step method is described below.

① Data fetching

The first step is the data fetching. It contains Features of BESS which consists with design range of BESS dimensions (kWh), module dimensions of BESS (kWh), module dimensions of power rating (kW) and planning optimization objective function. The parameters necessary for the GA algorithm are also imported in this step.

② Extraction of representative load demand curves

The load demand curves for the standard year were approached using principle component analysis and clustered using k-mean method. After alteration according to the chronological nature, representative load demand profiles are chosen from those profiles is computed.

③ Create initial population

An initial population of individuals is the starting point of the process. Each individual is represented using a string, in terms of alphabet (string of 1s and 0s). Every individual represents the capacity of BESS. The parent groups are initialized stochastically in this step.

④ Fitness function

The fitness function determines how fit an individual is(the fitness function is load standard deviation). MATLAB's fmincon solver is used to determine the optimal BESS operation for each population for corresponding the minimum load standard deviation (LSD). This step is performed for each individual member of the population in turn and results in fitness score. Based on the fitness score of an individual, we determine whether it will be selected for breeding.

⑤ Evolution via GA

Each individual progeny member of a population is evaluated for fitness in step 4 of the evaluation of the fitness of an individual generation. Selective breeding, crossbreeding, and mutation took place on the population in order to generate the offspring population. An elite algorithm is used to blend the parent and offspring populations together to form the next generation. Step 6 should be followed if the current generation is a final generation; otherwise, update the number of generations, reset the year to 1, and go to step 4.

⑥ Obtain the results of the capacity of the aggregated battery

An optimal capacity of the aggregated battery results from the GA search, which has the minimum LSD.

⑦ Optimization of distributed battery capacity for single building

In this step, GA is used to optimize the capacity of distributed batteries (kWh) installed in individual buildings based on aggregated battery capacity, which aims to minimize load limitations.

⑧ Calculating feasible solutions using LP

After the eighth step, the battery capacity of all batteries to be tested is calculated. We can use linear programming and combine other factors to assign the battery capacity.

3.5.7 Evaluation Indicators

Peak demand (PD) on an electrical grid is simply the highest electrical power demand that has occurred over a specified period. In this study, peak demand is characterized as annual.

Load factor (LF) is defined as the average load ratio over a given period to the maximum demand (peak demand) occurring in that period. In other words, the load factor is the ratio of energy consumed in a given period of the times of hours to the peak load, which has occurred during that particular period. The load factor means how efficiently we use energy. It is the measure of the utilization of electrical power during a given period to the maximum power which would have been utilized in that period. The load factor plays an essential role in the cost of generation per unit. The higher the load factor, the smaller will be the generation cost for the same maximum demands. Load factor is described as the stability of the annual load, which is determined as:

$$LF = \frac{load_{mean}}{load_{\max}} \tag{3-55}$$

Net present value (NPV) is the difference between the present value of cash inflows and the present value of cash outflows over a period of time. NPV is used in capital budgeting and investment planning to analyze the profitability of a projected investment or project. Ignore the operation and maintenance cost, the NPV of user side can be determined as:

$$NPV = \sum \frac{B_n}{(1+i)^n} - C_0 \tag{3-56}$$

where B_n, Co_o and n are the annual benefit of the PVB system, initial investment and generic year n= [1,2,3,...j], i is discount rate. In this paper, we adopt the Fukuoka Bank‘s annual interest rate: 4.5% [25].

PBP (payback period) are acknowledged indicator to evaluate the economic performance of renewable systems, that regards both cost and revenue of the whole system. It becomes the crucial one to conduct a comprehensive life cycle analysis of the PVB system. The annual revenue equals to the sum of the revenues caused by the saved electricity cost from the direct-use PV electricity, as well as the revenue of electricity sold back to the grid. The PBP (yr) can be presented as follows:

$$PBP = C_0 + \frac{\sum C_n / (1+i)^n}{(\sum B_n / (1+i)^n) / m} \tag{3-57}$$

where m is the minimum year the total revenue of the system is larger than the total cost.

References

[1] Prieto J-I, García D. Global solar radiation models: A critical review from the point of view of homogeneity and case study. Renewable and Sustainable Energy Reviews. 2021:111856.

[2] Dubayah R, Rich PM. Topographic solar radiation models for GIS. International journal of geographical information systems. 1995;9:405-19.

[3] Chai T, Draxler RR. Root mean square error (RMSE) or mean absolute error (MAE)?–Arguments against avoiding RMSE in the literature. Geoscientific model development. 2014;7:1247-50.

[4] Gupta HV, Kling H, Yilmaz KK, Martinez GF. Decomposition of the mean squared error and NSE performance criteria: Implications for improving hydrological modelling. Journal of hydrology. 2009;377:80-91.

[5] Joyce A, Rodrigues C, Manso R. Modelling a PV system. Renewable energy. 2001;22:275-80.

[6] Rasheed M, Al-Darraji MN, Shihab S, Rashid A, Rashid T. Solar PV Modelling and Parameter Extraction Using Iterative Algorithms. Journal of Physics: Conference Series: IOP Publishing; 2021. p. 012059.

[7] Ismail MS, Moghavvemi M, Mahlia TMI. Techno-economic analysis of an optimized photovoltaic and diesel generator hybrid power system for remote houses in a tropical climate. Energy Conversion and Management. 2013;69:163-73.

[8] Tamilselvi S, Gunasundari S, Karuppiah N, Razak RK A, Madhusudan S, Nagarajan VM, et al. A review on battery modelling techniques. Sustainability. 2021;13:10042.

[9] Divya KC, Østergaard J. Battery energy storage technology for power systems—An overview. Electric Power Systems Research. 2009;79:511-20.

[10] INSULATORS N. Sodium sulfur battery. In: Group EIB, editor.

[11] Zhang C, Li K, Mcloone S, Yang Z. Battery modelling methods for electric vehicles-A review. 2014 European Control Conference (ECC): IEEE; 2014. p. 2673-8.

[12] Bayram IS, Shakir MZ, Abdallah M, Qaraqe K. A survey on energy trading in smart grid. 2014 IEEE Global Conference on Signal and Information Processing (GlobalSIP): IEEE; 2014. p. 258-62.

[13] Zhou Y, Wu J, Long C. Evaluation of peer-to-peer energy sharing mechanisms based on a multiagent simulation framework. Applied Energy. 2018;222:993-1022.

[14] Wang Y, Saad W, Han Z, Poor HV, Başar T. A game-theoretic approach to energy trading in the smart grid. IEEE Transactions on Smart Grid. 2014;5:1439-50.

[15] Zhang C, Wu J, Zhou Y, Cheng M, Long C. Peer-to-Peer energy trading in a Microgrid. Applied Energy. 2018;220:1-12.

[16] Soto EA, Bosman LB, Wollega E, Leon-Salas WD. Peer-to-peer energy trading: A review of the literature. Applied Energy. 2021;283:116268.

[17] Conejo AJ, Morales JM, Baringo L. Real-time demand response model. IEEE Transactions on Smart Grid. 2010;1:236-42.

[18] Albadi MH, El-Saadany EF. A summary of demand response in electricity markets. Electric power systems research. 2008;78:1989-96.

[19] Ministry of Economy T, and Industry. Current Status and Future of Negawatt Trading. 2016.

[20] Astriani Y, Shafiullah GM, Shahnia F. Incentive determination of a demand response program for microgrids. Applied Energy. 2021;292.

[21] Torriti J, Hassan MG, Leach M. Demand response experience in Europe: Policies, programmes and implementation. Energy. 2010;35:1575-83.

[22] Mirjalili S. Genetic algorithm. Evolutionary algorithms and neural networks: Springer; 2019. p. 43-55.

[23] Kumar M, Husain D, Upreti N, Gupta D. Genetic algorithm: Review and application. Available at SSRN 3529843. 2010.

[24] Lambora A, Gupta K, Chopra K. Genetic algorithm-A literature review. 2019 international conference on machine learning, big data, cloud and parallel computing (COMITCon): IEEE; 2019. p. 380-4.

[25] bank F. Fukuoka Bank‘s annual interest rate

Chapter 4

DATA RESOURCES AND ENERGY CONVERSION ANALYSIS

DATA RESOURCES AND ENERGY CONVERSION ANALYSIS

4.1 Weather data sources 4-1

4.2 Energy sources 4-3

4.2.1 Load sources 4-3

4.2.2 Distributed network 4-12

4.2.3 Data Processing 4-14

References 4-16

4.1 Weather data sources

In this work, a public dataset with meteorological parameters is used. Data are collected from January 2000 to December 2021 at seven Japanese observations. The geographical locations are plotted in Fig 4-1. Adopted dataset is recorded by the Japan Meteorological Agency [1] [2] [3]. Table. 4-1 summarizes the description of the meteorological parameters.

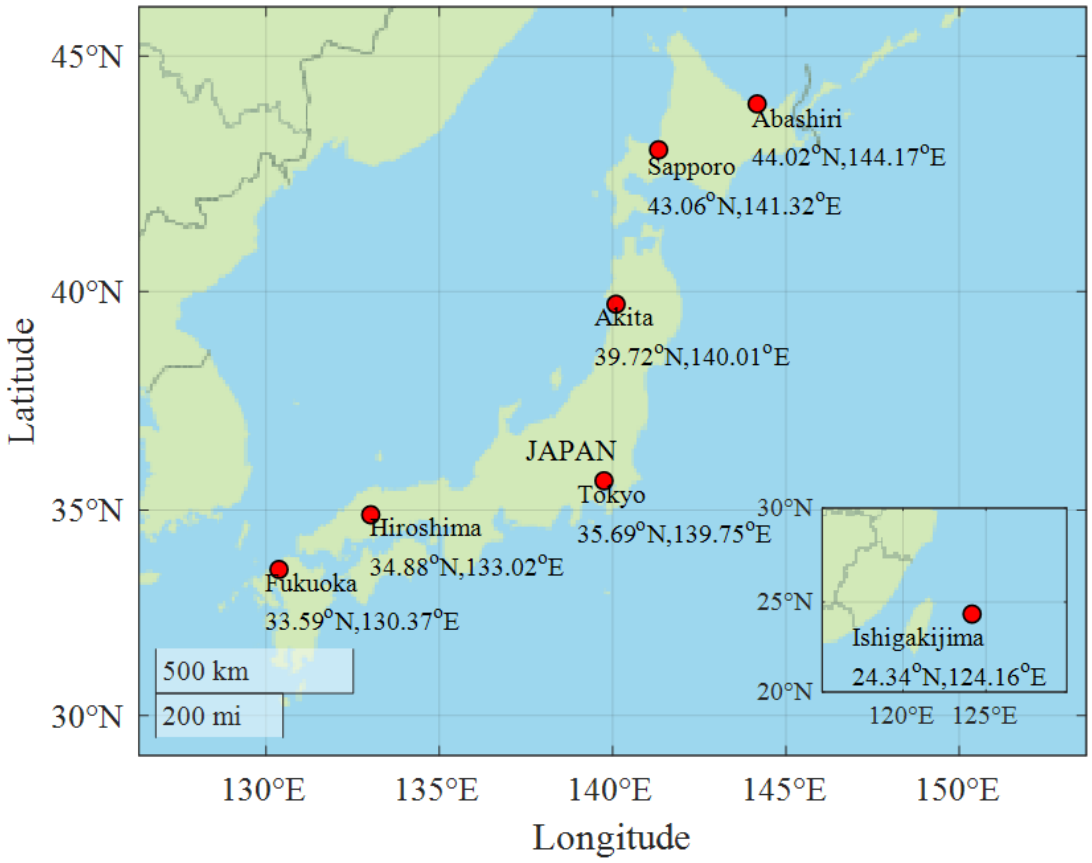

Fig. 4-1 Locations of meteorological observations referenced in this study: latitude(degrees), longitude(degrees).

Table. 4-1 Surface Meteorological Parameters

Surface Meteorological Parameter	Symbol	Unit	Resolution	Description
Air temperature	*T*	℃	1h	
Relative humidity	*RH*	%	1h	
Cloud cover	*CC*	-	3h	
Weather type	*WT*	-	3h/1h	
Sunshine duration	*SD*	-	1h	

Precipitation	*PR*	mm	1h
Wind speed	*WS*	m/s	1h
Wind direction	*WD*	-	1h
Visibility	*VI*	Km	3h/1h
Dewpoint temperature	T_d	℃	1h
Water vapor pressure	*WVP*	hPa	1h
Atmospheric pressure	P_a	hPa	1h
Solar radiation	*I*	MJ/m^2	1h

Table. 4-2 Cloud cover symbol description

Symbol	Description	Numericalization
blank	No observations	blank
--	No clouds are observed	0
0.0	If clouds are present but cloud cover is less than 0.1	0
0	If clouds are present but cloud cover is less than 1	0
0+	Cloud cover is more than 0.1 but less than 1	0.5
1	One-tenth of the total cloud cover	1
2	Two-tenths of the total cloud cover	2
3	Three-tenths of the total cloud cover	3
4	Four-tenths of the total cloud cover	4
5	Five-tenths of the total cloud cover	5
6	Six-tenths of the total cloud cover	6
7	Seven-tenths of the total cloud cover	7
8	Eight-tenths of the total cloud cover	8
9	Nine-tenths of the total cloud cover	9

10-	If cloud cover is 10 but there are areas with no clouds	9.5
10	The total cloud cover	10

Table. 4-3 Weather type description

Symbol	Description
1	Mostly clear and sunny
2	Sunny
3	Slightly cloudy
4	Cloudy
5	Mist
6	Dust storm
7	Drifting snow
8	Fog
9	Drizzle
10	Rain
11	Sleet
12	Snow
13	Hail
14	Hailstorm
15	Thunderstorm

4.2 Energy sources

4.2.1 Load sources

As seen in Fig. 4-1, the geographical distribution of installed wind and PV power, shows that Tokyo dominates in PV, followed by Kyushu, Kansai, and Hokkaido, and that Kyushu dominates in the wind, followed by Tokyo, Hokkaido, and Kansai.

① Kyushu Electric Power

Due to economic growth and the advancement of electrification, the demand for electricity in Kyushu has increased year by year. From the time when the company was founded (1951), the energy structure was hydropower and coal power, and then to oil power. Since the oil crisis in the 1970s, nuclear power and other energy sources, coal, LNG, oil power, and hydropower have developed in a balanced manner. Starting in 2011, fossil fuel consumption, fuel costs, and CO2 emissions will increase due to the increase in thermal power generation due to the closure of nuclear power plants (as shown in Fig. 4-2 and Fig.4-3), the installed capacity of power generation is also increased with the time. Since the oil crisis, the policymakers have been aiming for the best mix of power sources that combines various power sources in a well-balanced manner from the perspectives of fuel procurement stability, power generation costs, and the impact on the global environment.

According to the existing data of energy production, the energy distribution in Kyushu is shown in Fig. 4-4. The development centered on group companies is promoted, such as solar power generation (mega solar) utilizing the site of a thermal power plant and wind power generation in consideration of harmony with the surrounding environment. Such as the construction of Sasebo Mega Solar Power.

Plant and Nagashima Wind Power Plant (as shown in Fig.4-5). The power generation of PV in Sasebo Mega Solar Power Plant is shown in Fig. 4-6. The PV power generation is changed with meteorological conditions. We can conclude that even on a clear day, it took about 2 hours to reach the rated output. As the power generation output of PV power generation changes greatly depending on the time and weather. In order to supply electricity in a stable manner, we are dealing with output fluctuations due to solar and wind power generation by adjusting the output by thermal power generation.

Kyushu island is located in the southwest of Japan as the third-largest island, surrounded by a spray of smaller islands that trail off in a long arc across the East China Sea. By the end of 2016, it has 12 million, covering 36782 kilometers, 11.2% of the national area. Currently, Kyushu electric power sales accounts of 9.2% of national power, components of power technologies are mainly composed of thermal power plants, nuclear, hydro, PV, geothermal, biomass, and wind. The seasonal or daily power demand variations based on history grid load from April. 2014 to March. 2015 is shown in Fig.1. During spring and autumn, it shows a relative flatten the daily demand curve, higher daily variations mainly occur in summer that the maximum demand reaches around 15220 MWh.

According to the annual energy manual published by Kyushu Electric Power, electricity consumption in the commercial sector accounts for approximately 15.7% of total electricity consumption in Kyushu. The small and medium enterprises (SMEs) which have similar electricity consumption structure account for approximately 69.7% of the commercial sectors in Kyushu. Among them, the retail and service industries account for approximately 51.8%. According to the above information, we assume that the SMEs retail and services users installing grid-supporting PV battery systems account for 5.67% of the total public grid load in Kyushu Island.

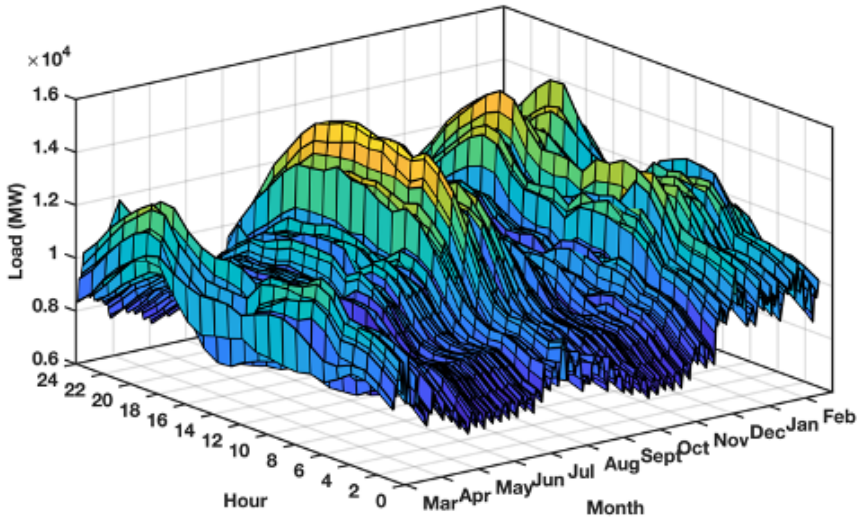

Fig. 4-2 Daily power demand in Kyushu public grid

② Higashida area in Kitakyushu City

The target area selected in this article is the Higashida area in Kitakyushu City, Japan, which serves as a key renovation and application test area for an environmentally friendly city. The target area has been selected as a new energy experimental demonstration area by the Ministry of Economy, Trade and Industry since 2010 [4] [5]. As shown in Fig 4-3, the blue coil area is the steel plant area, and the red coil area is the smart community demonstration area, which uses heat, hydrogen, solar energy, wind power and other energy sources to achieve energy self-sufficiency. In 2011, the application demonstration of hydrogen energy in the target area began, hoping to establish a model of hydrogen energy society to promote nationwide.

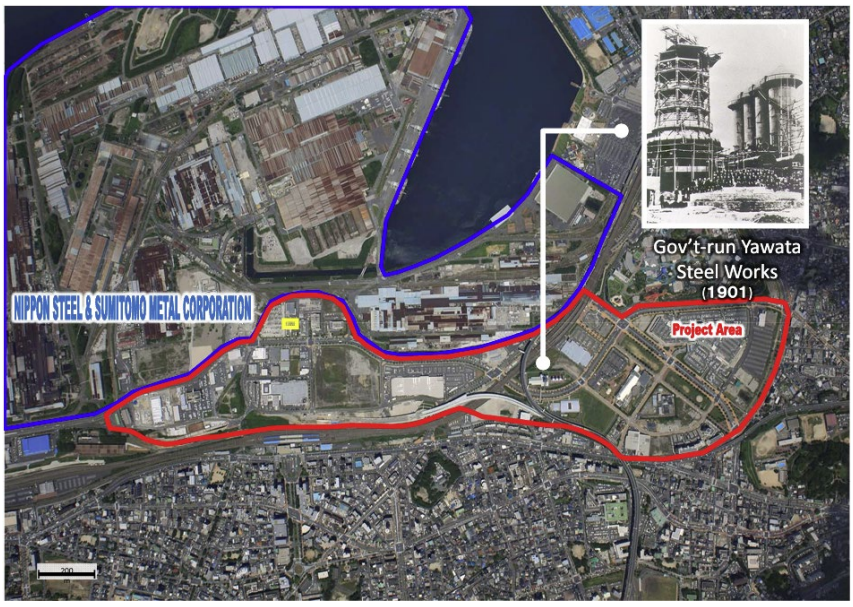

Fig. 4-3 Smart community in Higashida area

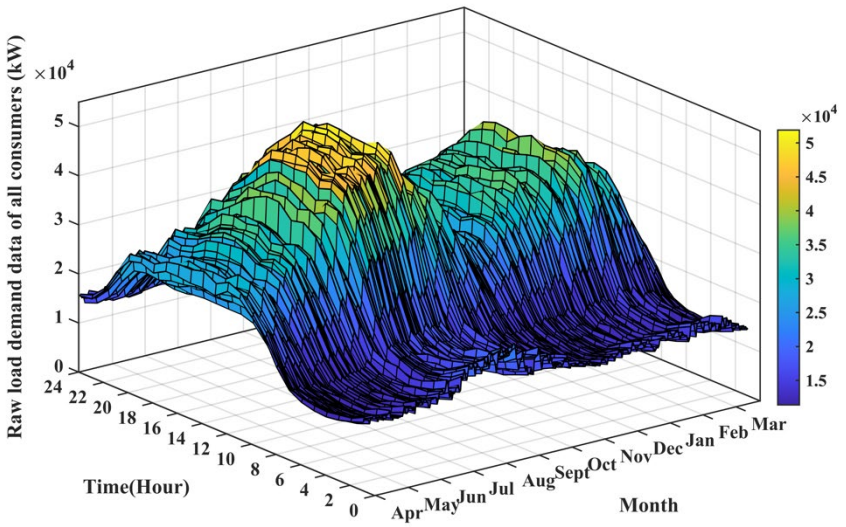

Fig. 4-4 Raw load demand data of all consumers in Higashida District

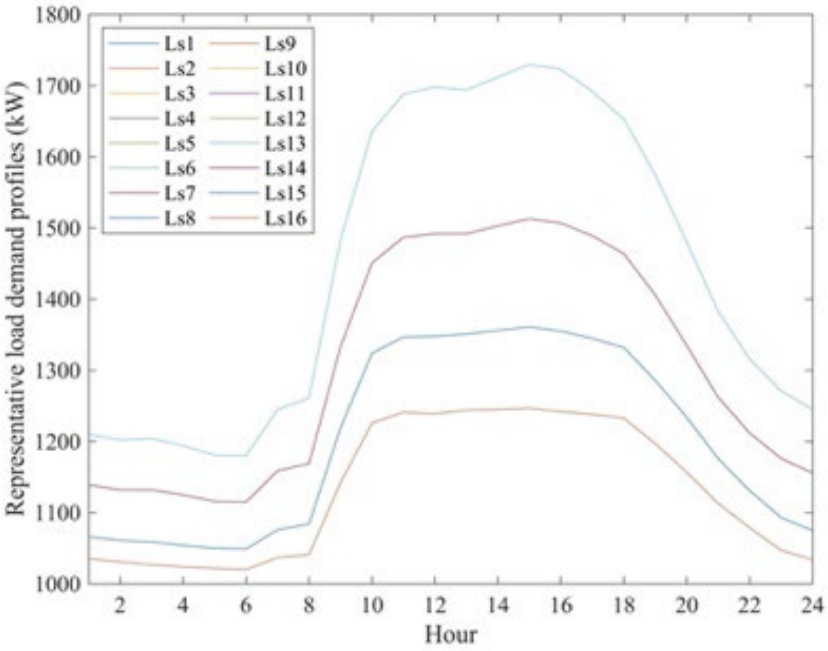

Fig. 4-5 Typical daily load of building (Building 4)

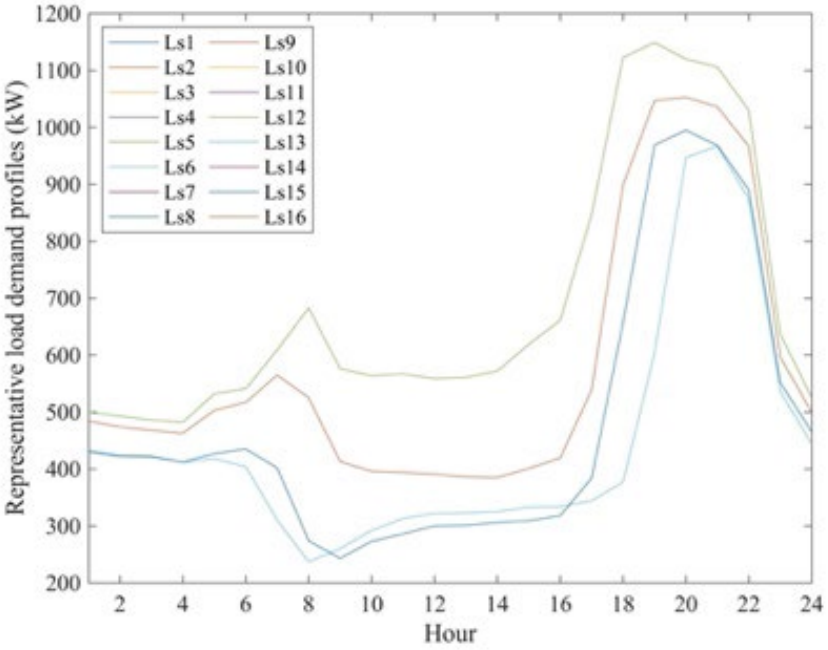

Fig. 4-6 Typical daily load of building (Building 16)

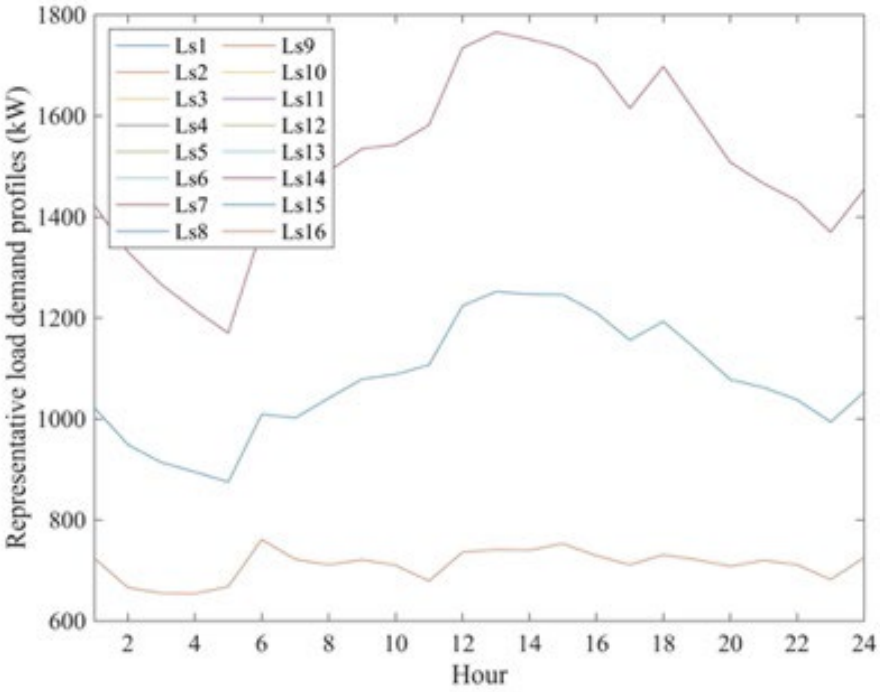

Fig. 4-7 Typical daily load of building (Building 5)

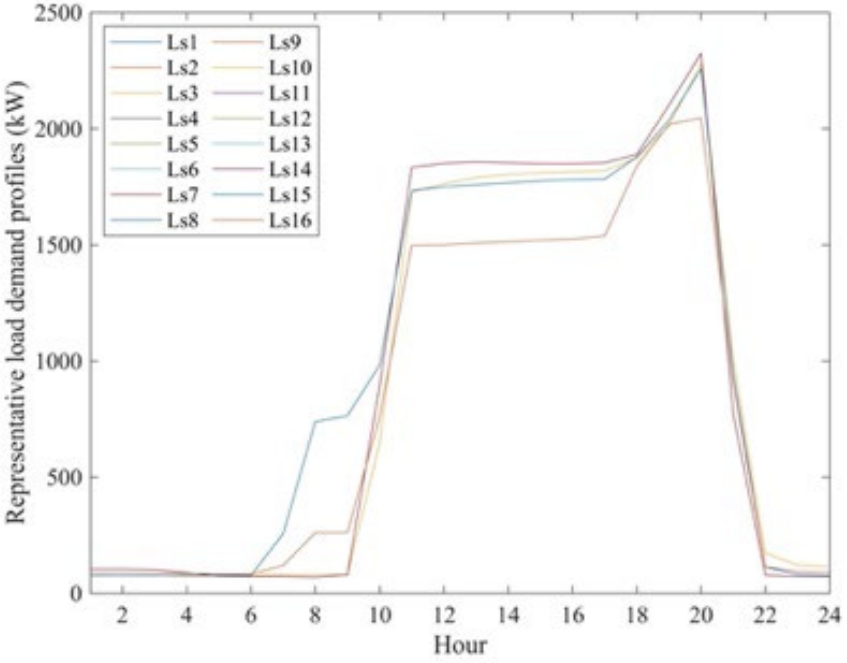

Fig. 4-8 Typical daily load of building (Building 28)

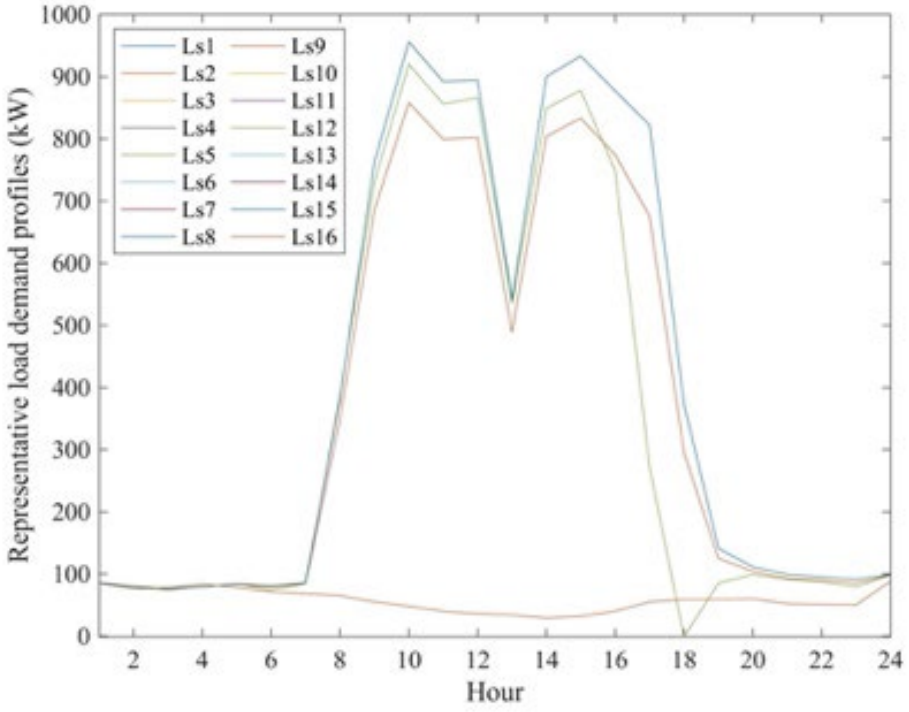

Fig. 4-9 Typical daily load of building (Building 36)

Table. 4-4 Basic information of the research target building

Building number	Daytime maximum electricity consumption (kWh)	Daytime minimum electricity consumption (kWh)	Daytime mean electricity consumption (kWh)	Business day (days)	Closing day (days)
B1	2928	9133	5501	365	0
B2	1463	17808	10176	321	44
B3	20332	39866	29323	365	0
B4	16856	22476	19368	365	0
B5	9973	24598	17194	365	0
B6	6594	13535	9272	365	0
B7	9161	14990	11221	365	0
B8	1972	21042	12035	255	110
B9	6547	12687	9108	365	0
B10	5487	6703	6226	365	0
B11	5627	8229	6813	365	0
B12	5730	8567	6641	365	0
B13	2086	5559	4039	365	0
B14	14018	20394	17351	365	0
B15	1511	5788	3728	365	0
B16	37656	20135	24176	365	0
B17	16595	6544	11456	255	110
B18	8518	2921	5496	255	110
B19	14564	8272	10767	365	0
B20	42629	17621	28649	365	0

B21	2973	629	1929	255	110
B22	5013	479	1676	185	180
B23	23705	12183	15919	365	0
B24	3286	554	2009	255	110
B25	5226	1242	2962	255	110
B26	15275	7424	9933	365	0
B27	19492	10580	14339	365	0
B28	22950	19629	20669	365	0
B29	30624	21094	23790	365	0
B30	10394	6338	8236	365	0
B31	26812	20239	22401	365	0
B32	46925	27017	35292	365	0
B33	8027	5734	6500	365	0
B34	32646	18038	23352	365	0
B35	9539	1393	7185	321	44
B36	6183	957	3846	255	110
B37	7822	3594	5120	365	0
B38	18407	4539	10600	255	110
B39	17754	12381	13790	365	0

The users adaptation under three different conditions are considered according to the degree of liberalization of the different buildings: (1) Case 1, Electricity consumption: according to the annual electricity consumption, three consumption level are divided, which are (a) Low: from 0~3,650,000 kWh (daily electricity consumption is less than 10,000 kwh); (b) Medium: from 3,650,000~7,300,000 kWh (daily electricity consumption is between 10,000 and 20,000 kwh); (c) High: from 7,300,000~ kWh (daily electricity consumption is higher than 20,000 kwh). (2) Case 2, Load curve types: (a) Daytime type (the main consumption of electricity is during the daytime); (b) Nighttime type (the main consumption of electricity is during the nighttime); (c)

Balanced. (3) Case 3, Electricity consumption cyclicality: according to the time difference of load, the three-cyclicality situation are discussed, which are (a) Constant (the daily load curve is not changed by the time); (b) Season based (there is a great difference in load curve according to different seasons); (c) Rest-day based (there is a great difference in load curve between working days and weekends).

Table. 4-5 Electricity consumption characteristics of buildings

Building	**1**	**2**	**3**	**4**	**5**	**6**	**7**	**8**	**9**	**10**
Electricity consumption	low	medium	high	high	high	medium	medium	medium	medium	low
Load curve types	Daytime type	Daytime type	Daytime type	Daytime type	Balanced	Nighttime type	Daytime type	Daytime type	Balanced	Daytime type
Cyclicality	Season based	Season based	Season based	Season based	Season based	Season based	Season based	Rest day based	Season based	Constant
Building	**11**	**12**	**13**	**14**	**15**	**16**	**17**	**18**	**19**	**20**
Electricity consumption	medium	low	low	medium	low	high	medium	low	low	high
Load curve types	Balanced	Balanced	Daytime type	Daytime type	Daytime type	Nighttime type	Daytime type	Daytime type	Daytime type	Daytime type
Cyclicality	Season based	Season based	Season based	Constant	Rest day based	Season based	Rest day based	Rest day based	Constant	Season based
Building	**21**	**22**	**23**	**24**	**25**	**26**	**27**	**28**	**29**	**30**
Electricity consumption	low	low	medium	low	low	medium	medium	high	high	medium
Load curve types	Daytime type	Daytime type	Daytime type	Daytime type	Daytime type	Daytime type	Daytime type	Daytime type	Daytime type	Balanced

Cyclicality	Rest day based	Rest day based	Constant	Rest day based	Rest day based	Season based	Constant	Constant	Constant	Season based
Building	**31**	**32**	**33**	**34**	**35**	**36**	**37**	**38**	**39**	**-**
Electricity consumption	high	high	low	high	low	low	low	medium	medium	-
Load curve types	Day time type	Day time type	Balanced	Nighttime type	Day time type	Daytime type	Day time type	Nighttime type	Day time type	-
Cyclicality	Season based	Season based	Season based	Season based	Rest day based	Rest day based	Season based	Rest day based	Constant	-

4.2.2 Distributed network

The Higashida Smart Community demonstration test is conducted in Yahata Higashida district of Kitakyushu City, that is redeveloping the former site of the Nippon Steel & Sumitomo Metal Corporation Yawata Works plant to promote next-generation urban development that symbiotically combines advanced urban infrastructure and the environment. More than 70 companies and organizations are the participants.

① Network

In Japan, electricity is transmitted at a reduced voltage. The voltage of the base trunk system in the project is 6600V, and power is supplied to the demand side by stepping down to 200V and 100V. The electricity generated is transmitted to the demand area through the grid while gradually lowering the voltage, but along the way it also includes electricity from renewable energy sources such as solar power installed in factories, office buildings, hospitals, etc. There are both power flow and reverse power flow. Demand-side energy such as small-scale solar power generation, stationary batteries, and electric vehicles (EVs) are introduced and installed at the consumer side (general households, stores, etc.) of the grid located at the end.

Due to the large amount of renewable energy imported, frequent voltage as well as power regulation is a big challenge. Therefore, the project area is equipped with a smart power conditioning system (PCS). The Smart PCS (consisting of a PCS and a controller) typically operates at around 400 to 600V. It converts the DC power generated by the autonomous operating system into AC power and boosts it to 6600V for connection to the main system.

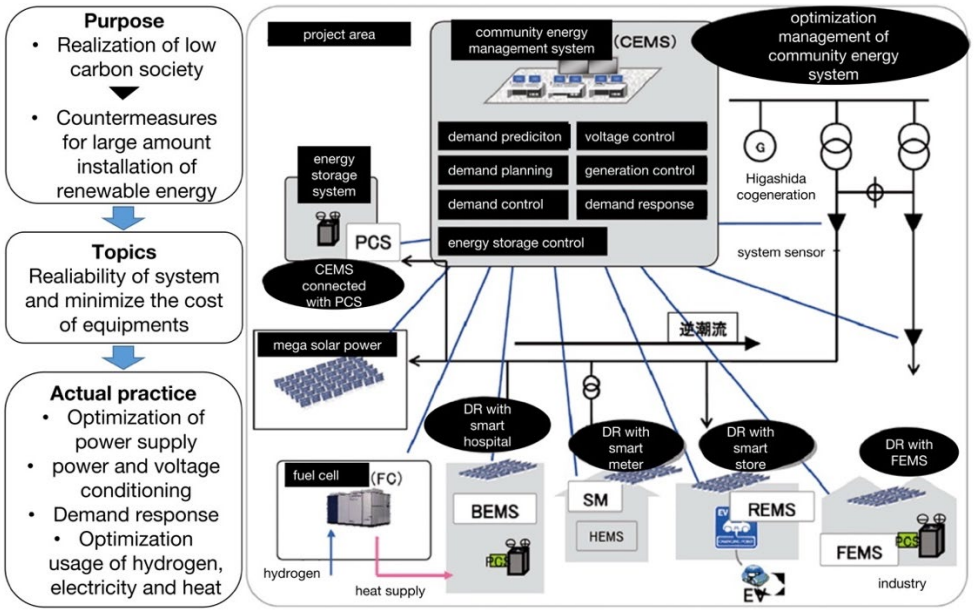

Fig. 4-10 Overall view of the CEMS (Community Energy Saving Station) in the Kitakyushu

On the other hand, the PV generation is another challenge. If the power generated by the solar panels exceeds the power consumption of the installation buildings (e.g. smart house) and appears reverse power flow, the main voltage of the system will increase. Therefore, if the distribution voltage may deviate from the appropriate value (101±6V: 95-107V) as specified in "Article 26 of the Electricity Utilities Act", it is necessary for the installer of the solar power facility to automatically prevent the reverse power flow. The community energy management center (CEMS) should anticipate this situation and output reactive power to the energy storage system to adjust the voltage appropriately [6].

② Advanced Metering and Communication Infrastructure

Low voltage (100V/200V) smart meters were installed in 230 homes within the community [7]. High voltage (6600V) smart meters were installed in 50 offices. The electricity consumption data of each household is sent to concentrator to aggregate and then transmitted to a CEMS (central).

This demonstration experiment in Kitakyushu chose the 920 MHz band for multi-hop communications because the 920 MHz band designation for low-power wireless systems does not require a license and the designation for low-power wireless systems is less expensive and less operational. The data between the internal display and the smart meter is updated frequently every minute, and the CEMS has real-time information on the demand side of the electricity consumption. In addition, CEMS can balance the electricity supply and demand by analyzing the past values of smart meters collected from each household based on weather forecasts such as the next day's weather and temperature. Therefore, our proposed aggregation of individual energy storage devices to achieve better load leveling is also able to be realized.

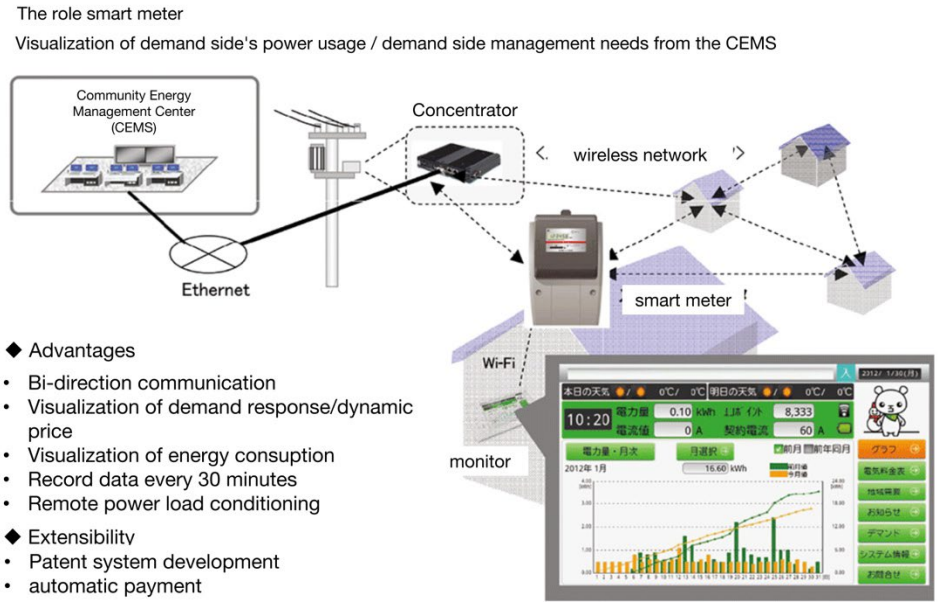

Fig. 4-11 Smart Meter System Configuration in Kitakyushu Demonstration

4.2.3 Data Processing

In this stage, the annual data set is processed using principal component analysis (PCA) to extract the most important features of each day. PCA is a feature extraction tool that is used to extract relevant information from a confusing data set. They can also reduce a complex data set to a lower dimension one while retaining, as much as possible, the variation present in the data to reveal the hidden structures that underlie it and filter out noise.

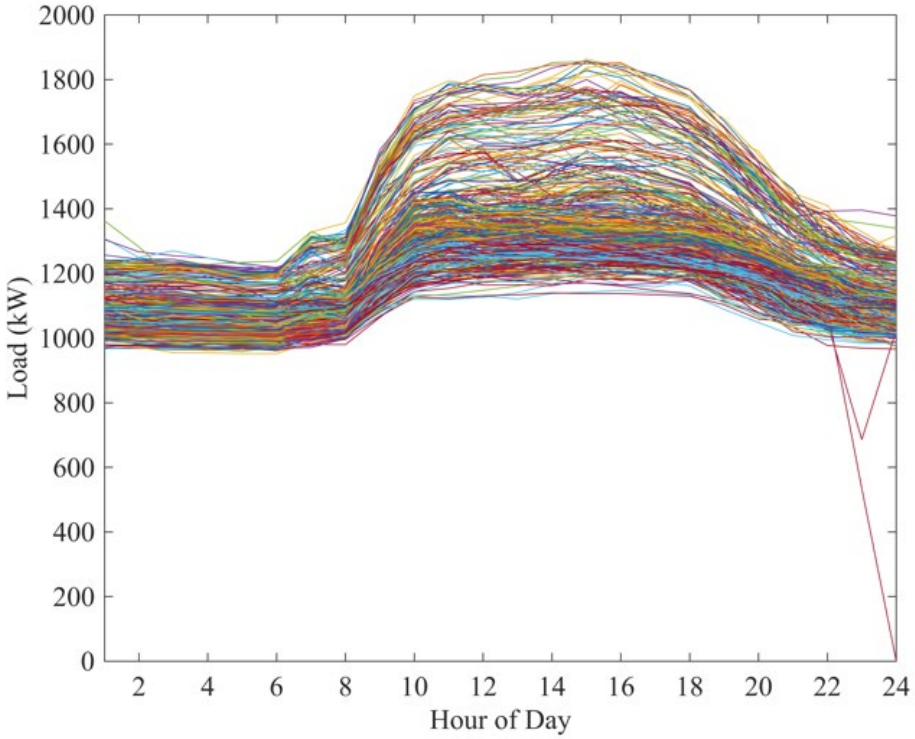

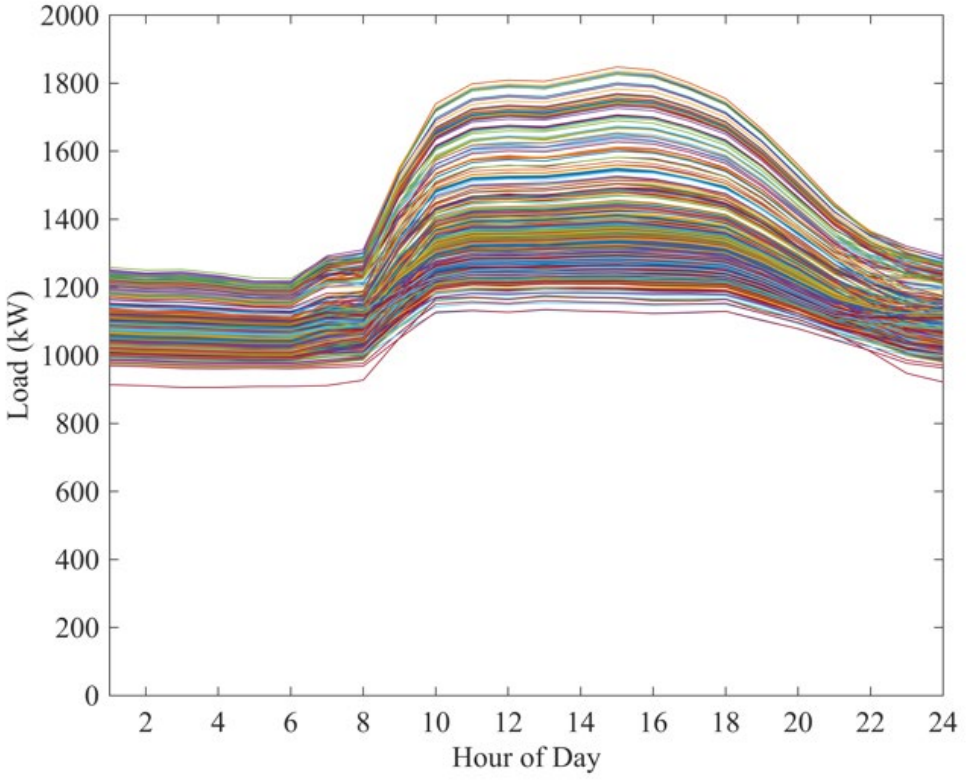

Fig. 4-12 Demonstration Aggregate load demand profiles of building 4 (a): Raw data (b): Reconstructed data using PCA

The use of 365 load demand profiles (i.e., one year data) in stochastic optimization for ESS sizing can be computationally very expensive. To reduce the computational complexity while retaining high accuracy, *k*-means clustering method is used in this paper. Hence, the reconstruction of aggregate load profiles with PCA is followed by clustering of aggregate load demand profiles into separate non-overlapping clusters using *k*-means clustering [8] [9].

To determine the optimal number of clusters, the elbow method is employed using within-cluster sum of square errors (SSE) as the validation index. In the elbow method, the SSE value is evaluated corresponding to different number of clusters and then plotted. Fig. 2 illustrates the variation of SSE against the number of clusters of one of user. It is observed from Fig.2 that SSE value sharply from 1 to 3, but hardly degrade beyond 3 clusters. Thus, 3 is the termed as optimal number of clusters of user No.3 in the elbow method. Fig.4 shows optimal number of clusters of all participating users. Among them, the optimal number of clusters for 20 users is 4, the optimal number of clusters for 18 users is 3, and one user is 5 and 6. In order to reduce the dimensionality, we choose 4 as the optimal number of clusters for all consumers.

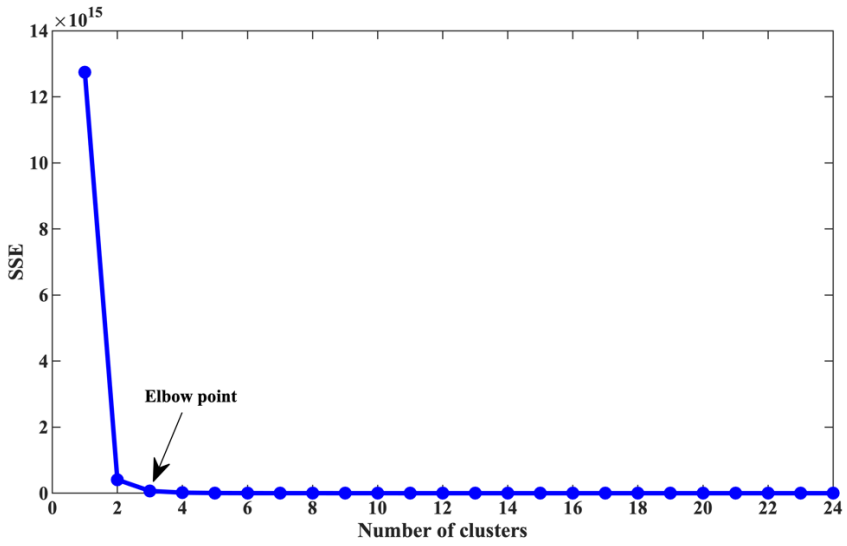

Fig. 4-13 Variation of SSE value with the number of clusters in the Elbow method

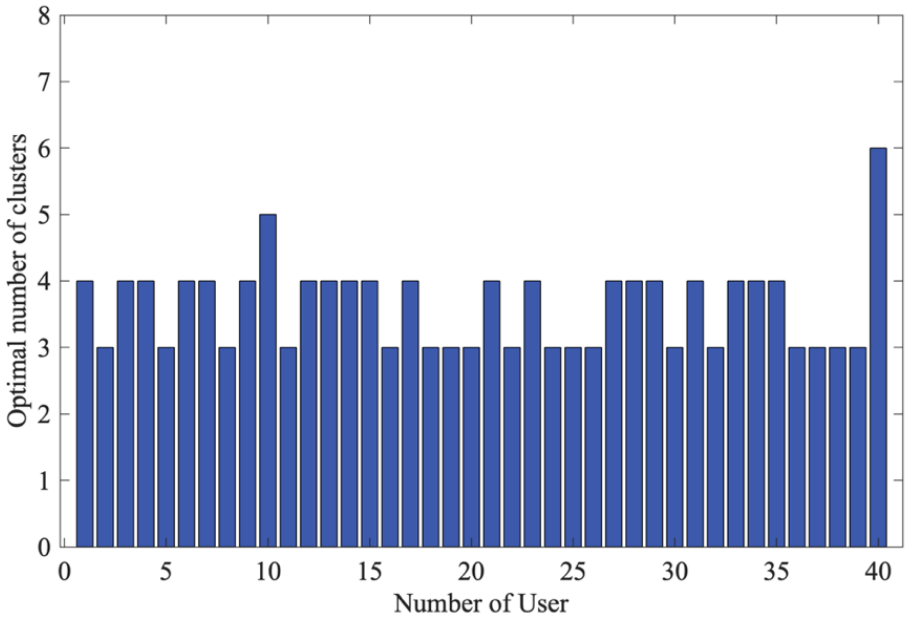

Fig. 4-14 Optimal number of clusters of all consumers

References

[1] Araki K. Meteorological Data Viewers at Japan Meteorological Agency. Proceedings of Seventh Workshop on Meteorological Operational Systems, ECMWF1999.

[2] Center JMAEC. Outline of Operational Numerical Weather Prediction at Japan Meteorological Agency: Japan Meteorological Agency; 1983.

[3] Shimose K-i, Ohtake H, da Silva Fonseca Jr JG, Takashima T, Oozeki T, Yamada Y. Improvement of the japan meteorological agency meso-scale model for the forecasting the photovoltaic power production: Modification of the cloud scheme. Energy Procedia.

2014;57:1346-53.

[4] Zheng Y, Novianto D, Zhang Y, Ushifusa Y, Gao W. Study on Residential Lifestyle and Energy Use of Japanese Apartment/Multidwelling Unit–An Investigation on Higashida Smart Community of Kitakyushu. Procedia-Social and Behavioral Sciences. 2016;216:388-97.

[5] Lu Y, Gao W, Kuroki S, Ge J. Household characteristics and electricity end-use under dynamic pricing in the collective housing complex of a Japanese smart community. Journal of Asian Architecture and Building Engineering. 2021:1-16.

[6] Gao W, Fan L, Ushifusa Y, Gu Q, Ren J. Possibility and challenge of smart community in Japan. Procedia-Social and Behavioral Sciences. 2016;216:109-18.

[7] Oga E, Kabasawa A. Social system demonstration of dynamic pricing in the Kitakyushu smart community creation project. FUJI ELECTRIC REVEIW. 2013;59:152-9.

[8] Yang J, Zhang D, Frangi AF, Yang J-y. Two-dimensional PCA: a new approach to appearance-based face representation and recognition. IEEE transactions on pattern analysis and machine intelligence. 2004;26:131-7.

[9] Mika S, Schölkopf B, Smola A, Müller K-R, Scholz M, Rätsch G. Kernel PCA and de-noising in feature spaces. Advances in neural information processing systems. 1998;11.

Chapter 5

DEVELOPMENT OF A NEW SOLAR RADIATION MODEL

DEVELOPMENT OF A NEW SOLAR RADIATION MODEL

5.1 Contents 5-1

5.2 Materials and Methodology 5-4

5.2.1 Analysis of global solar radiation models 5-4

5.2.2 A new concept from layer-by-layer weakening theory 5-5

5.2.3 Methods 5-6

5.2.4 Solar Geometry 5-7

5.2.5 Data collection 5-9

5.2.6 Processing flow 5-10

5.2.7 Statistical test methods 5-12

5.3 Result and discussion 5-13

5.3.1 Model Establishment 5-13

5.3.2 Overall forecast result 5-18

5.3.3 Available for rainy and cloudy conditions 5-26

5.3.4 Interpretability 5-29

5.3.5 Comparison and Expansion 5-29

5.4 Application 5-33

5.5 Conclusion 5-35

Appendix A 5-36

References 5-39

5.1 Contents

As the population grows and urbanization accelerates, the energy crisis and environmental issues are becoming increasingly prominent [1, 2]. Solar energy is one of the most attractive renewable sources of electricity and heat, as it has the advantages of no pollution, wide distribution, and abundant reserves [3, 4]. Solar energy has been widely used in various fields such as photovoltaic power generation [5], building energy saving [6, 7], weather forecasting [8], climate change monitoring [9], and agricultural drought [10]. As the primary data of solar energy, solar radiation is of great importance for various applications in the building sector, such as air conditioning design, thermal simulation of buildings, and passive solar house design. Additionally, the intermittent, fluctuating, and random nature of solar energy makes integrating PV power into the grid a very challenging task (e.g., the severe curtailment of generation [11] or lack of resilience in the face of failures and disturbances [12, 13]). Accurate and reliable solar radiation information can optimize the management between the entire system and the grid, thus facilitating better integration of solar energy and building energy systems [14]. Unfortunately, for economic reasons, there are far fewer weather stations that observe hourly solar radiation than those that observe general meteorological parameters (e.g., temperature, relative humidity, wind speed, and sunshine duration). Accordingly, in an effort to overcome these difficulties, it is necessary to develop models for estimating solar radiation based on general meteorological parameters.

Firstly, general meteorological parameters can be analyzed by regression with solar radiation to establish empirical models. Due to the simplicity of the expression form, it is widely used in its long development. The parameters commonly used in this empirical solar model are sunshine duration, temperature, or a mixture of other meteorological parameters. The initial sunshine duration model was first proposed by Angstrom in 1924 [15]. It is based on the analysis of the ratio of measured daily solar radiation to theoretical clear-sky solar radiation and the ratio of measured daily sunshine duration to the theoretical maximum possible sunshine duration. Then Prescott (1940) modify this model by replacing the clear-sky solar radiation with theoretical extraterrestrial solar radiation, which is more readily available; this modified form is called the Angstrom-Prescott model [16]. Since then, based on the Angstrom-Prescott model, different scholars have refined and improved the model [17] [18] [19] [20] [21]. Similarly, some scholars have developed linear, polynomial, exponential, and power functions between the clear sky index and the maximum, minimum, and average temperatures, and temperature differences [22] [23, 24] [25]. One of the classic models is the power function model proposed by Hargreaves using daily temperature differences and extraterrestrial solar radiation [23]. The models mentioned above are convenient for calculating daily solar radiation. Daily solar radiation is valuable for some specific applications, such as assessing the maximum output potential of solar generation. Nevertheless, for other scientific engineering applications, such as thermal utilization and heat gain in buildings, hourly solar radiation are increasingly required.

An hourly solar model is initially developed by Zhang and Huang for Beijing and Guangzhou, China [26]. Zhang and Huang use common meteorological parameters such as temperature, humidity and cloud cover to establish a polynomial relationship with hourly solar radiation [27].

It uses observed cloud cover data to reflect the effect of clouds on solar radiation under all-day conditions. The accuracy of the Zhang model has been verified in many previous studies [28] [29] [30]. Despite the fact that the many advantages of the Zhang and Huang model the cloud data used are not recorded numerically but as described: clear, scattered, broken, overcast, obscured and partially obscured [26]. Hence, the Zhang and Huang model needs to be deeply studied. In addition, although the authors claim that the proposed model can be adapted to all-sky conditions, there are still many technical difficulties in the study of clouds, and more evidence is needed to show that cloud cover is correlated with all-sky conditions.

In recent years, there has been an increasing interest in machine learning models, such as different artificial neural networks and support vector machine (SVM) models to estimate solar radiation. AI-Alawi and AI-Hinai [31] use a multi-layer feed-forward network and back-propagation training algorithm for analyzing the relationship between global radiation and climate variables. The results show that using location, month, average pressure, average temperature, average vapor pressure, average relative humidity, average wind speed and average sunshine hours as inputs, an accuracy of approximately 93% and an average absolute percentage error of 7.30 are achieved. Lazzús, J.A.et al. [32] have developed an artificial neural network using data measured from weather stations to estimate the hourly global solar radiation in La Serena (Chile). Then, an R-square value of 0.94 is found, indicating a strong correlation between hourly global solar radiation and meteorological data. Kaba, K. et al. [33] train the model using the Self-Regulating Particle Swarm Optimization algorithm. The parameters sunshine hours, cloud cover, maximum temperature, and minimum temperature are selected as inputs and 16 different input combinations were constructed. The results show that the deep learning model produces very accurate and comparable results in estimating the daily global solar radiation. Hassan, M.A. et al. have compared gradient boosting decision tree, random forest, multilayer perception, decision tree and SVM and concluded that SVM produced the highest accuracy but is 39 times more computationally expensive than the other models. As a result, many improved SVM models have been proposed [34]. In addition, researchers are keen to integrate multiple deep learning techniques, called Ensemble-based machine-learning models. Basaran, K., A. et al. [35] develop Ensemble-based machine-learning models based on SVM, multilayer perception, and decision tree, then give us a reference conclusion as compared to the single models, Ensemble-based machine-learning models improved the RMSE significantly. Gao, Y. et al. [36] develop a deep Long short-term memory-based generative model for multi-step solar irradiation prediction for at least 24 hours in the future. Peng, T. et al. [37] propose a hybrid model by combining the Bi-directional long short-term memory model sine cosine algorithm and complete ensemble empirical mode decomposition with adaptive noise for solar radiation prediction. The effectiveness of the Bi-directional long short-term memory network in processing solar radiation time series data and improving the prediction accuracy is demonstrated. Zhou Y. et al. [38] provide a comprehensive and systematic review of all important aspects of machine learning models, including input parameters, feature selection, and model development and presents a guide for machine learning models in solar radiation prediction. This is despite the fact that many studies have shown that the prediction accuracy of machine learning is generally higher than that of general empirical models, as a branch of data science, machine learning models have difficulty in

giving proper interpretation among the input parameters. Some researchers are trying to construct appropriate models to improve the interpretability as well as the credibility of the results. Gao, Y. et al. [39] investigate the interpretability of the temporal and spatial dependence of the prediction process through attentional mechanisms and graph neural networks. The results show that solar radiation is directly related to month, time, temperature, infiltration rainfall, water vapor pressure and radiation time. However, current findings are far from satisfactory.

The solar radiation estimation models mentioned above have high accuracy and wide applicability, they are mostly statistical or data-driven models. But it is difficult to guarantee that the forecasts will remain convincing when conditions change (e.g., geographic climate and weather conditions). Consequently, a proper theoretical basis is necessary for high-precision solar radiation prediction. In 1981, Richard E. Bird and Roland L. Hulstrom [40] first proposed a layer-by-layer weakening solar radiation model which divided the weakening layers into six layers: mixed gas layer, ozone layer, Rayleigh layer, water vapor layer, aerosol layer and cloud layer. The model is theoretically clear and consistent with the laws of nature. However, in the calculation of Bird model, the weakening effect is reflected by the transmittance, and it is necessary to consider the transmittance of each layer, which is complicated to use in practice. Chen et al. [41] refer to some data from NCEP/NCAR and some information about the terrain to improve the Bird model as input items. The results show that the accuracy of the model is improved by 7.58%, but it is greatly reduced in cloudy conditions. The accuracy of the model is limited by the resolution of the data. Su, G. et al. [42] modify the weakening solar radiation model by using relative humidity and air quality index. The result show that the R value of the layer-by-layer weakening model is increased by 5.74% and 41.27% compared with the existing beam solar radiation model and diffuse solar radiation model. Unfortunately, typical weakening models use data from satellite observations and invert them with specialized software. The collection and processing of satellite data is a huge challenge for the general weather station. The low resolution of satellite data also makes it difficult to meet the spatial and temporal adaptability requirements in practical applications.

Additionally, most of the models are developed based on clear-sky conditions. Nevertheless, it is increasingly required that hourly solar radiation models maintain a high level of accuracy and confidence in complex weather conditions, especially, nowadays with the frequent occurrence of extreme weather. Based on the aforementioned studies, the knowledge gaps identified in this paper are as follows:

• The relationship between easily obtainable meteorological parameters and solar radiation has not been sufficiently explored. In particular, the solar radiation’s weakening effect in the atmosphere.

• Seldom solar radiation models focus on the transmission rule of solar radiation, which is detrimental to the credibility of the results and the improvement of the models.

• The hourly solar radiation model development and validation for long-term and under multiple weather conditions are neglected.

In this regard, the contribution of this work is as follows:

• Low-cost meteorological parameters (relative humidity, precipitation, weather, etc.) are used to construct a highly accurate hourly solar radiation model.

• Based on the classical layer-by-layer weakening solar radiation theory, a new weakening solar radiation model is proposed.

• The proposed model is established and calibrated under a variety of weather conditions to maintain more strong adaptability to cloudy and rainy days.

The rest of the paper is organized as follows. In Section 2, the materials and methodology of the proposed model is presented. The result and discussion are described in Section 3. Finally, the conclusions are presented in Section 4.

5.2 Materials and Methodology

5.2.1 Analysis of global solar radiation models

Many global solar radiation models attempt to estimate the ratio between the radiation incident on the surface water plane and a radiation threshold (usually extraterrestrial radiation). Firstly, it is dimensionless and has a clear physical meaning, it can be expressed as the transmittance of solar radiation in the atmosphere on a clear or cloudy day. Therefore, the ratio can be referred to as the clearness index. As described in Section 1.2, a large number of studies [43] have tried to establish a functional relationship between the clearness index and general meteorological parameters (e.g. sunshine duration, temperature, humidity, and their combinations), and this class of models can be described by the following equation:

(5-1)

where I is the global solar radiation. I_0 is the extraterrestrial solar radiation. $f(\sigma)$ is a function expression containing meteorological parameters. They are mostly accurate when dealing with monthly values or daily resolution forecasts. This is because the meteorological parameters used provide feedback on the seasonal variation of solar radiation (accumulated values over time). But most of these models are not applicable when the resolution becomes hourly or instantaneous values. The reason is that a denominator close to zero due to the formal characteristics of the fraction can lead to a large amount of computational error in the prediction results. Normally, the daily accumulated value of extraterrestrial solar radiation in Japan is about 10~40 MJ/m2, while at sunrise and sunset, the extraterrestrial solar radiation is close to zero and this cannot be ignored. Also the distribution of solar radiation is not continuous and does not satisfy L'Hospital's rule. Therefore, the limit value of the ratio of two infinitesimals cannot be found by deriving the derivative. In addition, since the negative quadrature of X is a growth function, errors in the observation and recording process can also cause unacceptable errors.

In addition, in fine-grained solar radiation forecasting efforts, transient changes in the state of the sky can lead to a substantial increase in the randomness of the solar radiation distribution.

Individual seasonal meteorological parameters such as temperature do not correlate well with instantaneous solar radiation. Therefore, a combination of multiple meteorological parameters especially physical quantities describing the state of the sky is a better choice.

5.2.2 A new concept from layer-by-layer weakening theory

Based on the literature review of battery sharing, and our work, the effectiveness of BESS at the individual as well as community level can be demonstrated to act for better energy planning. However, when moving up to the city level of service recipients, there is still some room for improvement in data utilization, interoperability, and integrated management of the technologies currently used in BESS applications. This section will present the upgrade of BESS service targets and the future directions. It is well known that cities are pagoda-shaped, from single buildings to community or to city, and the higher up it is, the more the individuals or systems involved will grow exponentially. The current BESS application techniques are mainly used only for specific buildings or groups within cities and do not take into account the level of the city. As a result, we have taken an important step forward in our work. We have expanded the application of BESS from individual buildings to the community level and are connecting customers scattered across the city through battery sharing. Accordingly, BESS will improve the connectivity between systems to fully integrate the various factors that affect energy generation and consumption in cities. In order to achieve city-level interaction, the application strategy of BESS still faces some challenges. First, since BESS cannot be separated from the analysis, utilization, and interaction of data. Therefore, energy data needs to be collected and shared at all levels of the city through an integrated IoT. And geospatial information and automation-based technologies need to be shared as well to reflect the changing spatial and environmental characteristics of the city.

Most of the meteorological data used in the existing layer-by-layer solar radiation weakening models (The specific functional expressions for this model are provided in A.2) come from the MODIS official website (https://modis.gsfc.nasa.gov/data/). The main input parameters include geographic parameters (land surface elevation, hillside slope, hillside azimuth, solar zenith angle, solar azimuth) and physical parameters (total cloud fraction, precipitable water content, ozone amount, aerosol optical depth, precipitation rate, and ground albedo). The MODIS meteorological data are collected from satellite photography and then reversed by professional software. Total cloud fraction is from the MODIS Atmosphere Level 2 cloud product (MYD/MOD06_L2), precipitable water content is from the MODIS Atmosphere Level 2 precipitable water vapor product (MYD/MOD05_L2), and ozone amount is obtained from the MODIS atmospheric profile product (MYD/MOD07_L2). The ground albedo is converted from the MODIS Surface Reflectance product (MYD/MOD09) using an algorithm for total shortwave albedo retrieval based on the assumption that the land surface behaves as Lambertian [44]. The details of the method can be found in [45, 46]. Despite accurate data, the collection and processing of satellite data is a non-negligible challenge for decentralized weather stations. Therefore, it is a better choice for weather stations to apply locally and simply obtain weather data. In addition, only the effect of precipitation on airborne moisture content is considered in the existing models. Still, precipitation does not directly reflect changes in airborne moisture due to seasonality and differences in weather types. Some studies have tried to correct the water vapor layer as well as the aerosol layer to improve the accuracy. However, the available results show that the

classical layer-by-layer solar radiation reduction model and his improved model are not satisfactory on cloudy and rainy days. Hence, the research in this work focuses on the application of locally available and simple meteorological parameters to develop a new layer-by-layer weakening solar radiation model that is usable on cloudy and rainy days.

Based on the classical layer-by-layer solar radiation model, the weakening process of solar radiation can be divided into six layers: mixed gas layer, ozone layer, Rayleigh layer, water vapor layer, aerosol layer and cloud layer (Fig. 5-1).

The precipitation, relative humidity, visibility, and cloud cover are added to the water vapor layer, aerosol layer and clouds layer respectively to make the solar radiation weakening models more reliable and easily applicated. Meanwhile, weather type and sunshine duration are considered as combined influencing factors. The specific concept is shown in Fig. 5-1.

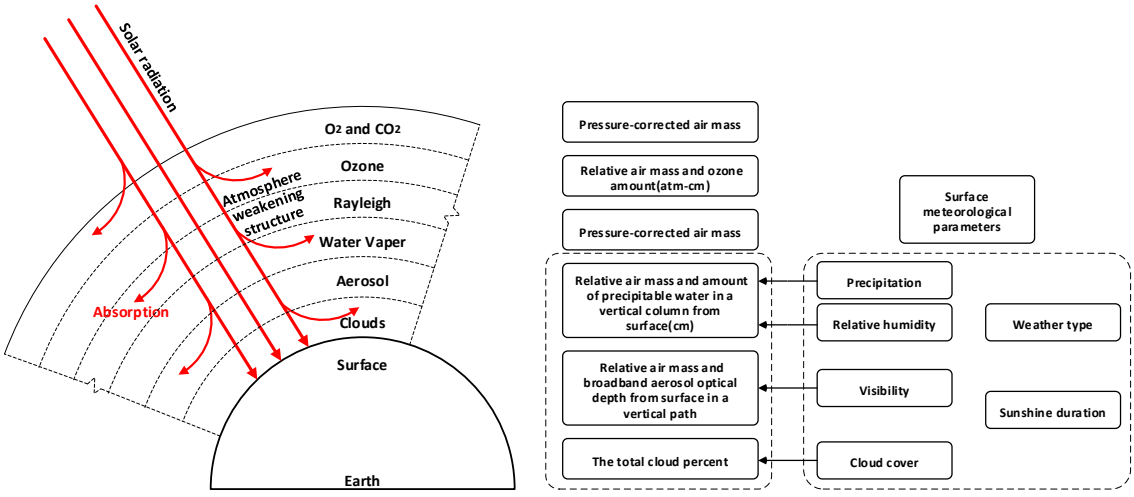

Fig. 5-1. The new concept of layer-by-layer weakening solar radiation models (Note: The layers shown only indicate the influence of radiation weakening and do not represent the physical composition of the atmosphere.)

5.2.3 Methods

The typical solar radiation weakening model for global solar radiation can be obtained using Eq.(A1) to Eq.(A7) in A.2. It is easy to understand that the typical weakening model functions the layer-by-layer weakening process of solar radiation as the transmittance of each layer to the radiation as shown in the Eq.(A2). Although the physical meaning of the expression is well defined, the complexity of the equation is significant. In addition, cloud cover is neglected in the typical weakening model because it is difficult to obtain by satellite retrieval, which is regarded as an influential factor in solar radiation estimation.

In an attempt to reduce the computational complexity while maintaining the physical meaning of the model. We propose the conceptual weakening model as follows:

$$I = I_0 - \Delta I \tag{5-2}$$

$$\Delta I = c_4 \cdot (c_1 \cdot L_a + c_2 \cdot L_w + c_3 \cdot L_c + c_0) \tag{5-3}$$

where I_0 is the extraterrestrial solar radiation. ΔI is loss value of solar radiation in the atmosphere (W/m2). L_a is the standard losses value in the aerosol layer (W/m2). L_w is the standard losses value in the water vapor layer (W/m2). L_c is the standard loss amount in the clouds layer. c_0 are c_4 the coefficients (dimensionless). Due to the homogeneity of the distribution of the mixed gas layer, the ozone layer, and the Rayleigh layer, it is possible to identify a constant value (c_0) for the loss value of solar radiation in these three layers.

5.2.4 Solar Geometry

① The extraterrestrial solar radiation

The circular motion performed by the Sun and the Earth results in a periodic variation of the angle of solar radiation in the horizontal plane. The solar radiation received on the horizontal surface is related to the solar incidence altitude and the incident direction. In the existing literature, the solar zenith angle is always considered an important variable to describe the position of the Sun. The solar altitude angle (θ) is estimated from the solar declination angle (δ), the geographical latitude (φ) and the solar hour angle (ω) as follow:

$$\sin\theta = \sin\varphi \sin\delta + \cos\varphi \cos\delta \cos\omega \tag{5-4}$$

The extraterrestrial solar radiation can be considered as the theoretical maximum of solar radiation on the surface. I_0 is obtained using Eq. (5):

$$I_0 = I_{sc} \cdot E_0 \cdot \sin\theta \tag{5-5}$$

where I_{sc} is the solar constant which is equal to 1361 W/m2. E_0 is the eccentricity factor. According to the Eq. (5), the temporal and seasonal trends of extraterrestrial solar radiation can be accurately described as shown in Fig. 5-2. Therefore, the extraterrestrial solar radiation can be used as the starting parameter of the proposed weakening model.

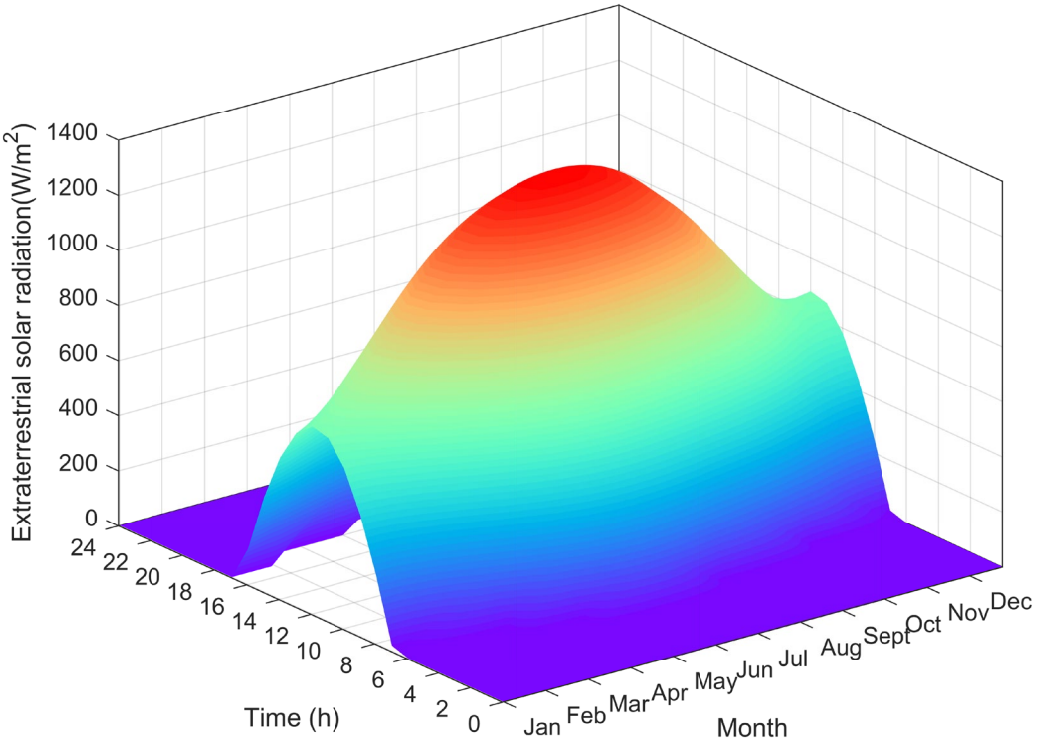

Fig. 5-2. The seasonal and daily trend of extraterrestrial solar radiation (Example site: Abashiri; example year: 2000).

② Solar radiation paths

Solar radiation needs to pass through the atmosphere before it reaches the surface. The relative position of the Sun and Earth is constantly altered, thus causing the length of solar radiation through the atmosphere always to change. Consequently, to properly analyze the intrinsic relationship between the weakening effects of solar radiation and meteorological parameters, it is necessary to consider the seasonal and daily trends of the length of solar radiation through the atmosphere. The solar altitude angle has attracted our attention because it serves as a very simple characterization variable for the relative position of the Sun and the Earth. As shown in Fig. 5-3, when the solar altitude angle is small, the solar radiation travels a long distance through the atmosphere and therefore the amount of weakening of the radiation is greater. As a result, Eq. and can be improved as follows:

$$\Delta I = \sin\theta \cdot (c_1 \cdot L_a + c_2 \cdot L_w + c_3 \cdot L_c + c_0) \tag{5-6}$$

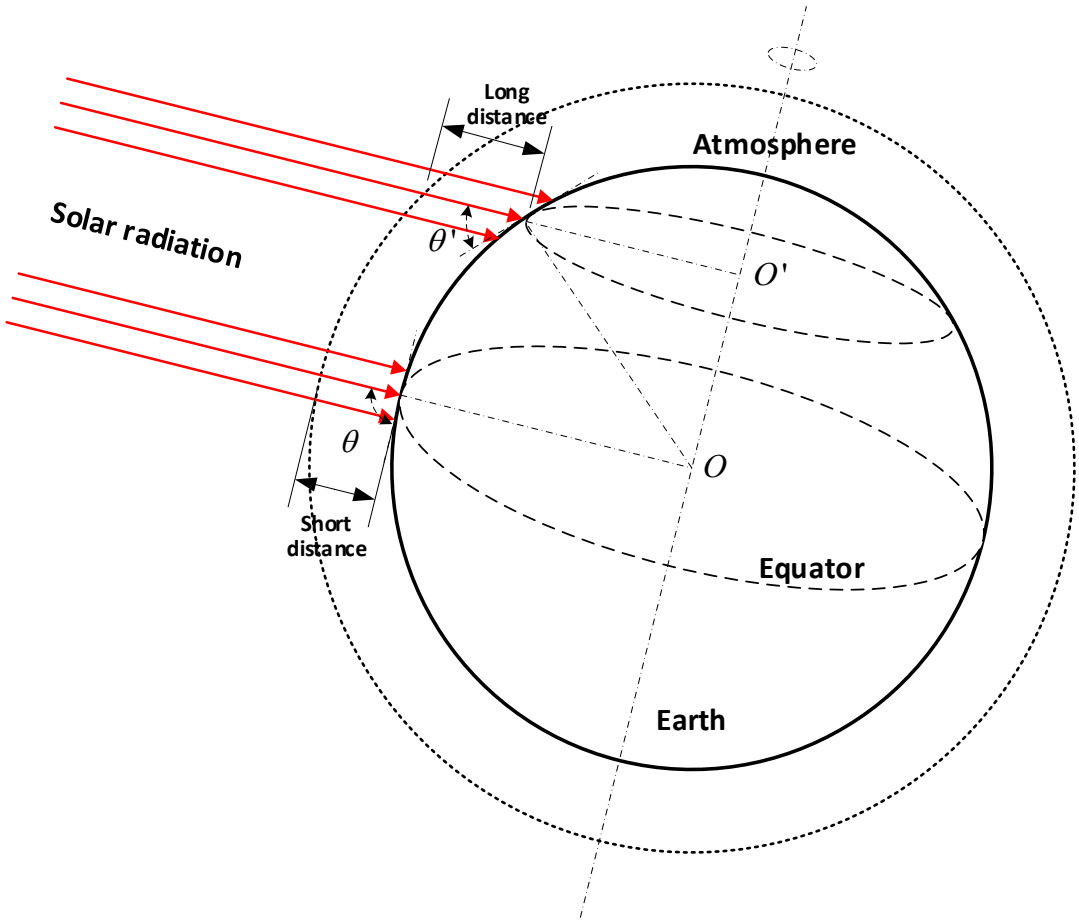

Fig. 5-3. The angle of incidence and path length of solar radiation

5.2.5 Data collection

In this paper, a public dataset with meteorological parameters is used. Data are collected from January 2000 to December 2021 at seven Japanese observations. The seven selected observation sites cover the geographical features of Japan well in order to prevent latitude and longitude differences from affecting the proposed model. The geographical locations are plotted in Fig. 5-4. Adopted dataset is recorded by the Japan Meteorological Agency. Table 5-1 summarizes the description of the meteorological parameters. All of those data have been inspected and quality controlled.

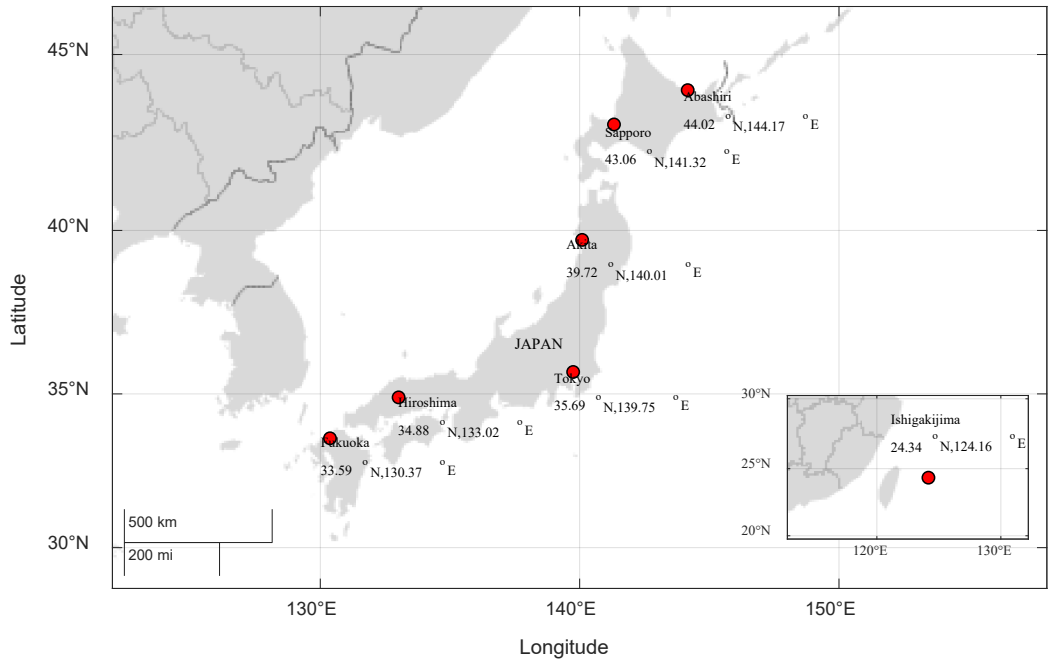

Fig. 5-4. Locations of meteorological observations referenced in this study: latitude (degrees), longitude (degrees).

Table 5-1 meteorological parameters from the observation sites

Surface Meteorological Parameter	Symbol	Unit	Resolution	Description
Relative humidity	*RH*	%	1h	-
Cloud cover	*CC*	dimensionless	3h	**Appendix Table** 5-1
Weather type	*W*	dimensionless	3h/1h	**Appendix Table** 5-2
Sunshine duration	*S*	hour	1h	-
Precipitation	*P*	mm	1h	-
Visibility	*V*	km	3h/1h	-
Solar radiation	*I*	MJ/m^2	1h	-

5.2.6 Processing flow

In this paper, based on the layer-by-layer weakening solar radiation, easily obtainable surface meteorological parameters are utilized to establish the weakened layer as a function of solar radiation in the following process:

- Data filtering. The raw data is first screened for missing values and outliers. Due to limitations in observation technology, weather stations will only provide weather type, cloud cover, and visibility at 3-hour resolution until 2019. Therefore, in order to maintain data consistency, data sets containing all of the above parameters are selected as data sources for the following analysis. After screening, the constructed dataset contains 205,722 sets of measurement data, of which 184,382 sets of data are used to build the model and 21,340 sets of data are used to verify the accuracy of the model. The data availability for each observation point is shown in Table 5-2.

- Modeling of solar radiation. The weakening value of solar radiation in the atmosphere is used as a medium to establish the functional relationship between meteorological parameters and the actual solar radiation received on the horizontal surface. Using the solar radiation data set from 1st January, 2000 to 31st December, 2018, the conventional functional forms such as exponential function, linear function, quadratic polynomial, and cubic polynomial are compared and analyzed. The best functional equation is determined.

- Model Validation. Finally, the proposed model is validated by the solar radiation measured in seven locations in Japan from 1st January, 2019 to 31st December, 2021 under 15 different weather conditions (which is summarized into three sky states), and the performance of the proposed model is evaluated.

Table 5-2 Data availability for each observation site

Site	Available data sets	Modeling data sets	Validation data sets
Abashiri	28,629	27,125	1,504
Sapporo	31,417	27,170	4,247
Akita	25,376	23,868	1,508
Tokyo	31,199	26,947	4,252
Hiroshima	30,697	26,539	4,158
Fukuoka	31,048	26,845	4,203

Ishigakijima	27,356	25,888	1,468
Total	205,722	184,382	21,340

5.2.7 Statistical test methods

In the existing literature, there are several statistical test methods used to evaluate the performance of the hourly solar radiation methods. The relative standard error (RSE), the root mean square error (RMSE), the relative root mean square error (rRMSE), Correlation coefficient (R), and Nash-Sutcliffe Equation (NSE) and are adopted in this study.

(1) Relative standard deviation (RSE)

The relative standard error can be calculated as follow:

$$RSE = \sqrt{\frac{1}{n}\sum_{i=1}^{n}\left(\frac{e_i - m_i}{m_i}\right)^2} \tag{5-7}$$

where e_i is the estimated value and m_i is the measured value.

(2) Root mean square error (RMSE)

The root mean square error can be calculated as follow:

$$RMSE = \sqrt{\frac{1}{n}\sum_{i=1}^{n}(e_i - m_i)^2} \tag{5-8}$$

(3) Relative root mean square error (rRMSE)

The relative root mean square error can be calculated as follow:

$$rRMSE = \frac{\sqrt{\frac{1}{n}\sum_{i=1}^{n}(e_i - m_i)^2}}{m_a} \times 100\% \tag{5-9}$$

where m_a is the average value of the measured value.

(4) Correlation coefficient (R)

The correlation coefficient can be calculated as follow:

$$R = \frac{\sum\left((m_i - m_a)(e_i - e_a)\right)}{\sqrt{\sum(m_i - m_a)^2 \sum(e_i - e_a)^2}} \tag{5-10}$$

where e_a is the average value of the estimated value and m_a is the average value of the measured value.

(5) Nash-Sutcliffe equation (NSE)

The Nash-Sutcliffe equation can be calculated as follow:

$$NSE = 1 - \frac{\sum (m_i - e_i)^2}{\sum (m_i - m_a)^2} \tag{5-11}$$

5.3 Result and discussion

5.3.1 Model Establishment

In this paper, relative humidity, cloud cover, weather type, precipitation, visibility and sunshine duration are chosen as possible characterization variables for the three weakened layers. The functional relationship Eq. is established as the basis. Their most suitable functional forms are discussed in this section. The linear function, quadratic polynomial function, cubic polynomial function, and exponential function are used for comparative analysis. The results are shown in Fig. 5-5. The color and the size of the circle represent the Pearson correlation coefficient (R) (closer to 1 means higher correlation). It can be seen that the correlation between ΔI and weather, cloud cover, relative humidity is higher. Meanwhile, R-value of the cubic polynomial function of all assumed parameters is the largest in all seven locations. As a result, the cubic polynomial function is used to establish the weakening solar radiation model. It needs to be declared that although only four forms of equations are shown in the main body for fitting, we actually used more than ten different equations (including logarithmic functions, power functions, logistic functions, etc.). Since the remaining equations are difficult or weakly related to functions, we have not chosen to show them in the main body for the sake of brevity.

The expression of the established function can be described as Eq.(5-12):

$$\Delta I = \sin\theta \cdot \begin{bmatrix} c_1 RH + c_2 RH^2 + c_3 RH^3 + c_4 CC + c_5 CC^2 + c_6 CC^3 + \\ c_7 W + c_8 W^2 + c_9 W^3 + c_{10} S + c_{11} S^2 + c_{12} S^3 + \\ c_{13} P + c_{14} P^2 + c_{15} P^3 + c_{16} V + c_{17} V^2 + c_{18} V^3 + c_0 \end{bmatrix} \tag{5-12}$$

where RH is the relative humidity (%). CC is cloud cover (dimensionless). W is weather type (dimensionless). S is sunshine duration (hour). P is the precipitation (mm). V is visibility (km). c_0 to c_{18} are the constants (dimensionless). After coefficient corrections, the coefficient tables for the seven regions are provided in Table 5-3.

(a) Site: Abashiri

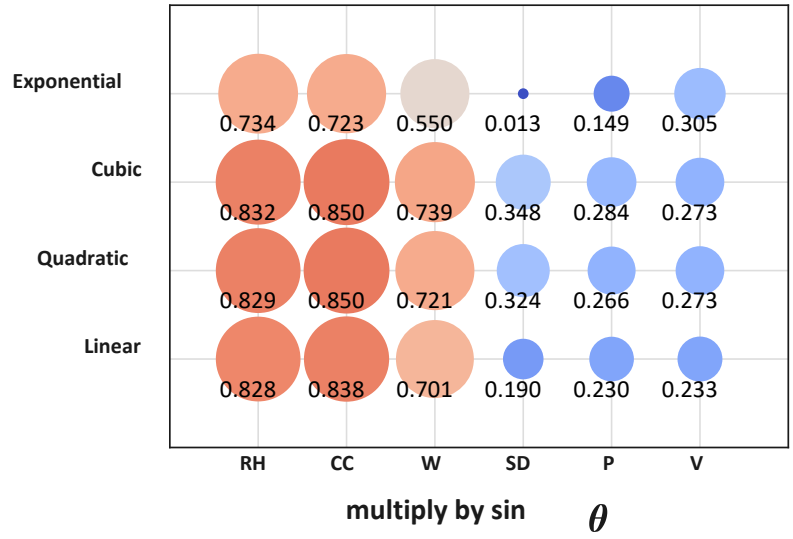

(b) Site: Sapporo

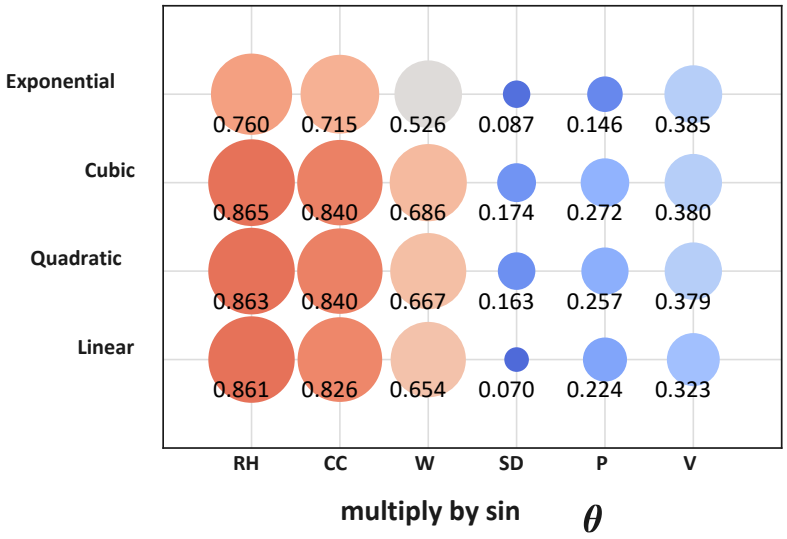

(c) Site: Akita

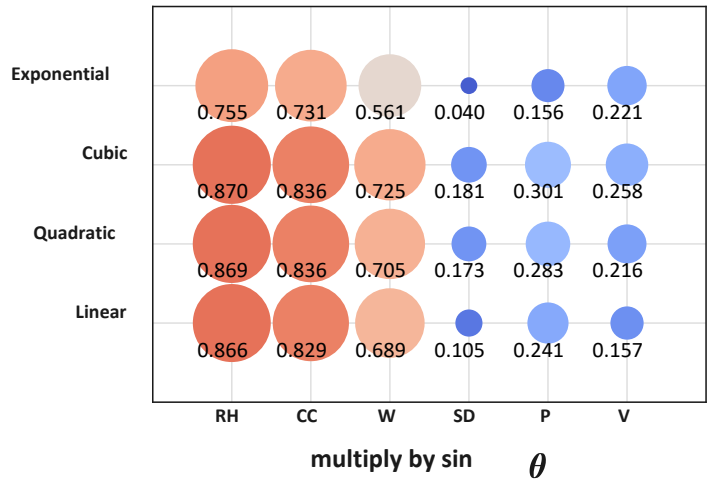

(d) Site: Tokyo

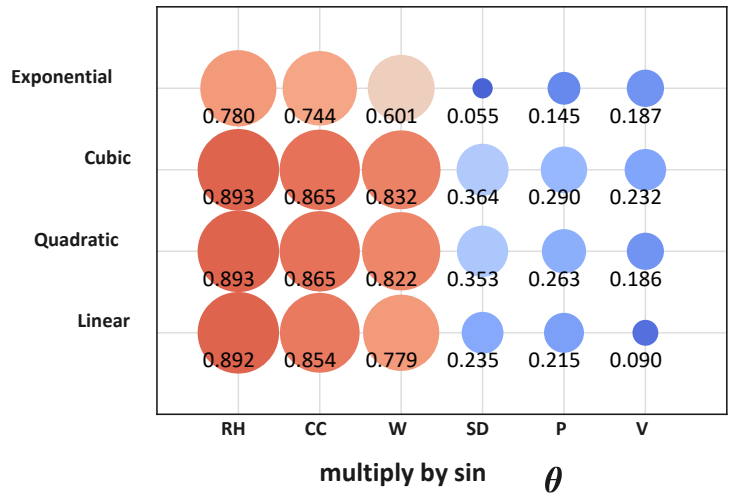

(e) Site: Hiroshima

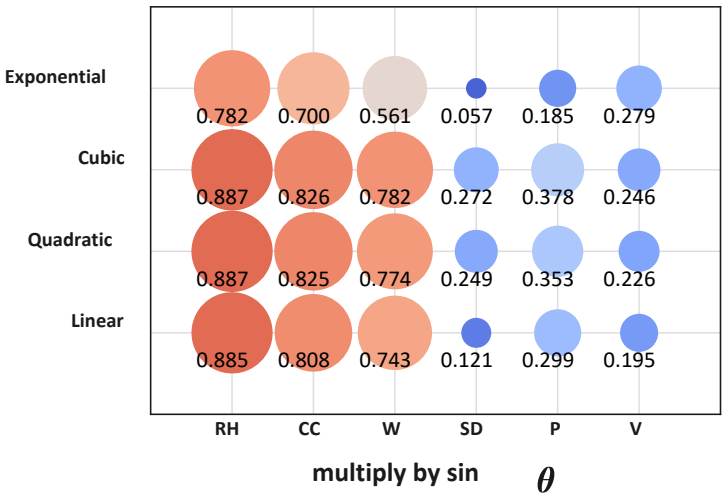

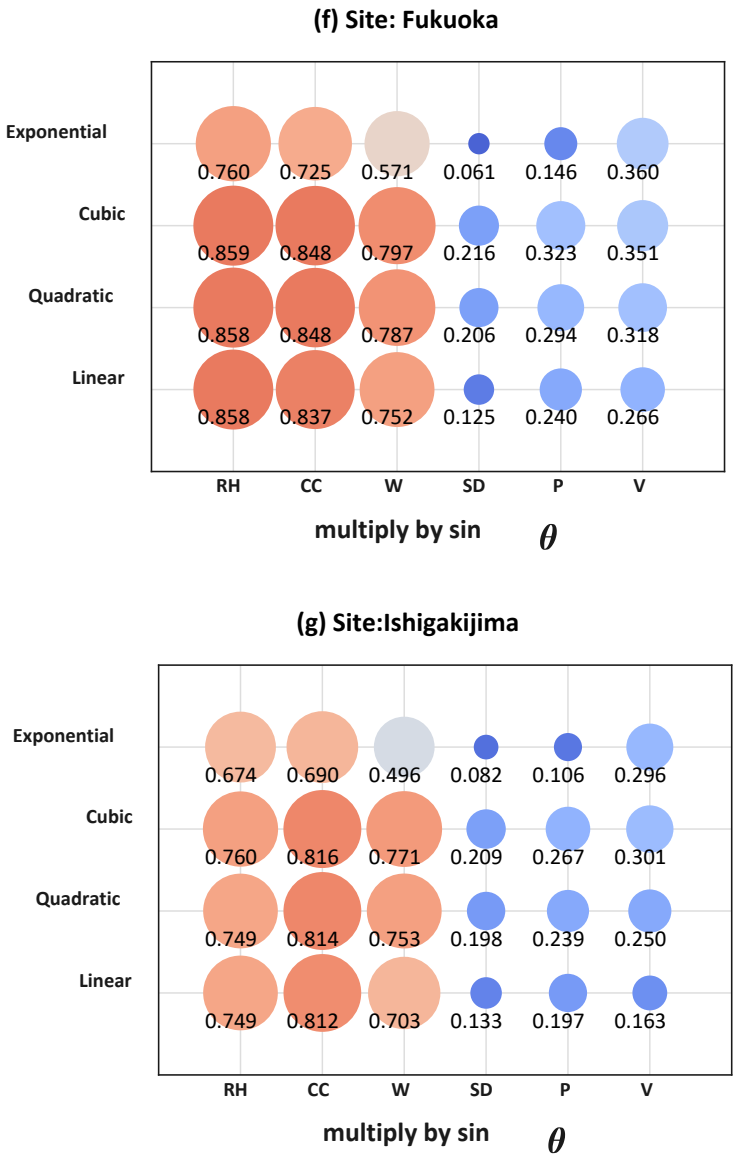

Fig. 5-5.Comparison of new solar radiation weakening models modified by different function forms (R)

Table 5-3Table of coefficients (Variables are normalized by min-max normalization)

Coefficient	Abashiri	Sapporo	Akita	Tokyo	Hiroshima	Fukuoka	Ishigakijima
c0	0.569	0.414	0.495	0.649	0.485	0.474	0.395
c1	0.663	0.051	-0.202	0.27	-0.68	-0.236	0.35
c2	-1.601	-0.013	0.678	0.062	2.226	1.104	-0.574
c3	1.218	0.418	-0.151	-0.085	-1.262	-0.648	0.493
c4	0.32	-0.254	-0.193	0.16	0.018	-0.139	0.69
c5	-0.758	0.223	0.023	-0.404	-0.347	0.07	-1.77
c6	0.579	0.082	0.224	0.333	0.428	0.143	1.37
c7	-0.67	0.607	1.084	-0.504	0.135	0.53	-0.458
c8	1.809	-0.462	-2.23	1.119	0.129	-0.478	1.229
c9	-1.336	-0.23	0.501	-0.588	-0.253	0.051	-0.771
c10	-0.936	-0.617	-0.677	-0.87	-0.591	-0.664	-0.653
c11	1.116	0.904	1.065	1.07	0.944	1.148	1.048
c12	-0.605	-0.498	-0.62	-0.602	-0.552	-0.7	-0.609
c13	1.233	0.392	0.238	0.262	0.342	0.714	0.857
c14	-3.083	-0.785	-0.245	-0.498	-0.6	-1.502	-2.229
c15	2.168	0.638	0.112	0.278	0.359	0.946	1.493
c16	0.873	0.436	0.286	-0.23	0.074	0.141	0.108
c17	-2.546	-0.787	-0.92	0.371	-0.123	-0.458	-0.446
c18	1.94	0.416	0.759	-0.156	0.06	0.357	0.362

5.3.2 Overall forecast result

Based on the consideration of environmental conditions and data reliability, it is chosen from 1st January, 2019 to 31st December, 2021 as the reference data for calculating the estimated radiation value through the proposed weakening model. The regression plot for validation data is indicated in Fig. 5-6. Seven representative observation sites are presented, i.e., Abashiri, Sapporo, Akita, Tokyo, Hiroshima, Fukuoka, and Ishigakijima (from north to south). It can be seen that the coefficient of determination (R2) of Abashiri, Sapporo, Akita, Tokyo, Hiroshima, Fukuoka, and Ishigakijima using the proposed weakening model are 0.93, 0.86, 0.88, 0.96, 0.9, 0.88 and 0.84, respectively (Fig. 5-6). The mean value of R2 is 0.89. In terms of trends, the regression analysis falls close to the fit line at all locations. Since the satellite data are difficult to obtain to compare the difference in accuracy with typical weakening solar radiation model, The Zhang and Huang model is chosen as the baseline model. Zhang and Huang model is developed based on the relationship between solar radiation, dry request temperature difference, relative humidity, and cloud cover, its accuracy is evaluated in many previous studies. The function expressions can be found in the appendix. After the coefficient calibration, the mean and the best value of R2 the Zhang and Huang model are 0.83 and 0.86 in seven locations, respectively (Fig. 5-7). As a result, the accuracy of the proposed model is improved by 7.59% on average and 11.63% on the best compared to the Zhang and Huang model.

The results of the other statistical parameters tested are summarized in Table 5-4 (includes R, RSE, RMSE, rRMSE and NSE). The closer R and NSE are to 1, and the closer RSE and RMSE are to 0, the more reliable and accurate the model are. The results show that the best and mean values of R, RSE, RMSE, and NSE are 0.979 (best), 0.945 (mean), 0.552 (best), 0.756 (mean), 59.024 (best), 88.2 (mean) and 0.946 (best), 0.884 (mean), respectively. The mean and best of rRMSE are 25.271% and 18.898%. In a previous study, J. Zhang et al. [47] has reviewed and compared the accuracy of various solar radiation prediction models and found that the RMSE of the hourly solar radiation model mostly ranged from 88.33 to 142.22 W/m2. W. Yao et al. [48] has compared the fifteen hourly solar radiation models (including eleven previous decomposition models and four proposed models), then give us the reference conclusion as the RMSE mostly ranged from 131.39 to 142.22 W/m2. Li M-F et al. [49] develop six solar radiation models from weather data such as sunshine duration, relative humidity, maximum and minimum temperatures were compared, and it is found that a large number of rRMSEs are concentrated between 24.97% and 41.05% based on 83 different stations. Compared with those results, it is observed that the proposed weakening model provides improved prediction accuracy to the measured values of global solar radiation.

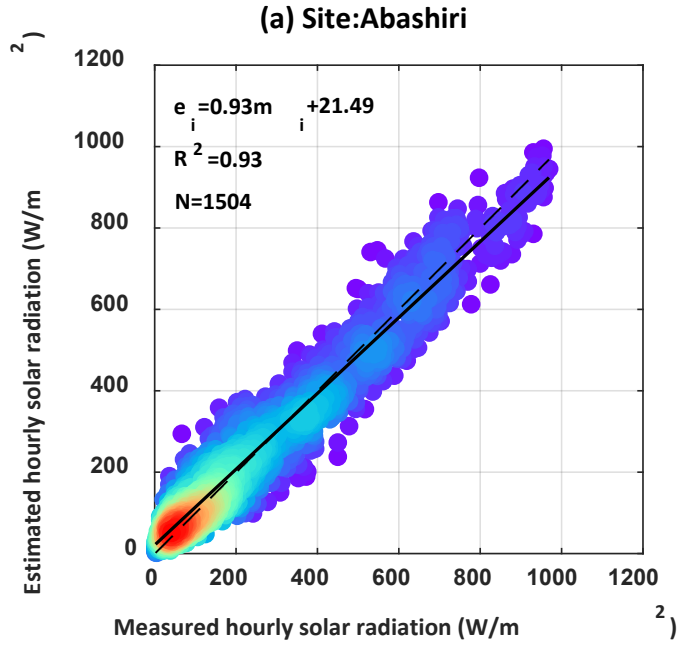
(a) Site:Abashiri
e i =0.93m i +21.49
R 2 =0.93
N=1504
Estimated hourly solar radiation (W/m 2)
Measured hourly solar radiation (W/m 2)
0
200
400
600
800
1000
1200

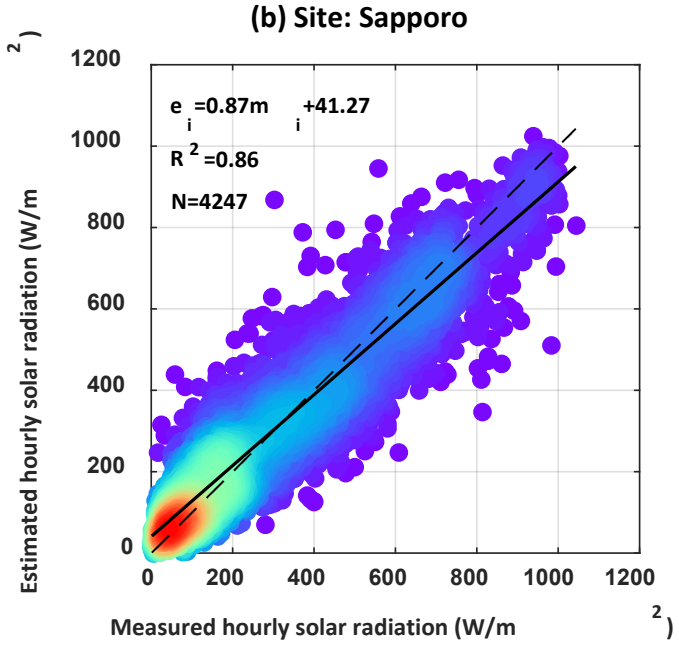
(b) Site: Sapporo
e i =0.87m i +41.27
R 2 =0.86
N=4247
Estimated hourly solar radiation (W/m 2)
Measured hourly solar radiation (W/m 2)
0
200
400
600
800
1000
1200

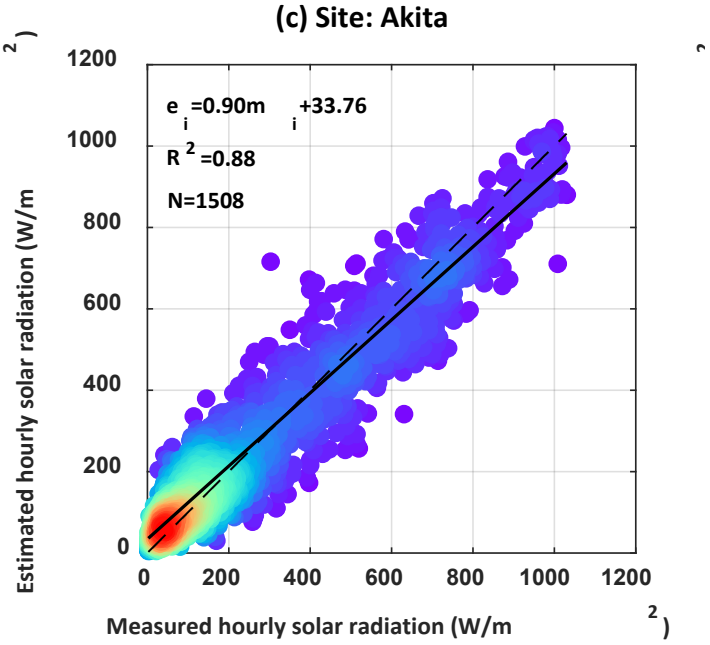
(c) Site: Akita
e i =0.90m i +33.76
R 2 =0.88
N=1508
Estimated hourly solar radiation (W/m 2)
Measured hourly solar radiation (W/m 2)
0
200
400
600
800
1000
1200

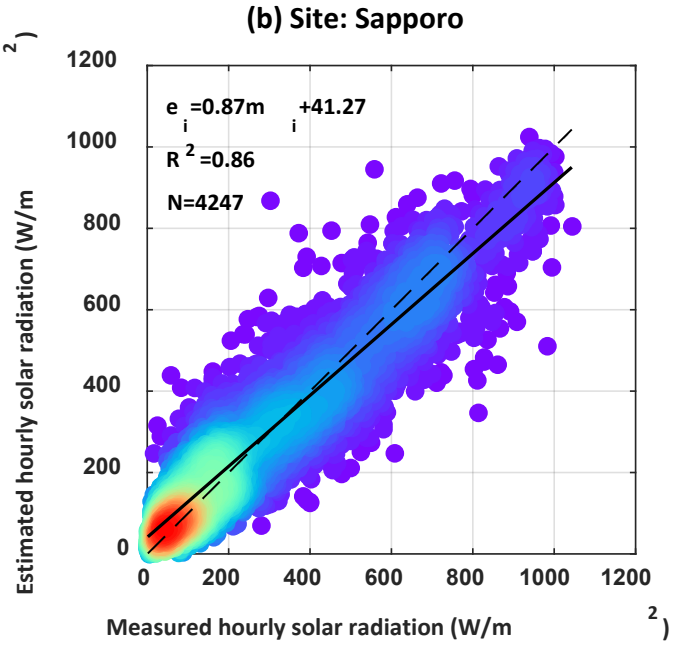
(b) Site: Sapporo
e i =0.87m i +41.27
R 2 =0.86
N=4247
Estimated hourly solar radiation (W/m 2)
Measured hourly solar radiation (W/m 2)
0
200
400
600
800
1000
1200

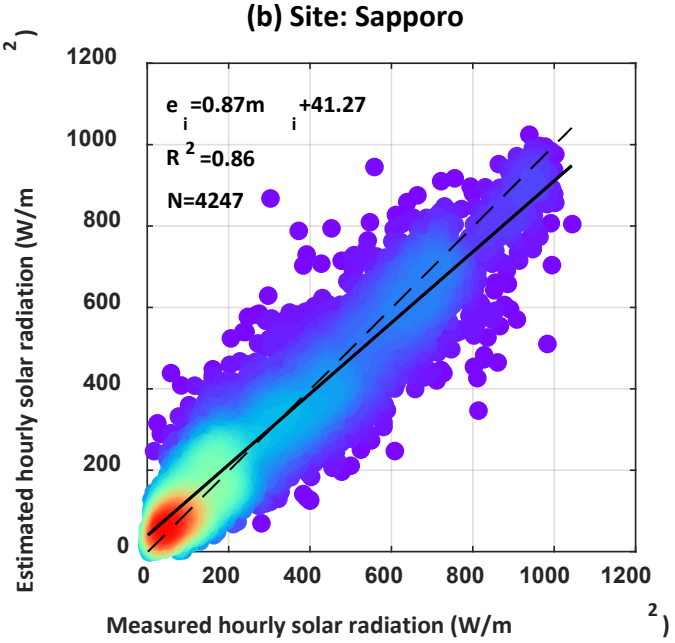
(b) Site: Sapporo
e i =0.87m i +41.27
R 2 =0.86
N=4247
Estimated hourly solar radiation (W/m 2)
Measured hourly solar radiation (W/m 2)
0
200
400
600
800
1000
1200

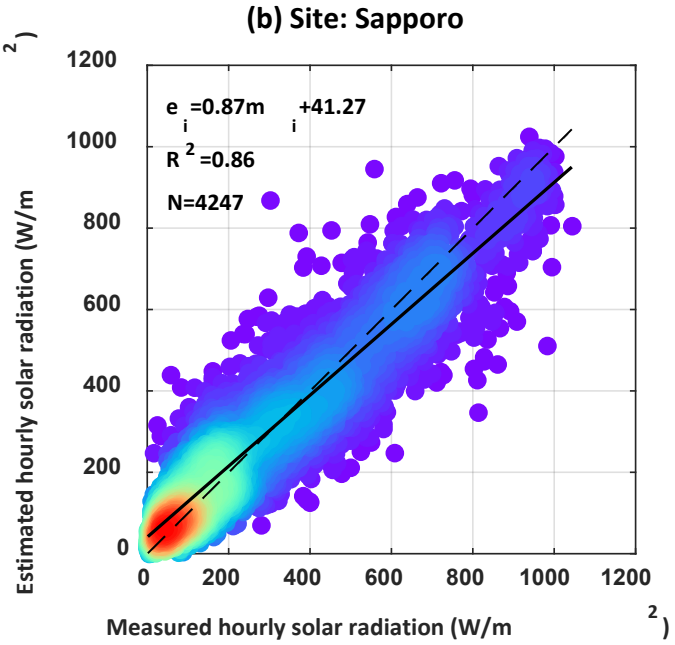
(b) Site: Sapporo
e i =0.87m i +41.27
R 2 =0.86
N=4247
Estimated hourly solar radiation (W/m 2)
Measured hourly solar radiation (W/m 2)
0
200
400
600
800
1000
1200

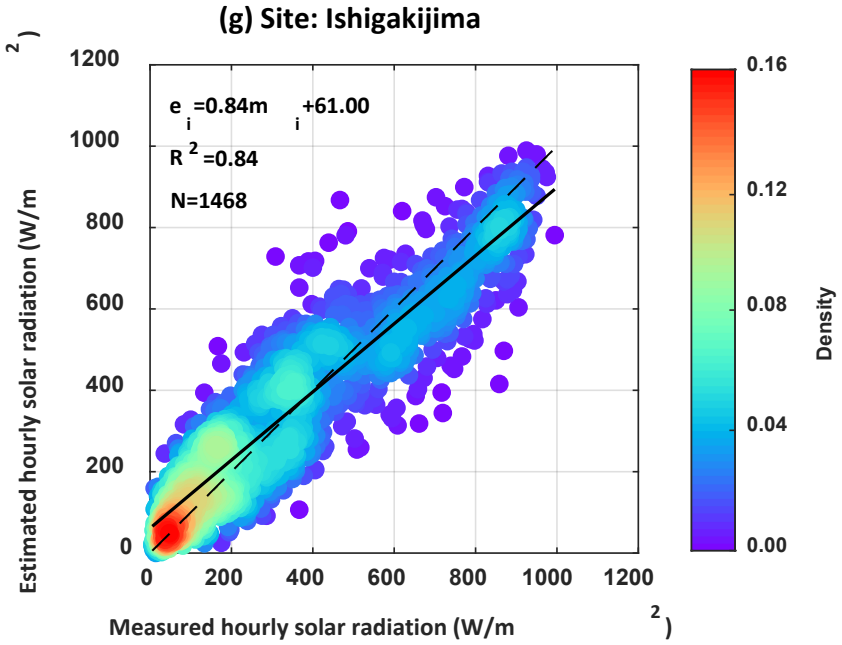

Fig. 5-6. Comparison of estimated to measured hourly solar radiation on horizontal surface for Japan (from 1st January, 2019 to 31st December, 2021)

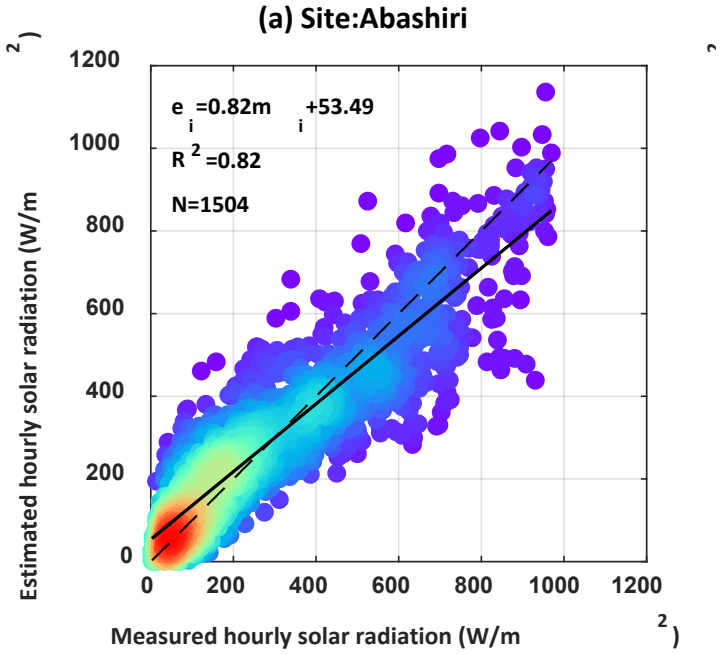

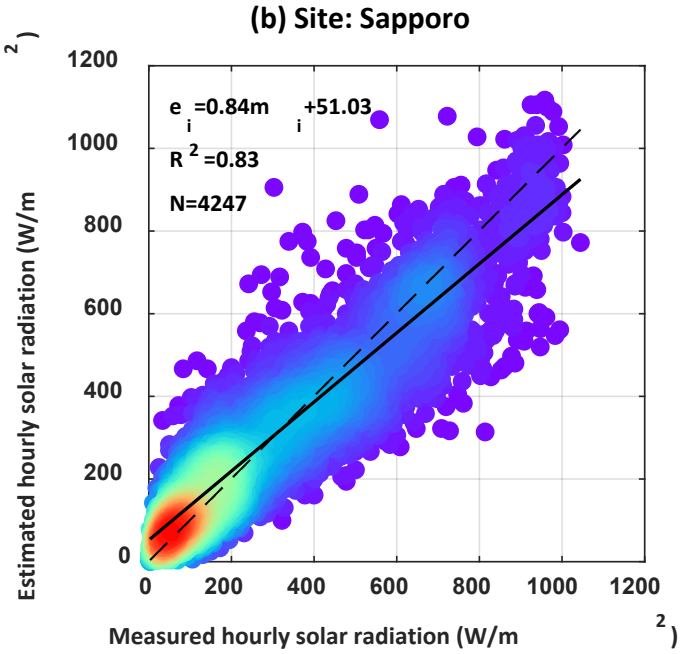
(b) Site: Sapporo
e i =0.84m i +51.03
R 2 =0.83
N=4247
Estimated hourly solar radiation (W/m 2)
Measured hourly solar radiation (W/m 2)
0
200
400
600
800
1000
1200

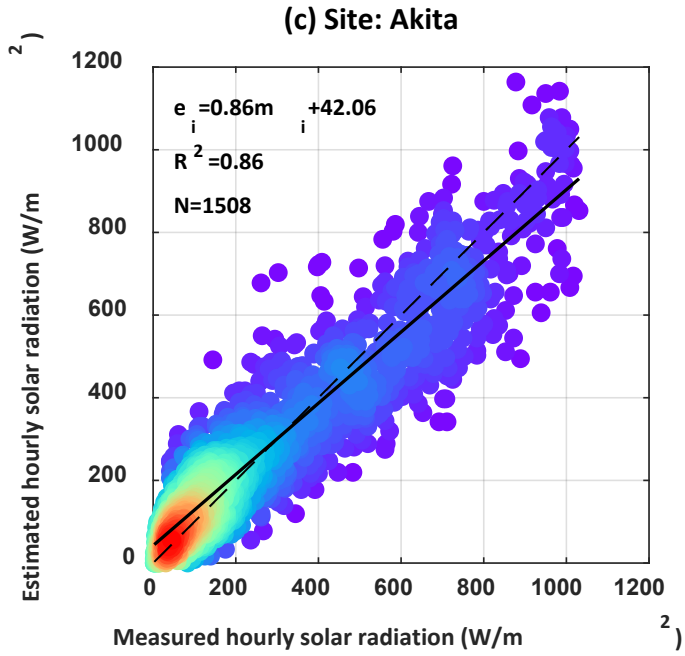
(c) Site: Akita
e i =0.86m i +42.06
R 2 =0.86
N=1508
Estimated hourly solar radiation (W/m 2)
Measured hourly solar radiation (W/m 2)
0
200
400
600
800
1000
1200

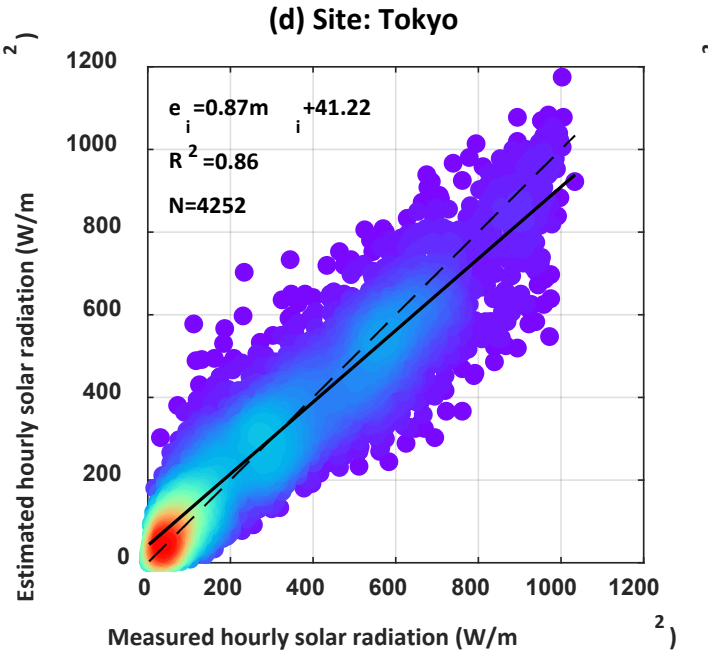
(d) Site: Tokyo
e i =0.87m i +41.22
R 2 =0.86
N=4252
Estimated hourly solar radiation (W/m 2)
Measured hourly solar radiation (W/m 2)
0
200
400
600
800
1000
1200

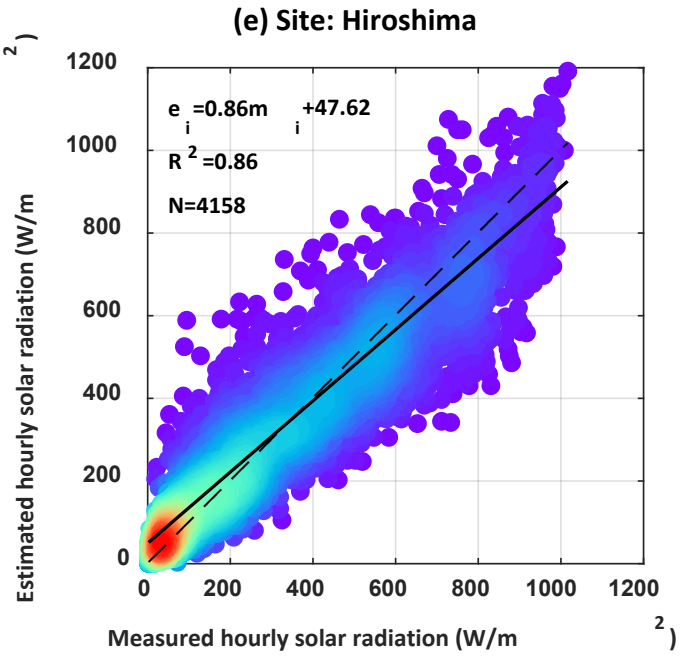
(e) Site: Hiroshima
e i =0.86m i +47.62
R 2 =0.86
N=4158
Estimated hourly solar radiation (W/m 2)
Measured hourly solar radiation (W/m 2)
0
200
400
600
800
1000
1200

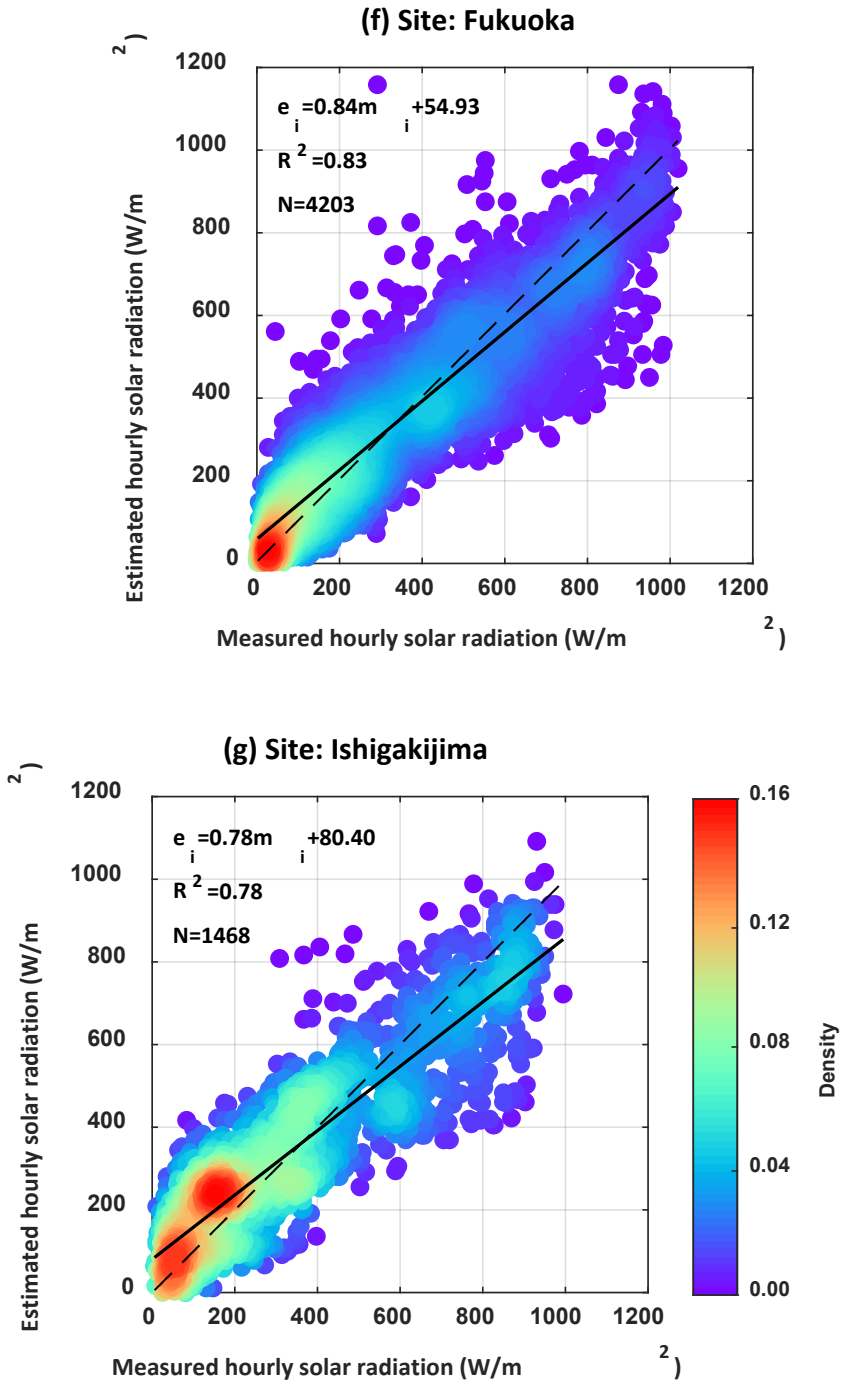

Fig. 5-7. Comparison of estimated to measured hourly solar radiation on horizontal surface for Japan of Zhang and Huang model (from1st January, 2019 to 31st December, 2021)

Table 5-4 Comparison of model's statistical parameters

Site	The proposed model					The Zhang and Huang model				
	R	RSE	RMSE	rRMSE	NSE	R	RSE	RMSE	rRMSE	NSE
Abashiri	0.965	0.404	62.748	21.047	0.929	0.905	1.516	103.751	34.801	0.781
Sapporo	0.930	0.821	89.462	28.768	0.858	0.911	1.216	103.201	33.187	0.803
Akita	0.938	0.666	82.407	27.195	0.896	0.927	1.398	101.096	33.362	0.839
Tokyo	0.979	0.552	59.024	18.898	0.946	0.926	1.118	94.445	30.241	0.847
Hiroshima	0.949	0.828	85.946	24.935	0.886	0.927	1.437	99.808	28.956	0.839
Fukuoka	0.938	0.612	95.139	28.531	0.859	0.910	1.539	110.930	33.266	0.802
Ishigakijima	0.917	1.415	104.880	28.912	0.815	0.883	1.281	125.980	34.733	0.715
Mean	0.945	0.756	82.800	25.271	0.884	0.912	1.358	105.602	32.649	0.803

5.3.3 Available for rainy and cloudy conditions

According to the literature review, almost all models of hourly solar radiation are based on clear sky conditions. Such models assume that weather conditions have no effect on the model and try to establish a direct relationship between solar radiation and surface meteorological parameters. This type of model has a high accuracy when extreme weather and cloud cover changes are not considered. It is also available to derive the maximum radiation on the surface under clear sky conditions. However, as climate change from year to year and the number of extreme weather events increases, solar radiation models for multiple kinds of weather are urgently needed. Therefore, the proposed weakening model is validated according to the weather classification in Table 5-5. The weather conditions were divided into three categories. They are sunny (clear conditions including mostly clear and sunny, sunny, and slightly cloudy), cloudy (turbid conditions including cloudy, mist, dust storm, drifting snow, and fog), and rainy (moisture mixing turbid conditions including drizzle, rain, sleet, snow, hail, hailstorm, and thunderstorm).

Theoretically, the more complex the weather conditions and the higher the turbidity in the atmosphere, the more challenging it is to predict solar radiation. However, the results show that the proposed weakening model has a better adaptation on cloudy and rainy days instead. The mean values of the coefficient of determination (R2) are 0.71, 0.90 and 0.96 for sunny, cloudy, and rainy conditions for the seven locations with the weakening value of solar radiation in the atmosphere as the prediction target (Fig. 5-8). The reason for this is that the proposed model is based on the atmospheric layer-by-layer weakening theory. When the atmospheric turbidity is high, the absorption as well as the diffusion effect of solar radiation, occurs strongly in the air. The weakening process is significant, so the relationship between the characterization factors (such as relative humidity, precipitation, and cloud cover) of the weakening layer and the weakening value of solar radiation is much easier to be observed.

Table 5-5 Weather classification

Symbol	Description	Definition
1	Mostly clear and sunny	
2	Sunny	Sunny
3	Slightly cloudy	
4	Cloudy	
5	Mist	
6	Dust storm	Cloudy
7	Drifting snow	
8	Fog	
9	Drizzle	
10	Rain	
11	Sleet	
12	Snow	Rainy
13	Hail	
14	Hailstorm	
15	Thunderstorm	

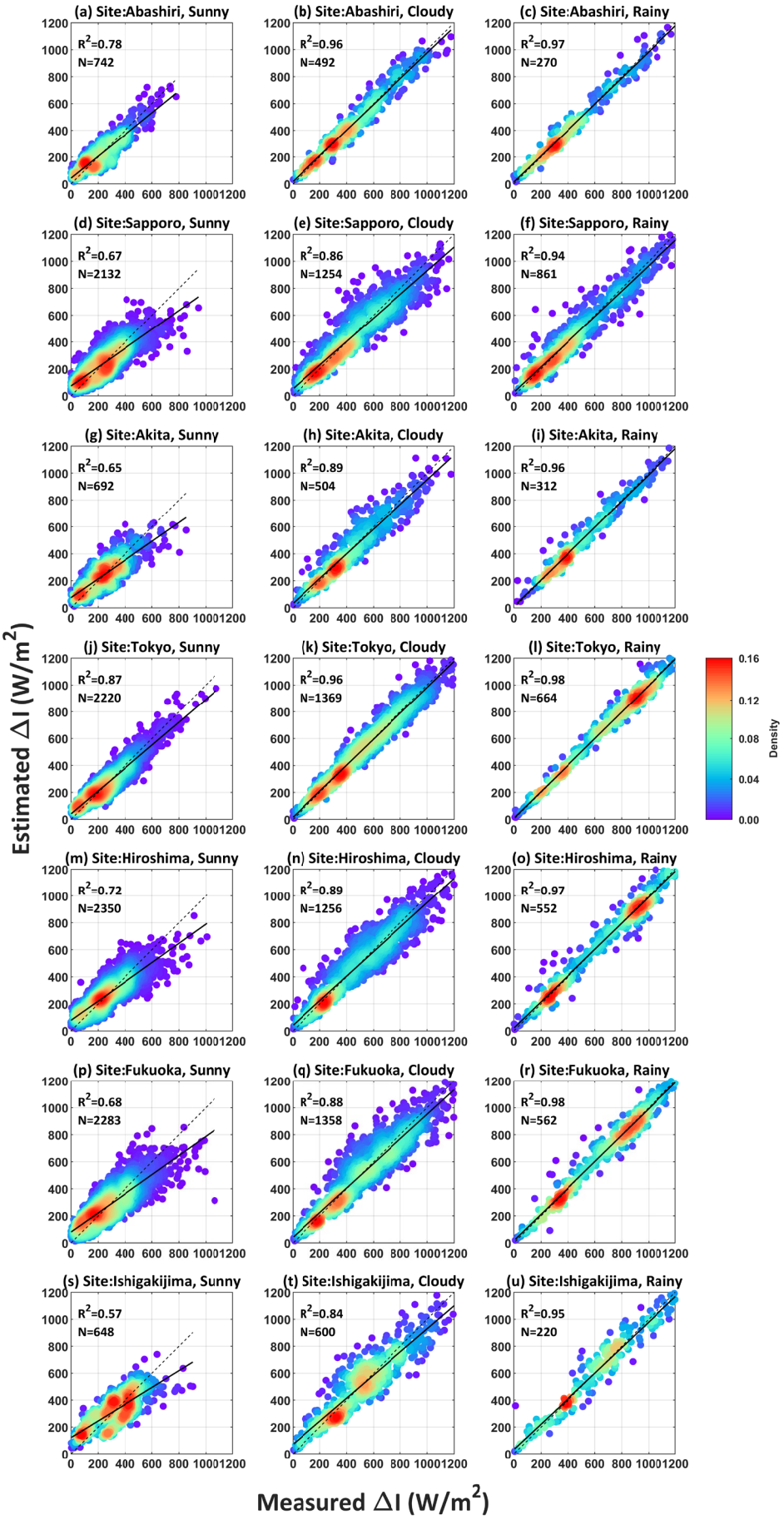
(a) Site:Abashiri, Sunny
R²=0.78
N=742
(b) Site:Abashiri, Cloudy
R²=0.96
N=492
(c) Site:Abashiri, Rainy
R²=0.97
N=270
(d) Site:Sapporo, Sunny
R²=0.67
N=2132
(e) Site:Sapporo, Cloudy
R²=0.86
N=1254
(f) Site:Sapporo, Rainy
R²=0.94
N=861
(g) Site:Akita, Sunny
R²=0.65
N=692
(h) Site:Akita, Cloudy
R²=0.89
N=504
(i) Site:Akita, Rainy
R²=0.96
N=312
(j) Site:Tokyo, Sunny
R²=0.87
N=2220
(k) Site:Tokyo, Cloudy
R²=0.96
N=1369
(l) Site:Tokyo, Rainy
R²=0.98
N=664
(m) Site:Hiroshima, Sunny
R²=0.72
N=2350
(n) Site:Hiroshima, Cloudy
R²=0.89
N=1256
(o) Site:Hiroshima, Rainy
R²=0.97
N=552
(p) Site:Fukuoka, Sunny
R²=0.68
N=2283
(q) Site:Fukuoka, Cloudy
R²=0.88
N=1358
(r) Site:Fukuoka, Rainy
R²=0.98
N=562
(s) Site:Ishigakijima, Sunny
R²=0.57
N=648
(t) Site:Ishigakijima, Cloudy
R²=0.84
N=600
(u) Site:Ishigakijima, Rainy
R²=0.95
N=220
0 200 400 600 800 1000 1200
0.16
0.12
0.08
0.04
0.00
Density
Estimated ΔI (W/m²)
Measured ΔI (W/m²)

Fig. 5-8. Comparison of estimated to measured hourly solar radiation weakening value in sunny cloudy and rainy situations (Coordinate axis as hourly loss value of solar radiation (W/m^2))

5.3.4 Interpretability

Interpretability is also very significant for solar radiation models because it can help us to better understand and improve the models. As shown in Fig. 5-5, the largest effects on the solar radiation weakening values are relative humidity, cloud cover, and weather type, which represent the tendency of solar radiation to be weakened in the water vapor layer, the clouds layer, and the mixed layer representing the turbid state, respectively. Of course, the distance of solar radiation through the atmosphere needs to be considered (multiply by $\sin\theta$). This is consistent with our physical perception. Although precipitation, and visibility, do not show a sufficient correlation in regression analysis. However, it is verified to contribute significantly to the coefficient of determination of the model. We believe that this might be related to the generally high visibility, low airborne suspended particulate matter (PM2.5 and PM10), and erratic precipitation at the chosen study site, Japan. Consequently, it is desirable to measure the data in other locations to evaluate the performance of the proposed model. Other meteorological parameters such as temperature, wind speed, barometric pressure, etc., are not adopted in our model. Because there is less evidence that these parameters may contribute to the weakening effect of solar radiation.

5.3.5 Comparison and Expansion

As described in Section 2.1, many models try to establish a functional relationship between the clearness index and general meteorological parameters (Eq. (1)), but this is not available in fine-grained solar radiation forecasting. In fact, a variant of Eq. (1) can be adapted to fine-scale solar radiation forecasting. This can be described by the Eq. (13):

$$I = I_0 \cdot f(\sigma) \tag{5-13}$$

Compared to Eq. (1), Eq. (13) does not generate additional computational errors. The Zhang and Huang model is typical of this category of models. The correlation coefficient calculated according to Eq. (13) is shown in A.4. The initial Zhang and Huang model uses relative humidity, 3-hour temperature difference, and cloud cover as input items. Recently, a new study [26] has improved the accuracy of the Zhang and Huang model by replacing the cloud cover with the sunshine duration. This is because the correlation between insolation time and solar radiation is more significant as shown in the **Appendix Fig**. 5-1 (a). In contrast, the proposed model can be described by Eq. (14):

$$I = I_0 - f(\sigma) \quad \text{or} \quad I_0 - I = \Delta I = f(\sigma) \tag{5-14}$$

According to Appendix Fig. 5-1 (b), relative humidity, weather type, and cloud cover are the best choices as input items in proposed model.

Consequently, in order to verify the performance of the proposed model, the proposed model is compared with seven commonly used solar radiation models. They include three models based on Eq. (1) (the Angstrom-Prescott model [15, 16], the Hargreaves model [23, 24], the Black model [50]), two models based on Eq. (13) (The Zhang and Huang model [27] and the improved Zhang and Huang model [26]), and two artificial neural network (ANN) models.

Table 5-6 shows the performance comparison between the proposed model and the commonly used models. Abashiri is chosen as the experimental site. The main evaluation metrics include the coefficients of determination (R2) of daily as well as hourly scales, the most important impression factors in the model, and the weather adaptation. Although the hourly solar radiation model is developed, it is also possible to calculate the model accuracy for 24 hours by summation. Models 1,2,3 as solar radiation models with single input variables to predict daily values have relatively low prediction accuracy. Also models 1 and 2 cannot be used for hourly scale forecasting because they use input variables at the daily value scale (maximum sunshine duration as well as maximum temperature difference). Model 3, although using daily mean cloud cover as input, can be replaced by hourly cloud cover to achieve hourly forecasts, but from the results, the accuracy of the forecasts is unsatisfactory (R2 equals 0.41). Thus, these single factor input models are difficult to meet the requirements of high-resolution solar radiation forecasting, and it is also difficult for a single factor to feedback the weather changes and therefore only applicable to sunny days. Models 4,5 and the proposed model are acceptable in terms of accuracy. And model 5 is an improved version of model 4. However, the determinants of the models are different, and the most relevant factor for model 5 is the sunshine duration while the cloud cover is the most relevant for the proposed model. Models 7 and 8 are the most commonly used artificial neural network models and they have the same topology (two-layer feedforward network with 10 layers of sigmoid hidden neurons and linear output neurons). They have the same inputs and outputs as models 5 and 6, respectively. There is no doubt that their accuracy is the highest. However, compared with models 5 and 6, they only improve the value of the coefficient of determination by 0.01, but lose the clear mathematical expressions and physical relationships.

The proposed model is based on separation, however in fact, physical interactions such as clouds and aerosol can produce feedback affecting transmission. Consequently, the interaction effects between meteorological parameters need to be considered. In statistics, when an explanatory variable affects the pathway of another explanatory variable to the dependent variable, it is usually expressed as the product of two separate variables [51]. Table 7 shows the comparison of the model accuracy after adding the interaction variables. Based on the correlation analysis, model 9 is chosen as the baseline model. Also, for simplicity, all variables are added to the model as linear equations. The results show that adding the interaction variables of cloud cover and weather, and sunshine duration with cloud cover, weather, and relative humidity, respectively, can improve the performance of the model. In particular, the interaction variable of sunshine duration and cloud cover (model 13) improves the R2 of the model by 0.08. Also, this is very easy to understand. This is because sunshine duration indicates in a strict sense whether the sun is blocked by clouds or not [52], while changes in cloudiness are usually accompanied by changes in relative position to the sun. The comparison with model 14 also shows that the increase in R2

does not simply come from adding variables either. Therefore, the inclusion of this interaction term is valid and physically meaningful. .

Table 5-6 Comparison with commonly available models

No.	Authors	Equation	Input parameters	R^2 (Daily)	R^2 (Hourly)	Determinant	Weather adaptability
1	Angstrom (1924) [15]-Prescott (1940) [16]	$\frac{I}{I_0} = c_0 + c_1 \frac{S_d}{S_0}$	Daily sunshine duration, theoretical sunshine duration	0.85	-	S_d	Clear day
2	Hargreaves and Samani (1982) [23]	$\frac{I}{I_0} = c_1 \Delta T^{0.5}$	Daily average temperature	0.63	-	ΔT	Clear day
3	Black (1956) [50]	$\frac{I}{I_0} = c_0 + c_1 C + c_2 C^2$	Mean total cloud cover during daytime observations	0.64	0.41	C	Clear day
4	Zhang and Huang (2002) [27]	$I = \left[I_{sc} \cdot \sin\theta \cdot \left\{ c_0 + c_1 CC + c_2 CC^2 + c_3 \left(T_n - T_{n-3} \right) + c_4 RH \right\} + d \right] / k$	Cloud cover, 3-hour temperature difference, relative humidity	0.82	0.82	T_n-T_{n-3}	Clear day
5	Chang Kai et.al (2020) [26]	$I = I_{sc} \cdot \sin\theta \cdot \left\{ c_0 + c_1 S + c_2 \left(T_n - T_{n-3} \right) + c_3 RH \right\} + c_4$	Sunshine duration, 3-hour temperature difference, relative humidity	0.92	0.92	S	Clear day
6	The proposed weakening model	$\Delta I = \sin\theta \cdot \begin{bmatrix} c_1 RH + c_2 RH^2 + c_3 RH^3 + c_4 CC + c_5 CC^2 + c_6 CC^3 + \\ c_7 W + c_8 W^2 + c_9 W^3 + c_{10} S + c_{11} S^2 + c_{12} S^3 + \\ c_{13} P + c_{14} P^2 + c_{15} P^3 + c_{16} V + c_{17} V^2 + c_{18} V^3 + c_0 \end{bmatrix}$	Relative humidity, cloud cover, weather type, sunshine duration, visibility, precipitation	0.93	0.93	CC	Rainy day
7	ANN1	Unclear	Sunshine duration, 3-hour temperature difference, relative humidity	0.93	0.93	Unclear	Clear day
8	ANN2	Unclear	Relative humidity, cloud cover, weather type, sunshine duration, visibility, precipitation	0.94	0.94	Unclear	Rainy day

Table 5-7 The proposed expansion model

No.	Equation	R^2 (hourly)
9	$\Delta I = \sin\theta \cdot \left(c_1 RH + c_2 CC + c_3 W\right)$	0.81
10	$\Delta I = \sin\theta \cdot \left(c_1 RH + c_2 CC + c_3 W + c_4 CC \cdot W\right)$	0.82
11	$\Delta I = \sin\theta \cdot \left(c_1 RH + c_2 CC + c_3 W + c_4 S \cdot W\right)$	0.87
12	$\Delta I = \sin\theta \cdot \left(c_1 RH + c_2 CC + c_3 W + c_4 S \cdot RH\right)$	0.87
13	$\Delta I = \sin\theta \cdot \left(c_1 RH + c_2 CC + c_3 W + c_4 S \cdot CC\right)$	0.89
14	$\Delta I = \sin\theta \cdot \left(c_1 RH + c_2 CC + c_3 W + c_4 S\right)$	0.84
15	$\Delta I = \sin\theta \cdot \left(c_1 RH + c_2 CC + c_3 W + c_4 S + c_5 S \cdot CC\right)$	0.91

5.4 Application

Solar radiation data has been a difficult data to obtain due to the cost involved in analysis as well as monitoring. For example, in Japan, out of more than 840 weather stations measuring air temperature, wind direction, wind speed, and relative humidity, only 48 weather stations measure solar radiation. The coverage of solar radiation data is very low. Therefore, when conducting PV efficiency assessments at sites where solar radiation observations are not available, data are typically only borrowed from the nearest solar radiation observation station. However, at longer distances, the differences in solar radiation can be significant because, likely, the weather in different cities is out of synchronization. Therefore, two methods are compared. The first one borrows data from the nearest solar radiation observatory to calculate the hourly power production of PV. The second one is to calculate the hourly power generation of PV by extrapolating the local solar radiation values from the local weather parameters.

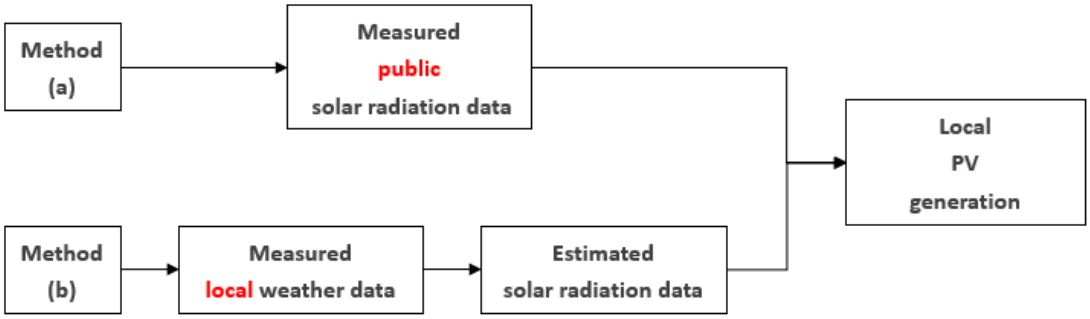

Fig. 5-9. Two methods to calculate solar PV generation in Kitakyushu

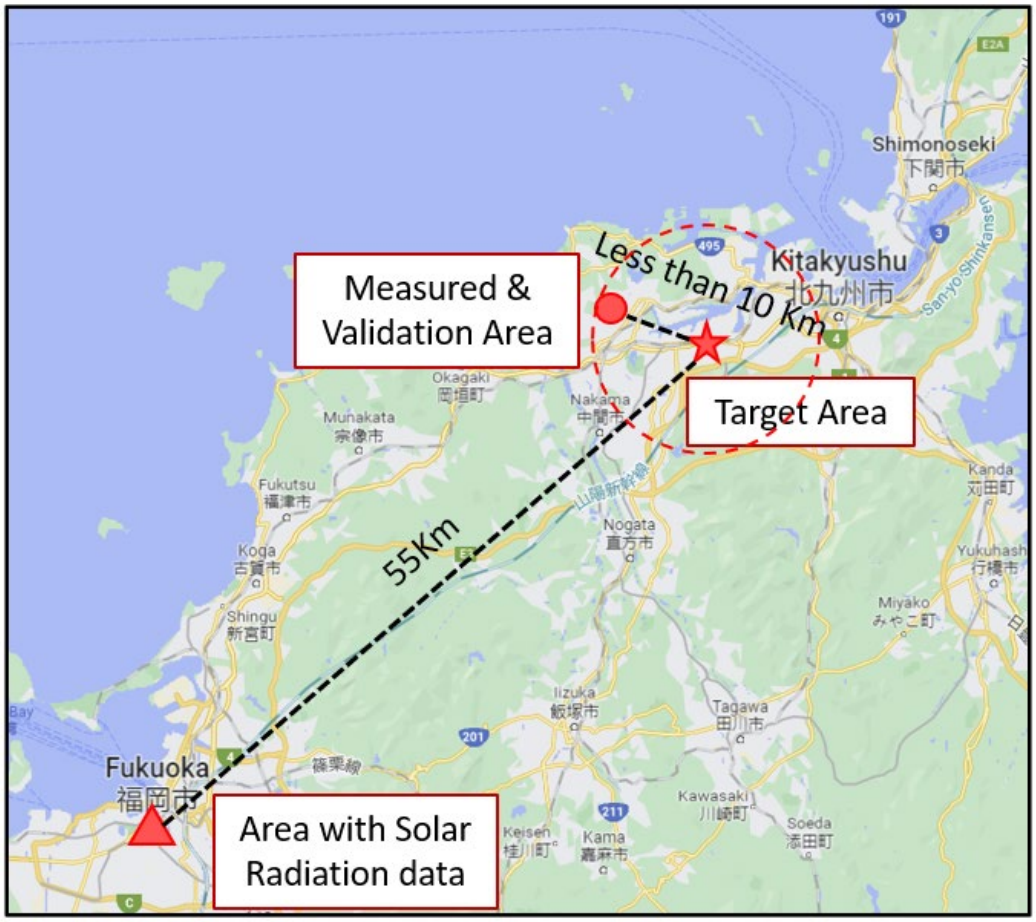

Fig. 5-10. Map of Target area and area with solar radiation data

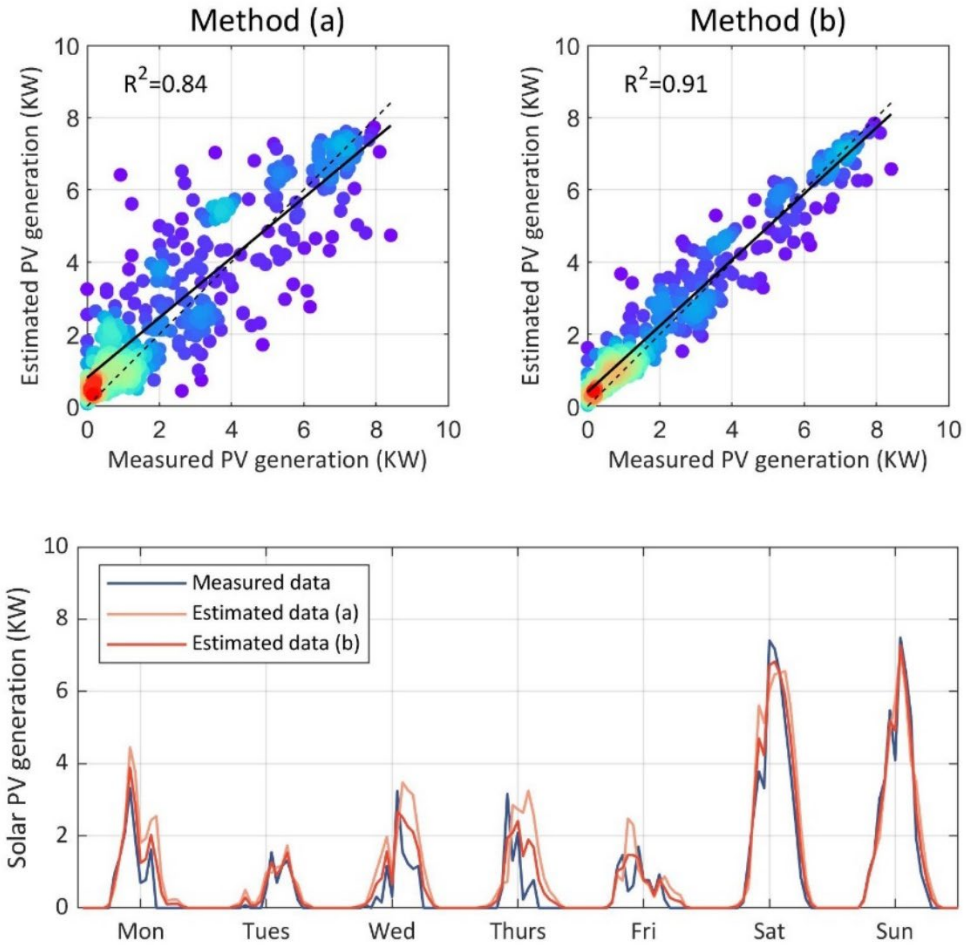

Fig. 5-11. Comparison of estimated to measured PV generation in Kitakyushu (July 2012)

In this case, the target area is in Kitakyushu city, but the nearest solar radiation observation site is in Fukuoka city, and the distance between them is 70 km. The location where local solar radiation values are calculated locally using weather data is less than 10 km from the target location.

The results for scenario a and scenario b are shown in Figure 5-11. Measured solar PV power data from July 2012 was used for validation. The optical module is the Panasonic module HIT N2285. The maximum power of a single module is 285W. 35 pieces are installed in total, with a total installed capacity of 10 KW. It can be found that the R2 of scenario a is 0.84. And the R2 of scenario b is 0.91. Scenario b improves the accuracy by 0.7 over scenario a.

5.5 Conclusion

In this study, a new hourly weakening solar radiation model was developed based on the layer-by-layer weakening theory. Over 200,000 sets of data collected from seven locations in Japan were used for modeling as well as validation. Considering the ease of data acquisition, we selected only six meteorological parameters that are easily available at weather stations as input variables. In addition, the accuracy of the model is tested in this paper under different weather conditions. The specific conclusions are as follows.

1) A new layer-by-layer weakening solar radiation model was proposed based on the attenuation process of solar radiation from the atmosphere to the ground. The mean and best values of R^2 are 0.89 and 0.96. Compared to the existing model, the accuracy of the proposed model was improved by 7.59% on average and 11.63% on best.
2) The weakening effect of solar radiation is taken as the main body of this work. The results of validation indicate that the proposed model has greater adaptability to cloudy and even rainy days since the weakening effect of solar radiation is more significant on cloudy and rainy days. This will provide a reference for most solar radiation models based on a clear sky condition to adapt to more complex weather conditions.
3) The proposed model is a generic framework so that the characterization factors of the weakening layer can be improved or replaced depending on the depth of the theory. The inclusion of interaction variables can significantly improve the performance of the model especially the interaction term of sunshine duration and cloud cover.

4) The proposed model is established and calibrated from over 20 years of meteorological data (spread over seven different locations throughout Japan) and under various weather conditions. Thus, a typical meteorological year (TMY) for Japan can be generated based on our method. This is valuable for certain applications or techniques, such as thermal simulation of buildings throughout the year.

Appendix A

A.1. Description of cloud cover and weather type in weather forecast

Appendix Table 5-1 Cloud cover symbol description

Symbol	Description	Numericalization
blank	No observations	blank
--	No clouds are observed	0
0.0	If clouds are present but cloud cover is less than 0.1	0
0	If clouds are present but cloud cover is less than 1	0
0+	Cloud cover is more than 0.1 but less than 1	0.5
1	One-tenth of the total cloud cover	1
2	Two-tenths of the total cloud cover	2
3	Three-tenths of the total cloud cover	3
4	Four-tenths of the total cloud cover	4
5	Five-tenths of the total cloud cover	5

6	Six-tenths of the total cloud cover	6
7	Seven-tenths of the total cloud cover	7
8	Eight-tenths of the total cloud cover	8
9	Nine-tenths of the total cloud cover	9
10-	If cloud cover is 10 but there are areas with no clouds	9.5
10	The total cloud cover	10

Appendix Table 5-2 Weather type description

Symbol	Description
1	Mostly clear and sunny
2	Sunny
3	Slightly cloudy
4	Cloudy
5	Mist
6	Dust storm
7	Drifting snow
8	Fog
9	Drizzle
10	Rain
11	Sleet
12	Snow
13	Hail
14	Hailstorm
15	Thunderstorm

A.2. The typical existing solar radiation weakening model

The typical existing solar radiation weakening model for calculating global solar radiation is as follows [41]:

$$I = I_b + I_d \tag{A1}$$

$$I_b = \frac{I_{sc} cos(\theta) T_r T_a T_w T_o T_u}{E_0} \tag{A2}$$

$$I_d = I_{as} + I_G \tag{A3}$$

$$T_w = 1 - 2.4959 \cdot X_w \left[\left(1 + 79.034 X_w\right)^{0.6828} + 6.385 X_w \right]^{-1} \tag{A4}$$

$$X_w = w_0 \left(\frac{p}{1013.25} \right)^{\frac{3}{4}} \left(\frac{283}{\eta} \right)^{\frac{1}{2}} \tag{A5}$$

$$\eta = 288 - 6.5 \cdot 10^{-3} z \tag{A6}$$

$$T_a = EXP\left[-\tau^{0.873} \left(1 + \tau - \tau^{0.7088}\right) m^{0.9108} \right] \tag{A7}$$

where I is global solar radiation on the horizontal surface (W/m2). I_b is beam solar radiation in clear sky on the horizontal surface (W/m2). I_d is diffuse solar radiation in clear sky on the horizontal surface (W/m2). I_{as} is atmosphere scattering of diffuse radiation (W/m2). I_G is solar radiation in clear sky on the horizontal surface from multiple reflections between ground and sky (W/m2). T_r is transmittance of Rayleigh scattering (dimensionless). T_a is transmittance of aerosol absorption and scattering (dimensionless). T_w is transmittance of water vapor absorption (dimensionless). T_o is transmittance of ozone absorption (dimensionless). T_u is transmittance of uniformly mixed gases (carbon dioxide and oxygen) (dimensionless). X_w is total amount of precipitation in slanted path (m). w_0 is precipitable water-vapor thickness under the actual condition (cm). η is an intermediate variable. z is altitude of studied position (m). m is air mass at actual pressure (dimensionless). τ is aerosol optical thickness (dimensionless).

A.3. The Zhang and Huang model

Zhang and Huang used common meteorological parameters such as temperature, humidity, and cloud cover to establish a polynomial relationship with hourly solar radiation [27]. It uses observed cloud cover data to reflect the effect of clouds on solar radiation under all-day conditions. The global solar radiation can be calculated as follows:

$$I = \left[I_{sc} \cdot \sin\theta \cdot \left\{ c_0 + c_1 CC + c_2 CC^2 + c_3 \left(T_n - T_{n-3} \right) + c_4 RH \right\} + d \right] / k \qquad \text{(A8)}$$

where I is global solar radiation on the horizontal surface (W/m2). θ is solar zenith angle (degree). I_{sc} is solar constant which is equal to 1361 W/m2. CC is cloud cover (dimensionless). T_n and T_{n-3} are the air temperature at time (n) and (n-3) (°C), respectively. RH is the relative humidity (%). c_0, c_1, c_2, c_3, c_4, d and k are the constants (dimensionless).

A.4. Correlation coefficients based on Eq. (13) and Eq. (14)

Appendix Fig. 5-1 shows the correlation coefficients based on Eq. (13) and Eq. (14), respectively. It can be found that the sensitivity of the two methods to various meteorological parameters is diverse. In the method based on actual solar radiation on the horizontal surface, sunshine duration, visibility, and three-hour temperature difference have the highest correlation to solar radiation values. This is because on a large scale, solar radiation reflects certain seasonal characteristics and therefore correlates better with meteorological parameters that can represent date or seasonal characteristics, such as sunshine duration and temperature differences. While in the proposed model, relative humidity, weather type, and cloudiness have the highest correlation on the solar radiation loss values. This is because the effect of these parameters on the reduction of solar radiation as it passes through the atmosphere is the most significant.

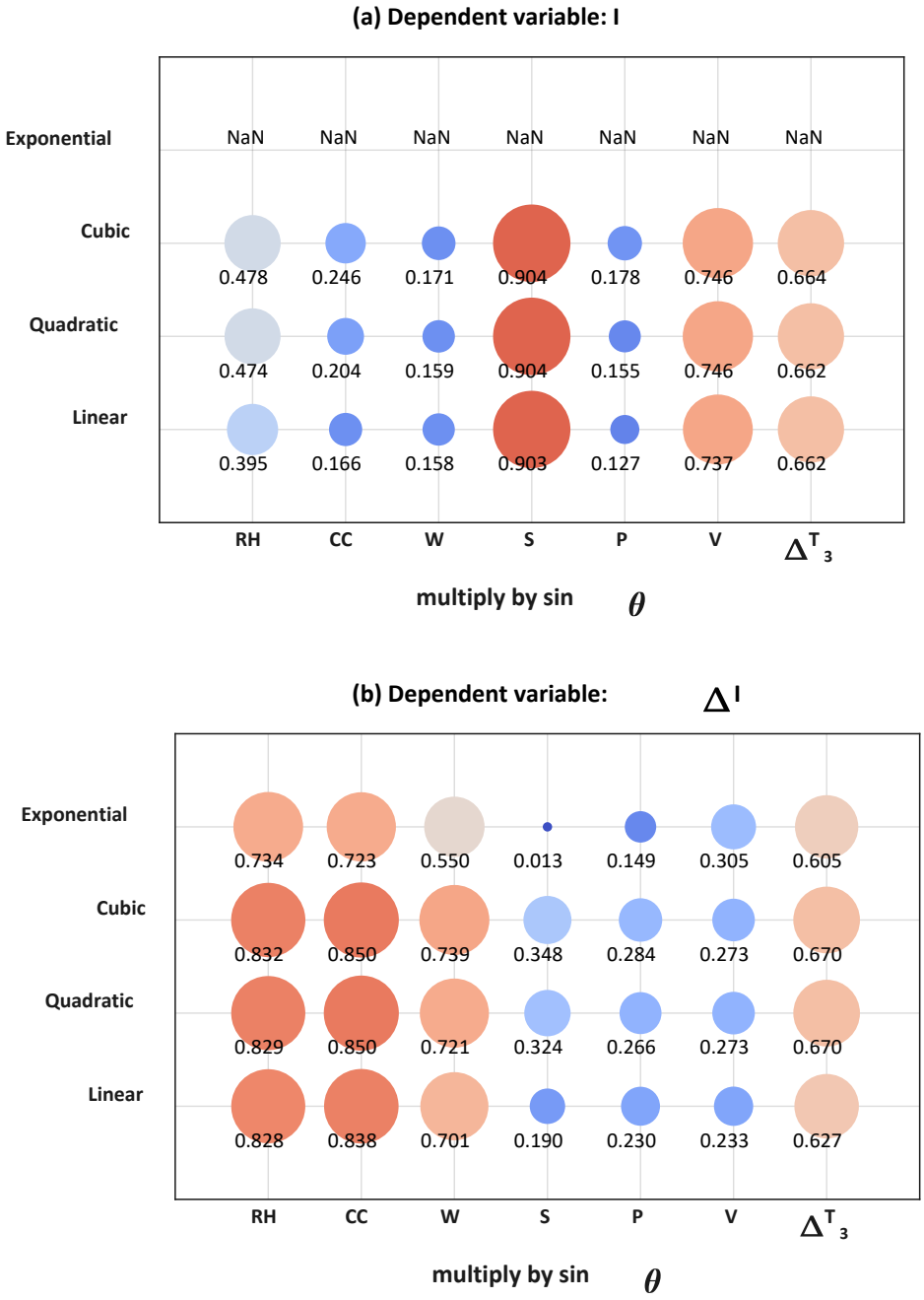

Appendix Fig. 5-1 Correlation coefficients (R) of the two methods for different meteorological parameters in Abashiri, (NaN means that the function form is not applicable to the method), ($\Delta T_3 = T_n - T_{n-3}$)

References

[1] Fattahi A, Diéguez MS, Sijm J, España GM, Faaij A. Measuring accuracy and computational capacity trade-offs in an hourly integrated energy system model. Advances in Applied Energy. 2021;1:100009.

[2] Pfeifer A, Herc L, Bjelić IB, Duić N. Flexibility index and decreasing the costs in

energy systems with high share of renewable energy. Energy Conversion and Management. 2021;240:114258.

[3] Van der Meer DW, Widén J, Munkhammar J. Review on probabilistic forecasting of photovoltaic power production and electricity consumption. Renewable and Sustainable Energy Reviews. 2018;81:1484-512.

[4] Yan J, Yang Y, Elia Campana P, He J. City-level analysis of subsidy-free solar photovoltaic electricity price, profits and grid parity in China. Nature Energy. 2019;4:709-17.

[5] Dai Y, Wang Y, Leng M, Yang X, Zhou Q. LOWESS smoothing and Random Forest based GRU model: A short-term photovoltaic power generation forecasting method. Energy. 2022;256:124661.

[6] Xiao L, Qin L-L, Wu S-Y. Proposal and application of comprehensive thermal comfort evaluation model in heating seasons for buildings with solar Trombe wall. Applied Thermal Engineering. 2022:118774.

[7] Yin Y, Chen H, Zhao X, Yu W, Su H, Chen Y, et al. Solar-absorbing energy storage materials demonstrating superior solar-thermal conversion and solar-persistent luminescence conversion towards building thermal management and passive illumination. Energy Conversion and Management. 2022;266:115804.

[8] Sward J, Ault T, Zhang K. Genetic algorithm selection of the weather research and forecasting model physics to support wind and solar energy integration. Energy. 2022:124367.

[9] Ji L, Wu Y, Sun L, Zhao X, Wang X, Xie Y, et al. Solar photovoltaics can help China fulfill a net-zero electricity system by 2050 even facing climate change risks. Resources, Conservation and Recycling. 2022;186:106596.

[10] Qiu R, Li X, Han G, Xiao J, Ma X, Gong W. Monitoring drought impacts on crop productivity of the US Midwest with solar-induced fluorescence: GOSIF outperforms GOME-2 SIF and MODIS NDVI, EVI, and NIRv. Agricultural and Forest Meteorology. 2022;323:109038.

[11] Li Y, Qian F, Gao W, Fukuda H, Wang Y. Techno-economic performance of battery energy storage system in an energy sharing community. Journal of Energy Storage. 2022;50:104247.

[12] Creutzig F, Agoston P, Goldschmidt JC, Luderer G, Nemet G, Pietzcker RC. The underestimated potential of solar energy to mitigate climate change. Nature Energy. 2017;2:1-9.

[13] Shabani M, Dahlquist E, Wallin F, Yan J. Techno-economic impacts of battery performance models and control strategies on optimal design of a grid-connected PV system. Energy Conversion and Management. 2021;245:114617.

[14] Dong J, Olama MM, Kuruganti T, Melin AM, Djouadi SM, Zhang Y, et al. Novel

stochastic methods to predict short-term solar radiation and photovoltaic power. Renewable Energy. 2020;145:333-46.

[15] Angstrom A. Solar and terrestrial radiation. Report to the international commission for solar research on actinometric investigations of solar and atmospheric radiation. Quarterly Journal of the Royal Meteorological Society. 1924;50:121-6.

[16] Prescott J. Evaporation from a water surface in relation to solar radiation. Trans Roy Soc S Aust. 1940;46:114-8.

[17] Asilevi PJ, Quansah E, Amekudzi LK, Annor T, Klutse NAB. Modeling the spatial distribution of Global Solar Radiation (GSR) over Ghana using the Ångström-Prescott sunshine duration model. Scientific African. 2019;4:e00094.

[18] Liu X, Mei X, Li Y, Porter JR, Wang Q, Zhang Y. Choice of the Ångström–Prescott coefficients: Are time-dependent ones better than fixed ones in modeling global solar irradiance? Energy Conversion and Management. 2010;51:2565-74.

[19] Liu X, Xu Y, Zhong X, Zhang W, Porter JR, Liu W. Assessing models for parameters of the Ångström–Prescott formula in China. Applied energy. 2012;96:327-38.

[20] Morf H. A stochastic solar irradiance model adjusted on the Ångström–Prescott regression. Solar Energy. 2013;87:1-21.

[21] Paulescu M, Stefu N, Calinoiu D, Paulescu E, Pop N, Boata R, et al. Ångström–Prescott equation: Physical basis, empirical models and sensitivity analysis. Renewable and Sustainable Energy Reviews. 2016;62:495-506.

[22] Almorox J, Bocco M, Willington E. Estimation of daily global solar radiation from measured temperatures at Cañada de Luque, Córdoba, Argentina. Renewable Energy. 2013;60:382-7.

[23] Hargreaves GH, Samani ZA. Estimating potential evapotranspiration. Journal of the irrigation and Drainage Division. 1982;108:225-30.

[24] Hargreaves GH, Samani ZA. Reference crop evapotranspiration from temperature. Applied engineering in agriculture. 1985;1:96-9.

[25] Li M-F, Fan L, Liu H-B, Guo P-T, Wu W. A general model for estimation of daily global solar radiation using air temperatures and site geographic parameters in Southwest China. Journal of Atmospheric and Solar-Terrestrial Physics. 2013;92:145-50.

[26] Chang K, Zhang Q. Development of a solar radiation model considering the hourly sunshine duration for all-sky conditions – A case study for Beijing, China. Atmospheric Environment. 2020;234.

[27] Zhang Q, Huang J, Lang S. SYMPOSIUM PAPERS-HI-02-16 Recent Developments in Availability of International Weather Data-Development of Typical Year Weather Data for Chinese Locations. ASHRAE Transactions-American Society of Heating Refrigerating Airconditioning Engin. 2002;108:1063-78.

[28] Chang K, Zhang Q. Improvement of the hourly global solar model and solar radiation for air-conditioning design in China. Renewable Energy. 2019;138:1232-8.

[29] Kim KH, Baltazar J-C, Haberl JS. Evaluation of meteorological base models for estimating hourly global solar radiation in Texas. Energy Procedia. 2014;57:1189-98.

[30] Kim KH, Oh JK-W, Jeong W. Study on solar radiation models in South Korea for improving office building energy performance analysis. Sustainability. 2016;8:589.

[31] S.M.Al-Alawi, H.A.Al-Hinai. An ANN-based approach for predicting global radiation in locations with no direct measurement instrumentation. Renewable Energy. 1998;14:199-204.

[32] Lazzús JA, Pérez Ponce AA, Marín J. Estimation of global solar radiation over the city of La Serena (Chile) using a neural network. Applied Solar Energy. 2011;47:66-73.

[33] Kaba K, Sarıgül M, Avcı M, Kandırmaz HM. Estimation of daily global solar radiation using deep learning model. Energy. 2018;162:126-35.

[34] Hassan MA, Khalil A, Kaseb S, Kassem MA. Exploring the potential of tree-based ensemble methods in solar radiation modeling. Applied Energy. 2017;203:897-916.

[35] Basaran K, Özçift A, Kılınç D. A new approach for prediction of solar radiation with using ensemble learning algorithm. Arabian Journal for Science and Engineering. 2019;44:7159-71.

[36] Gao Y, Miyata S, Akashi Y. Multi-step solar irradiation prediction based on weather forecast and generative deep learning model. Renewable Energy. 2022;188:637-50.

[37] Peng T, Zhang C, Zhou J, Nazir MS. An integrated framework of Bi-directional long-short term memory (BiLSTM) based on sine cosine algorithm for hourly solar radiation forecasting. Energy. 2021;221.

[38] Zhou Y, Liu Y, Wang D, Liu X, Wang Y. A review on global solar radiation prediction with machine learning models in a comprehensive perspective. Energy Conversion and Management. 2021;235.

[39] Gao Y, Miyata S, Akashi Y. Interpretable deep learning models for hourly solar radiation prediction based on graph neural network and attention. Applied Energy. 2022;321.

[40] Bird RE, Hulstrom RL. Simplified clear sky model for direct and diffuse insolation on horizontal surfaces. Solar Energy Research Inst., Golden, CO (USA); 1981.

[41] Chen R, Kang E, Ji X, Yang J, Wang J. An hourly solar radiation model under actual weather and terrain conditions: A case study in Heihe river basin. Energy. 2007;32:1148-57.

[42] Su G, Zhang S, Hu M, Yao W, Li Z, Xi Y. The modified layer-by-layer weakening solar radiation models based on relative humidity and air quality index. Energy. 2022;239.

[43] Prieto J-I, García D. Global solar radiation models: A critical review from the point of view of homogeneity and case study. Renewable and Sustainable Energy Reviews.

2021:111856.

[44] Liang S. Narrowband to broadband conversions of land surface albedo I: Algorithms. Remote sensing of environment. 2001;76:213-38.

[45] Van Laake PE, Sanchez-Azofeifa GA. Mapping PAR using MODIS atmosphere products. Remote Sensing of Environment. 2005;94:554-63.

[46] Xu X, Du H, Zhou G, Mao F, Li P, Fan W, et al. A method for daily global solar radiation estimation from two instantaneous values using MODIS atmospheric products. Energy. 2016;111:117-25.

[47] Zhang J, Zhao L, Deng S, Xu W, Zhang Y. A critical review of the models used to estimate solar radiation. Renewable and Sustainable Energy Reviews. 2017;70:314-29.

[48] Yao W, Li Z, Xiu T, Lu Y, Li X. New decomposition models to estimate hourly global solar radiation from the daily value. Solar Energy. 2015;120:87-99.

[49] Li M-F, Tang X-P, Wu W, Liu H-B. General models for estimating daily global solar radiation for different solar radiation zones in mainland China. Energy conversion and management. 2013;70:139-48.

[50] Black J. The distribution of solar radiation over the earth's surface. Archiv für Meteorologie, Geophysik und Bioklimatologie, Serie B. 1956;7:165-89.

[51] Jaccard J, Wan CK. LISREL approaches to interaction effects in multiple regression: sage; 1996.

[52] Chakchak J, Cetin NS. Investigating the impact of weather parameters selection on the prediction of solar radiation under different genera of cloud cover: A case-study in a subtropical location. Measurement. 2021;176:109159.

Chapter 6

ENERGY SHARING FOR SELF-SUFFICIENT IN SOLAR COMMUNITY

ENERGY SHARING FOR SELF-SUFFICIENT IN SOLAR COMMUNITY

6.1 Contents 6-1

6.2 System formulation 6-7

6.2.1 Basic idea of energy sharing structure 6-7

6.2.2 Introduction of typical design scenarios of BESS 6-8

6.3 Methodology 6-9

6.3.1 Data sources 6-9

6.3.2 PV and battery modeling 6-10

6.3.3 Internal pricing mechanism 6-11

6.3.4 Aggregator managed demand response 6-12

6.4 Energy flow and simulation 6-13

6.4.1 Energy flow 6-13

6.4.2 Energy losses 6-17

6.4.3 Objective functions 6-18

6.4.4 Optimization 6-18

6.5 Case study 6-21

6.5.1 Situation analysis 6-21

6.5.2 Energy sharing participation willingness evaluation 6-23

6.5.3 The results of optimized BESS configuration 6-26

6.5.4 Losses comparison at community-levels 6-27

6.5.5 Transmission loss optimization during battery sharing process 6-28

6.5.6 Performance comparison of single building 6-29

6.5.7 DR performance evaluation (Scenario SCB&SDB) 6-31

6.5.8 Economic performance comparison 6-33

6.6 Sensitivity analysis of parameters 6-34

6.7 Conclusions 6-36

References 6-37

6.1 Contents

With the rapid decline in the price of photovoltaic (PV), the growth in installation of PV systems has increased significantly, and the trend is likely to continue according to International Energy Agency Photovoltaic Power Systems Programme (IEA PVPS, 2020) [1]. The lower prices have attracted many commercial buildings to become producers who generate electricity from local renewable energy resources (RES) and consume it locally or sell it to the grid. The surplus energy generated by the dynamic mismatch between solar power and local demand can be sold to the grid through a feed-in tariff (FIT). However, as PV penetration increases and its intermittent output puts management pressure on the public grid, governments have had to promote local consumption of distributed energy resources (DERs) by reducing the FIT to reduce the impact on public grid stability [2]. Meanwhile, under the impact of the pandemic, the governments have understandably redistributed public funding to combat the Covid-19 in a way that leaves less available for renewable energy incentives and tax credits [3]. Japan has fully opened its retail electricity market since April 2016 [4]. The resulting positive impact is that the liberalization of the energy market has increased public support for RES [5]. Therefore, energy sharing [6], [7] have increased opportunities to improve the local energy self-consumption rate and the spread-ability of RES in the future. With direct energy sharing, communities still face the issue of not being able to consume all the surplus energy. Battery sharing [8], [9] is considered to be an effective solution to the above issue.

Energy sharing refers to energy transactions between consumers and producers or between producers, where surplus electricity from producers can be shared between neighbors. Energy sharing allows producers to sell energy to their neighbors for more profit, as well as makes the DERs to be better utilized [7]. Energy sharing networks can be broadly split into two categories, autonomous energy sharing and supervised sharing. In autonomous energy sharing mode, it allows users with full control over their DERs, without requiring a central control system. Most of the existing literature on energy sharing has focused on different mechanisms based on this community framework. A small-scale local market needs to be formed within the community. This market is mainly based on a decentralized model through auction model [9], [10], blockchain [11], [12] and bilateral contracts [13]. Game theory provides a good theoretical framework for this structure. Cintuglu et al.[14] presented a real-time implementation of multiagent-based game theory reverse auction for microgrid market operations featuring conventional and DERs. Cui et al.[15] used the Stackelberg approach realized a distributed game-based pricing market for solar PV prosumers within a microgrid to undertake energy sharing. In this mode, the advantages are, selling energy locally can be more profitable than selling to the grid, so incentives to engage producers in energy sharing are usually not needed in this model. The disadvantage is, in order to prevent long waits in the transaction process, communication systems with a lot of computational power are usually needed to perform the bidding of energy prices [16]. In addition, everyone in the community will participate individually without any cooperation. However, several studies have pointed out the Nash equilibrium of a non-cooperative game may not be the best solution [7], [17].

Under the supervised energy sharing mode, energy sharing within the community is managed by a third-party entity. Simpler communication systems and less data processing are required within the community because no bids need to be executed. Olivella-Rosell et al. [18] proposed

a new aggregator type called Smart Energy Service Provider to schedule flexible energy resources. Ottesen et al. [19] considered the capability of an aggregator providing flexibility services to the broader grid. Motalleb et al. [20] constructed a theoretical model of the competition between demand response aggregators for selling energy previously stored in an aggregation of storage devices.

Due to the limitations of load characteristics, direct energy sharing is not sufficient for communities to achieve high penetration of energy self-consumption. Existing studies have shown that energy sharing networks with battery energy storage systems (BESS) can save significant amounts of money for producers in a community while increasing energy self-consumption within the community [21]. Nguyen et al. [22] proposed an optimization model to maximize the economic benefits for rooftop PV-battery distributed generation in an energy trading environment. The goal of the proposed model is to investigate the feasibility of such renewable source participated energy trading by examining the economic benefits. Dong et al.[23] proposed an agent-based model to investigate and analyze community energy storage based on a range of criteria. Parra et al.[24] optimized the performance including equivalent full cycles and round trip efficiency of lead-acid and lithium-ion batteries performing demand load shifting are quantified as a function of the size of the community. BESSs with different sharing structures (distributed and centralized, respectively) of the kind found in sharing communities have also been shown to have different techno-economic properties. Rodrigues et al. [25] considered the optimal BESS sizing and operation in an energy sharing network under different BESS ownership structures. Huang and Sun et al.[26] proposed a hierarchical design method of distributed batteries in solar power shared building communities, with the purpose of reducing the battery capacity and minimizing the energy loss in the sharing process. The above study demonstrates that both different BESS structure designs (distributed and centralized) are economically feasible in energy sharing communities. But the interaction between energy sharing and BESS size and the optimal location of BESS units is ignored.

In modern power system, all system operators have a fundamental need to be responsive to the appropriate level to which they will function to achieve maximum reliability of overall power system [27, 28]. The overview of recent advances and future key benefits of demand-side management states that distributed generation should be integrated with demand response (DR) mechanisms which is an emerging strategy to deal with peak demand, energy management, reliability and economy of contemporary distribution system [29]. The combination of smart grid and energy storages and resultant policy recommendations have been discussed by Amoretti et al.[30] and Zame et al.[31]. Contreras-Ocanaet al. [32]showed that aggregators and storage units are likely to cooperate in the long-term using Nash bargaining theory. F. Mohamad et al. [33] proposed a method that optimally deployed BESSs and determined their capacity in a two-part framework to minimize solar energy curtailment, by considering network topology and power flow constraints to maximize their cooperation among BESSs by pooling all their capacities to store surplus solar power. Chen et al.[34] studied the coordination of groups of residential consumers for demand response. In addition, many scholars have pointed out that at this stage in Japan, the economic performance of BESS is heavily dependent on government subsidies, and we must seek new ways to improve the economic performance of BESS [35], [36]. Excitingly, through aggregation, BESS can

participate in DR to relieve the pressure on the grid for peaking, saving the supply side expenditure on peaking plants. Therefore power companies are also willing to work with aggregators by paying a fee when there are enough regulable users to participate in DR. Astriani Y et al[37] indicated that the power companies needs to allocate around 40% of its DR profit so that the commercial customer's DR deployment costs are paid back within its lifetime. Thus, there is a great prospect for providing services through aggregating BESSs.

Based on the aforementioned studies, the techno-economic performance brought by optimal sizing and number of different BESS sharing structures and the interaction between aggregator-managed BESS and smart grid is highly underestimated. To address the knowledge gaps identified above, we shared a techno-economic study of a PV-BESS system for a multi-commercial buildings energy sharing community and verified the feasibility by whole-life cost analysis. The major contributions of this work are as follows.

- Energy sharing and battery sharing are enabled to increase the self-consumption of renewable energy in the community, thereby eliminating the requirement for large-sized BESS and power feedback to the grid.
- The optimal number and position in the private battery sharing community are optimized by a constrained multivariate genetic algorithm.
- Loads in commercial buildings are considered to have a higher economic value than loads in residential buildings because of the potential for the loads to affect the business within the building. Therefore, the techno-economic performance of the BESS in the energy sharing community is investigated using a practical example of a multi-commercial building containing a 12-month hourly load profile.
- The BESS's effect on system benefits through an aggregator is discussed, which can be the different application of demand response (DR).

The rest of the paper is organized as follows. In Section 2, the introduction of typical design scenarios of BESS is presented. The methodology and simulation are presented in Section 3. The result of the case study is described in 4 while the discussion and sensitivity analysis are presented in Section 5. Finally, the conclusions are presented in Section 6.

Nomenclature

Abbreviations

BESS Battery energy storage system

DR Demand response

FIT Feed-in-tariff

PV Photovoltaic

RES Renewable energy resources

IDB Individual design for distributed BESS

SCB Shared design for centralized BESS

SDB Shared design for distributed BESS

SDR Supply and demand ratio

NPV Net present value

SCR Self-consumption rate

GA Genetic algorithm

SOC State of charge

TOU Time of use

Set

t Index for time, t ={1,2,…24}

d Index for time, d ={1,2,…365}

yr Index for year

j Index for number of buildings

Variable

C_{inv} Investment cost

E Energy (kWh)

E_{net} Net power (kWh)

E_{load} Power demand (kWh)

E_{pv} PV generation power (kWh)

E_{sur} Surplus sharing power (kWh)

E_{cha} Charging power (kWh)

E_{dis} Discharging power (kWh)

R Solar radiation

R_{ref} Reference solar radiation

T_c Normal cell temperature

T_{air} Ambient temperature

T_{ref} Reference temperature

N_T Panel temperature coefficient

p_{pv} Produced power by a PV module

$P_{R,PV}$ Rated power of PV panel

Pr_{sell} Selling price

Pr_{buy} Buying price

Pr_{cont} Fixed incentive price

Pr_{va} Nighttime electricity price

λ_{sell} Feed-in-tariff price

λ_{buy} Grid TOU price

η_{cha} Charge efficiency

η_{dis} Discharge efficiency

η_{trans} Transmission efficiency

α Discount rate

β Compensating factor

Cap Capacity of BESS

pw Rated power of BESS

Pro_{DR}^{fix} Fixed incentive

Pro_{DR}^{perf} Performance-based incentive

$Loss_{tot}$ Total energy losses

$Loss_{cha/dis}$ Energy losses in battery charging and discharging process

$Loss_{sur}$ Energy losses in surplus sharing process

$Loss_{pvs}$ Energy losses in surplus PV storage sharing process

$Loss_{bat}$	Energy losses in remaining battery sharing process
k	Compensation rate

6.2 System formulation

6.2.1 Basic idea of energy sharing structure

In this research, we focus on the locally consumption of PV and improve the economic feasibility of BESS in the commercial community. Without considering subsidies and incentives, the economic benefits of batteries come from the consumption of local PV generation and economic arbitrage. PV generation is firstly used directly then is shared to the other buildings, finally charged into BESS. Due to the characteristics of commercial buildings, although there is a large surplus of PV generation, it represents only a small proportion of the annual consumption. (Fig.1). Therefore, we consider the charging power comes from PV generation and grid. Energy sharing is divided into three types which are displayed in Fig.2: PV surplus sharing (i.e., using surplus PV power to meet the electricity demand of other buildings) and battery storage sharing, where battery storage sharing is divided into two categories, surplus PV storage sharing (i.e., storing surplus PV in batteries in other buildings) and remaining battery sharing (i.e., discharging remaining battery capacity to other buildings). To explore the impact of different sharing structures on improving community energy self-consumption as well as economic performance, this paper investigates the following three BESS sharing structures, namely (a) Individual design for distributed BESS (IDB); (b) Shared design for centralized BESS (SCB); (c) Shared design for distributed BESS (SDB). Fig.3 summarizes the operational strategies of the three sharing structures. The operational strategies of BESS can be divided into two categories. In scenario IDB, the capacity of BESS is determined by the power deviation of each building. Each BMS manages its own resource so as to every BESSs cannot participate in demand response. And in scenario SCB and SDB, the other community prosumers should be considered for all BESSs. The aggregator centrally manages individual decentralized resources. Thus, each building can participate in a demand response program by an aggregator.

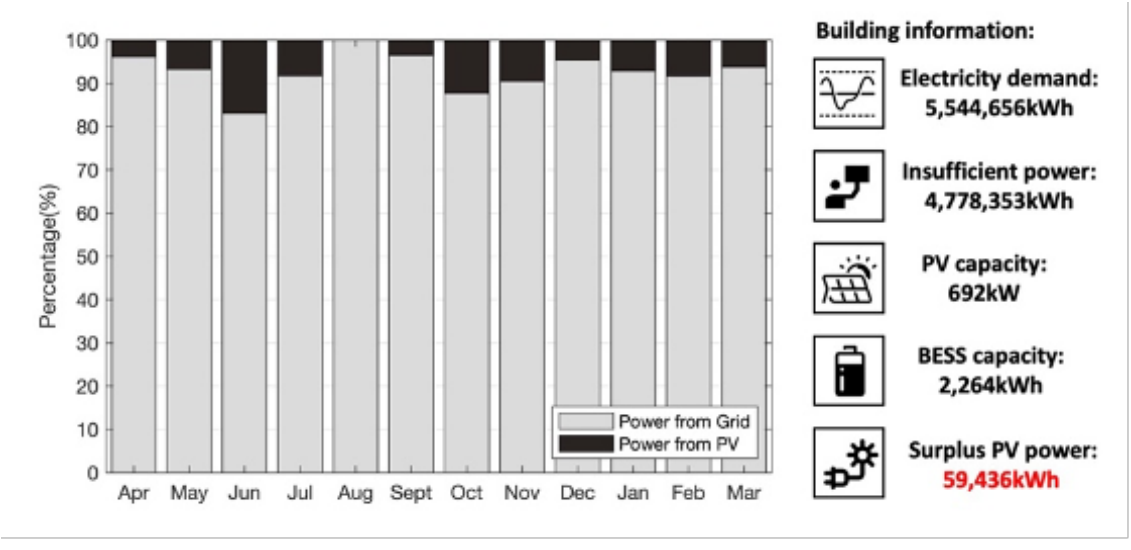

Fig. 6-1. BESS charging structure of a typical commercial building

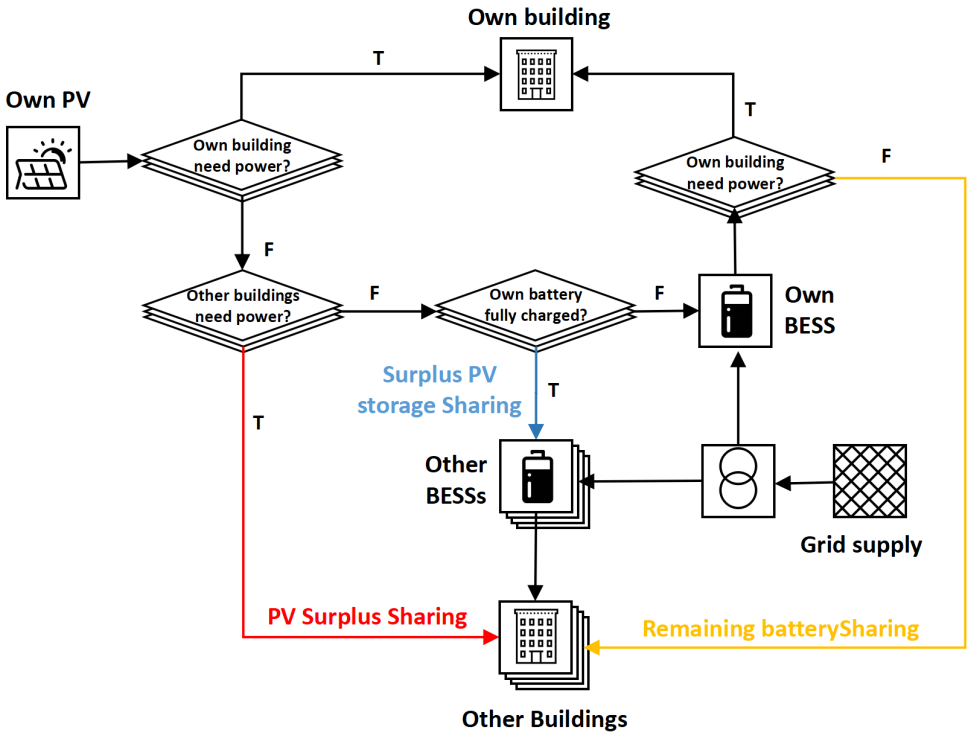

Fig. 6-2. Surplus and insufficient power exchange in the energy sharing community

6.2.2 Introduction of typical design scenarios of BESS

① Individual design for distributed BESS (IDB)

This is a typical individual BESS deployment structure. First, buildings can decide whether to share surplus power with other buildings, depending on the internal price within the community. If the internal price is sufficient to stimulate producers to voluntarily share their surplus power, the surplus power from these buildings can be sent to the building community to meet the electricity demand of other buildings with insufficient generation capacity (i.e., surplus sharing). If there is still surplus power after meeting the community's demand, the surplus power will be stored in its own battery. In the evening, the building draws power from its own battery. In this scenario, only surplus sharing is enabled. Buildings cannot draw power from other buildings' batteries. The transmission of electricity is done inside the building; therefore, we consider that the transmission loss of electricity is zero.

② Shared design for centralized BESS (SCB)

There is a centralized battery in the community, and it is managed by an aggregator. The aggregator is a broker that facilitates energy sharing between buildings. The surplus power from the building satisfies other buildings in the community that have insufficient power. (i.e., surplus sharing). After compensating the supply and demand inside the community, the surplus/insufficient power will be stored/ acquired from the centralized battery. In this scenario, due to this long-distance power charging/discharging, a large amount of power loss is generated. And the sharing of energy is done using three methods, surplus sharing, surplus PV storage sharing, and remaining battery sharing.

③ Shared design for distributed BESS (SDB)

Buildings can deploy private BESSs. Same as centralized BESS, the surplus power from the building satisfies other buildings that have insufficient power in the community. (i.e., surplus sharing). And through an internal sharing network, after compensating the supply and demand inside the community, the surplus power can first be stored through its own battery, then it can also be stored through the batteries of other buildings. In this scenario, the sharing of energy is done using three methods, surplus sharing, surplus PV storage sharing and remaining battery sharing.

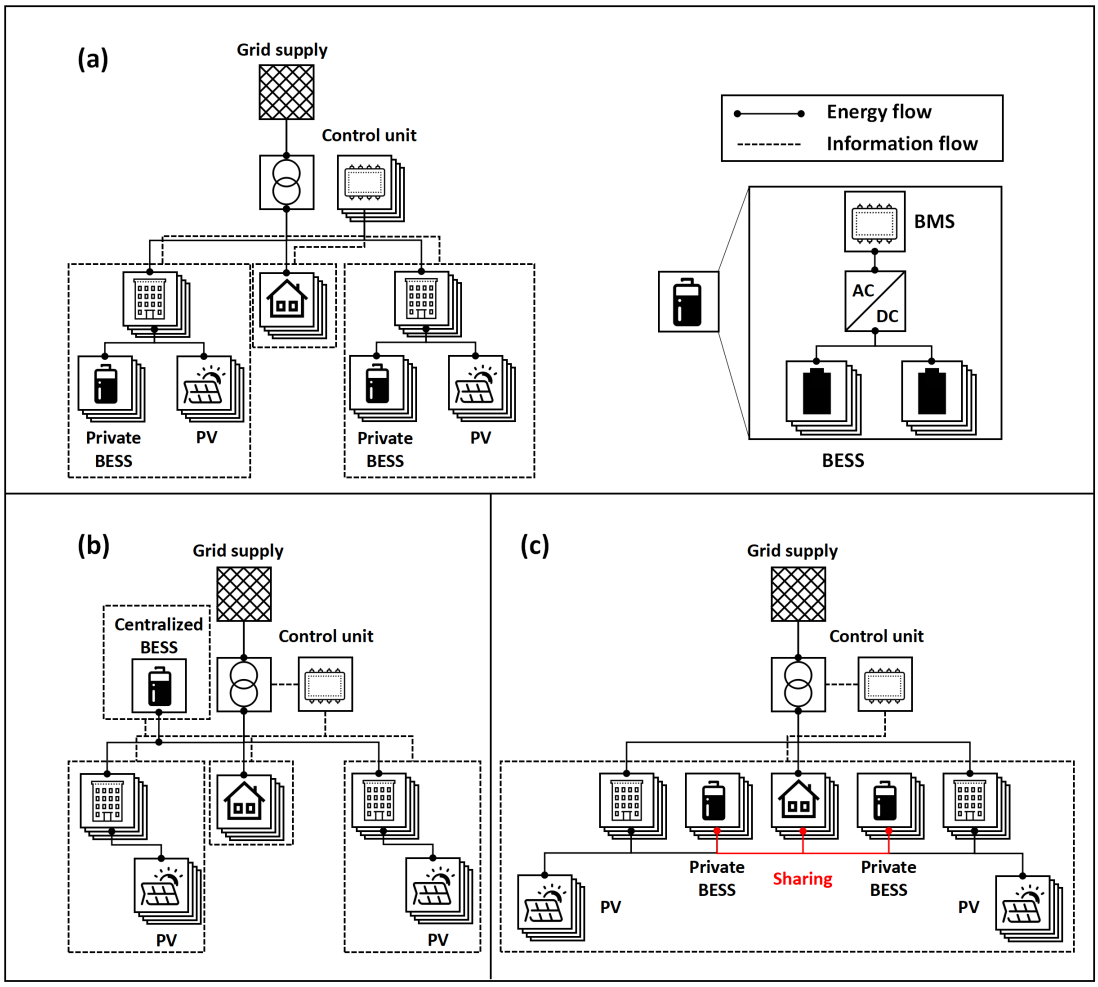

Fig. 6-3. The operation strategies of three BESS sharing structure design approaches. (a), Individual design for distributed BESS; (b), Shared design for centralized BESS; (c), Shared design for distributed BESS

6.3 Methodology

6.3.1 Data sources

In this research, the power load data is collected from a smart community located in the Kitakyushu city of Japan. And we collected the hourly load data from April 2013 to March 2014. The weather data in Fukuoka is provided by Japan Meteorological Agency [38]. The target community is within the scope of Kyushu power grid. Therefore, the price we choose comes from the official website of Kyushu Electric Power [39]. The electricity price model we chose is the seasonal-hourly price. The specific prices are shown in Table1.

Table 6-1. Commercial electricity price in Kyushu Electric Power

Basic capacity fee (Yen/kW)	Period (season)	Period (hour)	Price (Yen/kWh)
2046	Spring, autumn and winter	Nighttime (23:00~8:00)	9.06
		Standard daytime (8:00-13:00; 16:00-23:00)	13.53
		Peak daytime (13:00-16:00)	16.95
	Summer	Nighttime (23:00~8:00)	9.06
		Standard daytime (8:00-13:00; 16:00-23:00)	14.48
		Peak daytime (13:00-16:00)	16.95

6.3.2 PV and battery modeling

① PV system modelling

We considered j users in the community, each of whom is equipped with a solar PV system. This paper adopt the Panasonic module HIT N245 as the objection of PV module [40]. The generated power of the PV module, by considering the received solar irradiance, can be determined by using Eq. (1) [41]:

$$p_{pv}(t) = P_{R,pv} \times (\frac{R}{R_{ref}}) \times [1 + NT \times (T_c - T_{ref})] \quad (6\text{-}1)$$

where $p_{pv}(t)$, $P_{R,PV}$, and R refer to the produced power by a PV module at time (t), the rated power of the utilized panel, and solar radiation, respectively. R_{ref} and T_{ref} denote the reference solar radiation (1000 W/m^2) and reference temperature (conventionally considered equal to 25℃), respectively. The panel temperature coefficient is shown by N_T and equals to $-3.7 \times 10^{-3}(1/℃)$ for mono and polycrystalline silicon cells [42]. The temperature of the cell can be determined by employing Eq. (2) as:

$$T_c = T_{air} + [(\frac{NOCT - 20}{800}) \times R] \quad (6\text{-}2)$$

where T_{air}, R and T_c are the ambient temperature (℃), solar radiation and the normal operating cell temperature (℃), respectively. $NOCT$ is a specification of the cell and is declared by the cell producer. By considering the number of panels as N_{pv}, the total generated power is determined by employing Eq. (3) as:

$$C_{pv} = N_{pv} \times p_{pv}(t) \quad (6\text{-}3)$$

② Battery system modelling

In recent years, battery energy storage technology has developed greatly. Among the many battery technologies that meet the requirements of large-scale energy storage, the overall characteristics of NAS batteries are most suitable for l arge-scale energy storage system applications, based on a combination of factors such as energy efficiency, installation cost, rated power discharge capacity and the size of the installation site [43, 44]. We chose NAS batteries as the power storage technology. NAS batteries have high capacity with no significant self-discharge and are very safe because they do not use toxic metals [44]. In addition, it has a high charge/discharge tolerance with an expected lifetime of 15 years. A crucial feature of BESS is the time coupling characteristic related to state of charge (SOC). During the charging and discharging process, the SOC (%) dynamics are defined by (4) and (5), respectively as:

$$SOC(t+1) = SOC(t) + \frac{\eta_{cha} \cdot \sum pw^j(t) \cdot \Delta T}{Cap^j} \tag{6-4}$$

$$SOC(t+1) = SOC(t) - \frac{\sum pw^j(t) \cdot \Delta T}{\eta_{dis} \cdot Cap^j} \tag{6-5}$$

where $SOC(t)$, s, yr denotes the state of charge of ESS at time period t in the year yr, η_{cha} , $\eta_{dis}$and Cap^j denote the charging and discharging efficiency and energy capacity of building j, respectively, of BESS. The BESS operation optimization is subject to the following constraints.

(a) SOC limit constraint -

$$SOC_{\min} \le SOC(t) \le SOC_{\max} \tag{6-6}$$

where SOC_{min} and SOC_{max} are the lower and upper limits of SOC.

(b) ESS operation power limit constraint –

$$-pwc \le pw \le pwc \tag{6-7}$$

where pwc denotes the rated power capacity of BESS. In our paper, in order to investigate the long-term economic potential of batteries with different sharing structures, we adopted a mature and commercially available NAS battery system for its field-proven 4,500 full cycle discharges and stabilized capability of charging and discharging. The rated power capacity of BESS is 16% of its capacity [44].

6.3.3 Internal pricing mechanism

In this study, we adopt the SDR internal pricing mechanism with a compensation factor. Because it provides an internal transaction price based on the energy demand conditions within the community during a specified period to ensure a more equitable distribution of benefits in energy trading [45]. The total selling power is from the PV generation and the total buying power is the building's demand. Thus, the SDR at a community at time t is defined as:

$$SDR(t) = \frac{E_{pv}^{tot}(t)}{E_{load}^{tot}(t)} \tag{6-8}$$

where $E_{pv}^{tot}(t)$ is the total supply power (kWh) and $E_{load}^{tot}(t)$ is the total demand power at time t. Buying and selling prices fluctuate at different times of the day and the price set is determined by:

$$Pr_{sell} = [Pr_{sell}(1), Pr_{sell}(2), \cdots Pr_{sell}(T)] \tag{6-9}$$

$$Pr_{buy} = [Pr_{buy}(1), Pr_{buy}(2), \cdots Pr_{buy}(T)] \tag{6-10}$$

where Pr_{sell} is the selling price at time t, Pr_{buy} is the buying price at time t. And T is a time series for a day with a time-step of ΔT, and it is represented as $T = \{1, 2, \ldots, 24\}$. The

internal trading prices depends on the buildings demand and solar PV generation at a particular period. Therefore, the selling and buying prices are defined as a function of the SDR. They are determined by:

$$Pr_{sell}(t) = f(SDR(t)) = \begin{cases} \dfrac{\left(\lambda_{sell}(t) + \beta(t)\right) \cdot \lambda_{buy}(t)}{(\lambda_{buy}(t) - \lambda_{sell}(t) - \beta(t)) \cdot SDR(t) + \lambda_{sell}(t) + \beta(t)}, 0 \le SDR(T) \le 1 \\ \lambda_{sell}(t) + \beta(t) / SDR(t), SDR(t) > 1 \end{cases} \tag{6-11}$$

$$Pr_{buy}(t) = f(SDR(t)) = \begin{cases} Pr_{sell}(t) \cdot SDR(t) + \lambda_{buy}(t) \cdot (1 - SDR(t)), 0 \le SDR(T) \le 1 \\ \lambda_{sell}(t) + \beta(t), SDR(t) > 1 \end{cases} \tag{6-12}$$

where $\lambda_{sell}(t)$ is the grid feed-in tariff energy price, (Notice: we adopt $\lambda_{sell} = 0$ in this case). $\lambda_{buy}(t)$ is the grid TOU supply energy price and $\beta(t)$ is the compensating factor restricted by:

$$0 \le \beta(t) \le \lambda_{buy}(t) - \lambda_{sell}(t) \tag{6-13}$$

6.3.4 Aggregator managed demand response

Energy sharing does not mean that the building directly controls its DERs; the building can use a third-party entity, such as an aggregator, to manage its resources. The aggregator has the ability to centrally manage individual decentralized resources. A building participates in a demand response program by an aggregator, referred to as 'negative trading'. This is an incentive-based demand response program where buildings can save electricity bills during peak hours based on a contract with the aggregator. The aggregator plays the role of a manager that controls the transaction by bundling many buildings and the demand for electricity on a per-building basis.

By shaving or shifting demand at the request of the aggregator, in addition to the reduced electricity bill, the building will receive the following incentives:

KW incentive (fixed per period): Since an event may be activated for any period of time specified in the contract, the building needs to have an appropriate system in place to respond upon activation. Therefore, the incentive will be paid based on the controllable capacity (kW), regardless of whether it is actually activated or not. The incentive is given to the consumer on an annual (kW-year) or monthly (kW-month) basis.

KWh incentive (performance based): Based on the actual performance of the DR events, such as the total kWh reduction during each DR event. The premise of the device is that: (1).The sustainable time for demand reduction is set in the range of 2 to 6 hours. (2).The number of hours required for response is set in the range of 10 to 100 hours as the number of hours of annual demand [46].

Load can be classified as shiftable load, controllable load, and shaveable load [37]. In order to reduce the impact of operations within commercial buildings, we only considered the response effect of shiftable load and the BESSs with shared ability are considered as tools to perform load shifting. (Note: Since aggregators do not have centralized control over individual design-based batteries, individual design for distributed BESS approach do not have the basis

to participate in demand response.) The demand response incentives for buildings can be described as:

$$pro_{DR} = \sum (pro_{DR}^{fixed} + pro_{DR}^{perf}) \tag{6-14}$$

where Pro_{DR}^{fixed} is fixed incentive of each consumer, and Pro_{DR}^{perf} is the performance-based incentive of each consumer.

$$pro_{DR}^{fixed} = cap^{j} \times pr_{cont} \tag{6-15}$$

$$pro_{DR}^{perf} = \sum_{d}^{D} \sum_{t}^{T} (RW_{act} \times RD_{act}(t,d)) \tag{6-16}$$

where$cap^{j}$is the capacity of the BESS, $Pr_{cont}$is fixed incentive price. RW_{act} is activation reward (Yen/kWh), and $RD_{act}(t,d)$ is the kWh reduction during DR event at time t.

6.4 Energy flow and simulation

6.4.1 Energy flow

For each building in the community a power balance between PV generation, the grid, and the building power demand is to be achieved. This is given by the following equation：

$$E_{net}^{j'}(t) = E_{net}^{j}(t) - \sum E_{sur}^{i,j}(t) + \eta_{trans} \times \sum E_{sur}^{i,j}(t) \tag{6-17}$$

where $E_{net}^{j}(t)$ is the building j's net power and $\mathrm{E}_{\mathrm{load}}^{\mathrm{j}}(t)$, $\mathrm{E}_{\mathrm{pv}}^{\mathrm{j}}(t)$ are the power demand and PV generation power at time t.

$$E_{net}^{tot}(t) = \sum E_{\mathrm{n}et}^{j}(t) \tag{6-18}$$

where$E_{net}^{tot}(t)$ is total net power in the building community. According to the total net demand situation of whole community, the PV surplus sharing power of each building $\mathrm{E}_{\mathrm{sur}}(\mathrm{t})$ can be described as follow:

$$E_{sur}(t) = \begin{bmatrix} 0 & E_{sur}^{2,1}(t) & \cdots & E_{sur}^{j,1}(t) \\ E_{sur}^{1,2}(t) & 0 & \cdots & E_{sur}^{j,2}(t) \\ \vdots & \vdots & \ddots & \vdots \\ E_{sur}^{1,j}(t) & E_{sur}^{2,j}(t) & \cdots & 0 \end{bmatrix} \tag{6-19}$$

where $E_{sur}(t)$ is a diagonalized vector, whose elements $E_{sur}^{i,j}(t)$ represent the PV surplus sharing from building i to building j at time t. To reduce communication costs, the PV surplus sharing between buildings is uniformly deployed by the aggregator based on demand/surplus. And the elements $E_{sur}^{i,j}(t)$ are limited by equation (20). The relationship with $E_{sur}(t)$ and $E_{net}^{tot}(t)$ is given by equation (21).

$$E_{sur}^{i,j}(t) \geq 0, \forall (E_{net}^{i}(t) \leq 0, E_{net}^{j}(t) \geq 0) \tag{6-20}$$

$$\sum E_{sur}(t) = E_{net}^{tot}(t) \tag{6-21}$$

Hourly energy mismatch of each building after PV surplus sharing can be described as follow:

$$E_{net}^{j'}(t) = E_{net}^{j}(t) - \sum E_{sur}^{i,j}(t) + \eta_{trans} \times \sum E_{sur}^{i,j}(t) \tag{6-22}$$

where $E_{net}^{j\prime}(t)$ is the building j 's net power after surplus sharing. η_{trans} is the transmission efficiency for energy sharing between buildings.

Depending on the BESS sharing structure, the operation of the BESS and energy flow are discussed by category.

(a) IDB:

In scenario IDB, the net load balance is given by equation (23). Each BESS manger its own energy mismatch, so the charge and discharge power can be defined as diagonal matrices, which are determined by equation (24) and equation (25).

$$\left|E_{net}^{j'}(t)\right| = \begin{cases} \dfrac{E_{cha}^{j}(t)}{\eta_{cha}}, if\,(E_{net}^{j'}(t) < 0) \\ 0, if\,(E_{net}^{j'}(t) = 0) \\ E_{dis}^{j}(t) \times \eta_{dis} + E_{grid}^{j}(t), if\,(E_{net}^{j'}(t) > 0) \end{cases} \tag{6-23}$$

$$E_{cha}(t) = \begin{bmatrix} E_{cha}^{1,1}(t) & 0 & \cdots & 0 \\ 0 & E_{cha}^{2,2}(t) & \cdots & 0 \\ \vdots & \vdots & \ddots & \vdots \\ 0 & 0 & \cdots & E_{cha}^{j,j}(t) \end{bmatrix} \tag{6-24}$$

$$E_{dis}(t) = \begin{bmatrix} E_{dis}^{1,1}(t) & 0 & \cdots & 0 \\ 0 & E_{dis}^{2,2}(t) & \cdots & 0 \\ \vdots & \vdots & \ddots & \vdots \\ 0 & 0 & \cdots & E_{dis}^{j,j}(t) \end{bmatrix} \tag{6-25}$$

where η_{cha} and η_{dis} are the chare/discharge efficiency of the BESS. $E_{cha}^{j,j}(t)$ and $E_{dis}^{j,j}(t)$ are the charge and discharge power from building j to building j at time t. The calculation of the charging/discharging states in scenario IDB are described as follows.

Charging state: When the building has surplus PV power generation, (i.e., $E_{net}^{j,\prime}(t) < 0$), the private battery is in a charging state. The battery charging rates $E_{cha}^{j,j}(t)$ (kW) should be limited by both the remaining storage capacity of the battery and the battery charging power.

$$E_{cha}^{j,j}(t)=\begin{cases}\left|E_{net}^{j'}(t)\right|\times\eta_{cha}, if\left(\left|E_{net}^{j'}(t)\right|\le pw^{j}\right)\\ pw^{j}, f\left(\left|E_{net}^{j'}(t)\right|> pw^{j}\right)\end{cases} \tag{6-26}$$

Discharging state: When the building has insufficient PV power generation, (i.e., $E_{net}^{j,\prime}(t) > 0$), the private battery is in a discharging state. The battery discharging rates $E_{dis}^{j,j}(t)$ (kW) should be limited by both the remaining storage capacity of the battery and the battery discharging power.

$$E_{dis}^{j,j}(t)=\begin{cases}\dfrac{\left|E_{net}^{j'}(t)\right|}{\eta_{dis}}, if\left(\left|E_{net}^{j'}(t)\right|\le pw^{j}\right)\\ pw^{j}, f\left(\left|E_{net}^{j'}(t)\right|> pw^{j}\right)\end{cases} \tag{6-27}$$

(b) SCB:

In scenario SCB, the net load balance is given by equation (28). The centralized BESS manger all energy mismatch, so the charge and discharge power can be defined as vectors, which are determined by equation (29) and equation (30). The calculation of the charging/discharging states in scenario SCB are described as equation (31) and equation (32).

$$\left|\sum E_{net}^{j'}(t)\right|=\begin{cases}\dfrac{E_{cha}(t)}{\eta_{cha}}, if\left(\sum E_{net}^{j'}(t)<0\right)\\ 0, if\left(\sum E_{net}^{j'}(t)=0\right)\\ E_{dis}(t)\times\eta_{dis}+\sum E_{grid}^{j}(t), if\left(\sum E_{net}^{j'}(t)<0\right)\end{cases} \tag{6-28}$$

$$E_{cha}(t)=\begin{bmatrix}E_{cha}^{1,1}(t) & E_{cha}^{2,2}(t) & \cdots & E_{cha}^{j,j}(t)\end{bmatrix} \tag{6-29}$$

$$E_{dis}(t)=\begin{bmatrix}E_{dis}^{1,1}(t) & E_{dis}^{2,2}(t) & \cdots & E_{dis}^{j,j}(t)\end{bmatrix} \tag{6-30}$$

Charging state: When the community has surplus PV power generation, (i.e., $\sum E_{net}^{j,\prime}(t) < 0$), the centralized battery is in a charging state. The battery charging rates $E_{cha}(t)$ (kW) should be limited by both the remaining storage capacity of the battery and the battery charging power.

$$E_{cha}(t)=\begin{cases}\left|E_{net}^{j'}(t)\right|\times\eta_{cha}, if\left(\left|E_{net}^{j'}(t)\right|\le pw^{j}\right)\\ pw^{j}, f\left(\left|E_{net}^{j'}(t)\right|> pw^{j}\right)\end{cases} \tag{6-31}$$

Discharging state: When the community has insufficient PV power generation, (i.e., $\sum E_{net}^{j,\prime}(t) > 0$), the centralized battery is in a discharging state. The battery discharging rates $E_{dis}(t)$ (kW) should be limited by both the remaining storage capacity of the battery and the battery discharging power.

$$E_{dis}(t)=\begin{cases}\dfrac{\left|E_{net}^{j'}(t)\right|}{\eta_{dis}}, if\left(\left|E_{net}^{j'}(t)\right|\le pw^{j}\right)\\ pw^{j}, f\left(\left|E_{net}^{j'}(t)\right|> pw^{j}\right)\end{cases} \tag{6-32}$$

(c) SDB:

In scenario SDB, the net load balance is given by equation (33). The shared private BESS not only manage its own energy mismatch, but also responses to the other building's requirement if there are remaining capacity. So the charge and discharge power can be defined as matrices, which are determined by equation (34) and equation (35). The calculation of the charging/discharging states in scenario SDB is described as equation (36) and equation (37).

$$\left|\sum E_{net}^{j'}(t)\right|=\begin{cases}\dfrac{\sum E_{cha}^{j}(t)}{\eta_{cha}}, if\left(\sum E_{net}^{j'}(t)<0\right)\\ 0, if\left(\sum E_{net}^{j'}(t)=0\right)\\ \sum E_{dis}^{j}(t)\times\eta_{dis}+\sum E_{grid}^{j}(t), if\left(\sum E_{net}^{j'}(t)>0\right)\end{cases} \tag{6-33}$$

$$E_{cha}(t)=\begin{bmatrix}E_{cha}^{1,1}(t) & E_{cha}^{2,1}(t) & \cdots & E_{cha}^{j,1}(t)\\ E_{cha}^{1,2}(t) & E_{cha}^{2,2}(t) & \cdots & E_{cha}^{j,2}(t)\\ \vdots & \vdots & \ddots & \vdots\\ E_{cha}^{1,j}(t) & E_{cha}^{2,j}(t) & \cdots & E_{cha}^{j,j}(t)\end{bmatrix} \tag{6-34}$$

$$E_{dis}(t)=\begin{bmatrix}E_{dis}^{1,1}(t) & E_{dis}^{2,1}(t) & \cdots & E_{dis}^{j,1}(t)\\ E_{dis}^{1,2}(t) & E_{dis}^{2,2}(t) & \cdots & E_{dis}^{j,2}(t)\\ \vdots & \vdots & \ddots & \vdots\\ E_{dis}^{1,j}(t) & E_{dis}^{2,j}(t) & \cdots & E_{dis}^{j,j}(t)\end{bmatrix} \tag{6-35}$$

Charging state: When the own building has surplus PV power generation, (i.e., $E_{net}^{j,\prime}(t)<0$), the private battery is in a charging state. And if the other buildings have surplus PV power generation while the battery has remaining capacity, (i.e.,$E_{net}^{j-1,\prime}(t)<0\cdots\vee E_{net}^{1,\prime}(t)<0$), the private battery can also be in a charging state. The battery charging rates $E_{cha}^{j}(t)$ (kW) should be limited by both the remaining storage capacity of the battery and the battery charging power.

$$E_{cha}^{j}(t)=\sum E_{cha}^{j,j}(t)=\begin{cases}pw^{j}, if\left(\left|E_{net}^{j'}(t)\right|> pw^{j}\right)\\ \left|E_{net}^{j'}(t)\right|\times\eta_{cha}+\left|E_{net}^{j-1'}(t)\right|\times\eta_{cha}\times\eta_{trans}, if\left(\left|E_{net}^{j'}(t)\right|\le pw^{j}\le\left|E_{net}^{j'}(t)+E_{net}^{j-1'}(t)\right|\right)\\ \left|E_{net}^{j'}(t)\right|\times\eta_{cha}+\left|E_{net}^{j'}(t)+E_{net}^{j-1'}(t)\right|\times\eta_{cha}\times\eta_{trans}, if\left(\left|E_{net}^{j-1'}(t)\right|\le pw^{j}\right)\end{cases} \tag{6-36}$$

Discharging state: When the own building has insufficient PV power generation, (i.e., $E_{net}^{j,\prime}(t) > 0$), the private battery is in a discharging state. And if the other buildings have insufficient PV power generation while the battery has remaining capacity, (i.e.,$E_{net}^{j-1,\prime}(t) > 0 \cdots \vee E_{net}^{1,\prime}(t) > 0$), the private battery can also be in a discharging state. The battery discharging rates $E_{dis}^{j}(t)$ (kW) should be limited by both the remaining storage capacity of the battery and the battery discharging power.

$$E_{dis}(t) = \sum E_{dis}^{j,j}(t) = \begin{cases} pw^{j}, if\left(\left|E_{net}^{j'}(t)\right| > pw^{j}\right) \\ \left|E_{net}^{j'}(t)\right| / \eta_{dis} + \left|E_{net}^{j-1'}(t)\right| / \eta_{dis} \times \eta_{trans}, if\left(\left|E_{net}^{j'}(t)\right| \le pw^{j} \le \left|E_{net}^{j'}(t) + E_{net}^{j-1'}(t)\right|\right) \\ \left|E_{net}^{j'}(t)\right| / \eta_{dis} + \left|E_{net}^{j'}(t) + E_{net}^{j-1'}(t)\right| / \eta_{dis} \times \eta_{trans}, if\left(\left|E_{net}^{j-1'}(t)\right| \le pw^{j}\right) \end{cases} \tag{6-37}$$

6.4.2 Energy losses

Due to the differences in distance from the BESS to the building in the three scenarios, the extensive energy loss during energy sharing process is bound to have an impact on the performance evaluation. Also, in the scenario SDB, different number and location of cells can produce differentiated results for the optimal operation of the BESS. Therefore, it is essential to discuss the energy losses. The total energy loss occurs during battery charging and discharging process, PV surplus sharing, and battery sharing process, which can be described as:

$$Loss_{tot} = Loss_{cha/dis} + Loss_{sur} + Loss_{pvs} + Loss_{bats} \tag{6-38}$$

where $Loss_{cha/dis}$ is the energy loss in the battery charging and discharging process, $Loss_{sur}$ is the energy loss in the surplus sharing process, $Loss_{pvs}$ is the energy loss in the surplus PV storage sharing process .and $Loss_{bats}$ is the energy loss in the remaining battery sharing process. The transmission losses (including remaining battery energy sharing and surplus PV storage sharing) of battery sharing within the community (within 1km) in this paper was assumed 8% and for the distributed surplus PV storage (inside) we assumed 0% because all energy exchange processes are occurred inside one building.

$$Loss_{cha/dis} = \sum E_{dis}(t) \times \left(\frac{1-\eta_{cha}}{\eta_{cha}}\right) \times \left(\frac{1-\eta_{dis}}{\eta_{dis}}\right) \tag{6-39}$$

$$Loss_{sur} = \sum E_{sur}(t) \times \eta_{trans} \tag{6-40}$$

$$Loss_{pvs} = \begin{cases} 0, if\,(IDB) \\ \sum E_{cha}(t) \times \eta_{trans}, i(SCB) \\ \sum (E^{j}_{cha}(t) - E^{j,j}_{cha}(t)) \times \eta_{trans}, i(SDB) \end{cases} \quad (6\text{-}41)$$

$$Loss_{bats} = \begin{cases} 0, if\,(IDB) \\ \sum E_{dis}(t) \times \eta_{trans}, i(SCB) \\ \sum (E^{j}_{dis}(t) - E^{j,j}_{dis}(t)) \times \eta_{trans}, i(SDB) \end{cases} \quad (6\text{-}42)$$

6.4.3 Objective functions

The optimal sizing and energy sharing problem can be formulated into a non-linear programming multi-objective model, with fist objective equation (43), maximizing the profitability of the BESS project and the second equation (44), maximizing the community's self-consumption of local PV generation, and the third equation (38), minimizing the total energy losses under the minimum BESS capacity.

$$NPV_{BESS} = \sum_{n=1}^{y} \frac{\sum (E_{dis}(t) - pr(t)) - (\sum E_{dis}(t) - \sum E_{cha}(t) -) \times pr_{va}}{(1+a)^{n}} - \sum cap^{j} \times c_{inv} \quad (6\text{-}43)$$

In the above, $\mathrm{Pr(t)}$ is the electricity price at time t. $\mathrm{Pr_{va}}$ the nighttime electricity price. And α is the discount rate. $\mathrm{C_{inv}}$ is the initial capital cost, which includes all inverters, power management and installation costs.

$$SCR = \frac{\sum \sum E^{j}_{du}(t) + \sum E_{sur}(t) + \sum E_{cha}(t)}{\sum \sum E^{j}_{pv}(t)} \quad (6\text{-}44)$$

where SCR is self-consumption rate, E_{du} is the directly used PV generation power(kWh).

6.4.4 Optimization

The optimization algorithm in this paper is a genetic algorithm (GA). It's a computational model to simulate the natural selection and genetic mechanism of Darwin's biological evolution theory [47]. GA shows its efficiency in dealing with BESS capacity optimization in many studies. M.K.Metwaly [48]. presented a multi-objective framework that optimizes the uprating of the line's real-time thermal rating and capacity of battery storage focused on WIND curtailment, network ageing and reliability. M.K.Metwaly [49] proposed a probabilistic evaluation method to evaluate various combinations of BESS power ratings and energy capacities based on the reliability of transmission networks. In this study, we focused on the possibility of battery share to reduce the total energy losses and increase the profitability of the BESS project and the community's self-consumption of local PV generation. The step-by-step methodology of GA is presented in Fig.4.

Table 2 summarizes input parameters used in the study, the unit price of battery was set to 24,300 Yen/kWh including the cost of installation and conversion. The subsidy to BESS from government was set to 33%. The maximum charging/discharging rate of each battery was assumed to be 16% of its capacity. The maximum depth of discharge was set to 90%. The FIT was assumed to be 0 Yen/kWh to encourage energy self-consumption. And the required PV power self-consumption rate wase adopt to 100%. The fixed incentive and activation reward of

DR are adopt to 4856 Yen/(kW· year) and 20.2 Yen/kWh according to the average winning price collected by the Ministry of Economy, Trade, and Industry in Japan [50]. Considering the small physical distance difference between different buildings in a community. To simplify the calculation, this study employs the same transmission efficiency for energy sharing between buildings.

Table 6-2. Input simulation parameters [44], [50], [51], [52]

Category	Parameters	Value	Unit
Economic Parameters	Battery investment cost (Including conversion & installation cost)	24,300	*Yen/kWh*
	Government Subsidy Ratio	33	*%*
	Discount rate	4.5	*%*
	FIT	0	*Yen/kWh*
	Fixed incentive	4856	*Yen/(kW·year)*
	Activation reward	20.2	*Yen/kWh*
Technical Parameters	NAS storage life cycle	15	*Year*
	Maximum depth of discharge	90	*%*
	Maximum charging/discharging rates	16	*%*
	Battery charge/discharge efficiency	92	*%*
	Power transmission loss rate	8	*%*
	Required PV power self-consumption rate	100	*%*

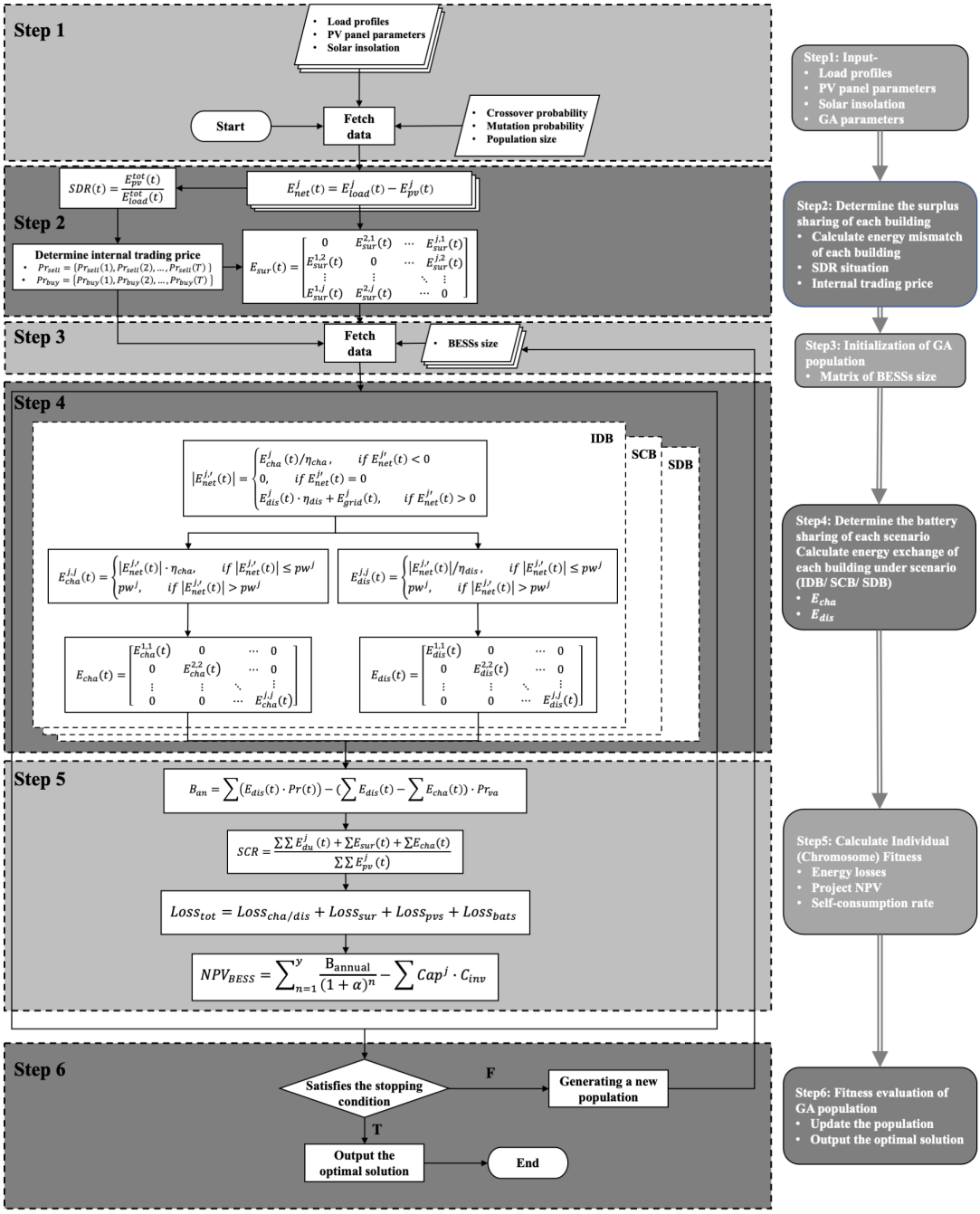
Step 1
Load profiles
PV panel parameters
Solar insolation
Start
Fetch data
Crossover probability
Mutation probability
Population size
Step 2
$SDR(t) = \frac{E_{pv}^{tot}(t)}{E_{load}^{tot}(t)}$
$E_{net}^{j}(t) = E_{load}^{j}(t) - E_{pv}^{j}(t)$
Determine internal trading price
$Pr_{sell} = \{Pr_{sell}(1), Pr_{sell}(2), \ldots, Pr_{sell}(T)\}$
$Pr_{buy} = \{Pr_{buy}(1), Pr_{buy}(2), \ldots, Pr_{buy}(T)\}$
$E_{sur}(t) = \begin{bmatrix} 0 & E_{sur}^{2,1}(t) & \cdots & E_{sur}^{j,1}(t) \\ E_{sur}^{1,2}(t) & 0 & \cdots & E_{sur}^{j,2}(t) \\ \vdots & \vdots & \ddots & \vdots \\ E_{sur}^{1,j}(t) & E_{sur}^{2,j}(t) & \cdots & 0 \end{bmatrix}$
Step 3
Fetch data
BESSs size
Step 4
IDB
SCB
SDB
$|E_{net}^{j,\prime}(t)| = \begin{cases} E_{cha}^{j}(t)/\eta_{cha}, & if\ E_{net}^{j\prime}(t) < 0 \\ 0, & if\ E_{net}^{j\prime}(t) = 0 \\ E_{dis}^{j}(t) \cdot \eta_{dis} + E_{grid}^{j}(t), & if\ E_{net}^{j\prime}(t) > 0 \end{cases}$
$E_{cha}^{j,j}(t) = \begin{cases} |E_{net}^{j,\prime}(t)| \cdot \eta_{cha}, & if\ |E_{net}^{j,\prime}(t)| \le pw^{j} \\ pw^{j}, & if\ |E_{net}^{j,\prime}(t)| > pw^{j} \end{cases}$
$E_{dis}^{j,j}(t) = \begin{cases} |E_{net}^{j,\prime}(t)|/\eta_{dis}, & if\ |E_{net}^{j,\prime}(t)| \le pw^{j} \\ pw^{j}, & if\ |E_{net}^{j,\prime}(t)| > pw^{j} \end{cases}$
$E_{cha}(t) = \begin{bmatrix} E_{cha}^{1,1}(t) & 0 & \cdots & 0 \\ 0 & E_{cha}^{2,2}(t) & \cdots & 0 \\ \vdots & \vdots & \ddots & \vdots \\ 0 & 0 & \cdots & E_{cha}^{j,j}(t) \end{bmatrix}$
$E_{dis}(t) = \begin{bmatrix} E_{dis}^{1,1}(t) & 0 & \cdots & 0 \\ 0 & E_{dis}^{2,2}(t) & \cdots & 0 \\ \vdots & \vdots & \ddots & \vdots \\ 0 & 0 & \cdots & E_{dis}^{j,j}(t) \end{bmatrix}$
Step 5
$B_{an} = \sum(E_{dis}(t) \cdot Pr(t)) - (\sum E_{dis}(t) - \sum E_{cha}(t)) \cdot Pr_{va}$
$SCR = \frac{\sum\sum E_{au}^{j}(t) + \sum E_{sur}(t) + \sum E_{cha}(t)}{\sum\sum E_{pv}^{j}(t)}$
$Loss_{tot} = Loss_{cha/dis} + Loss_{sur} + Loss_{pvs} + Loss_{bats}$
$NPV_{BESS} = \sum_{n=1}^{y} \frac{B_{annual}}{(1+\alpha)^{n}} - \sum Cap^{j} \cdot C_{inv}$
Step 6
Satisfies the stopping condition
F
Generating a new population
T
Output the optimal solution
End
Step1: Input-
Load profiles
PV panel parameters
Solar insolation
GA parameters
Step2: Determine the surplus sharing of each building
Calculate energy mismatch of each building
SDR situation
Internal trading price
Step3: Initialization of GA population
Matrix of BESSs size
Step4: Determine the battery sharing of each scenario Calculate energy exchange of each building under scenario (IDB/ SCB/ SDB)
E_{cha}
E_{dis}
Step5: Calculate Individual (Chromosome) Fitness
Energy losses
Project NPV
Self-consumption rate
Step6: Fitness evaluation of GA population
Update the population
Output the optimal solution

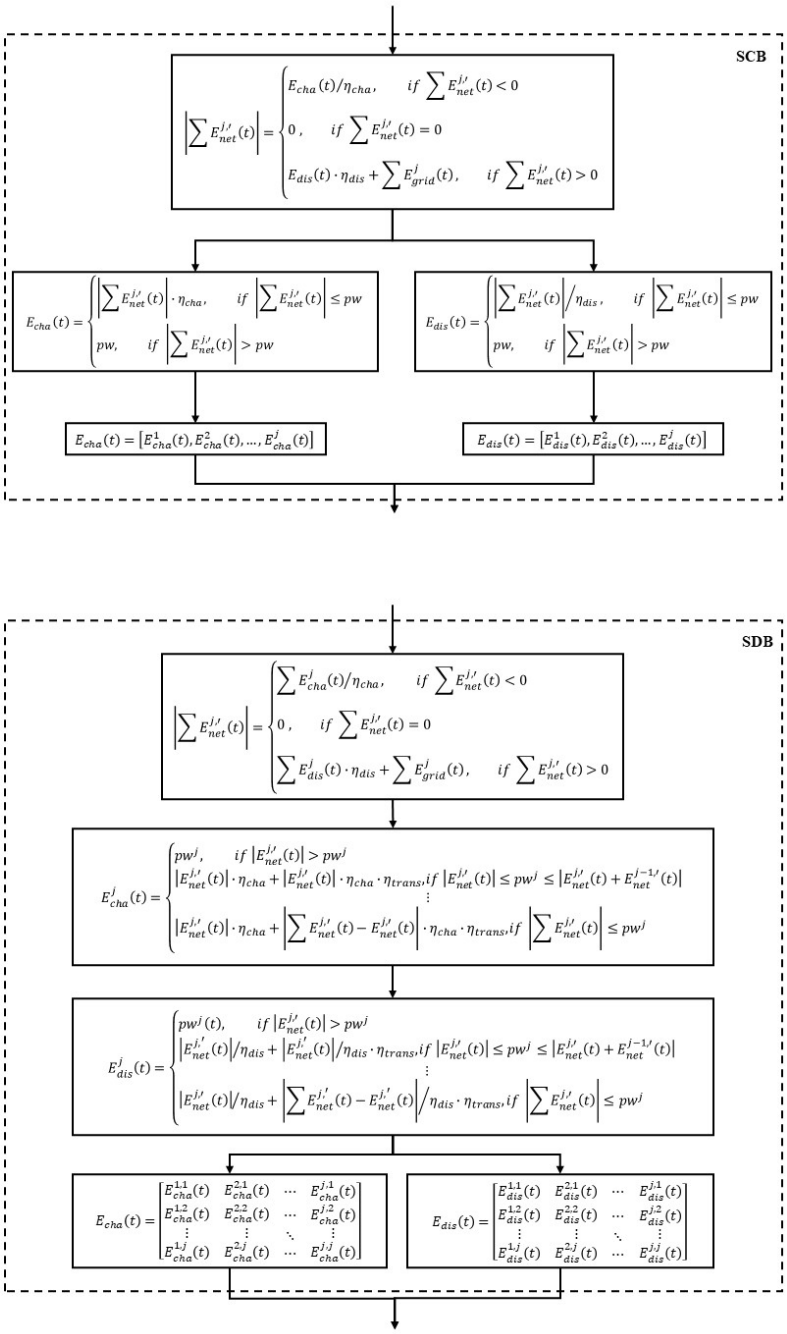

Fig. 6-4. The operation flow of genetic algorithm

6.5 Case study

6.5.1 Situation analysis

① Building electricity and PV generation

Fig. 5 displays the annual electricity consumption and the PV generation power of the selected buildings. The annual electricity consumption is in the range of 4,438,000~5,545,000 kWh. The installed PV capacity have shown in Table 3.

Table 6-3. The schedule and the installed PV capacity of each building

	Schedule (opening hours)	PV installation area (m^2)	PV capacity (kW)
Building 1	8:00-19:00 (Mon ~Sat.)	3488	692
Building 2	9:00-18:00 (Mon ~Sun.)	6048	1200
Building 3	10:00-21:00 (Mon ~Sun.)	4417	817
Building 4	00:00-24:00 (Mon ~Sun.)	1411	280
Building 5	00:00-24:00 (Mon ~Sun.)	1397	277
Building 6	9:00-20:00 (Mon ~Sun.)	7408	1470

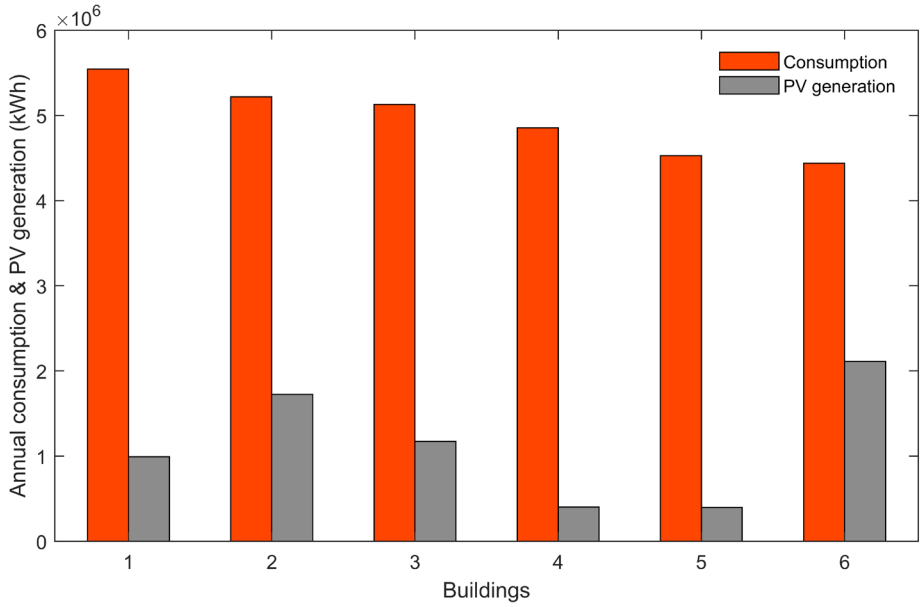

Fig. 6-5. Annual electricity consumption and supply of the buildings in the commercial community

② Load and PV profiles

Each selected building has different activities and different physical characteristics in terms of size, design, and age, resulting in different demand profiles. Fig. 6 shows the load profiles of the six buildings. Building 1 and Building 2 are exhibition buildings. Note that building 1 is only open from Monday to Saturday (This is called regular holiday and is a common business model in Japan.), therefore, the characteristics of load profiles is different between workdays and Sunday. Building 3 and building 6 are large shopping mall. Building 4 is a railroad service center. Building 5 is a gas station. Both buildings 4 and 5 are 24-hour operation. Usually, consumers are more active in building 5 from 18:00 to 23:00, so the electricity demand is significantly higher at this time.

Fig. 7 shows the PV power generation of six buildings on an average sunny day.

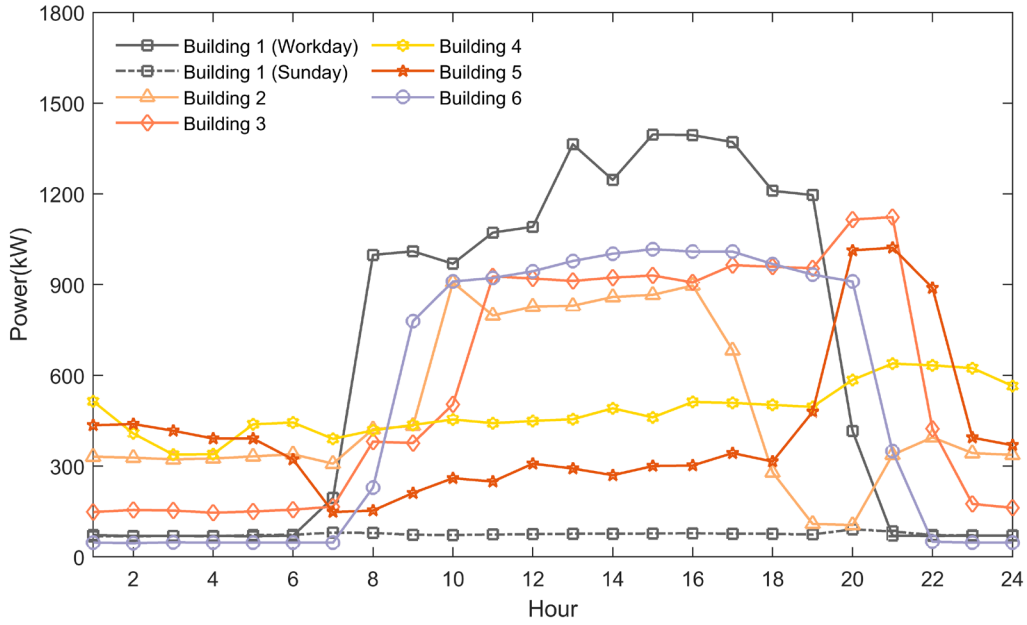

Fig. 6-6. Representative daily load demand profiles of six buildings

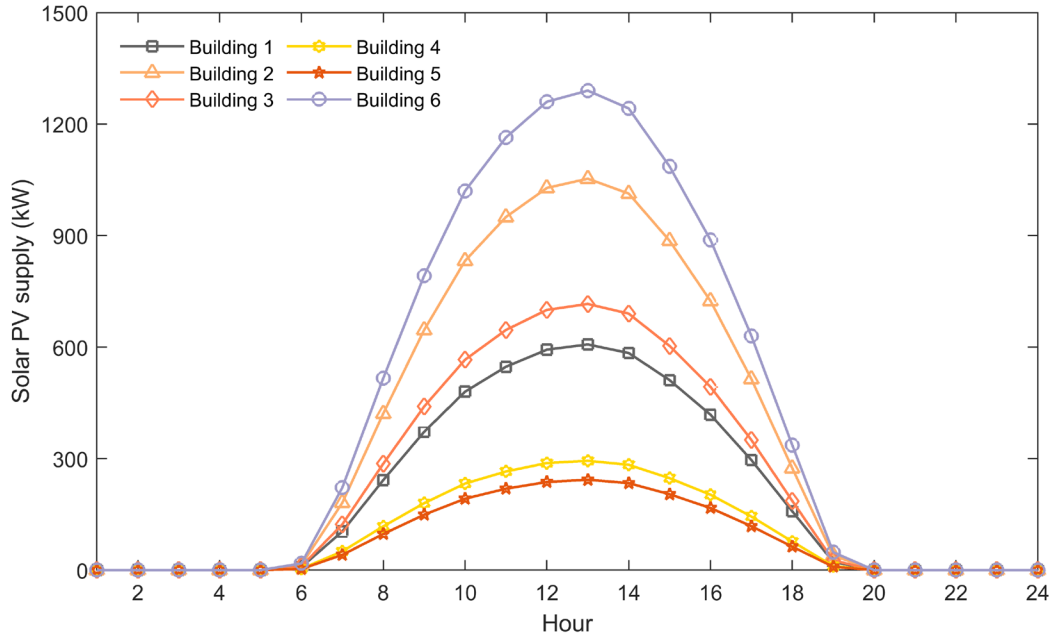

Fig. 6-7. PV generation of six Buildings

6.5.2 Energy sharing participation willingness evaluation

For the consumers, as the internal buying price in the energy sharing community will be never higher than the price of electricity bought from the grid, the energy bill of consumers will be always lower when participating in energy sharing than under the P2G energy trading.

However, in commercial buildings, building has the ability to consume all of the surplus PV power through the individual battery system. When the internal price is low, the producer's sale of surplus PV brings lower profit than investing in the battery, and in this condition, the

producers in the community tend to invest in the individual battery rather than surplus sharing. Therefore, the threshold value of the compensation factor needs to be considered to increase the willingness of energy sharing participants. In ref [16], the compensation factor was discussed in the form of a fixed price. But in this case, the energy exchange requirements occur across different price zoom and most of them occur in standard and peak daytime (Fig.8). If we adopt the fixed compensation factor, the low compensation factor will undermine the producers' income in standard and peak daytime. (According to Eq. (13), the fixed compensation factor means the $\beta(t)$ is always less than 9.06 yen in this case.) Therefore, we adopt the hourly compensation factor to improve economic benefits in standard and peak daytime, which can be defined as:

$$\beta(t) = \kappa \cdot \left(\lambda_{buy}(t) - \lambda_{sell}(t)\right),\ \kappa \in (0,1). \tag{45}$$

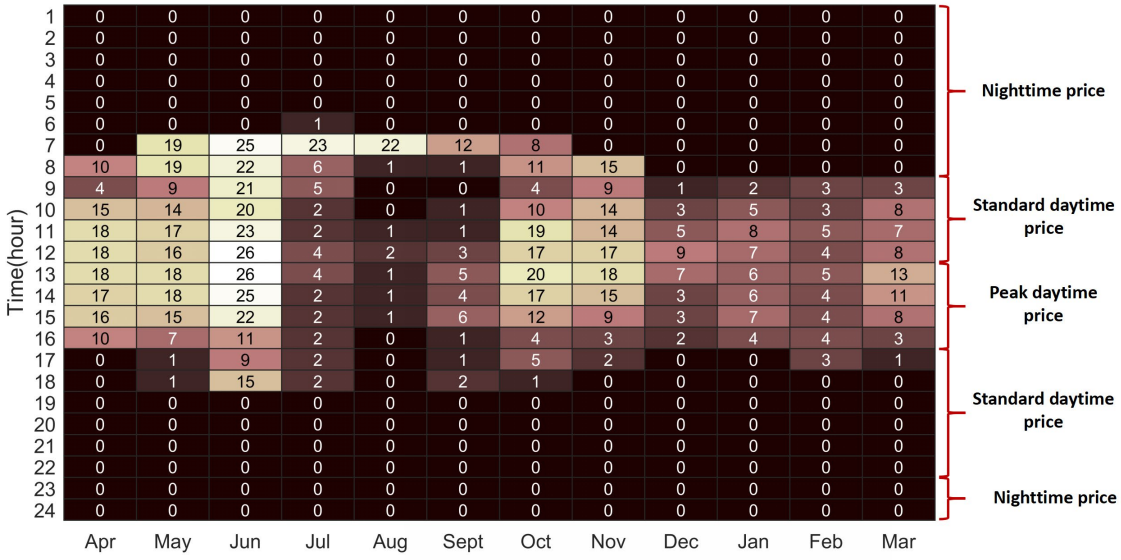

Fig. 6-8. The energy mismatch situation of the whole community (Note: the number represents the frequency of the energy exchange requirements)

Table.4 shows three scenarios of representative compensation prices.Fig.9 illustrates the internal buying and selling prices under the scenarios. Fig.10 shows the net income for communities investing in individual BESS and centralized BESS with different compensation factors, and it can be obtained that an increase in the compensation factor increases the net income of the PV-BESS system within the community. Thus, the compensation factor is an economic incentive for the buildings to participate in surplus sharing. Lower compensation factors (scenario a) can stimulate surplus sharing among individual BESS buildings, while only scenario c can stimulate surplus sharing in communities with centralized BESS installed, because investing in individual BESS leads to much lower income than the centralized BESS before surplus sharing.

Table 6-4. Scenarios of hourly compensation factors

Scenarios	Nighttime	Standard daytime	Peak daytime	Standard daytime(summer)
a	2.718	4.059	5.085	4.452
b	4.53	6.765	8.475	7.42
c	7.248	10.824	13.56	11.872

To incentivize buildings to participate in energy sharing, we choose the scenarios c (i.e., a compensation factor equals to 13.56 at peak daytime; 10.824 at standard daytime; 11.872 at summer standard daytime; 7.248 at nighttime) for the techno-economic analysis of the three BESS sharing scenarios.

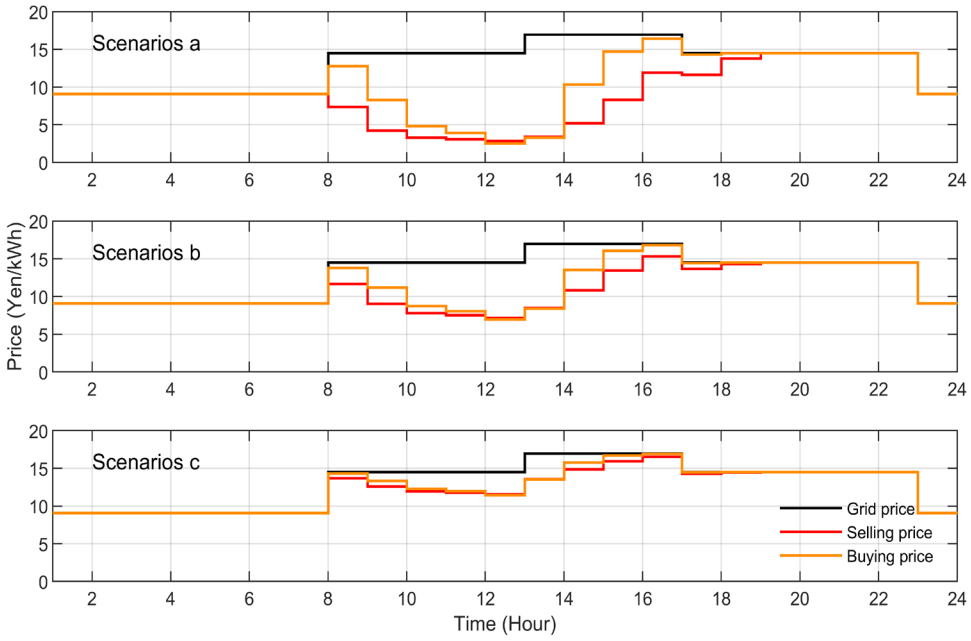

Fig. 6-9. Internal price under different compensation factor

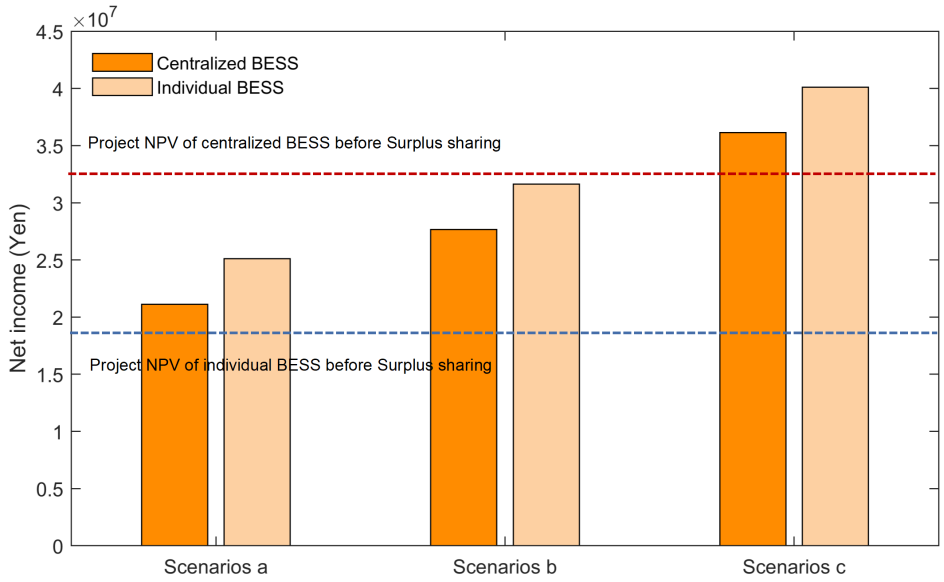

Fig. 6-10. Net income of Individual and centralized BESS under different compensation factor

6.5.3 The results of optimized BESS configuration

The model is optimized with maximizing the self-consumption rate and minimizing the energy losses under lowest BESS capacity. The results of optimization is presented in Table 5. Shared BESS structure (SCB/SDB) have same battery capacity and are 38.8% less than Scenario IDB. In scenario baseline, energy loss due to system operation is zero, but 226,658 kWh surplus PV is lost due to the lack of appropriate system. Compared with the baseline (Without BESS), the self-consumption rate of IDB, SCB, SDB is increased by 19.83%, 16.77% and 19.63%. It is noted that the self-consumption rate in Scenario IDB is more improved than Scenario SDB because some of the PV generation in Scenario SDB is lost in the sharing process, which will be discussed in detail in the section 4.4. Conventionally, BESSs are by default placed on buildings(building 1, 2, 6 in IDB) where solar energy is largely curtailed, so that surplus solar power can be stored immediately without undergoing delivery over transmission lines. But in the optimization results is the exact opposite. It is because scenario SDB maximize their cooperation among BESSs by pooling all their capacities to store surplus solar power, will be discussed in detail in the section 4.5.

Table 6-5. The optimization results under different scenarios

		Scenario 1: Individual design for distributed BESS	Scenario 2: Shared design for centralized BESS	Scenario 3: Shared design for distributed BESS	Scenario 4: Baseline (W/O ESS)
Battery capacity (kWh)	**Building 1**	2266	-	122	-
	Building 2	2066	-	521	-
	Building 3	920	-	1702	-
	Building 4	0	-	1482	-
	Building 5	88	-	88	-
	Building 6	2460	-	858	-

Aggregator	-	4773	-	-
Community	7800	4773	4773	-
Self-consumption (%)	98.96	96.44	98.8	82.59
Energy losses (kWh)	220,698	261,038	131,743	0 (226,658 surplus PV loss)

6.5.4 Losses comparison at community-levels

Fig.11 compares the energy losses in the three scenarios. In scenario IDB, the energy losses occurs mainly during the surplus sharing and the charging and discharging process of the BESS. In scenarios SCB and SDB, energy losses also occurs in the transfer of surplus PV storage sharing and battery sharing process. Since the battery capacity of scenario IDB is much larger than that of scenario SCB and SDB, the losses generated by battery storage power are also much larger (92.9% of the total). In scenario IDB, the operation of the BESS occurs inside the building, thus the transmission loss of using the battery is zero. In the scenario SCB, all energy exchange of battery occurs outside the buildings, so it leads to the largest proportion of battery sharing losses (48.8% of the total). In addition, scenario SCB keeps relatively large proportion of battery storage loss (44.2% of the total). Therefore, the total losses in the scenario SCB are the largest. Loss due to battery sharing is much lower in scenario SDB than in scenario SCB. This is because the buildings can operate their own BESS as part of the power storage and access the surplus PV through the BESS of other buildings in the community, thereby reducing the long-distance transmission of power. Finally, the total losses in the scenario SDB are the smallest.

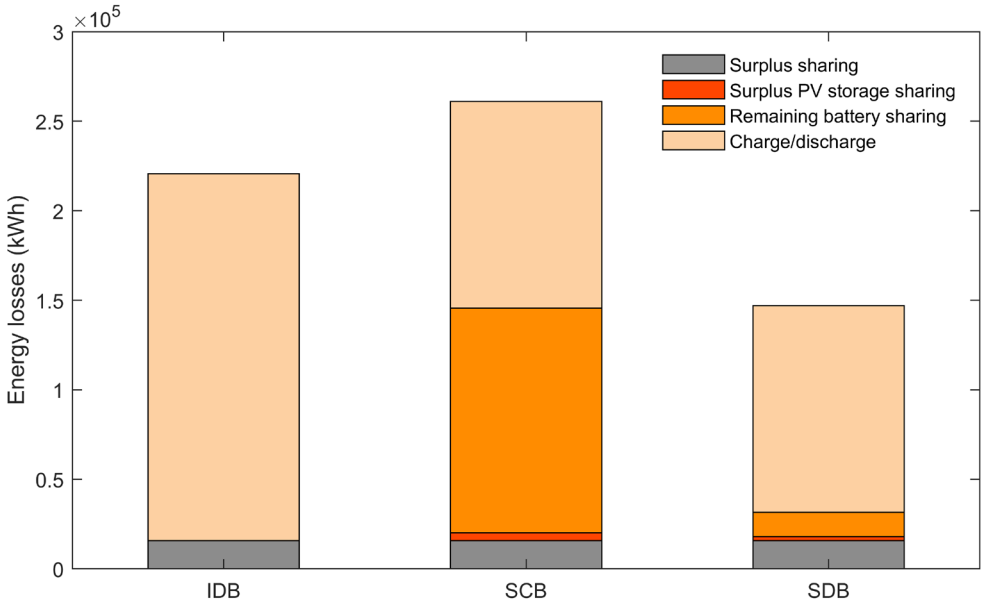

Fig. 6-11. Energy loss of whole building community of different scenarios

6.5.5 Transmission loss optimization during battery sharing process

The shared BESSs considers the energy mismatch situation for all buildings in the community, and the number as well as the position of the installation have an impact on the transmission loss.

Fig.12 shows the effect of different number of BESSs on transmission losses inside a building. (We consider the centralized BESS as 0 batteries inside the buildings). It is concluded that the increase in the number of batteries reduces the energy loss of battery sharing process. The reason is buildings can first use their own batteries for basic storage requirements, thereby reducing unnecessary energy exchange between different buildings. Compared to scenario SCB (0 batteries inside the buildings), an optimized distributed energy sharing community reduce transmission losses by up to 98%.

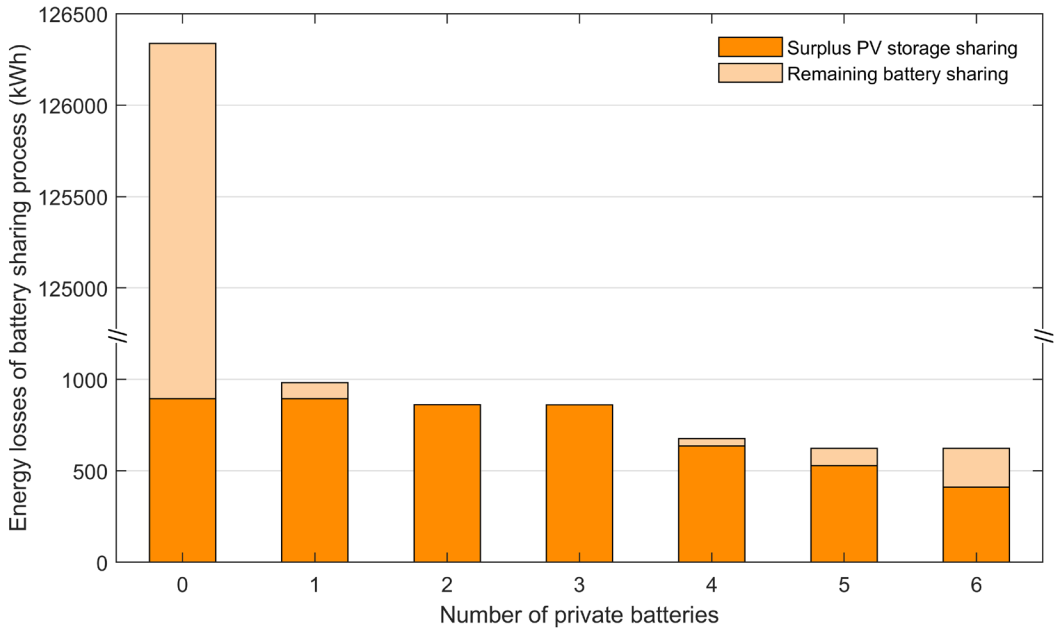

Fig. 6-12. Energy loss of battery sharing process

Fig.13 estimates the surplus PV generation status of each building in the community. The buildings are divided into two categories, producers (building 1, 2 and 6) and consumers (building 3, 4 and 5), based on the total amount of PV remaining power after surplus sharing.

The position of the battery demonstrates different technical characteristics depending on the building which it belongs. Fig.14 presents the energy loss of battery sharing process for the two position properties (producer priority and consumer priority, respectively). Conventionally, BESSs are by default placed on buildings (producer priority) where solar energy is largely curtailed, so that surplus solar power can be stored immediately without undergoing delivery over transmission lines. But Fig.13(a) shows deploying BESS in the producers (building 1, 2 and 6) have significant high remaining battery sharing losses and low surplus PV storage sharing losses. The reason is that the large amount of surplus PV generation is charged in the buildings' own battery without transmission losses. But the battery is remained large capacity which should be discharged to the other buildings with high transmission losses. Deploying BESS in the consumers (building 3, 4 and 5) have low energy losses, because the consumer

buildings have insufficient power which allows the discharging of local BESS, despite some surplus PV storage sharing losses. Because the remaining battery sharing is significantly higher than surplus PV sharing.(0 batteries in Fig.11). Therefore, prioritizing the deployment of batteries in consumer buildings is more applicable than in producer buildings.

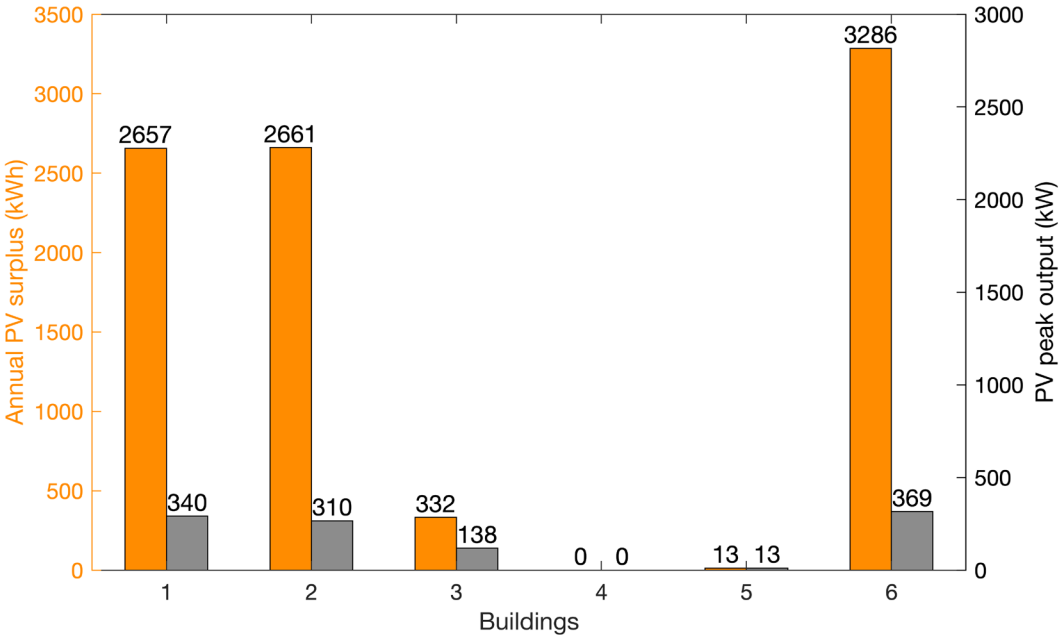

Fig. 6-13. Annual PV surplus and PV peak output of each building after PV surplus sharing

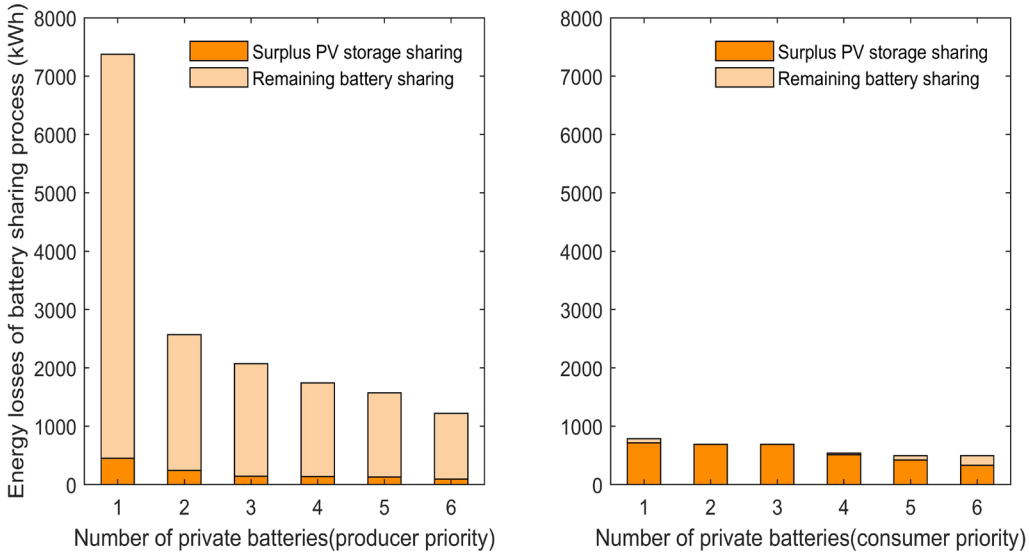

Fig. 6-14. Energy loss of battery sharing process under two positional attributes (a) producer priority; (b) consumer priority.

6.5.6 Performance comparison of single building

This section presents the battery operation and energy exchange in a typical week, with an example of a producer building and a consumer building, respectively. Fig.15 represents the producer (building 6). Fig.16 represents the consumer (building 3). Where a positive value of energy flow indicates power demand, and a negative value indicates power surplus.

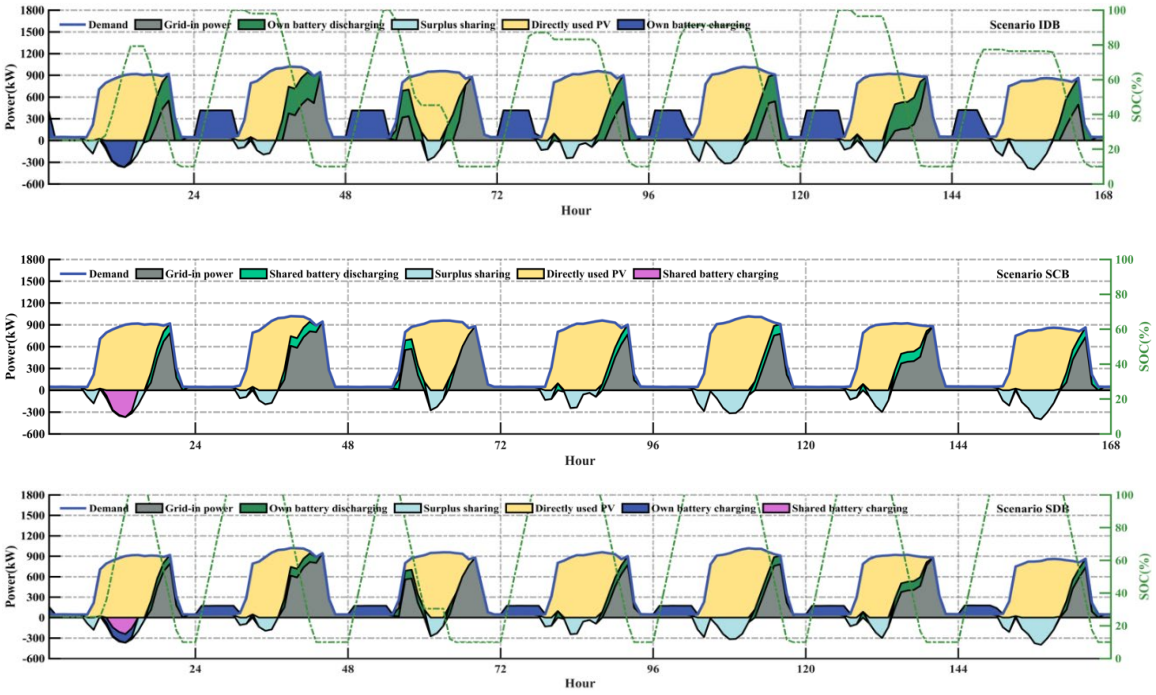

Fig. 6-15. The battery operation and energy exchange of building 6 in a typical week

For producer:

In the scenario IDB, the surplus PV can first be shared with other buildings in the community through surplus sharing (the light blue section). BESS can store surplus PV (negative section in blue) or charge from the grid at night (positive section in blue), but for producers, the large amount of PV generation reduces the building's demand for electricity in battery discharging period (gray and green sections). This results in the building loads being concentrated in a very short period of time (between 18:00 and 22:00).Due to the limitation of rated power capacity, the independent battery cannot be completely discharged in four hours even if it works as the maximum power (NAS batteries require at least six hours to a fully discharging). Therefore, a full charge/discharge cycle cannot be completed on most days of the week, such as the first, fourth, fifth, seventh days. The SOC of those days only reach 80-90%. The reason is that due to the limitation of rated power capacity, the over-concentrated demand in a short time cannot allow the fully discharging of the battery.

In the scenario SCB, the surplus PV is stored in a centralized BESS (purple section). The centralized BESS is deployed outside the building, so it does not draw power from that building. Since the BESS is centrally controlled by the aggregator, the discharge of the battery can be based on community-wide considerations. In contrast to the scenario IDB, the building use the centralized battery to store surplus PV without considering remaining battery capacity.

In scenario SDB, the surplus PV is first stored in its own battery until the battery is fully charged (negative section in blue), and then the surplus PV is stored in other buildings through storage sharing (purple section). Due to the smaller size of the BESS than in the scenario IDB, the BESS complete a full DOD on all days of the week.

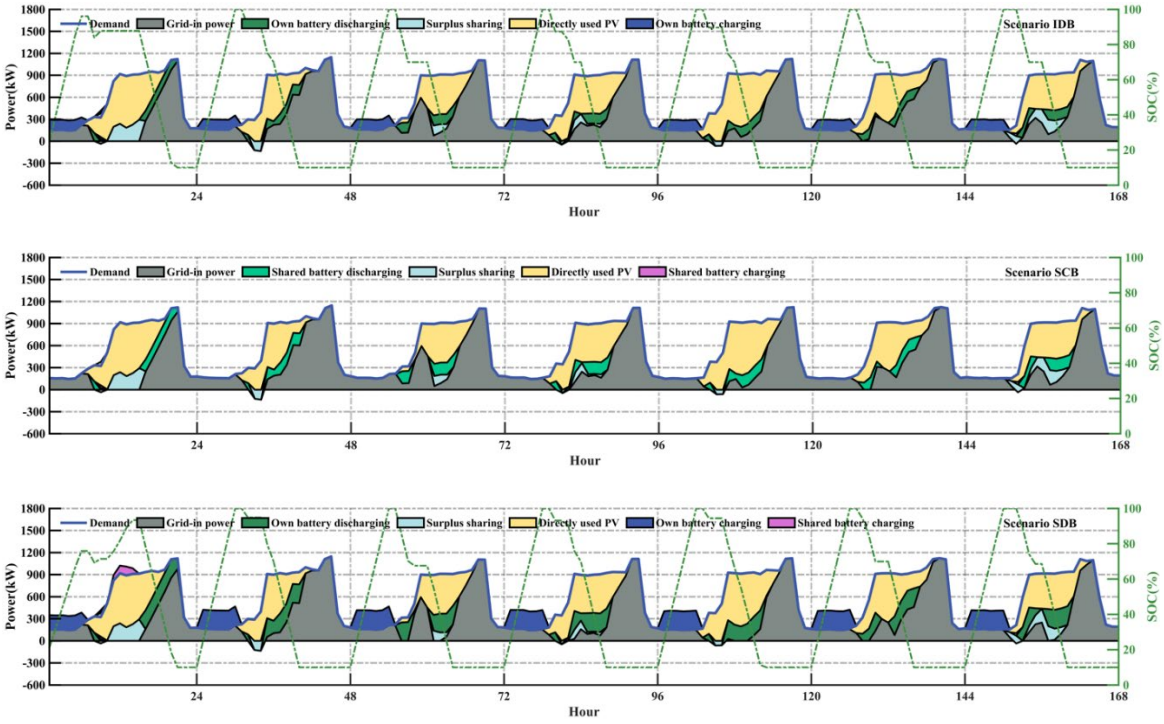

Fig. 6-16. The battery operation and energy exchange of building 3 in a typical week

For consumer:

In scenario IDB, the building draw the surplus PV from other buildings to meet the demand (light blue section). Second, the building does not have a large amount of surplus PV and is designed with a low BESS capacity. Since the building maintains a high-power demand even after using direct PV and surplus PV, the BESS complete a full DOD for most days of the week.

In scenario SCB, a small amount of the building's surplus PV is stored in a centralized BESS (purple section).

In scenario SDB, the BESS stores a small amount of surplus PV in the building, while it can store surplus PV in other buildings (purple section). Due to the high consumption of the building, the BESS complete a full DOD on most days of the week even if the capacity of the BESS is increased.

In scenario IDB, the utilization of the producer's battery is low because there is no battery sharing. In scenario SCB, the utilization of the batteries is high, but all storage processes occur outside the building and the power loss is high. In scenario SDB, both producer's and consumer's batteries in the community maintain high utilization and only a small amount of energy is exchanged between the two parties.

6.5.7 DR performance evaluation (Scenario SCB&SDB)

According to the Ministry of Economy, Trade, and Industry in Japan, the peaking load is around 1% of total (equals 88 hours in a year). But demand response in Japan remains in the proof stage, only 0.3% of time is field-proven (equals 30 hours in a year) [46]. Thus, we take the Kyushu electricity demand (2013-2014) as a study object, setting 0.5% of the annual peak demand as a catastrophic event to test the community's performance in responding to demand response. The cumulative activation time can reach 50 hours a year, with a total shifted power of 35,800 kWh. Fig.17 illustrates the actual responding power in each month of the year. It is

observed that the BESS participation in the grid DR occurs mainly in August with a total shifted power of 28,640 kWh (80% of the total). In addition, a small number of time periods are activated in September/ January/ March. Fig.18 illustrates a typical energy flow of the BESSs involved in DR on 30th Aug. DR event typically occurs between 13:00 and 18:00. Thus, it can be appreciated that the BESSs perform an effective peak shift when a DR event occurs.

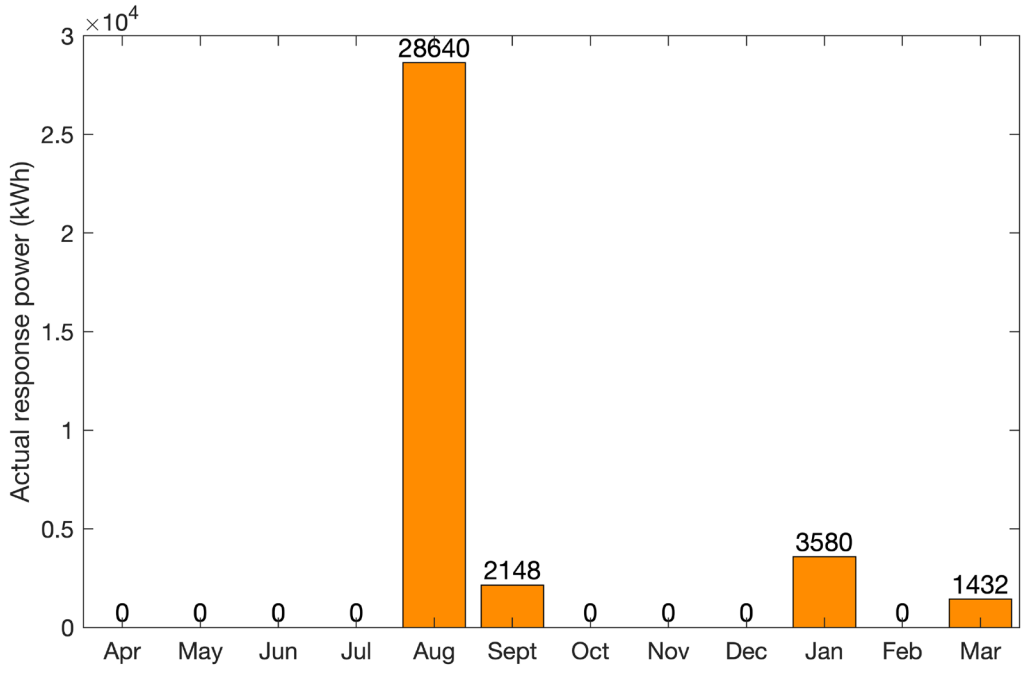

Fig. 6-17. Actual response power of whole community

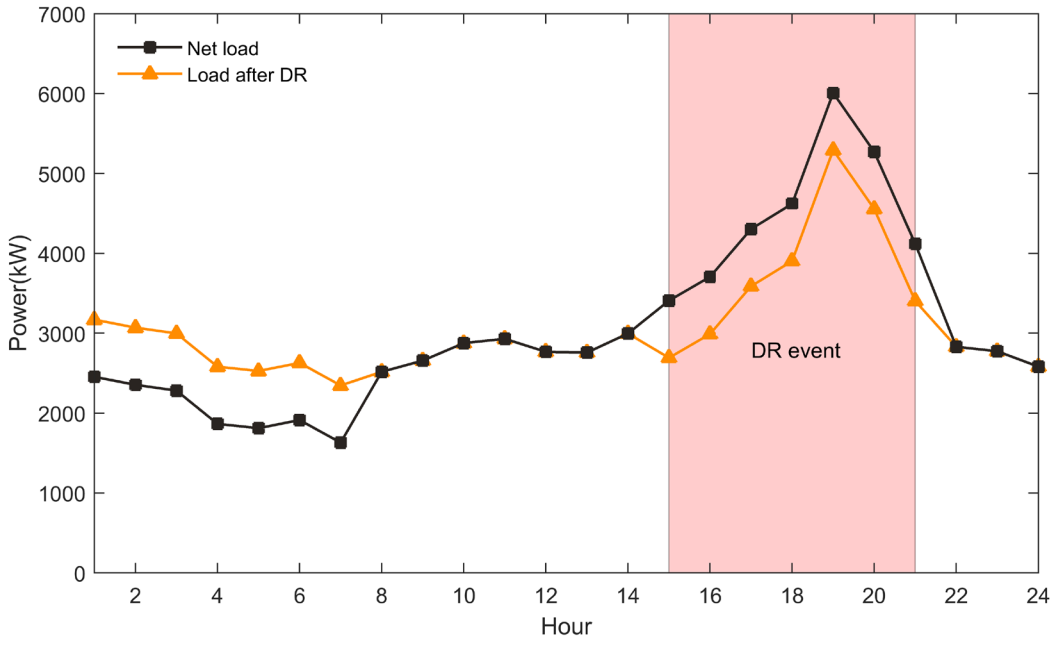

Fig. 6-18. Power change of whole community with shiftable DR (30th. Aug.)

6.5.8 Economic performance comparison

Table 6 displays the aggregated BESS size, investment cost, and project NPV for the three scenarios, and Table 7 illustrates the BESS size of the building and the size savings relative to scenario IDB. The aggregated capacity of scenario IDB is 7800 kWh, and the aggregated capacity of both scenario SCB and scenario SDB is 4773 kWh. Scenario SCB and SDB approaches save 38.8% of capacity compared to scenario IDB, and the initial investment is significantly lower (i.e., 38.8% lower). Scenario IDB has the lowest NPV while with the highest energy self-sufficiency and self-consumption rates due to the lowest PV sharing loss, and Scenario SCB and SDB have significantly higher NPV than IDB NPV due to the BESS grid DR. It is interesting to note that without participation in the DR programme, the IDB scenario yields a higher NPV than the SCB. The reason is that for profitable projects with similar return rate on investment(ROI), the higher investment will achieve high NPV value. In this case, although the ROI of the scenario IDB is lower than SCB, but due to the significant higher investment, the final NPV is much higher.

In Scenario SCB, buildings can participate in energy sharing and reduce energy costs without investment. Scenario SDB increases the BESS size of consumers (building 3, 4) and decreases the BESS size of producers (building 1, 2 and 6) because the proportion of remaining battery sharing is higher than the surplus PV storage sharing. The BESS size of Building 5 has not changed because it does not have high power PV generation and with low power demand. However, it still can be considered as a resource to reduce energy costs, for example, by participating in DR.

Table 6-6. The economic performance of BESS under different scenarios

	Scenario 1: Individual design for distributed BESS	Scenario 2: Shared design for centralized BESS	Scenario 3: Shared design for distributed BESS	Scenario 4: Baseline (W/O ESS)
Battery capacity (kWh)	7800	4773	4773	-
Battery investment (Yen)	126,360,000	77,328,000	77,328,000	-
Project NPV (W/O DR benefit) (Yen)	12,994,031	9,023,265	14,214,883	
Return on Investment (W/O DR benefit) (%)	10.27	10.40	11.23	-
Project NPV (Yen)	12,994,031	54,129,959	59,321,576	-
Payback period (W/O DR benefit) (Year)	13.3	12.91	11.94	-
Payback period (Year)	13.3	7.66	6.42	-

Table 6-7. Comparison of the design results under different scenarios

	Scenario 1: Individual design for distributed BESS		Scenario 2: Shared design for centralized BESS			Scenario 3: Shared design for distributed BESS		
	Battery capacity (kWh)	Battery investment (Yen)	Battery capacity (kWh)	Battery investment (Yen)	Size Saving (%)	Battery capacity (kWh)	Battery investment (Yen)	Size Saving (%)
Building 1	2266	55,080,000	-	-	100	122	1,980,000	94.6
Building 2	2066	50,220,000	-	-	100	521	8,442,000	74.8
Building 3	920	22,356,000	-	-	100	1702	27,576,000	-85
Building 4	0	0	-	-	100	1482	24,012,000	-
Building 5	88	2,106,000	-	-	100	88	1,4040,00	0
Building 6	2460	59,778,000	-	-	100	858	13,896,000	65.1
Aggregator	-	-	4773	77,328,000	-	-	-	-
Community	7800	126,360,000	4773	77,328,000	38.8	4773	77,328,000	38.8

6.6 Sensitivity analysis of parameters

In this section we perform a scalable analysis of the shared design for distributed BESS. With reference to the results of the parameter setting and optimization process, a sensitivity analysis is performed on the following parameters: number of producers, number of demand responses, and battery cost.

We replaced the demand profiles of buildings 3, 4 and 5 with building 6 profiles, respectively, to investigate the effect of the number of producers on the shared design for distributed BESS. The results in Fig.19 show that that the battery size increases with the number of producers in the community, while the direct surplus sharing increases and then decreases with the number of producers. This is because an increase in a small amount of PV production can facilitate direct surplus PV sharing within a community, while as the number of consumers continues to decrease, PV generation has exceeded peak demand due to changes in load distribution, and buildings must rely on larger BESSs to meet PV self-consumption.

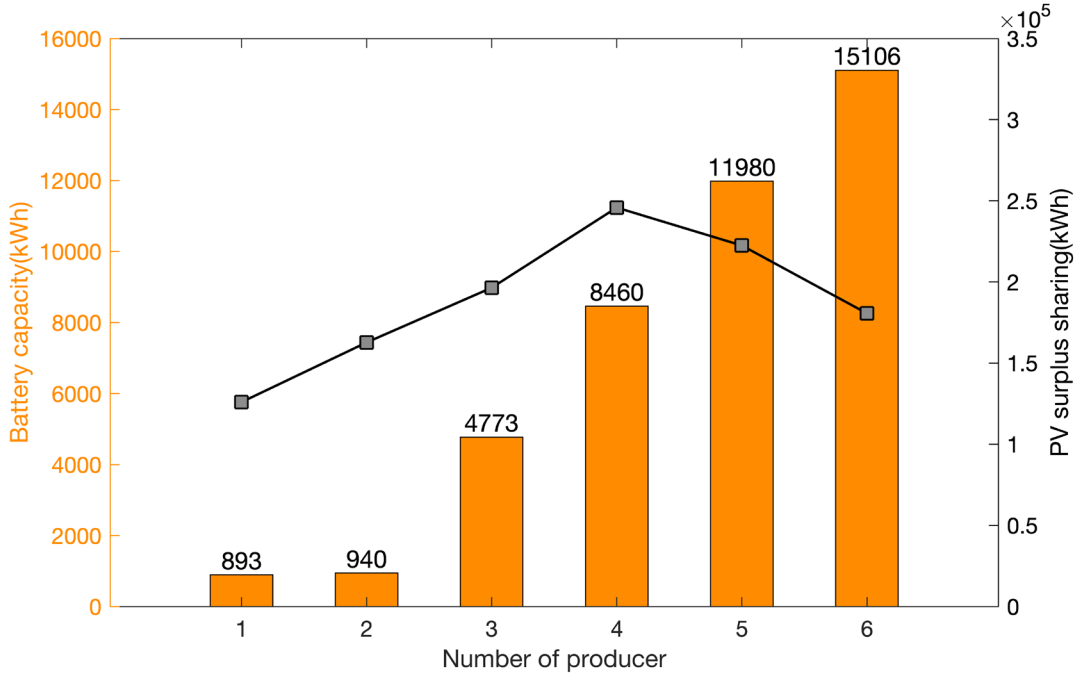

Fig. 6-19. BESS capacity and surplus sharing versus number of producers within a community

Table 8 shows the project NPV corresponding to different demand response hours and the expected decline in battery cost, and it can be noticed that as the time of responses increases, the project NPV increases due to the fact that the actual incentive received by the project increases. One of the benefits of demand response is that the buildings receive the base cost of contracting even if the number of responses required throughout the year is 0. In addition, as the battery price declines, the project NPV increases significantly and the PBP is shortened significantly.

Table 6-8. Sensitivity analysis of parameters

DR hour (hour)	**0**	**25**	**50**	**75**	**100**
Project NPV (Yen)	51,555,166	55,438,371	59,321,576	63,204,781	63,204,781
Payback period (year)	6.80	6.60	6.42	6.24	5.95
Battery price (Yen/kWh)	**24,000**	**21,000**	**18,000**	**15,000**	**12,000**
Project NPV (Yen)	51,555,166	76,505,576	85,097,576	93,689,576	102,281,576
Payback period (year)	6.42	5.50	4.61	3.76	2.94
Incentive price	16.16	18.18	20.2	22.22	24.24
(Yen/kWh) Project NPV	57,768,294	58,544,935	59,321,576	60,098,217	60,874,858
(Yen)					
Payback period (year)	6.49	6.45	6.42	6.38	6.35

6.7 Conclusions

The purpose of this study is to improve the feasibility of battery sharing by optimizing the techno-economic performance of battery sharing in an energy sharing community. For validation, two different BESS sharing structures, namely shared design for centralized BESS and the shared design for distributed BESS have been compared with the traditional user owned BESS (Individual design for distributed BESS). First, we optimize the BESS size under different battery sharing structures and then discuss the BESS installation position and quantity by a multi-objective genetic algorithm. In terms of economics, aggregation control of shared BESS and participation in grid demand response are used to improve the economic performance, and their effectiveness is verified by whole-life cost analysis. The performance of surplus sharing and storage sharing within the energy sharing community was investigated in the context of the Kyushu region of Japan.

The main conclusions of this study are summarized as follows:

(1). The economic analysis shows that the shared design approach leads to a significant reduction in battery capacity at the community level (i.e., a 38.8% reduction). The payback period of the investment is shortened by 44.6%. This suggests that the economic benefits of PV- BESS systems can be effectively increased through the deployment of battery sharing. In addition, as the high initial investment is still required currently, the active incentives of the DR play a critical role in the economic assessment (i.e., a 46.4% reduction in payback period). Therefore, a combination of battery-based applications with multiple technologies can be the key solution to successful BESS deployment.

(2). A loss-based technical analysis shows that compared to the shared design for centralized BESS, an optimized distributed battery sharing community reduces transmission losses by up to 98%. The reason is the increase in the number of batteries within a community can reduce unnecessary energy exchange between different buildings. The requirement of remaining battery sharing accounts for a larger proportion than surplus PV storage sharing, thereby prioritizing the deployment of batteries in buildings with much insufficient power is more applicable.

(3). As the development of electrification in the future and the pressure on the grid for peak shaving continues to increase, BESS will have greater application value as a flexible DR response tool.

(4). With the expected declines in equipment prices in the future, the PBP of the shared BESS will gradually be shortened. The battery sharing is expected to be more economical considering future trends, and it have more development prospects.

This paper focused on arbitrage opportunity under different sharing structures of BEESs. And the environmental factors, and network capacity limit are set as constants in this study. With the practical application of battery sharing and the evolvement of network capacity, it is a strong possibility to access the value of storage to consumers in providing non-economic benefits such as power system reliability. As a future work, the battery sharing model will be evaluated in a more comprehensive manner, taking into account various indicators such as grid reliability, economy and environmental aspects. Meanwhile, some researchers have proposed that combining the BESS system with the dynamic thermal rating system can improve the reliability of the system and enhance the integration of renewable energy [53, 54] . Accordingly,

coordination with different systems may also one of the key points to make good use of battery sharing system. The inclusion of those possibility will also be a part of future research.

References

[1] Gandhi O, Kumar DS, Rodríguez-Gallegos CD, Srinivasan D. Review of power system impacts at high PV penetration Part I: Factors limiting PV penetration. Solar Energy. 2020;210:181-201.
[2] Li Y, Gao W, Ruan Y. Performance investigation of grid-connected residential PV-battery system focusing on enhancing self-consumption and peak shaving in Kyushu, Japan. Renewable Energy. 2018;127:514-23.
[3] Sovacool BK, Furszyfer Del Rio D, Griffiths S. Contextualizing the Covid-19 pandemic for a carbon-constrained world: Insights for sustainability transitions, energy justice, and research methodology. Energy Research & Social Science. 2020;68.
[4] Shin KJ, Managi S. Liberalization of a retail electricity market: Consumer satisfaction and household switching behavior in Japan. Energy Policy. 2017;110:675-85.
[5] Nicolli F, Vona F. Energy market liberalization and renewable energy policies in OECD countries. Energy Policy. 2019;128:853-67.
[6] Vand B, Ruusu R, Hasan A, Manrique Delgado B. Optimal management of energy sharing in a community of buildings using a model predictive control. Energy Conversion and Management. 2021;239.
[7] Jiang A, Yuan H, Li D. A two-stage optimization approach on the decisions for prosumers and consumers within a community in the Peer-to-peer energy sharing trading. International Journal of Electrical Power & Energy Systems. 2021;125.
[8] Taşcıkaraoğlu A. Economic and operational benefits of energy storage sharing for a neighborhood of prosumers in a dynamic pricing environment. Sustainable Cities and Society. 2018;38:219-29.
[9] Tushar W, Chai B, Yuen C, Huang S, Smith DB, Poor HV, et al. Energy Storage Sharing in Smart Grid: A Modified Auction-Based Approach. IEEE Transactions on Smart Grid. 2016;7:1462-75.
[10] Bandara KY, Thakur S, Breslin J. Flocking-based decentralised double auction for P2P energy trading within neighbourhoods. International Journal of Electrical Power & Energy Systems. 2021;129.
[11] Mengelkamp E, Gärttner J, Rock K, Kessler S, Orsini L, Weinhardt C. Designing microgrid energy markets. Applied Energy. 2018;210:870-80.
[12] Khalid R, Javaid N, Almogren A, Javed MU, Javaid S, Zuair M. A Blockchain-Based Load Balancing in Decentralized Hybrid P2P Energy Trading Market in Smart Grid. IEEE Access. 2020;8:47047-62.
[13] Morstyn T, Teytelboym A, McCulloch MD. Bilateral Contract Networks for Peer-to-Peer Energy Trading. IEEE Transactions on Smart Grid. 2019;10:2026-35.
[14] Cintuglu MH, Martin H, Mohammed OA. Real-Time Implementation of Multiagent-Based Game Theory Reverse Auction Model for Microgrid Market Operation. IEEE Transactions on Smart Grid. 2015;6:1064-72.

[15] Cui S, Wang YW, Liu N. Distributed game-based pricing strategy for energy sharing in microgrid with PV prosumers. IET Renewable Power Generation. 2017;12:380-8.
[16] Long C, Wu J, Zhou Y, Jenkins N. Peer-to-peer energy sharing through a two-stage aggregated battery control in a community Microgrid. Applied Energy. 2018;226:261-76.
[17] Jia L, Tong L. Dynamic Pricing and Distributed Energy Management for Demand Response. IEEE Transactions on Smart Grid. 2016;7:1128-36.
[18] Olivella-Rosell P, Bullich-Massagué E, Aragüés-Peñalba M, Sumper A, Ottesen SØ, Vidal-Clos J-A, et al. Optimization problem for meeting distribution system operator requests in local flexibility markets with distributed energy resources. Applied Energy. 2018;210:881-95.
[19] Ottesen SØ, Tomasgard A, Fleten S-E. Prosumer bidding and scheduling in electricity markets. Energy. 2016;94:828-43.
[20] Motalleb M, Ghorbani R. Non-cooperative game-theoretic model of demand response aggregator competition for selling stored energy in storage devices. Applied Energy. 2017;202:581-96.
[21] Lüth A, Zepter JM, Crespo del Granado P, Egging R. Local electricity market designs for peer-to-peer trading: The role of battery flexibility. Applied Energy. 2018;229:1233-43.
[22] Nguyen S, Peng W, Sokolowski P, Alahakoon D, Yu X. Optimizing rooftop photovoltaic distributed generation with battery storage for peer-to-peer energy trading. Applied Energy. 2018;228:2567-80.
[23] Dong S, Kremers E, Brucoli M, Rothman R, Brown S. Techno-enviro-economic assessment of household and community energy T storage in the UK. Energy Conversion and Management. 2020.
[24] Parra D, Norman SA, Walker GS, Gillott M. Optimum community energy storage system for demand load shifting. Applied Energy. 2016;174:130-43.
[25] Rodrigues DL, Ye X, Xia X, Zhu B. Battery energy storage sizing optimisation for different ownership structures in a peer-to-peer energy sharing community. Applied Energy. 2020;262.
[26] Huang P, Sun Y, Lovati M, Zhang X. Solar-photovoltaic-power-sharing-based design optimization of distributed energy storage systems for performance improvements. Energy. 2021;222.
[27] Jimada-Ojuolape B, Teh J. Impact of the Integration of Information and Communication Technology on Power System Reliability: A Review. IEEE Access. 2020;8:24600-15.
[28] Jimada-Ojuolape B, Teh J. Surveys on the reliability impacts of power system cyber–physical layers. Sustainable Cities and Society. 2020;62.
[29] Kakran S, Chanana S. Smart operations of smart grids integrated with distributed generation: A review. Renewable and Sustainable Energy Reviews. 2018;81:524-35.
[30] Amoretti M. Towards a peer-to-peer hydrogen economy framework. International Journal of Hydrogen Energy. 2011;36:6376-86.
[31] Zame KK, Brehm CA, Nitica AT, Richard CL, Schweitzer Iii GD. Smart grid and energy storage: Policy recommendations. Renewable and Sustainable Energy Reviews. 2018;82:1646-54.
[32] Contreras-Ocana JE, Ortega-Vazquez MA, Zhang B. Participation of an Energy Storage Aggregator in Electricity Markets. IEEE Transactions on Smart Grid. 2019;10:1171-83.

[33] Mohamad F, Teh J, Lai C-M. Optimum allocation of battery energy storage systems for power grid enhanced with solar energy. Energy. 2021;223.
[34] Chen C, Wang J, Kishore S. A Distributed Direct Load Control Approach for Large-Scale Residential Demand Response. IEEE Transactions on Power Systems. 2014;29:2219-28.
[35] Wang Y, Gao W, Qian F, Li Y. Evaluation of economic benefits of virtual power plant between demand and plant sides based on cooperative game theory. Energy Conversion and Management. 2021;238.
[36] Qian F, Gao W, Yang Y, Yu D. Economic optimization and potential analysis of fuel cell vehicle-to-grid (FCV2G) system with large-scale buildings. Energy Conversion and Management. 2020;205.
[37] Astriani Y, Shafiullah GM, Shahnia F. Incentive determination of a demand response program for microgrids. Applied Energy. 2021;292.
[38] Agency JM. Solargis, radiaiton and wethear data.
[39] Kyuden Electric CO I. Commercial dynamic electricity price.
[40] Panasonic Solar HIT photovaltic module.
[41] Wu B, Maleki A, Pourfayaz F, Rosen MA. Optimal design of stand-alone reverse osmosis desalination driven by a photovoltaic and diesel generator hybrid system. Solar Energy. 2018;163:91-103.
[42] Ismail MS, Moghavvemi M, Mahlia TMI. Techno-economic analysis of an optimized photovoltaic and diesel generator hybrid power system for remote houses in a tropical climate. Energy Conversion and Management. 2013;69:163-73.
[43] Divya KC, Østergaard J. Battery energy storage technology for power systems—An overview. Electric Power Systems Research. 2009;79:511-20.
[44] INSULATORS N. Sodium sulfur battery. In: Group EIB, editor.
[45] Zhou Y, Wu J, Long C. Evaluation of peer-to-peer energy sharing mechanisms based on a multiagent simulation framework. Applied Energy. 2018;222:993-1022.
[46] Ministry of Economy T, and Industry. Current Status and Future of Negawatt Trading. 2016.
[47] Yan Z, He A, Hara S, Shikazono N. Modeling of solid oxide fuel cell (SOFC) electrodes from fabrication to operation: Microstructure optimization via artificial neural networks and multi-objective genetic algorithms. Energy Conversion and Management. 2019;198.
[48] Metwaly MK, Teh J. Optimum Network Ageing and Battery Sizing for Improved Wind Penetration and Reliability. IEEE Access. 2020;8:118603-11.
[49] Metwaly MK, Teh J. Probabilistic Peak Demand Matching by Battery Energy Storage Alongside Dynamic Thermal Ratings and Demand Response for Enhanced Network Reliability. IEEE Access. 2020;8:181547-59.
[50] Ministry of Economy T, and Industry. The fixed incentive and activation reward of demand response.
[51] bank F. Fukuoka Bank‘s annual interest rate
[52] Ministry of Economy T, and Industry. Government Subsidy to battery energy storage system.

[53] Teh J, Lai C-M. Reliability impacts of the dynamic thermal rating and battery energy storage systems on wind-integrated power networks. Sustainable Energy, Grids and Networks. 2019;20.
[54] Teh J, Lai C-M, Muhamad NA, Ooi CA, Cheng Y-H, Mohd Zainuri MAA, et al. Prospects of Using the Dynamic Thermal Rating System for Reliable Electrical Networks: A Review. IEEE Access. 2018;6:26765-78.

Chapter 7

ENERGY SHARING FOR LOAD LEVELING IN SOLAR PV COMMUNITIY

ENERGY SHARING FOR LOAD LEVELING IN SOLAR PV COMMUNITIY

7.1 Contents 7-1

7.2 System description 7-4

7.2.1 Basic concept of cloud-based battery sharing framework 7-4

7.3 Methodology 7-5

7.3.1 General process 7-5
7.3.2 Battery energy storage system 7-7
7.3.3 Energy flow 7-7
7.3.4 Energy flow modeling 7-10
7.3.5 Performance metrics 7-11
7.3.6 Optimization 7-12

7.4 Case study 7-15

7.4.1 Situational analysis 7-15
7.4.2 Optimal battery capacity at aggregation level 7-16
7.4.3 Result of BESS in implementing load leveling 7-16
7.4.4 Aggregated battery capacity comparison with individual design 7-19
7.4.5 Optimization at single building level 7-19
7.4.6 Building features and optimal sizing of BESS 7-21
7.4.7 Closing day 7-22

7.5 Future direction of battery sharing 7-24

7.6 Conclusions 7-25

References 7-26

7.1 Contents

Buildings are now responsible for around 55% of total electricity use[1]. Electricity consumption in the building sector shows irregular characteristics and is reflected in two main portions. The first part is the valley of low energy demand. This valley indicates periods of low energy demand and energy prices. Conversely, periods with high energy demand create peaks or ceilings in the load profile [2]. This irregularity in consumption leads to inefficiencies in energy supply as well as uncertainty (because conventional electricity suppliers were designed and built with average electricity demand rather than maximum demand). To worsen the situation, energy consumption in the building sector continues to grow due to population growth and increasing per capita income [3]. In Japan, after the Great East Japan Earthquake in 2011 [4], the safety of nuclear energy has been seriously questioned, thus, it remains heavily dependent on imported fossil fuels which provides 88% of the Japan's total primary energy supply (TPES) in 2019 [1, 5]. Large-scale power outages and year-round electricity bill hikes are also plaguing Japan due to insufficient conventional power generation capacity and changes in the international situation. As a result, Japan is urgently upgrading its energy system. Integrating energy storage systems(ESS) into the power system is one of the solutions being proposed to improve the grid's reliability and performance [6, 7]. Distribution networks can utilize ESS for a number of grid applications including mitigating the renewable resources uncertainties [8], micro-grid applications [9] risk mitigation in electricity market [10].The other significant benefit at distribution side is that ESS can contribute in time shifting of energy output[11], for example excess generated energy is stored energy at off peak or low price periods and then stored energy is dispatched during the high demand, high price or low generation periods. It also achieve the performance on smoothing the load pattern be decreasing the on-peak and increasing the off-peak loads in one day, knowns as load leveling [2]. In addition, the planners would need to build only sufficient generating capacity to meet average rather than peak electrical demand by installing large-scale electricity storage facilities. [12]. Consequently, ESS can be a critical element in helping to regulate the city's peak demand by implementing load leveling. Among the various available ESS technology types, Battery Energy Storage System (BESS) has attracted considerable attention with clear advantages like a fast response, controllability, and geographical independence [13-16].

In spite of the fact that the use of BESS for load leveling can bring significant economic advantages, the high overall investment of BESS remains an issue [17]. It is therefore crucial that the BESS is optimally sized. Those on the application of BESS to cope with load leveling problem can be broadly categorized as two categories, centralized battery storage and distributed battery storage. The majority of the existing studies in the literature propose optimal manipulation and sizing for BESS. Some researchers also examine the optimal policy for charging and discharging power based on two different optimization objectives [18]. The first is to minimize the difference between the peak and valley demand, the second is to minimize the daily variance in load. The storage devices have been used to reduce the peak of the load profile and therefore, lessen the planning and operational costs. Allocation of the ESS is incorporated into the network planning problem [19]. A mixed integer nonlinear programming

(MINLP) model was proposed to solve it utilizing a particle swarm optimization algorithm (PSO) [20]. As a result of the simulation, both the cost and technical performance of the network is improved. To improve the reliability level of the distribution network, Saboori H et.al have been proposed as an investment plan of ESSs. With the energy not supplied (ENS) index, the level of system reliability is elevated, and system failures are minimized through optimal ESS planning. In order to perform load leveling and improve voltage curve in the networks, a bi-objective optimization model was proposed [2]. For economic assessment, a stochastic cost–benefit analysis framework for allocating centralized energy storage systems (ESS) in the networks is proposed to achieve load balancing [21]. An algorithm was presented to solve the issue of load leveling and losses minimization in the networks impacted by temporary service restoration activities but they have not considered optimal allocation [22]. [23] introduced a metric of five indexes to evaluate the technical performances of load peak shaving for a test house in Northern Ireland but have not considered optimal operation. In addition, the mobile BESS technology can provide services and economic benefits by connecting to the grid (such as vehicle-to-grid system). However, some researchers pointed out that the increased integration of electric vehicles is expected to have a negative impact on power quality, and investment costs of the microgrid. Hence, a decentralized energy management system, based on multi-agent systems, was developed for the efficient charging of electric vehicles [24], to achieve approximately 17% peak load reduction and 29% load variances reduction.

The various papers mentioned above discuss strategies for the placement of BESS to improve the load leveling performance of the building sector and propose solutions in terms of optimal location and size. Most importantly, it demonstrates the feasibility of BESS participation in grid management in terms of economics. As the price of battery systems decreases, battery systems, whether centralized or distributed (It will be explained in detail in section 3.3), are expected to become an attractive application for the building sector. Centralized energy storage not only requires operational and size optimization considerations but also requires additional consideration of battery siting and distribution system upgrades due to large transient branch circuit current changes over long distances. The conventional design methods of distributed system are based on single building energy allocation for sizing the distributed batteries, so, they neglect the interaction that we call it ‘energy sharing’ in this paper, between the smart grid, smart buildings and distributed energy storage to achieve better energy management practices.

With the rapid growth of the sharing economy around the world, a new proprietary idea of community centric sharing has recently emerged into the energy market [25]. Unlike traditional individually owned BESSs and large utility-level BESSs, customers in a community can provide optimal energy management services through energy sharing (for example, using remaining power to match the power needs in the same community) and storage sharing (for example, using the battery to take remaining power to or out of the building community) [26, 27]. A peer-to-peer (P2P) energy sharing paradigm involving hybrid solar-wind renewable energy systems, battery storage, and grid-connected commercial prosumers (a high-rise office and hotel) was proposed[28]. And they found that the proposed P2P sharing operation with storage sharing can promote the self-consumption from 0.591 to 0.795 and reduce the net cost.

[29] established a shared economy model that enables residential communities to share solar power generation and storage capacity is investigated. The result is that it saves an average of €615 per year compared to operating alone. Peer-to-peer (P2P) energy trading framework was proposed [30], enabling distributed photovoltaic (PV) consumers and prosumers to participate in a community sharing market created by a stakeholder. [31] proposed a bi-objective mixed-integer linear programming approach for managing clusters of buildings equipped with shared electrical energy storage. Therefore, the uneconomic use case for batteries may become profitable when individual EES assets are aggregated into a large portfolio to provide grid-scale ancillary services [32].

At this stage, large-scaled battery is mainly utilized for load levelling in electricity plants by supplying power. The power generated by the electricity suppliers due to low needs (for example at dawn or on the off-peak hours) and charged to the battery during periods of overgeneration and discharged to the buildings during the electricity shortage periods because of high needs (for example on the peak hours). Economic viability is the major critical element in large battery implementations because of the high initial costs. However, the utilization rate of large BESS for load levelling can be low due to fluctuating demand. In addition, large BESS also have high transmission loss due to size and distance limitations. On the other side, the ability to perform energy arbitrage is the biggest motivation for individual users to install BESS. Therefore, through energy sharing, private BESSs can perform in load levelling to reduce the peaking stress of the power supply, saving expenses for peaking power generators. Electricity suppliers are also willing to cooperate with individuals to share information and optimize energy use by paying a fee. As a result, stakeholder-based information exchange is essential to enable energy sharing between buildings where load balancing is performed and electricity suppliers. Hence, wide area monitoring system(WAMS) based on real-time measurement and monitoring is becoming a key solution in the key areas of online stability, situational awareness, grid planning. The possibility of monitoring and controlling the operation of the whole power system for achieve real-time, dynamic control of the power has been proved [33]. [34] studied the performance of communication in dense networks with wireless energy harvesting (WEH)-enabled sensor nodes. [35] proposed an information sharing strategy based on linked data for improved management of Net-zero communities. This strategy systematically integrates stakeholders' engagement by using energy performance indicators as information carriers and linked data as engagement channels.

Contents

With the development and application of technologies such as blockchain and the Internet of Things(IoT), the outstanding flexibility and rapid response of BESS has been proven. With the increasing impact of distributed energy on the grid, BESS and the sharing strategy have gradually become the most effective means to improve the utilization of distributed energy in the community. Most of the literature mentioned above focuses on this area. They suggest that co-investment by producers and consumers can effectively reduce energy costs, avoid unnecessary investments, and increase BEES utilization. This novel trading model enhances community resilience by reducing the community's reliance on the main grid and increasing the

ability to participate in demand response (DR) to achieve better generation balancing. Many studies have also discussed the role of appropriate pricing models in sharing(through auction model, blockchain and bilateral contracts[36]), as this directly affects the incentives of Peer-to-Peer participants to participate in energy sharing. However, there is a lack of understanding of the impact of sharing strategies on battery sizing across multiple buildings (especially non-residential buildings), and it is unclear whether community or grid-level battery sharing will provide the best solution for load leveling performance. To address the knowledge gaps identified above, based on the information sharing and energy sharing strategy of linked data, we try to achieve load leveling by gathering individual BESS.

The main achievements of this work are listed below:

we develop an energy sharing framework between the distribution network and the individual batteries for allocation of distributed ESS for community load leveling application.

- Representative load profiles (RLP) for non-residential buildings were extracted by clustering and feature analysis methods, and the optimal deployment of BESS in the RLP with sharing framework was discussed, and these results provide promising insights into battery sharing.
- We propose a generic sharing model that takes into account the interaction between various hierarchies in the city, and the application of BESS is expanded from the individual building to the community level and finally to the city, giving a basis for efficient energy sharing for city hierarchies in the future.

The rest of the paper is organized as follows: the basic idea of cloud- based battery sharing is presented in Section 2. The general process and proposed methodology are presented in Section 3. The results and discussion are proposed in Section 4. In the end, we present the conclusions in Section 5.

7.2 System description

7.2.1 Basic concept of cloud-based battery sharing framework

The proposed energy sharing network allows for potential users to benefit from operating the BESS and to participate in energy trading. Real-time energy monitoring and physiographic data from multiple perspectives will help to build a database in the cloud-based battery sharing community (Figure 1). It means, all energy participants including power producers and customers, and energy components including distributed generation systems, consumers, battery system which decentralized within a community can be interlinked and influence among each component.

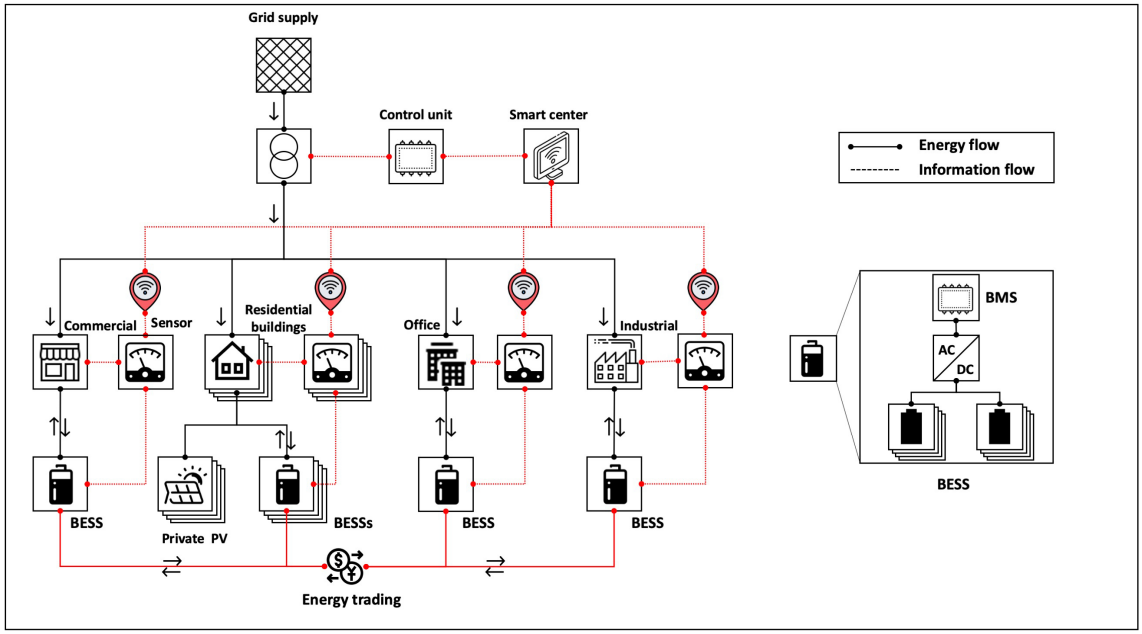

Fig. 7-1. The concept of the cloud-based battery sharing framework

7.3 Methodology

7.3.1 General process

Raw power demand data are collected with meters from a smart community in Japan. A one-hour time-step is used for monitoring the active power, reactive power. In this study, only active power is considered. Raw electricity demand data is provided in a single column format, with each row corresponding to within a selected time range. Data formatting is performed by extracting the Daily Load Profile (DLP) of annual data set. It is difficult for utilities to analyze the large number of DLPs from different customers. Especially when the volume of customer data is very large or the study time is very long, it can be a very challenging task. A common solution is to assign a representative load profile(RLP) to each customer. RLP is usually calculated by averaging DLPs over a period of time. Therefore, each customer is represented by one RLP rather than many DLPs. There are various methods of clustering algorithm, three of most applied are self-organizing maps(SOM) [37], hierarchical clustering [38] and K-means [39]. Due to the characteristics of the clustering algorithm, it always assigns DLPs that follow the same consumption pattern to the same group. Commercial buildings do not undergo significant changes in DLP due to stable commercial activities. K-means algorithm stand out for its better clustering effect, stronger interpretability, fast convergence and other advantages [40, 41] as applied to non-residential building performance analysis [42]. Conversely, the application of clustering algorithms is a challenge when dealing with highly variable data sets (e.g., residential customers, which do not reuse specific appliances or electrical equipment at the same time of day). At this point, if clustering is performed using algorithms such as K-means and distance metrics such as Euclidean distance, a customer's DLP may be assigned to many different clusters. Therefore, SOM was proved to be the most suitable for residential customers [43]. The strategy of hierarchical clustering is to first treat each object as a cluster,

and then merge these atomic clusters into larger clusters until all objects are in a cluster or some end condition is satisfied[44]. Once two clusters are merged, they are not undone so that the computational storage is costly. Therefore, its disadvantages are obvious: 1) the computational complexity is too high; 2) the singular values can have a significant impact (e.g., caused by maintenance or temporary closures). As a result, we adopt the *k*-means clustering algorithm to reduce the calculation sophistication while retaining high accuracy in this paper. The specific steps are as follows:

- After that, the annual data set is processed using principal component analysis (PCA) to extract the most important features of each day. Feature extraction is a technique for extracting meaningful information from a confusing data set by using PCA. In addition, they can reduce complex data sets to a lower dimension one while retaining the variation to reveal hidden structures that underlie them and eliminate noise [45].
- Accordingly, after reconstructing the total load curves using Principle component analysis, the daily load demand curves are clustered into independent non-overlapping clusters [39].
- Then, the feature-based daily load profiles are used as the input items to search the optimal set of BESS deployments. Meanwhile, feature extraction is used to provide the physical meaning to identified the results (Fig.2).

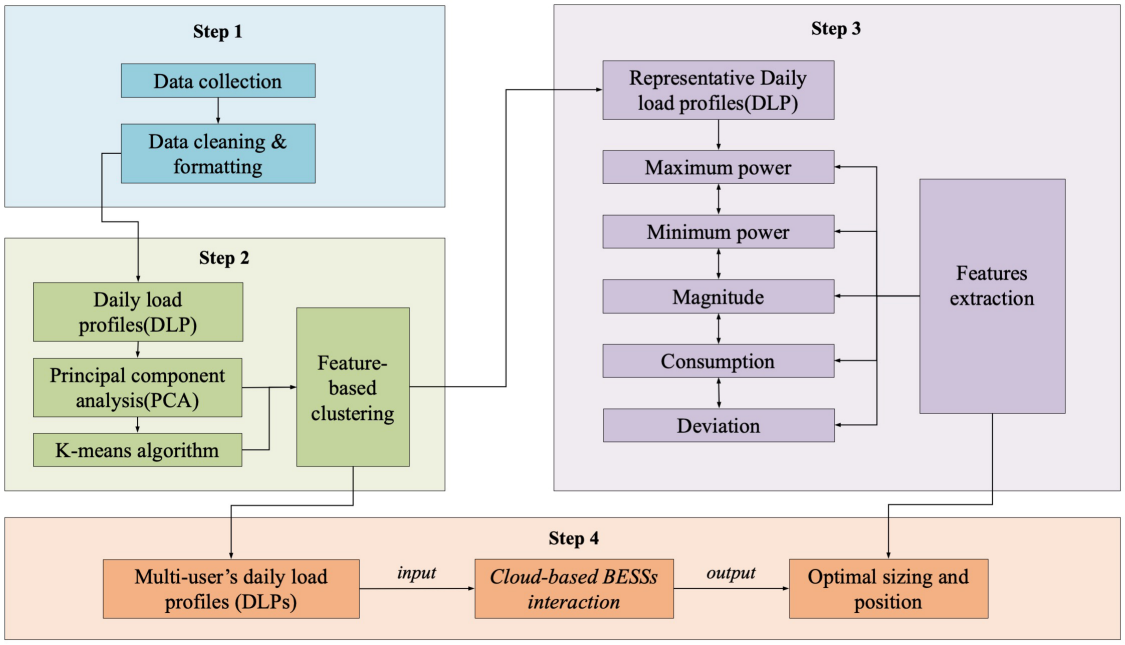

Fig. 7-2. General process

7.3.2 Battery energy storage system

In the past few decades, battery energy storage system has significantly improved because of the fast declined price. What's more, Battery energy storage systems have the ability to transform the "production-consumption" energy paradigm into a new "production-storage-consumption" paradigm. In the case study, we select the Sodium-sulfur battery (NAS) technology as the electricity power storage tool because of its high energy efficiencies [14, 46]. For the input and output of power, the state of the battery is changing. We build a model to calculate the storage system. The state of charge (SOC) and power rating of the battery are mostly used to develop a realistic model. During the charging and discharging process, the state of charge of the battery can be described by the equation. (4) and (5), respectively as:

$$SOC(t+1) = SOC(t) + \frac{\eta_{cha} \cdot \sum pw^j(t) \cdot \Delta T}{Cap^j} \tag{7-1}$$

$$SOC(t+1) = SOC(t) - \frac{\sum pw^j(t) \cdot \Delta T}{\eta_{dis} \cdot Cap^j} \tag{7-2}$$

where $SOC(t)$ is the state of charge of BESS, η_{cha} and η_{dis} denote the charging and discharging efficiency of BESS. Cap^{j} is the energy capacity of BESS in the building j. $E^j_{BESS}(t)$ is energy state at the time (t), respectively. Battery cycle aging has been one of the main considered factors in the performance of BESS technology as far as BESS lifetime is involved. During charging and discharging, battery performance, especially energy capacity, decreases as a result of oxidation and reduction reactions between the positive and negative electrodes. Consequently, under the following conditions, the battery will not be degraded due to overcharging or over discharging.

(a) Maximum SOC constraint –

$$E^i_{BESS} \geq SOC_{\min} \tag{7-3}$$

$$E^i_{BESS} \leq SOC_{\max} \tag{7-4}$$

where SOC_{min} is the lowest limitation of SOC, and SOC_{max} is the highest limitation of SOC.

(b) BESS operation power rating limitation -

$$\left| \frac{E^i_{BESS}}{\Delta T} \right| \leq pwc \tag{7-5}$$

where pwc denotes the rated power capacity of BESS.

7.3.3 Energy flow

Load transfer management is the main work of load leveling. The purpose is to optimize the allocation and rational use of power resources, improve the economic operation of the power

grid by changing the time and method of power consumption, increase the utilization of facilities, and at the same time benefit to customers.

-*(a).Aggregated BESS*

The community's buildings are equipped with a single centralized battery, which is usually mounted on the outside of the structure. The capacity and power of the aggregated BESS is defined by the load demand of all buildings in community. The aggregated BESS is charged when the load demand is low (e.g., at night) and discharged when the load demand is high to relieve the instantaneous supply pressure on the power plant and to improve the energy efficiency. This is a conventional application of a large BESS on the distribution network side [21]. And since all processes take place outside the building, the overall peak shaving performance is not affected by the individual building. Hence, there is no need to consider the load of a single consumer, it easily reach a stable state both on-peak and off-peak periods, like the red line in Fig.3 (a).

-*(b).Distributed BESS*

Each building has its own individual battery. Energy exchange is based on single building energy allocation. The conventional solution is to deploy BESS inside the building to achieve load leveling on an individual level according to its own load demand. For example, in [47], the authors take a demand-driven approach to determining residential battery capacity of individual household demand for both load smoothing and peak shaving. The results show that the BESS can successfully achieve load smoothing and keep the cell size within the design allowance. However, due to the complexity of building types (e.g. shopping malls and office buildings have very varied electricity consumption habits), when the number of buildings in a community becomes large (with dozens or even hundreds of buildings), such a solution will become inefficient. And, each BESS is installed individually, there is no interchange of information between them and the whole system will become unpredictable. Hence, although it is possible to maintain a smooth load profile at an individual level, the final balance performance is difficult to predict and control due to the involvement of multiple users(Fig.3 (b)). In the above mentioned literature [47], the innovation is that they also compared the battery capacity required for a single house with the battery capacity required for the total needs of a group of households (20 households). Aggregation reduces battery demand per house by 50% for load smoothing and 90% peaking. This means that allowing battery resources to be shared among users may result in smaller battery deployments per house to achieve the same level of load smoothing [48]. Consequently, under the cloud-based energy sharing framework, the individual BESS have the capability to manger the energy of the other buildings in the community. The relationship between the distribution network and the individual batteries is developed so that the individual consumer's management system can adjust the charging and discharging power by means of the peak information of the distribution network. However, the disadvantage is the capacity and power of the distributed battery are limited by their own load demand. Based on benefits considerations, the discharge power is limited by its own load demand. Therefore, when the load demand is compensated by own battery at a certain moment, the remaining power is charged to the other buildings in the community (battery storage sharing).

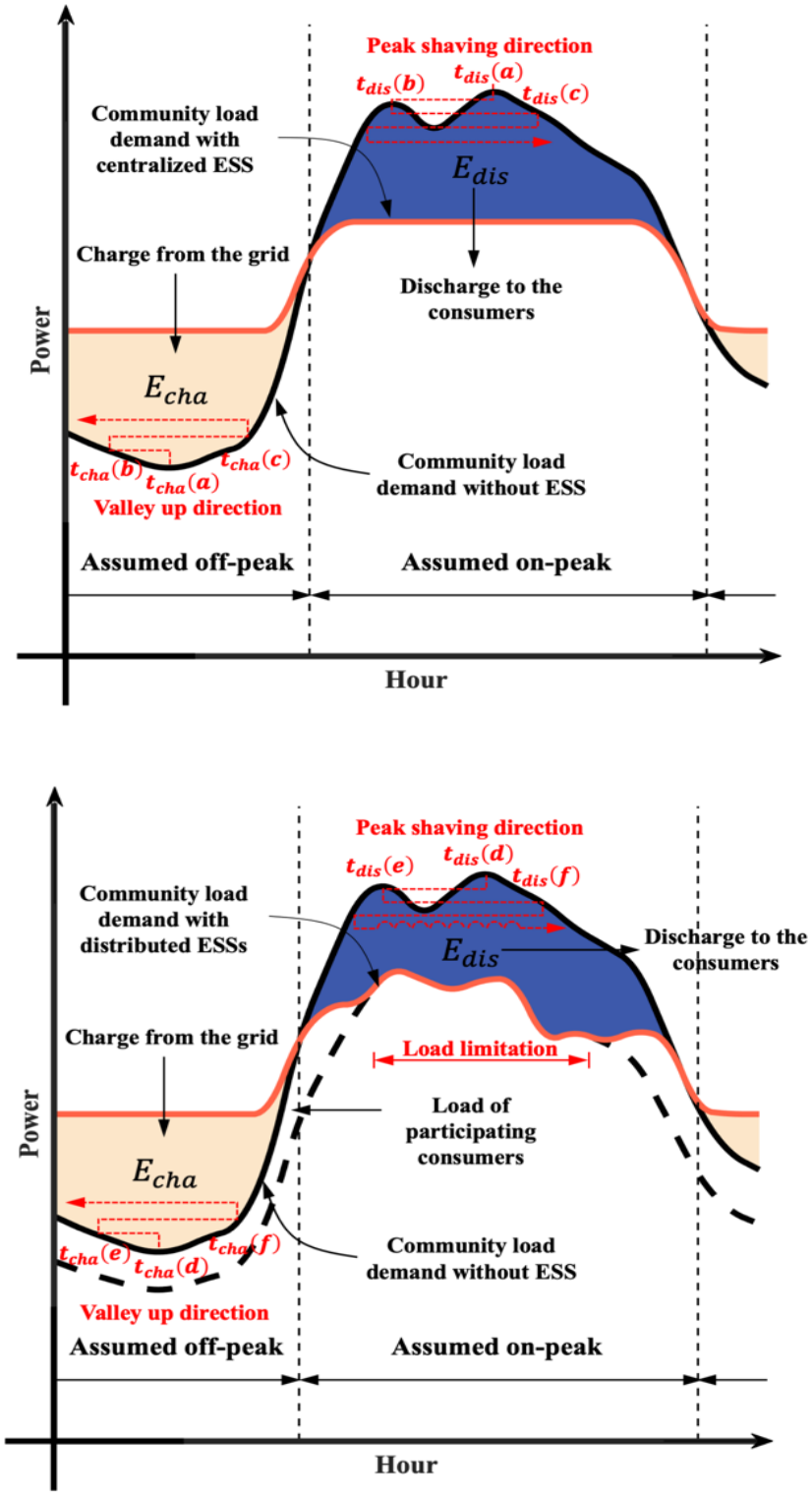

Fig. 7-3. Principle of load leveling and key figure of energy flow with/without information exchange

7.3.4 Energy flow modeling

The energy system configuration may vary depending on the grid and the components of the energy flow. As an example, the following equation can be used to represent the load balance between components of the system:

$$E_{net}^{j}(t) = E_{grid}^{j}(t) - E_{BESS}^{j}(t) \tag{7-6}$$

where $E_{net}^{j}(t)$ is the net load demand of end-user. $E_{gird}^{j}(t)$ is the electricity from the external grid, and $E_{\mathrm{BESS}}^{j}(t)$ donates the net electricity exchange of BESS. t is the index that indicates the time period of each hour of the day. Due to the cloud-based energy sharing framework, the individual battery not only charge or discharge electricity power to own building, but also store or use the remaining power or access to electricity in the building community. Therefore, the interaction with net load and the private BESS of whole community can be defined as equation.(7). The matrix provides a visual representation of the energy exchange between buildings, so that the charge and discharge power between buildings can be defined by equation (8) and equation (9).

$$\left|\sum E_{net}^{j'}(t)\right| = \begin{cases} \dfrac{\sum E_{cha}^{j}(t)}{\eta_{cha}}, if\left(\sum E_{net}^{j'}(t) < 0\right) \\ 0, if\left(\sum E_{net}^{j'}(t) = 0\right) \\ \sum E_{dis}^{j}(t) \times \eta_{dis} + \sum E_{grid}^{j}(t), if\left(\sum E_{net}^{j'}(t) > 0\right) \end{cases} \tag{7-7}$$

$$E_{cha}(t) = \begin{bmatrix} E_{cha}^{1,1}(t) & E_{cha}^{2,1}(t) & \cdots & E_{cha}^{j,1}(t) \\ E_{cha}^{1,2}(t) & E_{cha}^{2,2}(t) & \cdots & E_{cha}^{j,2}(t) \\ \vdots & \vdots & \ddots & \vdots \\ E_{cha}^{1,j}(t) & E_{cha}^{2,j}(t) & \cdots & E_{cha}^{j,j}(t) \end{bmatrix} \tag{7-8}$$

$$E_{dis}(t) = \begin{bmatrix} E_{dis}^{1,1}(t) & E_{dis}^{2,1}(t) & \cdots & E_{dis}^{j,1}(t) \\ E_{dis}^{1,2}(t) & E_{dis}^{2,2}(t) & \cdots & E_{dis}^{j,2}(t) \\ \vdots & \vdots & \ddots & \vdots \\ E_{dis}^{1,j}(t) & E_{dis}^{2,j}(t) & \cdots & E_{dis}^{j,j}(t) \end{bmatrix} \tag{7-9}$$

Charging state: The individual BESS is in charging state at the nighttime when the electricity price is on the off-peak price. The charging power of private BESS can be defined as follow:

$$E_{cha}^{j}(t) = \sum E_{cha}^{j,j}(t) = \begin{cases} pw^{j}, if\left(\left|E_{net}^{j'}(t)\right| > pw^{j}\right) \\ \left|E_{net}^{j'}(t)\right| \times \eta_{cha} + \left|E_{net}^{j-1'}(t)\right| \times \eta_{cha} \times \eta_{trans}, if\left(\left|E_{net}^{j'}(t)\right| \le pw^{j} \le \left|E_{net}^{j'}(t) + E_{net}^{j-1'}(t)\right|\right) \\ \left|E_{net}^{j'}(t)\right| \times \eta_{cha} + \left|E_{net}^{j'}(t) + E_{net}^{j-1'}(t)\right| \times \eta_{cha} \times \eta_{trans}, if\left(\left|E_{net}^{j-1'}(t)\right| \le pw^{j}\right) \end{cases}$$

(7-10)

Discharging state: The private BESS is in a discharging state at the day time, when the building has insufficient power, (i.e., $E_{net}^{j,\prime}(t) > 0$). And if the other buildings have insufficient power while the battery has remaining capacity, (i.e.,$E_{net}^{j-1,\prime}(t) > 0 \cdots \vee E_{net}^{1,\prime}(t) > 0$), the private battery can also be in a discharging state. The discharging power of private BESS can be defined as follow:

$$E_{dis}(t) = \sum E_{dis}^{j,j}(t) = \begin{cases} pw^j, if\left(\left|E_{net}^{j'}(t)\right| > pw^j\right) \\ \left|E_{net}^{j'}(t)\right| / \eta_{dis} + \left|E_{net}^{j-1'}(t)\right| / \eta_{dis} \times \eta_{trans}, if\left(\left|E_{net}^{j'}(t)\right| \le pw^j \le \left|E_{net}^{j'}(t) + E_{net}^{j-1'}(t)\right|\right) \\ \left|E_{net}^{j'}(t)\right| / \eta_{dis} + \left|E_{net}^{j'}(t) + E_{net}^{j-1'}(t)\right| / \eta_{dis} \times \eta_{trans}, if\left(\left|E_{net}^{j-1'}(t)\right| \le pw^j\right) \end{cases}$$

(7-11)

7.3.5 Performance metrics

① Load leveling

As of today, the definition of load leveling is not clear. The purpose of load leveling is to perform a more stabilized and balanced load curve. And it is to avoid frequent transitions between peak and troughs so that reduce the peak supply pressure on the electricity supplier. Therefore, load leveling can be interpreted as a small fluctuation of electricity consumption data. Xu L et al. [49] proposed that using standard deviation to measure the fluctuation from statistics.

The SD corresponding to scenario is defined as:

$$SD = \sqrt{\frac{\sum [E_{load}(t) + \sum E_{BESS}(t) - E_{mean}(t)]^2}{N}} \tag{7-12}$$

where $E_{load}(t)$ denotes the system base load demand at time period t, respectively. $E_{mean}(t)$ is the mean load demand value. T is a time period for one day. And j is the set of all buildings, which is represented as $j \in \{1,2,\dots,39\}$.In this study, SD of load curves(LSD) is used to determine the load curve. The lower the standard deviation value, the more stabilized the load curve will be.

② Transmission losses

Energy sharing requires reliance on the distribution network to share surplus battery capacity to other buildings within the community. Generally, smaller power network will occur higher transmission losses. Although the electricity may travel a few miles or less on low-voltage distribution lines, losses are high at the community level network. Meanwhile, the different operation of batteries due to its location and capacities will cause different energy losses. Therefore, energy loss cannot be ignored in shared energy communities. In addition, losses are

incurred during the charging or discharging of the BESS. The total energy loss can be described as:

$$Loss_{tot} = Loss_{cha/dis} + Loss_{trans} \tag{7-13}$$

where $Loss_{cha/dis}$ is the conversion losses due to the BESS charging or discharging. $Loss_{trans}$ is the transmission losses due to the surplus battery sharing through the distribution network. In this paper, the distance to buildings within the community is within 1km, the transmission losses due to the energy sharing is defined as equation.(13) and equation.(14). The transmission loss rate is assumed as 8%. It is noted that the loss rate of building taking of storing power from or into own building is 0% since the energy exchange takes place within its own building.

$$E_{ex}(t) = \begin{bmatrix} 0 & E_{ex}^{2,1}(t) & \cdots & E_{ex}^{j,1}(t) \\ E_{ex}^{1,2}(t) & 0 & \cdots & E_{ex}^{j,2}(t) \\ \vdots & \vdots & \ddots & \vdots \\ E_{ex}^{1,j}(t) & E_{ex}^{2,j}(t) & \cdots & 0 \end{bmatrix} \tag{7-14}$$

$$Loss_{trans} = \sum E_{ex}(t) \times \eta_{trans} \tag{7-15}$$

③ Economic indicator

The net present value of an investment is the difference between the present value of cash flows and the present value of cash outflows over time. The NPV is a tool used in capital budgeting and investment planning to determine whether a planned investment or project will be profitable. Ignore the operation and maintenance cost, the NPV of BESS can be determined as:

$$NPV_{BESS} = \sum_{n=1}^{y} \frac{\sum (E_{dis}(t) - pr(t)) - (\sum E_{dis}(t) - \sum E_{cha}(t) -) \times pr_{va}}{(1+a)^n} - \sum cap^j \times c_{inv} \tag{7-16}$$

In the above, NPV_{BESS} donates the Net present value of BESS. $Pr(t)$ is the electricity price at time (t). And i is the discount rate. y is the lifecycle of project. C_{inv} is the investment fee. It includes the inverters, equipment costs, installation costs and initial conservation costs.

7.3.6 Optimization

This section describes the design and optimization methods of distributed BESS within an energy sharing community. The first step is to obtain the electrical load profile of the entire community by evaluating each building. In the second step, the battery capacity at the aggregation level is optimized using a genetic algorithm (GA) using the aggregation level power/demand as input parameters, with the goal of maximizing the load leveling performance of the community. The objective function of this step can be described as:

$$J_{fitness} = \begin{cases} \min(SD) \\ \max(NPV_{BESS}) \end{cases} \tag{7-17}$$

The output of this step is considered to be the minimum capacity required to achieve the required energy performance (load leveling) for the entire community. In step 3, nonlinear programming (NLP) is used to optimize the capacity of the distributed batteries installed in each building) to minimize storage sharing (i.e., power exchange with other batteries) and thus reduce the associated energy losses. The objective function of NLP is represented by equation (7-18).

$$J_{NLP} = \min(\sum E_{ex}(t) \times \eta_{trans}) \tag{7-18}$$

A step-by-step method is described below. Figure 4 is a flow chart depicting the method.

(1).Data fetching-

The first step is the data fetching. It contains Features of BESS which consists with design range of BESS dimensions (kWh), module dimensions of BESS (kWh), module dimensions of power rating (kW) and planning optimization objective function. The parameters necessary for the GA algorithm are also imported in this step.

(2). Extraction of representative load demand curves-

The load demand curves for the standard year were approached using principle component analysis and clustered using *k*-mean method. After alteration according to the chronological nature, representative load demand profiles are chosen from those profiles is computed.

(3). Create initial population-

An initial population of individuals is the starting point of the process. Each individual is represented using a string, in terms of alphabet (string of 1s and 0s). Every individual represents the capacity of BESS. The parent groups are initialized stochastically in this step.

(4). Fitness function-

The fitness function determines how fit an individual is(the fitness function is load standard deviation). MATLAB's fmincon solver is used to determine the optimal BESS operation for each population for corresponding the minimum load standard deviation (LSD). This step is performed for each individual member of the population in turn and results in fitness score. Based on the fitness score of an individual, we determine whether it will be selected for breeding.

(5). Evolution via GA-

Each individual progeny member of a population is evaluated for fitness in step 4 of the evaluation of the fitness of an individual generation. Selective breeding, cross-breeding, and mutation took place on the population in order to generate the offspring population. An elite algorithm is used to blend the parent and offspring populations together to form the next generation. Step 6 should be followed if the current generation is a final generation; otherwise, update the number of generations, reset the year to 1, and go to step 4.

(6). Obtain the results of the capacity of the aggregated battery -

An optimal capacity of the aggregated battery results from the GA search, which has the minimum LSD.

(7). Optimization of distributed battery capacity for single building -

In this step, GA is used to optimize the capacity of distributed batteries (kWh) installed in individual buildings based on aggregated battery capacity, which aims to minimize load limitations.

(8) Calculating feasible solutions using LP -

After the eighth step, the battery capacity of all batteries to be tested is calculated. We can use linear programming and combine other factors to assign the battery capacity.

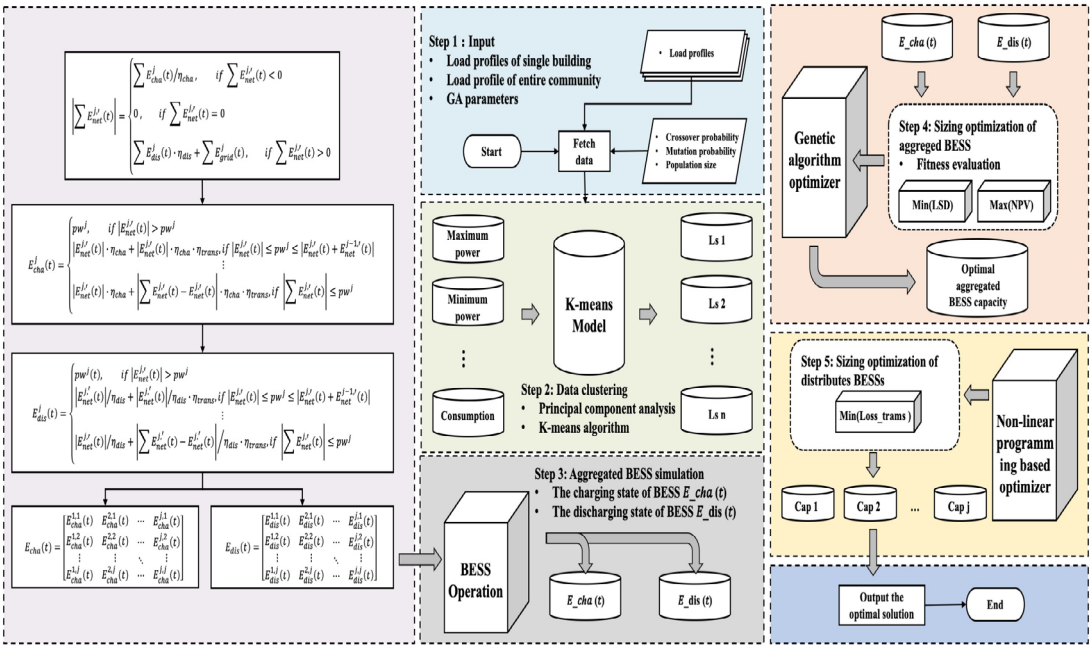

Fig. 7-4. The operation flows

Table 1 provides an overview of input variables utilized in the study; the investment price of battery energy storage system is 25,000 Yen/kWh. It is including the inverters, equipment costs, installation costs and initial conservation costs. The discount rate is set to 4.5% according to the Fukuoka bank. The power rating of each BESS is limited as 16% of its capacity. The upper limit of discharging depth is 90%. The power transmission loss rate is set as 8%. The parameters of genetic algorithm are also summarized in the Table.1.

Table 7-1. Input simulation parameters [46], [50], [51], [52]

Category	Variables	Value	Unit
Economic Variables	BESS investment fee (Including conversion & installation cost)	25,000	*Yen/kWh*
	Discount rate	4.5	*%*
Technical Variables	Battey life cycle	15	*Yr*
	Maximum discharging depth (DOD)	90	*%*
	Power rating of battery	16	*%*

	Conversion efficiency	92	%
	Electricity transmission loss rate	8	%
Optimization Variables	Population sizes	80	-
	Number of iterations	200	-
	Minimum value of crossover probability	0.58	-
	Maximum value of crossover probability	0.86	-
	Maximal value of mutation	0.096	-
	Minimum value of mutation probability	0.05	-

7.4 Case study

7.4.1 Situational analysis

In the paper, we collected the load profile data from a commercial community in Japan. The date of measurement is from April 2013 and March 2014. The data set contain annual load data of thirty-nine buildings are used to form the load matrix (365 days x 24 data point/day). It is a typical community dominated by commercial practices. The thirty-nine buildings cover different common activities of a commercial community including supermarket, hotel, factory, convenience store, gas station, shopping mall, stadium, exhibition hall, clinic, station service center, office and restaurant. The daily electricity consumption curves of whole community are shown in Fig.5. Due to the chronological nature of the commercial activities, the electricity consumption of daytime is extremely higher than that in the night-time. The peak annual electricity consumption is concentrated in the summer (June, July, and August).

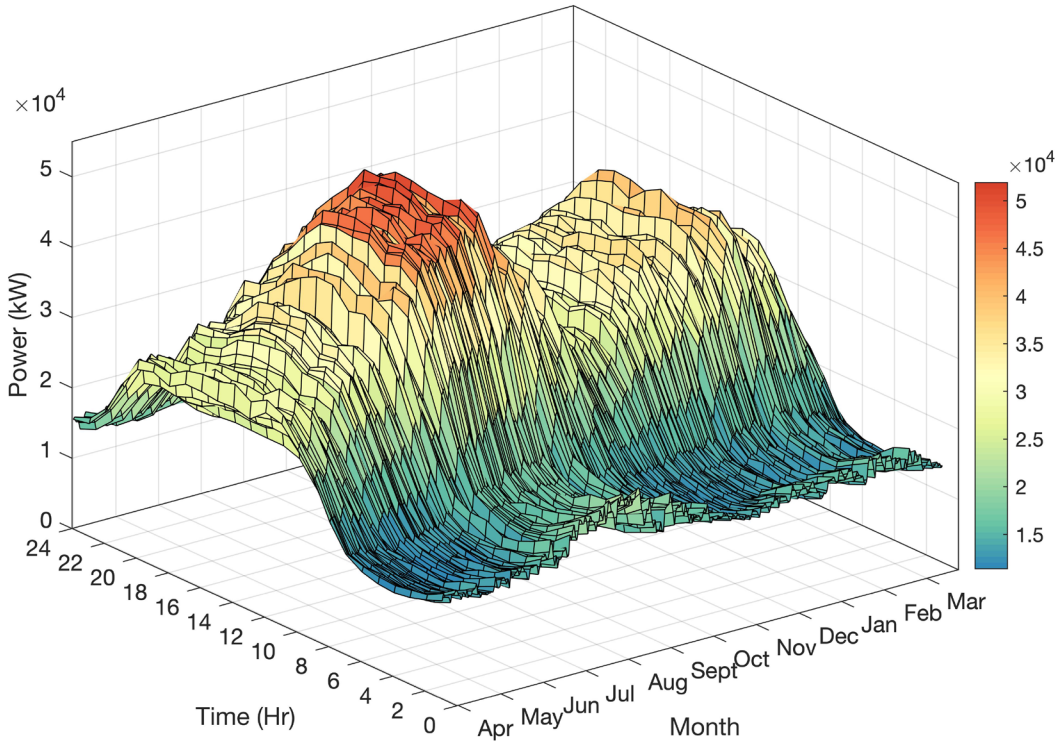

Fig. 7-5. The load profiles of the whole community

7.4.2 Optimal battery capacity at aggregation level

Fig. 6 shows the curve of load leveling performance with BESS capacity at aggregation level. In the initial part of the curve, the LSD decreases at a very fast rate as the aggregated capacity increases, while near the lowest point (98120 kWh/3960) the rate of decrease becomes slow. Then, with the increasing of the BESS sizes, the load leveling performance become worse. Meanwhile, the range area of energy losses are plotted with green color in Fig.6. It is growing higher due to the increasing of the BESS' sizes. The reason is that the number of energy exchanges is becoming more frequent. Therefore, the optimal BESS capacity at aggregation level is 98120 kWh.

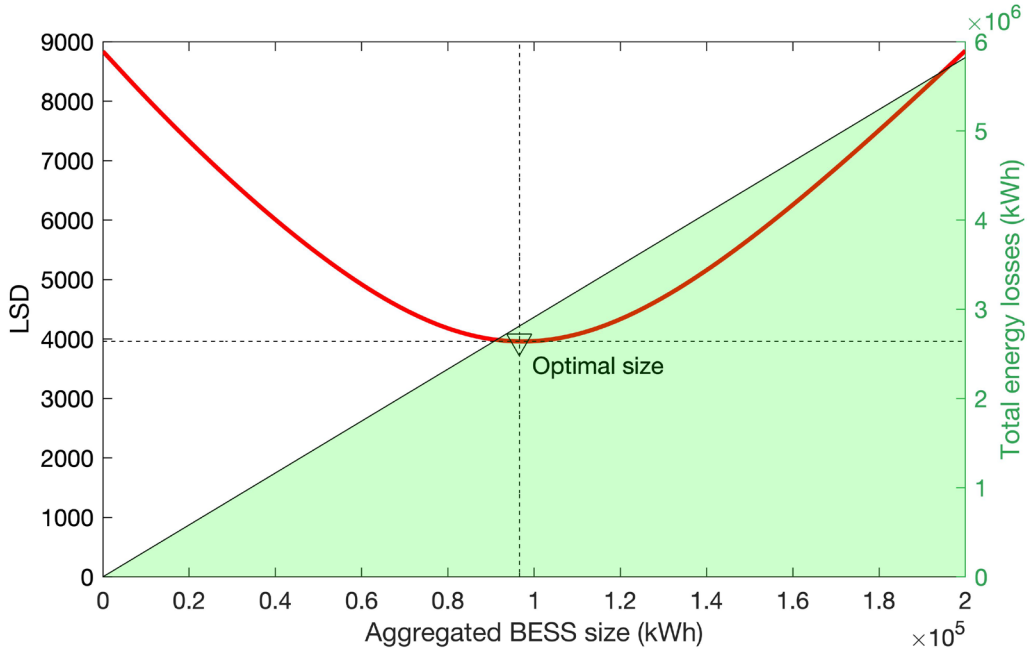

Fig. 7-6. The load standard deviation and energy losses under different battery sizes

7.4.3 Result of BESS in implementing load leveling

We select four most representative days among the whole year to verify the validity of BESS for load leveling. Each represents the most significant day of the year for each of the four seasons. The load curve for the whole community with and without BESS operation, is plotted in Fig.7. The capacity of battery is the optimal size of 98,120 kWh which is discussed in section 4.2. The SOC of virtual aggregated BESS is also shown in Fig. 7(green line), which represents the comprehensive operation capability of the distributed batteries. The figure conclude that there is a large fluctuation in the community load without BESS (black line). The peak demand is 44,300 kWh at noon while the valley demand is 13,123 kWh at 4:00 am in summer. The difference between peak and valley is over 30,000 kWh. Optimal BESS operation results in the BESS charging from 0am to 8am and discharging from 10am to 8pm. The green part represents charging and the blue part represents discharging. Therefore, The difference between the peak and valley is greatly reduced and the peak become significantly flatter (red line). In winter, although the peak demand is 28390 kW, the optimal BESS operation also reduce the difference between peak and valley. Compared with the case of no BESS, the peak demand is reduced as 26.6%. It shows that optimal BESS operation can be effectively in implementing load leveling.

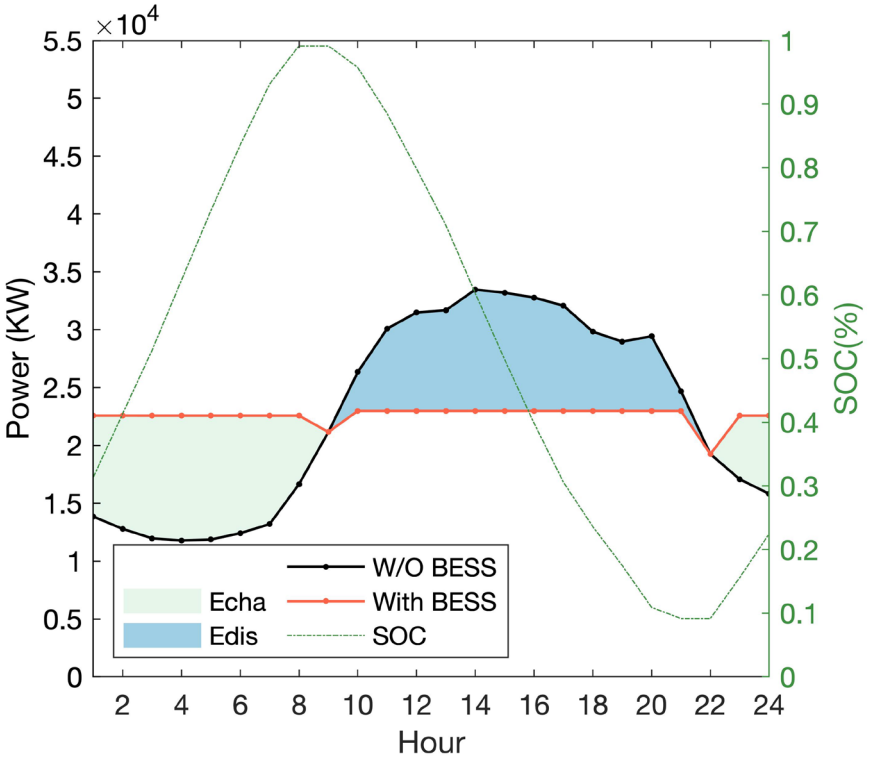
×10^4
Power (KW)
SOC(%)
Hour
W/O BESS
With BESS
SOC
Echa
Edis

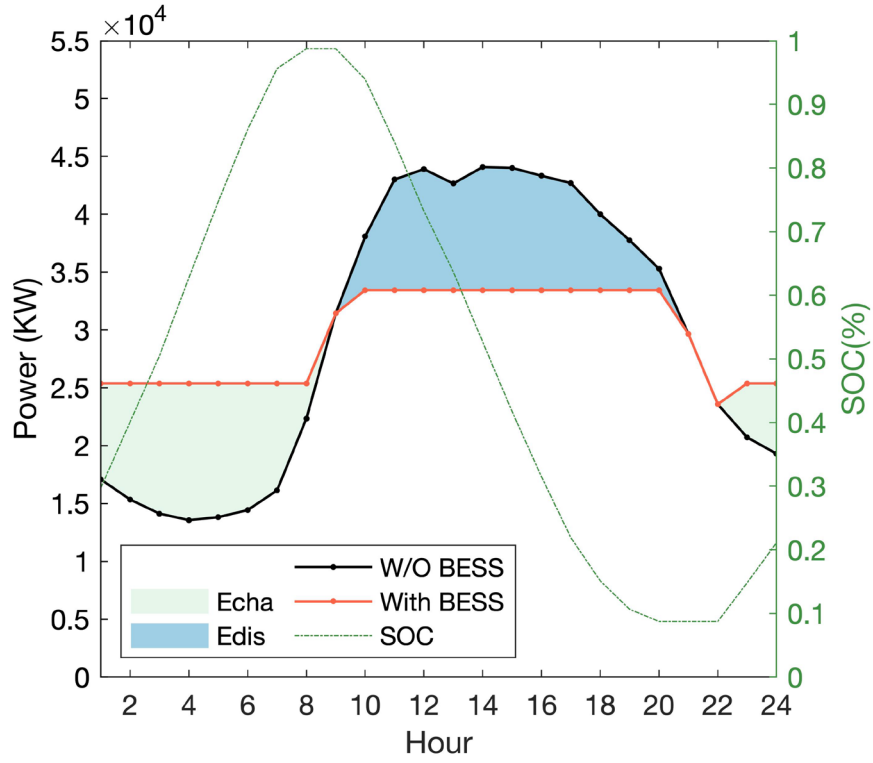
×10^4
Power (KW)
SOC(%)
Hour
W/O BESS
With BESS
SOC
Echa
Edis

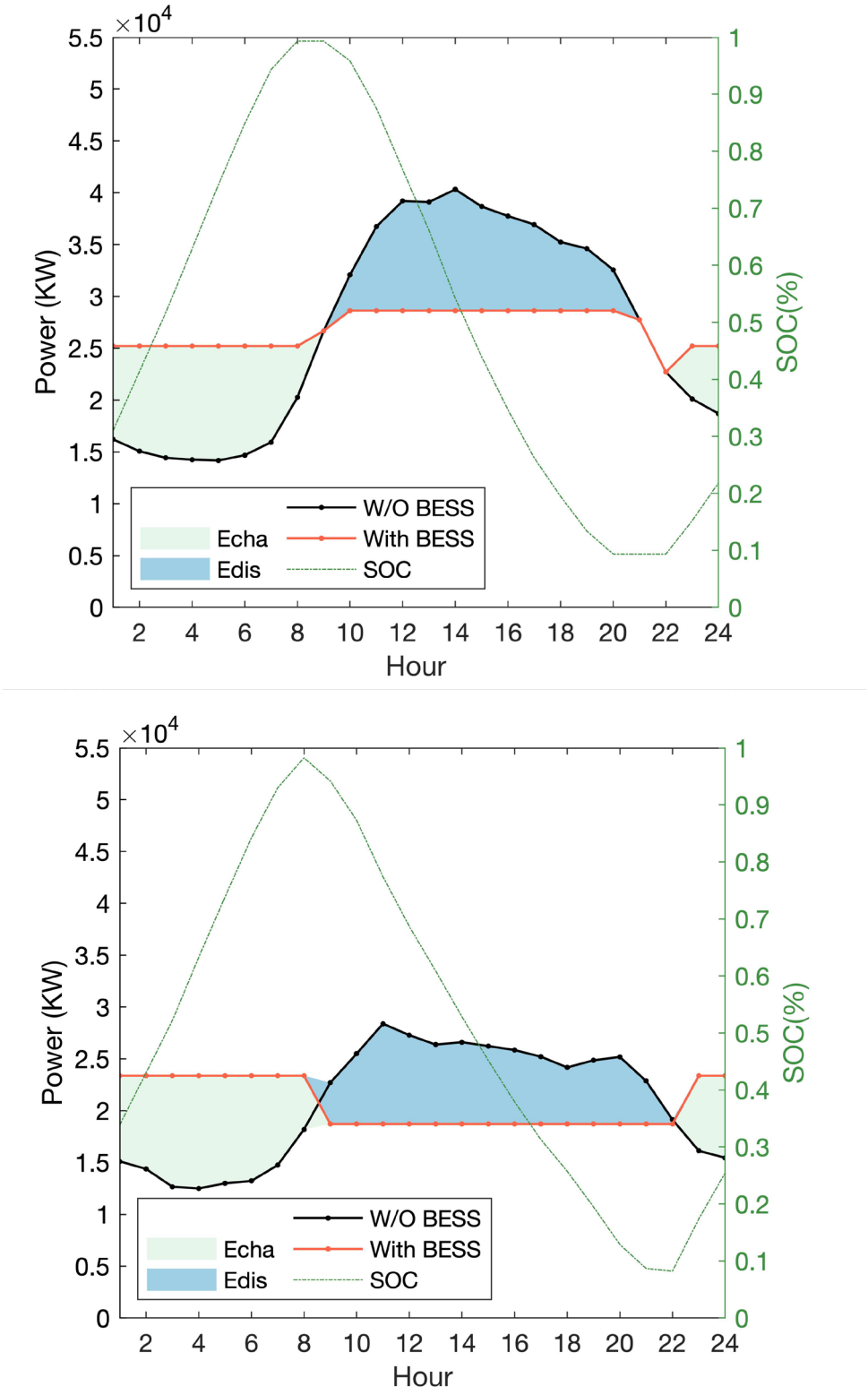

Fig. 7-7. Aggregate load profile with and without (W/O) BESS ((a).15th May; (b). 15th Aug; (c). 16th Nov; (d). 17th Feb)

7.4.4 Aggregated battery capacity comparison with individual design

Table 2 compares the results and performances with the battery sharing design method and normal individual design method. In the perspective of load leveling performance, the LSD value of individual design is 4113, while the other method is 3960. Compared with the situation without BESS (scenario 1), they are reduced by over half. It means both design methods offer good performance. The aggregated capacity of the distributed batteries is 113,056 kWh under the individual design and operation scenario (scenario 2). While the aggregated capacity of the distributed batteries to achieve better load leveling performance is 98,120 kWh in Scenario 3. The aggregated battery capacity is significantly reduced (i.e., 13.2% decrease) compared with Scenario 2. Correspondingly, the initial investment of battery is significantly reduced in Scenarios 3.

Table 7-2. Comparison of the results under individual design and shared design

	Scenario 1: W/O BESS	Scenario 2: Individual design	Scenario 3: Shared design
Aggregated battery capacity (Unit: kWh)	0	113,056	98,120
Load standard deviation (LSD)	8,838	4,113	3,960

7.4.5 Optimization at single building level

Due to the benefit of energy sharing framework, the private BESSs manger all energy flow with the community. The limitations of deploying batteries inside buildings is greatly reduced, as the surplus capacity can be consumed inside other buildings. It provides a great deal of flexibility in the BESS deployment. However, buildings with variety of curves are showing the different feature of BESS operation. The flexibility of BESS deployment of single buildings is presented in Fig.8 as optimal range BESS capacities. It indicates that BESS deployment flexibility varies greatly between buildings. We select three scenarios who have same BESS capacity at the aggregation level (98120 kWh) but with different capacity of each building. It is noted that in the case of scenario a, all the buildings deploy the batteries under the optimal sizes. The energy flow of three scenarios is plotted in Fig.9. In the case of scenario, a, all energy flow of batteries occur within the own buildings so that there is no energy loss of energy exchange with buildings. In the case of scenario b, some buildings (such as building 1, 2, 21 & 22) fist discharge to own buildings, but they still have remaining capacity, they share the batteries to the other building in order to achieve the load leveling performance. Therefore, there is 333,697 kWh energy losses occurred in the energy sharing process. In the case of scenario c, there is much higher remaining battery capacities in buildings so that the energy losses are much higher.

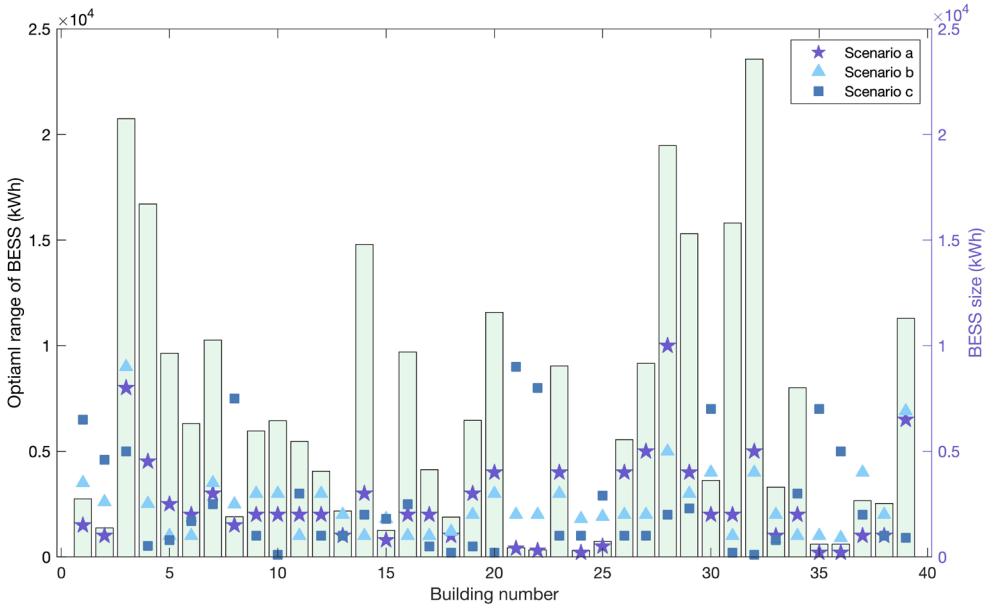

Fig. 7-8. Optimal BESS capacity of single buildings

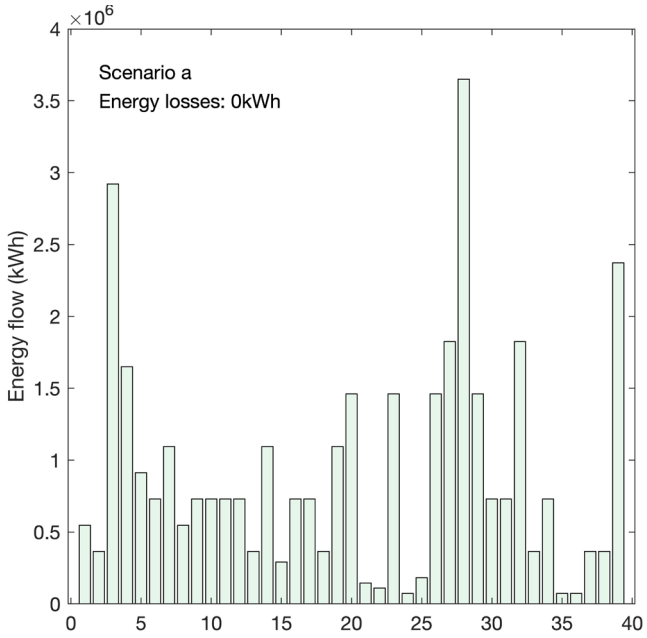

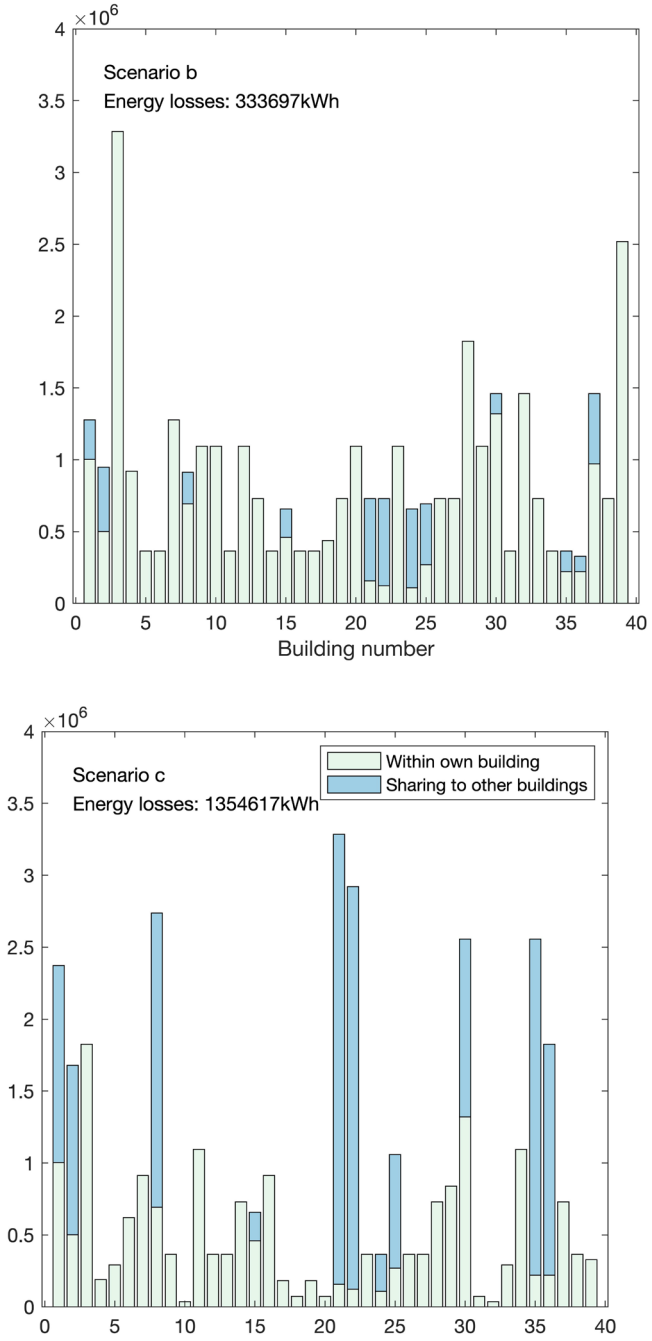

Fig. 7-9. Energy losses comparison under different scenarios

7.4.6 Building features and optimal sizing of BESS

From the comparison of scenario a, b and c, it indicates that the different sizes in the buildings will affect the energy losses. And the case of scenario a achieves 0 kWh energy losses, because all buildings consume all batteries charged power so that there is no energy exchange within buildings. In the case of scenario b and c, there always remains surplus power charged by batteries. The reason is some buildings are not required of electric power at much time, but they install over-sizing batteries. Therefore, the building load features, and the battery sizes are

highly dependent. Due to the characteristics and operations of the battery, the power from the grid is charged to the battery at night and discharged to the building at daytime. Figure 10 illustrates the relationship between daytime electricity consumption (from10:00 a.m. to 22:00 p.m. in this case) and optimal battery capacity for all buildings. Where the daytime electricity consumption is shown as a box plot, the dots represent the 4 most representative sets of data points and the red boxes are 95% confidence intervals. It can be noticed that the battery capacity of the building is always below the minimum value of daytime electricity consumption, this is because when the capacity is greater than the minimum value the battery capacity remains surplus power. The optimal capacity depends on the lowest daytime electricity consumption.

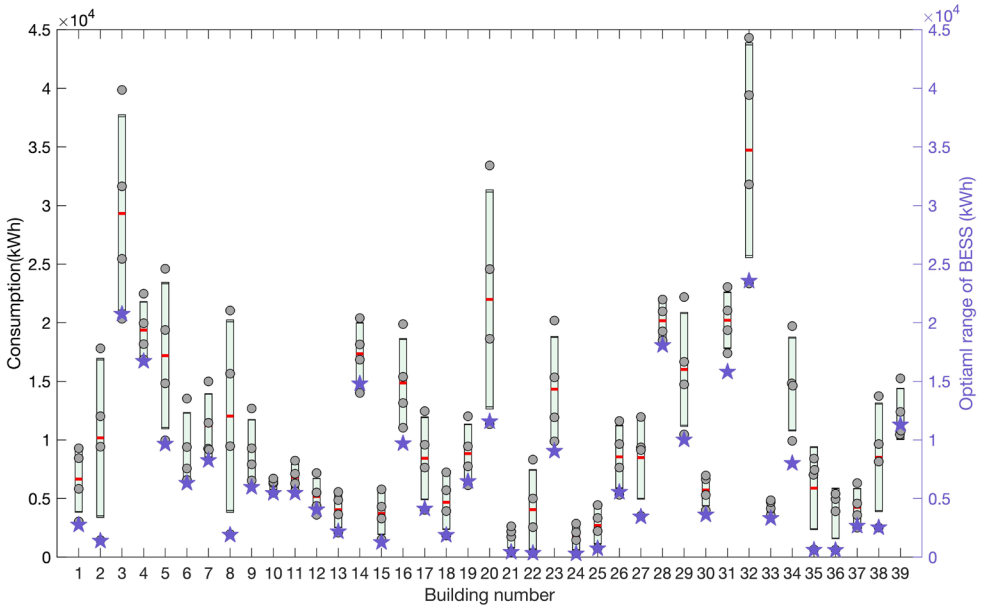

Fig. 7-10. The relationship with the daytime consumption and optimal capacity of single buildings

7.4.7 Closing day

The optimal capacity depends on the lowest daytime electricity consumption. Commercial activities are the determinants of electricity consumption in commercial buildings. On working days, buildings have a high demand for electricity to cope with busy commercial activities (e.g., air conditioning, lights, operation of factory production equipment), but on closing days, buildings have little demand for large amounts of electricity consumption and require only a small amount of power to keep equipment on standby (e.g., network, security, and some storage equipment). In the Fig.11, it is noted that the building 2, 8 and 22 also have relatively high consumption but the optimal BESS capacity are at a low level. Therefore, rest days can have a significant impact on battery sharing as well as battery capacity in a shared framework. We select four buildings which have similar annual electricity consumption as a case study. Two of the buildings (B9 and B11) have no closing days, and electricity consumption is relatively stable throughout the year. One building (B35) has a closing day on Sunday. One building (B22) has two closing days on Saturdays and Sundays. The daily electricity consumption curves are

plotted in Fig.11. It can be clearly seen that there is a clear difference between business days and closing days in B22 and B35.

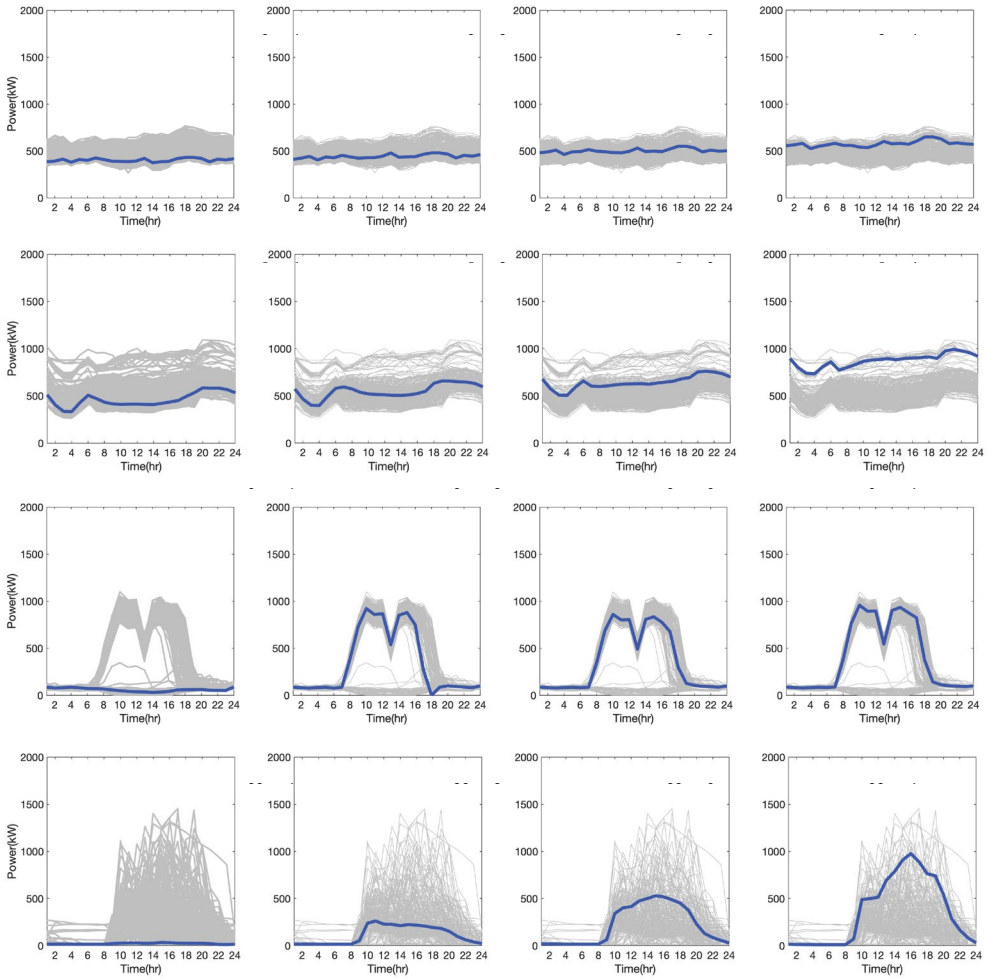

Fig. 7-11. The load curves of four typical buildings

Batteries with a capacity of 2,000kWh were installed in all four buildings. The operation of the battery between buildings can be clearly seen in Fig. 12. During weekdays, all buildings have high power consumption during the day, so all batteries have to be discharged from their own buildings and there is no energy exchange. On Saturdays, the batteries in B22 will be shared between B9 and B11 since B22 is a closing day and there is almost no power consumption during the daytime. On Sundays, the remaining battery capacity in B22 and B35 will be shared between B9 and B1, as B22 and B35 are on the closing days. Buildings with two closing days on one week lose 14.3% more energy than those with one day.

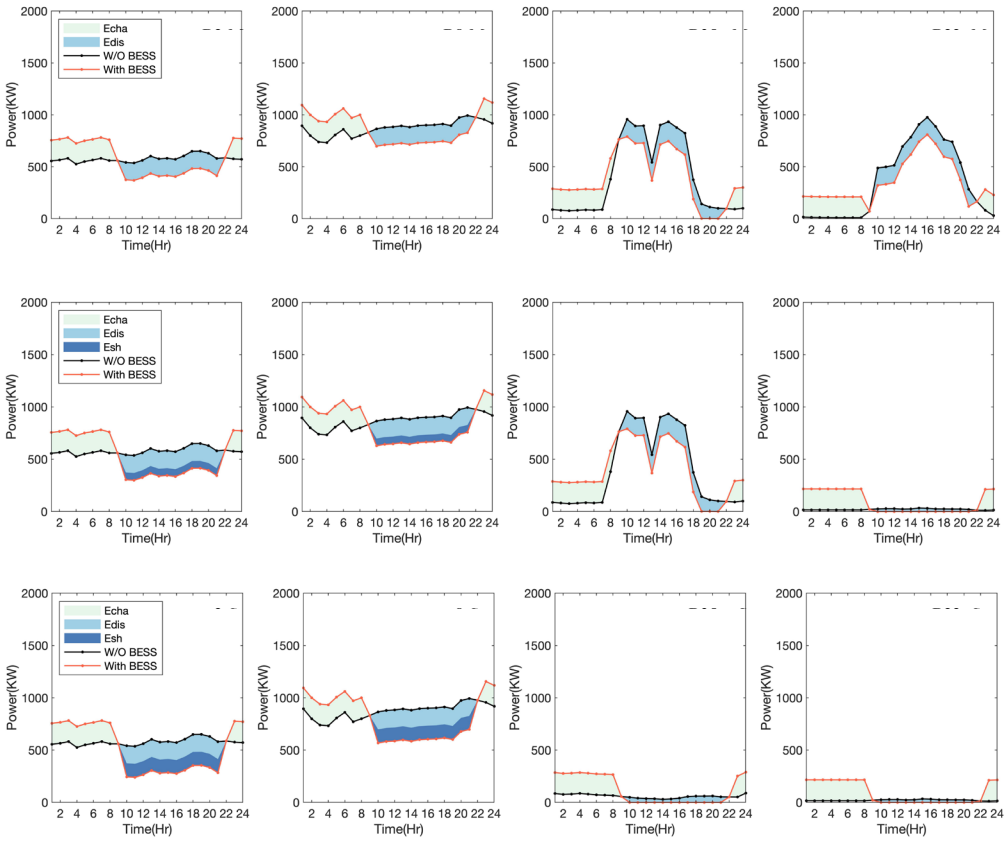

Fig. 7-12. The energy exchange between four buildings

7.5 Future direction of battery sharing

Based on the literature review of battery sharing, and our work, the effectiveness of BESS at the individual as well as community level can be demonstrated to act for better energy planning. However, when moving up to the city level of service recipients, there is still some room for improvement in data utilization, interoperability, and integrated management of the technologies currently used in BESS applications. This section will present the upgrade of BESS service targets and the future directions. It is well known that cities are pagoda-shaped, from single buildings to community or to city, and the higher up it is, the more the individuals or systems involved will grow exponentially. The current BESS application techniques are mainly used only for specific buildings or groups within cities and do not take into account the level of the city. As a result, we have taken an important step forward in our work. We have expanded the application of BESS from individual buildings to the community level and are connecting customers scattered across the city through battery sharing. Accordingly, BESS will improve the connectivity between systems to fully integrate the various factors that affect energy generation and consumption in cities. In order to achieve city-level interaction, the application strategy of BESS still faces some challenges. First, since BESS cannot be separated from the analysis, utilization and interaction of data. Therefore, energy data needs to be collected and shared at all levels of the city through an integrated IoT. And geospatial

information and automation based technologies need to be shared as well to reflect the changing spatial and environmental characteristics of the city.

7.6 Conclusions

In this paper, we enabled the energy sharing framework to optimize the control strategy and allocation method of the distributed battery system that can be exploited to achieve better optimization for load leveling through investigating the interaction between buildings with the distributed battery system and the distribution network. Firstly, we proposed the advantages of energy sharing to analyze the differences and of centralized and distributed energy storage in dealing with load-leveling problems. And we establish a strategy to move the peak-to-valley difference for the battery management system. Then we combine the advantages of centralized energy storage and propose a size allocation method in distributed energy storage to optimize load leveling performance and reduce the battery capacity at the aggregation level. The proposed distributed battery system, which is applied in typical community with 39 buildings in Japan, is simulated to analyze the load leveling performance.

The major conclusions of this paper are showed as bellow:

(1). The results indicate that the optimal solution obtained with the energy sharing structure performs load leveling effectively. It achieved the 26.6% of peak shaving rate.

(2). Compared with the individual operation, the energy sharing model achieves better load leveling performance of the public grid, while it reduces the battery capacity by 13.2% at aggregation level.

(3). The energy sharing is a generic framework for decomposing the optimal BESS allocation problem into individual optimal sizes of BESS within buildings. This approach allows to obtain optimal solutions by reducing unnecessary energy exchange between buildings. On the other hand, the approach also allows to obtain near-optimal solutions for the whole system (with energy losses) due to the different investment budgets and preferences of the buildings. This gives flexibility in the placement of the BESS, and investors can choose the solution according to their investment budget, other available investment opportunities and their preferences.

(4). Commercial buildings have great potential for BESS placement because of their fixed power consumption patterns. The optimal BESS capacity in commercial buildings depends on the lowest daytime power consumption. Among them, commercial buildings with closing days have limitations on BESS deployment. On closing days, buildings can only use BESS by sharing. Buildings with two closing days on one week lose 14.3% more energy than those with one day.

(5). The proposed method highlights the possibility of cooperation between consumers. It provides a blueprint for the implementation of regional battery sharing.

As a result of current development, many buildings are now producing their own electricity from local PV panels and selling it to the grid. Moreover, PV penetration and its intermittent output place additional management burdens on the public grid. There is no consideration of the impact of PV penetration or power trading on the design of individual BESS in this study. Thus, future work will consider a techno-economic case of a PV-battery system for building energy sharing communities to find out the interaction between coordinated energy storage system and smart grid.

References

[1] Global A. Global status report for buildings and construction. Global Alliance for Buildings and Construction. 2020.
[2] Mehrjerdi H. Simultaneous load leveling and voltage profile improvement in distribution networks by optimal battery storage planning. Energy. 2019;181:916-26.
[3] Al Shawa B. The ability of Building Stock Energy Models (BSEMs) to facilitate the sector's climate change target in the face of socioeconomic uncertainties: A review. Energy and Buildings. 2022;254:111634.
[4] Li Y, Gao W, Ruan Y. Performance investigation of grid-connected residential PV-battery system focusing on enhancing self-consumption and peak shaving in Kyushu, Japan. Renewable Energy. 2018;127:514-23.
[5] Cozzi L, Gould T, Bouckart S, Crow D, Kim T, Mcglade C, et al. World Energy Outlook 2020. vol. 2020;2050:1-461.
[6] Child M, Bogdanov D, Breyer C. The role of storage technologies for the transition to a 100% renewable energy system in Europe. Energy Procedia. 2018;155:44-60.
[7] Zhang C, Wei Y-L, Cao P-F, Lin M-C. Energy storage system: Current studies on batteries and power condition system. Renewable and Sustainable Energy Reviews. 2018;82:3091-106.
[8] Zhao H, Wu Q, Hu S, Xu H, Rasmussen CN. Review of energy storage system for wind power integration support. Applied energy. 2015;137:545-53.
[9] Comodi G, Giantomassi A, Severini M, Squartini S, Ferracuti F, Fonti A, et al. Multi-apartment residential microgrid with electrical and thermal storage devices: Experimental analysis and simulation of energy management strategies. Applied Energy. 2015;137:854-66.
[10] Zheng Y, Dong ZY, Luo FJ, Meng K, Qiu J, Wong KP. Optimal allocation of energy storage system for risk mitigation of DISCOs with high renewable penetrations. IEEE Transactions on Power Systems. 2013;29:212-20.
[11] Wong LA, Ramachandaramurthy VK, Taylor P, Ekanayake J, Walker SL, Padmanaban S. Review on the optimal placement, sizing and control of an energy storage system in the distribution network. Journal of Energy Storage. 2019;21:489-504.
[12] Van der Linden S. Bulk energy storage potential in the USA, current developments and future prospects. Energy. 2006;31:3446-57.
[13] Energy stroage study-Funding and knowledge sharing priorities. 2015.
[14] Divya KC, Østergaard J. Battery energy storage technology for power systems—An overview. Electric Power Systems Research. 2009;79:511-20.
[15] Dunn BK, Haresh; Tarascon, Jean-Marie. Electrical Energy Storage for the Grid: A Battery of Choices. Materials for grid energy. 2011.
[16] Mahlia TMI, Saktisahdan TJ, Jannifar A, Hasan MH, Matseelar HSC. A review of available methods and development on energy storage; technology update. Renewable and Sustainable Energy Reviews. 2014;33:532-45.
[17] Sparacino RJKGFRAR. Economic analysis of grid level energy storage for the application of load leveling. 2012 IEEE Power and Energy Society General Meeting. 2012.

[18] Lu C, Xu H, Pan X, Song J. Optimal Sizing and Control of Battery Energy Storage System for Peak Load Shaving. Energies. 2014;7:8396-410.
[19] Saboori H, Hemmati R, Abbasi V. Multistage distribution network expansion planning considering the emerging energy storage systems. Energy Conversion and Management. 2015;105:938-45.
[20] Saboori H, Hemmati R, Jirdehi MA. Reliability improvement in radial electrical distribution network by optimal planning of energy storage systems. Energy. 2015;93:2299-312.
[21] Trivedi A, Chong Aih H, Srinivasan D. A stochastic cost–benefit analysis framework for allocating energy storage system in distribution network for load leveling. Applied Energy. 2020;280.
[22] Duerr S, Ababei C, Ionel DM. A Case for Using Distributed Energy Storage for Load Balancing and Power Loss Minimization in Distribution Networks. Electric Power Components and Systems. 2020;48:1063-76.
[23] Jankowiak C, Zacharopoulos A, Brandoni C, Keatley P, MacArtain P, Hewitt N. Assessing the benefits of decentralised residential batteries for load peak shaving. Journal of Energy Storage. 2020;32:101779.
[24] Boglou V, Karavas CS, Karlis A, Arvanitis K. An intelligent decentralized energy management strategy for the optimal electric vehicles' charging in low-voltage islanded microgrids. International Journal of Energy Research. 2022;46:2988-3016.
[25] Kang H, Jung S, Lee M, Hong T. How to better share energy towards a carbon-neutral city? A review on application strategies of battery energy storage system in city. Renewable and Sustainable Energy Reviews. 2022;157:112113.
[26] Huang P, Lovati M, Zhang X, Bales C. A coordinated control to improve performance for a building cluster with energy storage, electric vehicles, and energy sharing considered. Applied Energy. 2020;268:114983.
[27] Roberts M. Impact of shared battery energy storage systems on photovoltaic self-consumption and electricity bills in apart.
[28] Zheng S, Huang G, Lai AC. Techno-economic performance analysis of synergistic energy sharing strategies for grid-connected prosumers with distributed battery storages. Renewable Energy. 2021;178:1261-78.
[29] Henni S, Staudt P, Weinhardt C. A sharing economy for residential communities with PV-coupled battery storage: Benefits, pricing and participant matching. Applied Energy. 2021;301:117351.
[30] He L, Liu Y, Zhang J. Peer-to-peer energy sharing with battery storage: Energy pawn in the smart grid. Applied Energy. 2021;297:117129.
[31] Dai R, Charkhgard H. Bi-objective mixed integer linear programming for managing building clusters with a shared electrical energy storage. Computers & Operations Research. 2018;96:173-87.
[32] Rappaport RD, Miles J. Cloud energy storage for grid scale applications in the UK. Energy Policy. 2017;109:609-22.

[33] Karavas C-SG, Plakas KA, Krommydas KF, Kurashvili AS, Dikaiakos CN, Papaioannou GP. A review of wide-area monitoring and damping control systems in Europe. 2021 IEEE Madrid PowerTech. 2021:1-6.
[34] Mekikis P-V, Antonopoulos A, Kartsakli E, Lalos AS, Alonso L, Verikoukis C. Information exchange in randomly deployed dense WSNs with wireless energy harvesting capabilities. IEEE Transactions on Wireless Communications. 2016;15:3008-18.
[35] Li Y, Hu S, Hoare C, O'Donnell J, García-Castro R, Vega-Sánchez S, et al. An information sharing strategy based on linked data for net zero energy buildings and clusters. Automation in Construction. 2021;124:103592.
[36] Wang J, Xie N, Ilea V, Bovo C, Xin H, Wang Y. Cooperative Trading Mechanism and Satisfaction-Based Profit Distribution in a Multi-Energy Community. Frontiers in Energy Research. 2021;9.
[37] Zhang T, Zhang G, Lu J, Feng X, Yang W. A new index and classification approach for load pattern analysis of large electricity customers. IEEE Transactions on Power Systems. 2011;27:153-60.
[38] Chicco G. Overview and performance assessment of the clustering methods for electrical load pattern grouping. Energy. 2012;42:68-80.
[39] Richard M-A, Fortin H, Poulin A, Leduc M-A, Fournier M. Daily load profiles clustering: a powerful tool for demand side management in medium-sized industries. Proceedings of the ACEEE Summer Study on Energy Efficiency in Industry, Denver, CO, USA. 2017:15-8.
[40] Bourdeau M, Basset P, Beauchêne S, Da Silva D, Guiot T, Werner D, et al. Classification of daily electric load profiles of non-residential buildings. Energy and Buildings. 2021;233:110670.
[41] Rajabi A, Eskandari M, Ghadi MJ, Ghavidel S, Li L, Zhang J, et al. A pattern recognition methodology for analyzing residential customers load data and targeting demand response applications. Energy and Buildings. 2019;203:109455.
[42] Miller C, Nagy Z, Schlueter A. A review of unsupervised statistical learning and visual analytics techniques applied to performance analysis of non-residential buildings. Renewable and Sustainable Energy Reviews. 2018;81:1365-77.
[43] McLoughlin F, Duffy A, Conlon M. A clustering approach to domestic electricity load profile characterisation using smart metering data. Applied energy. 2015;141:190-9.
[44] Wang S, Liu H, Pu H, Yang H. Spatial disparity and hierarchical cluster analysis of final energy consumption in China. Energy. 2020;197:117195.
[45] Yilmaz S, Chambers J, Patel MK. Comparison of clustering approaches for domestic electricity load profile characterisation-Implications for demand side management. Energy. 2019;180:665-77.
[46] INSULATORS N. Sodium sulfur battery. In: Group EIB, editor.
[47] Mair J, Suomalainen K, Eyers DM, Jack MW. Sizing domestic batteries for load smoothing and peak shaving based on real-world demand data. Energy and Buildings. 2021;247:111109.
[48] Bayliss CR, Bayliss C, Hardy B. Transmission and distribution electrical engineering: Elsevier; 2012.

[49] Xu L, Pan Y, Lin M, Huang Z. Community load leveling for energy configuration optimization: Methodology and a case study. Sustainable cities and society. 2017;35:94-106.
[50] Ministry of Economy T, and Industry. The fixed incentive and activation reward of demand response.
[51] bank F. Fukuoka Bank‘s annual interest rate
[52] Ministry of Economy T, and Industry. Government Subsidy to battery energy storage system.

Chapter 8

CONCLUSION AND PROSPECT

CONCLUSION AND PROSPECT

8.1 Conclusion 8-1

8.2 Prospect 8-3

8.2.1 Future direction of solar energy 8-3

8.2.2 Future direction of battery sharing 8-4

8.1 Conclusion

The power sector plays an important role in energy conservation and emission reduction. Renewable energy, especially solar PV, has been growing steadily in recent years. The development of solar energy can not only reduce the use of fossil energy, but also increase the energy self-sufficiency rate. After the implementation of the FiT system in 2011, there has been an explosive growth in the import of solar PV. However, solar power generation exhibits unstable output characteristics as it is affected by weather conditions. Large-scale introduction can affect the stability of the grid (e.g., the severe curtailment of generation or lack of resilience in the face of failures and disturbances). Therefore, this study considers the unstable weather conditions and proposes the concept of energy sharing to increase the chances of local energy self-consumption and renewable energy penetration in the future. At the same time, we aim to explore the interactions between smart grids, smart buildings and distributed energy storage to achieve better energy management practices

The main works and results can be summarized as follows:

In Chapter 1, RESEARCH BACKGROUND AND PURPOSE OF THE STUDY. The research backgrounds of energy resources are introduced in Chapter1, which is including the current status and bottleneck of integrational energy development. As well as the significant of developing solar energy. Then, the development and status of solar energy in world and Japan is well introduced. It is essential to developing solar energy in the communities to dealing with the problem of fossil fuel shortage. At last, the research purpose and logical framework is shown in order to support reviewers understand the content of this paper.

In Chapter 2, LITERATURE REVIEW. The relevant research of this paper is well reviewed in this Chapter. The commonly used solar radiation models and the calculation methods, and then summarizes the characteristics of the existing models and the application scenarios are also well explained. Then, the performance of power generation systems combining renewable energy sources with energy storage devices and their applications in urban grids are introduced further. A detailed description and summary of the emerging types of sharing economies, reviewing the economic performance of energy sharing as well as the technical means are also reviewed. Overall, the review in this section focuses on the development of solar radiation models, the application of renewable energy in the grid, the metrics for assessing the impact of renewable energy on the grid, and the methodology.

In Chapter 3, METHODOLOGY. The keyword of this paper is load in solar energy, battery energy storage system, energy sharing economy. Therefore, the methodology employed including, the development of a new solar radiation model with higher adaptability to the weather, the technical aspects of the grid impact of renewable energy penetration, and the modeling of batteries and the optimization methods are summarized in Chapter 3. Secondly, the economics metrics, where the dynamic payback period of PV is established. And the energy flow of the proposed energy sharing framework is also proposed in this chapter. It helps us to understand the interplay of load in solar energy, demand side, power grid, and battery energy storage system to seek an ideal electricity production composition.

In Chapter 4, DATA RESOURCE AND ENERGY CONVERSION ANALYSIS. The data resources and energy conversion analysis in this paper are presented in Chapter 4. The parameters of weather are obtained from historical data observed by the Japan Meteorological Agency. In this paper, the regional power grid of the Higashida Smart Community in Kyushu is selected to describe the generation composition and load profile.

In Chapter 5, DEVELOPMENT OF NEW SOLAR RADIATION MODEL. A new hourly weakening solar radiation model is developed based on the layer-by-layer weakening theory. Over 200,000 sets of data are collected from seven locations in Japan were used for modeling as well as validation. Considering the ease of data acquisition. A new layer-by-layer weakening solar radiation model was proposed based on the attenuation process of solar radiation from the atmosphere to the ground. The mean and best values of R2 are 0.89 and 0.96. Compared to the existing model, the accuracy of the proposed model was improved by 7.59% on average and 11.63% on best. The weakening effect of solar radiation is taken as the main body of this work. The results of validation indicate that the proposed model has greater adaptability to cloudy and even rainy days since the weakening effect of solar radiation is more significant on cloudy and rainy days. This will provide a reference for most solar radiation models based on a clear sky condition to adapt to more complex weather conditions. The proposed model is a generic framework so that the characterization factors of the weakening layer can be improved or replaced depending on the depth of the theory. The inclusion of interaction variables can significantly improve the performance of the model especially the interaction term of sunshine duration and cloud cover. The proposed model is established and calibrated from over 20 years of meteorological data (spread over seven different locations throughout Japan) and under various weather conditions. Thus, a typical meteorological year (TMY) for Japan can be generated based on our method. This is valuable for certain applications or techniques, such as thermal simulation of buildings throughout the year.

In Chapter 6, ENERGY SHARING FOR SELF-SUFFICIENT IN SOLAR COMMUNITY. The purpose of this study is to improve the feasibility of battery sharing by optimizing the techno-economic performance of battery sharing in a solar energy sharing community. The economic analysis shows that the shared design approach leads to a significant reduction in battery capacity at the community level (i.e., a 38.8% reduction). The payback period of the investment is shortened by 44.6%. This suggests that the economic benefits of PV- BESS systems can be effectively increased through the deployment of battery sharing. In addition, as the high initial investment is still required currently, the active incentives of the DR play a critical role in the economic assessment (i.e., a 46.4% reduction in payback period). Therefore, a combination of battery-based applications with multiple technologies can be the key solution to successful BESS deployment. A loss-based technical analysis shows that compared to the shared design for centralized BESS, an optimized distributed battery sharing community reduces transmission losses by up to 98%. The reason is the increase in the number of batteries within a community can reduce unnecessary energy exchange between different buildings. The requirement of remaining battery sharing accounts for a larger proportion than surplus PV storage sharing, thereby prioritizing the deployment of batteries in buildings with much insufficient power is more applicable. As the development of electrification in the future and

the pressure on the grid for peak shaving continues to increase, BESS will have greater application value as a flexible DR response tool. With the expected declines in equipment prices in the future, the PBP of the shared BESS will gradually be shortened. The battery sharing is expected to be more economical considering future trends, and it have more development prospects.

In Chapter 7, ENERGY SHARING FOR LOAD LEVELING IN SOLAR PV COMMUNITIY. We enabled the energy sharing framework to optimize the control strategy and allocation method of the distributed battery system that can be exploited to achieve better optimization for load leveling through investigating the interaction between buildings with the distributed battery system and the distribution network. The results indicate that the optimal solution obtained with the energy sharing structure performs load leveling effectively. It achieved the 26.6% of peak shaving rate. Compared with the individual operation, the energy sharing model achieves better load leveling performance of the public grid, while it reduces the battery capacity by 13.2% at aggregation level. The energy sharing is a generic framework for decomposing the optimal BESS allocation problem into individual optimal sizes of BESS within buildings. This approach allows to obtain optimal solutions by reducing unnecessary energy exchange between buildings. On the other hand, the approach also allows to obtain near-optimal solutions for the whole system (with energy losses) due to the different investment budgets and preferences of the buildings. This gives flexibility in the placement of the BESS, and investors can choose the solution according to their investment budget, other available investment opportunities and their preferences. Commercial buildings have great potential for BESS placement because of their fixed power consumption patterns. The optimal BESS capacity in commercial buildings depends on the lowest daytime power consumption. Among them, commercial buildings with closing days have limitations on BESS deployment. On closing days, buildings can only use BESS by sharing. Buildings with two closing days on one week lose 14.3% more energy than those with one day. The proposed method highlights the possibility of cooperation between consumers. It provides a blueprint for the implementation of regional battery sharing.

In Chapter 8, CONCLUSION AND PROSPECT. A summarized of each Chapter is concluded.

8.2 Prospect

8.2.1 Future direction of solar energy

Solar energy is one of the best options for meeting future energy needs because it outperforms other renewable energy sources in terms of availability, cost effectiveness, accessibility, capacity and efficiency. Most home solar panels have an efficiency of about 10-20%, another drawback of solar technology. However, more efficient (10~>20%) solar panels are also available at higher prices. Performance limitations of other components (e.g., batteries, inverters, etc.) are other areas with considerable room for improvement. Another obvious disadvantage is that solar energy can only be utilized during daylight hours and works most efficiently when the sun is shining. Therefore, in areas where weather or climate conditions are not sustainable, solar energy may not be the most reliable source of energy. Therefore, in the

future, solar technology combined with energy storage systems is the better choice.

8.2.2 Future direction of battery sharing

Based on the literature review of battery sharing, and our work, the effectiveness of BESS at the individual as well as community level can be demonstrated to act for better energy planning. However, when moving up to the city level of service recipients, there is still some room for improvement in data utilization, interoperability, and integrated management of the technologies currently used in BESS applications. This section will present the upgrade of BESS service targets and the future directions. It is well known that cities are pagoda-shaped, from single buildings to community or to city, and the higher up it is, the more the individuals or systems involved will grow exponentially. The current BESS application techniques are mainly used only for specific buildings or groups within cities and do not take into account the level of the city. As a result, we have taken an important step forward in our work. We have expanded the application of BESS from individual buildings to the community level and are connecting customers scattered across the city through battery sharing. Accordingly, BESS will improve the connectivity between systems to fully integrate the various factors that affect energy generation and consumption in cities. In order to achieve city-level interaction, the application strategy of BESS still faces some challenges. First, since BESS cannot be separated from the analysis, utilization, and interaction of data. Therefore, energy data needs to be collected and shared at all levels of the city through an integrated IoT. And geospatial information and automation-based technologies need to be shared as well to reflect the changing spatial and environmental characteristics of the city.